

Copyright

By

Jaime Fernando Argudo

2003

**Evaluation and Synthesis of Experimental Data  
for Autoclaved Aerated Concrete**

**by**

**Jaime Fernando Argudo, P.E.**

**Thesis**

Presented to the Faculty of the Graduate School of

The University of Texas at Austin

in Partial Fulfillment

of the Requirements

for the Degree of

**Master of Science in Engineering**

**The University of Texas at Austin**

**August 2003**

**Evaluation and Synthesis of Experimental Data  
for Autoclaved Aerated Concrete**

**Approved by  
Supervising Committee:**

---

**Richard Klingner, Supervisor**

---

**James Jirsa, Reader**

## **Dedication**

To my wife Maggy, and our children  
Carolina, Fernanda and Jaime Javier

## **Acknowledgements**

The research described in this thesis was conducted at the Phil M. Ferguson Structural Engineering Laboratory (FSEL) at the University of Texas at Austin, from May to August 2002, with financial support from the Autoclaved Aerated Concrete Products Association (AACPA). The Author thanks the AACPA for their financial assistance, and FSEL Faculty and Staff for their hospitality and kindness.

The work described in this thesis was part of an experimental and analytical research project (1998 – 2003) carried out at FSEL to develop design provisions for Autoclaved Aerated Concrete (AAC) elements and structures. Most of the work on that project was carried out directly by PhD students, Jennifer Tanner and Jorge Varela, to whom I express my gratitude for their continuous input, contributions and constructive criticism during the development of this thesis. I also appreciate and thank their cooperation to share information and data produced by them, and their interest to use the outcome of this research as an input for their PhD dissertations. Much of the data evaluated and synthesized in this thesis was developed by Prof. Fouad Fouad of the University of Alabama at Birmingham; this thesis would not have been possible without that work.

I express my deepest gratitude and recognition to Professor Dr. Richard Klingner, supervising professor of this thesis and of the AAC project, for his guidance and for the opportunity he gave me to learn about AAC, a material of which I knew almost nothing before. I would also like to thank Professor Dr. James O. Jirsa for his technical contributions as a reader of this thesis and member of its supervising committee.

I also want to acknowledge and thanks to the following institutions for the financial assistance and academic support provided for the fulfillment of my MSE degree at The University of Texas at Austin: Universidad Católica de Santiago de Guayaquil – Ecuador; Fundación Nacional para la Ciencia y la Tecnología del Ecuador (FUNDACYT); The Leo Rowe Fund from The Organization of the American States (OAS); The Latin-American Scholarship Program for American Universities (LASPAU); the Department of Civil Engineering of the University of Texas at Austin; and The Walter L. and Reta Mae Moore Graduate Fellowship in Civil Engineering.

August, 2003

## **Abstract**

# **Evaluation and Synthesis of Experimental Data for Autoclaved Aerated Concrete**

Jaime Fernando Argudo, M.S.E.

The University of Texas at Austin, 2003

Supervisor: Richard E. Klingner

Autoclaved aerated concrete (AAC) is a lightweight uniform cellular concrete that is well known and used in Europe, but relatively new in the United States, where design and construction provisions, and material specifications, are now being developed for its use.

In this thesis, available data for key mechanical properties of AAC are evaluated and synthesized. The data were originally produced at the University of Texas at Austin, the University of Alabama at Birmingham, and elsewhere.

The synthesized data are then used to develop a technical justification for proposed design provisions for ACC elements and structures.

# Table of Contents

<b>CHAPTER 1 INTRODUCTION .....</b>	<b>1</b>
1.1 Historical Perspective.....	1
1.2 The European Model Code: RILEM Recommended Practice, 1993 ....	2
1.3 Scope of Work.....	3
1.4 Objective of this Thesis.....	6
1.5 Organization of this Thesis .....	6
<b>CHAPTER 2 BACKGROUND OF AVAILABLE DATA ON AAC .....</b>	<b>8</b>
2.1 Introduction.....	8
2.2 Criteria for Data Evaluation .....	8
2.2.1 Consistency of Data .....	8
2.2.2 Completeness of Data.....	9
2.3 Available Data.....	9
2.3.1 Data from Hebel – Germany .....	9
2.3.2 Data from The University of Alabama at Birmingham (UAB).....	10
2.3.3 Data from Construction Technology Laboratories (CTL) .....	11
2.3.4 Data from The University of Texas at Arlington .....	11
2.3.5 Data from The University of Texas at Austin .....	13



<b>CHAPTER 3</b>	<b>EVALUATION AND SYNTHESIS OF AVAILABLE DATA ON MECHANICAL PROPERTIES OF AAC</b>	<b>14</b>
3.1	General	14
3.2	Compressive Strength of AAC	14
3.2.1	Available Information regarding Compressive Strength	14
3.2.2	Discussion of Results for Compressive Strength of AAC	15
3.3	Stress-Strain Behavior and Modulus of Elasticity of AAC	22
3.3.1	Information regarding Modulus of Elasticity	22
3.3.2	Discussion of Results for Modulus of Elasticity of AAC	23
3.4	Tensile Strength of AAC	28
3.4.1	Information regarding Tensile Strength of AAC	28
3.4.2	Discussion regarding Splitting Tensile Strength of AAC	30
3.4.3	Discussion of Relationship between Modulus of Rupture and Splitting Tensile Strength	35
3.4.4	Discussion regarding Modulus of Rupture of AAC using Combined UAB and UT Austin Data	37
3.4.5	Relationship between Modulus of Rupture ( $f_r$ ) and Compressive Strength ( $f_{AAC}$ )	43
3.5	Tensile Bond between AAC and Bedding Mortar	45
3.5.1	Information regarding Tensile Bond between AAC and Bedding Mortar	45
3.5.2	Discussion regarding Tensile Bond Strength for Masonry Mortar using Combined UAB and UT Austin Data	46
3.6	Tensile Bond between AAC and Thin-bed Mortar	46
3.6.1	Information regarding Tensile Bond between AAC and Thin-bed Mortar	46
3.6.2	Discussion of Results regarding Tensile Bond between AAC and Thin-bed Mortar	47

3.7	Shear Bond between AAC and Thin-bed Mortar .....	50
3.7.1	Information regarding Shear Bond between AAC and Thin-bed Mortar... ..	50
3.7.2	Discussion of Results regarding Shear Bond between AAC and Thin-bed Mortar .....	50
3.8	Direct Shear Strength of AAC .....	54
3.9	Freeze-Thaw Resistance of AAC .....	56
3.10	Variation in the Compressive Strength of AAC with Moisture Content .....	56
<b>CHAPTER 4 DESIGN PROVISIONS FOR REINFORCED AAC FLOOR PANELS.....</b>		<b>57</b>
4.1	Organization of Work on Design Provisions for Reinforced AAC Panels .....	57
4.2	Approach For Developing Design Provisions.....	58
4.3	Bond Strength between Factory-Installed Wire Reinforcement and AAC .....	59
4.3.1	Information regarding Bond Strength between Welded Wire Reinforcement and AAC.....	59
4.3.2	Discussion regarding Anchorage Failure of Tensile Reinforcement for UAB Panel Tests.....	59
4.3.3	Design Proposal for Anchorage Capacity .....	63
4.4	Flexural Design of AAC Beam Elements .....	66
4.4.1	Nominal Flexural Capacity ( $M_n$ ).....	66
4.4.2	Minimum Flexural Reinforcement Ratio .....	66
4.4.3	Flexural Design of Tension- and Compression-Controlled AAC Elements under ACI 318-02 .....	68
4.5	Control of Deflections.....	68
4.6	Shear Design of AAC Beam Elements .....	70
4.6.1	Shear Capacity of AAC ( $V_{AAC}$ ).....	70

4.6.2	Shear Strength provided by Shear Reinforcement ( $V_s$ ).....	72
4.6.3	Design Shear Capacity ( $\phi V_n$ ) .....	72
4.6.4	Predicted Shear Capacities of Reinforced AAC Floor Panels Tested at UAB and CTL .....	73
4.7	Design Example of an AAC Floor Panel .....	75
4.7.1	Design data.....	75
4.7.2	Control of Deflections.....	76
4.7.3	Shear capacity .....	82
4.7.4	Anchorage .....	82
4.7.5	Flexural capacity .....	83
4.7.6	Wall-panel connection, shear force on bearing critical section.....	84
<b>CHAPTER 5 SUMMARY, CONCLUSIONS AND RECOMMENDATIONS .....</b>		<b>86</b>
5.1	Summary.....	86
5.2	Conclusions.....	86
5.2.1	Available data are sufficient to develop design provisions for reinforced AAC panels .....	86
5.2.2	Use of specified compressive strength as key independent variable.....	87
5.2.3	Quality assurance for compressive strength is essential .....	87
5.2.4	Flexural and shear strength of the material can be controlled by the tensile bond capacity at the interface between AAC and the mortar.....	87
5.2.5	Good construction practices can significantly increase the tensile bond capacity at the interface between AAC and the mortar.....	88
5.3	Recommendations for Future Research Work .....	88

<b>APPENDIX A</b>	<b>DESIGN PROVISIONS FOR REINFORCED AAC SHEAR WALLS AND FLOOR DIAPHRAGMS.....</b>	<b>90</b>
<b>APPENDIX B</b>	<b>ACI 523.5R-XX GUIDE FOR USING AUTOCLAVED AERATED CONCRETE PANELS.....</b>	<b>171</b>
<b>APPENDIX C</b>	<b>PROPOSED CODE DESIGN PROVISIONS AND COMMENTARY .....</b>	<b>222</b>
<b>APPENDIX D</b>	<b>COMPLEMENTARY SECTIONS TO CHAPTERS 3 AND 4 .....</b>	<b>281</b>
<b>REFERENCES</b>	<b>.....</b>	<b>295</b>
<b>VITA</b>	<b>.....</b>	<b>297</b>

## List of Tables

Table 3.1	Summary of results for compressive strength and density from UAB and UT Austin .....	17
Table 3.2	Change in correlation coefficients for compressive strength and modulus of rupture tests.....	21
Table 3.3	Modulus of elasticity for load perpendicular to the direction of rise for tests at UAB and UT Austin.....	24
Table 3.4	Modulus of elasticity for load parallel to the direction of rise for UAB.....	25
Table 3.5	Results of C1006 splitting tensile strength tests performed at UT Austin.....	32
Table 3.6	Ratios between measured modulus of rupture at C1386 density and splitting tensile strength estimated using oven-dry density for different classes of AAC .....	36
Table 3.7	Modulus of Rupture – UAB Method 1 .....	38
Table 3.8	Modulus of Rupture – UAB Method 2 .....	38
Table 3.9	Modulus of Rupture of AAC specimens with thin-bed mortar joints (UAB, Method 2).....	47
Table 3.10	Shear Tests on AAC with and without thin-bed mortar - UAB Method.....	52
Table 4.1	Organization of primary responsibility for development of design provisions for AAC elements .....	58
Table 4.2	Comparison of anchorage demand to anchorage resistance for reinforced panels tested at UAB .....	62
Table 4.3	Summary of predicted and observed modes of failure for floor panels tested at UAB.....	74
Table 4.4	Summary of predicted and observed modes of failure in ACCOA panels .....	74

## List of Figures

Figure 1.1	Objectives of program for developing draft design provisions for AAC at The University of Texas at Austin (Klingner, et al., 2003).....	5
Figure 3.1	Compressive strength versus dry density with ASTM C1386 requirements .....	18
Figure 3.2	Compressive strength versus calculated density corresponding to a 10% moisture content for tests performed at UT Austin and UAB.....	18
Figure 3.3	Variation of compressive strength versus calculated density at a moisture content of 10%.....	21
Figure 3.4	Direction-of-rise convention for specimens tested by UT Austin and UAB for Modulus of Elasticity .....	23
Figure 3.5	Modulus of elasticity versus calculated density at 10% moisture content for load perpendicular to the direction of rise in UAB and UT Austin .....	26
Figure 3.6	Modulus of elasticity versus calculated density at 10% moisture content for all tests performed at UAB .....	27
Figure 3.7	Modulus of elasticity versus compressive strength for loading parallel to the direction of rise at UAB and UT Austin .....	27
Figure 3.8	UAB test set up for Modulus of Rupture, “Method 1” .....	29
Figure 3.9	UAB test set up for Modulus of Rupture, “Method 2” .....	29
Figure 3.10	Direction-of-rise convention for specimens tested by UAB for Modulus of Rupture (Method 1) .....	30
Figure 3.11	Splitting tensile strength versus density .....	33
Figure 3.12	Splitting tensile strength versus compressive strength.....	33
Figure 3.13	Comparison between Dutch Standards and UT Austin relationships for specified design tensile strength ( $f_t'$ ) versus compressive strength ( $f_{AAC}$ ) .....	35
Figure 3.14	Modulus of rupture versus density for Method 1 (stresses parallel to the direction of rise) .....	39
Figure 3.15	Modulus of rupture versus density for Method 1 (stresses perpendicular to the direction of rise) .....	39
Figure 3.16	Modulus of rupture versus density for Method 2 (stresses parallel to the direction of rise) .....	40
Figure 3.17	Modulus of rupture versus compressive strength for Method 1 (stresses parallel to direction of rise).....	42

Figure 3.18	Modulus of rupture versus compressive strength for Method 1 (stresses perpendicular to direction of rise).....	42
Figure 3.19	Modulus of rupture versus compressive strength for Method 2 (stresses parallel to the direction of rise).....	43
Figure 3.20	Relationship between $f_r$ and $f_{AAC}$ based on UAB and UT Austin data (Method 2) .....	45
Figure 3.21	Tensile bond strength versus density .....	49
Figure 3.22	Tensile bond strength versus compressive strength .....	49
Figure 3.23	Shear strength of AAC units and thin-bed mortar versus density .....	53
Figure 3.24	Shear strength of AAC units and thin-bed mortar versus compressive strength .....	53
Figure 3.25	Relationship between direct shear strength ( $f_v$ ) and compressive strength ( $f_{AAC}$ ) .....	56
Figure 4.1	Free-body diagram of panel section .....	60
Figure 4.2	Resistance mechanism based on cross-wires functioning in bearing.....	61
Figure 4.3	Simple supported AAC Floor Panel.....	75
Figure 4.4	Cracked transformed section (h = 10 in.).....	78
Figure 4.5	Cracked transformed section (h = 12 in.).....	80
Figure 4.6	Detail of panel bearing area .....	84

# CHAPTER 1

## Introduction

### 1.1 HISTORICAL PERSPECTIVE

Aerated concrete was first developed as a lightweight material consisting of combinations of cement and quicklime silica sand, slag, pulverized fly ash, or other siliceous fine aggregates, in the form of a fine powder. The powder is mixed with water to form a slurry, and air or other gas (usually hydrogen) is introduced into the slurry. Due to initial hydration of the cement, accelerated by the heat produced by the quicklime, the mixture sets, acquiring a uniform cellular structure (CEB, 1978).

In the early 1920s Dr. Axel Eriksson, then Assistant Professor for Building Techniques at the Royal Institute of Technology in Stockholm, invented an aerated concrete that he called “gas concrete.” This new material was later called Autoclaved Aerated Concrete (AAC); its industrial manufacture was developed in Sweden in 1929 as a combination of the technique for producing a cellular concrete by the introduction of a gas-forming agent, and the technique for hardening concrete through autoclaving (RILEM, 1992). AAC is usually factory produced, high-pressure steam-cured, and available for used in pre-cast units for floors, walls, roofs and lintels. The density of AAC is 25 to 60 pcf (3.94 E-06 to 9.45 E-06 N/mm<sup>3</sup>).

From 1929, it took another 10 to 20 years until reinforced AAC elements were developed and first used mainly in Scandinavia as roof and floor units and wall panels. The Second World War temporarily halted the expansion in the use



of AAC, but after 1950, AAC did successfully expand in Europe and Asia (RILEM, 1992).

Siporex, Ytong (Germany), Durox, Hebel (Germany), and H+H (Denmark) have become the most important AAC producers worldwide. From 1955 to 1972, a Siporex plant operated near Montreal, Canada, representing the first and only attempt to introduce AAC in North America before the 1990s.

The production of AAC in the United States and Mexico started in the early and mid-1990s, with the opening of plants by Hebel (later Matrix and then Babb), Ytong Florida (later Aercon Florida), ACCOA, and E-Crete in the US, and of a plant by Contec Mexicana in Mexico.

## **1.2 THE EUROPEAN MODEL CODE: RILEM RECOMMENDED PRACTICE, 1993**

Extensive research on AAC has been developed in Europe by RILEM (International Union of Testing and Research Laboratories for Materials and Structures). RILEM's first Symposium on Autoclaved Aerated Concrete was held in Göteborg, Sweden in 1960 (RILEM, 1960)

In 1978 the Comité Euro-international du Béton (CEB) published the first manual on AAC design and construction technology (CEB, 1978). That publication served as the starting point for the subsequent development of unified European design provisions for AAC.

The Proceedings of the 2nd International Symposium, held at the Swiss Federal Institute of Technology (EPFL) in Lausanne in March 1982, included a

detailed bibliography of almost 500 references on AAC (RILEM, 1983). At that time, the need was recognized for evaluating the experimental data and theoretical studies that had been collected throughout Europe.

At the RILEM General Council meeting held in Mexico City in September 1982, Technical Committee 78-MCA (Model Codes for AAC based on RILEM Test Methods) was set up. Another RILEM Technical Committee, 51-ALC (Test Methods for Autoclaved Lightweight Concrete), was already active preparing recommendations for test methods to characterize relevant properties of AAC. In many European countries, national standards and recommendations on selected topics already existed in 1982. For this reason RILEM Technical Committee 78-MCA started his work collecting and comparing existing standards from eighteen different countries, and published a working document in 1984 (RILEM, 1984).

In 1993, RILEM Technical Committees 78-MCA and 51-ALC published the first edition of “*Autoclaved Aerated Concrete: Properties, Testing, and Design*”- *RILEM Recommended Practice* (RILEM, 1993). That document was prepared as a European model code, is used throughout Europe and Asia, and is cited as a key reference in research studies conducted in the University of Alabama at Birmingham and the University of Texas at Austin.

### **1.3 SCOPE OF WORK**

As AAC products were introduced in the United States, it became clear that there was a need for methods of test and design provisions compatible with US material specifications, design codes and construction practices for masonry and reinforced concrete.

Because RILEM methods of test are not equivalent to those of ASTM, and are often not written in mandatory language, the RILEM Recommend Practice is not useful for evaluating the performance of AAC units for use in the United States. Similarly, RILEM Design Provisions cannot be conveniently used for design in the US, because they are relatively unknown in the US, they differ in approach, organization and style from ACI 318 and the Masonry Standards Joint Committee provisions, and they are difficult to reference in US model codes.

To address this issue, a comprehensive program for development of draft design provisions was begun at The University of Texas at Austin. The objective of that program is shown schematically in Figure 1.1. Draft design provisions for unreinforced masonry elements of AAC would follow the format of the 2002 MSJC Code and Specification; draft design provisions for reinforced AAC panels would follow the format of ACI 318-02; and each set of provisions would in turn reference appropriate ASTM specifications for materials, methods of test, and other items as appropriate.

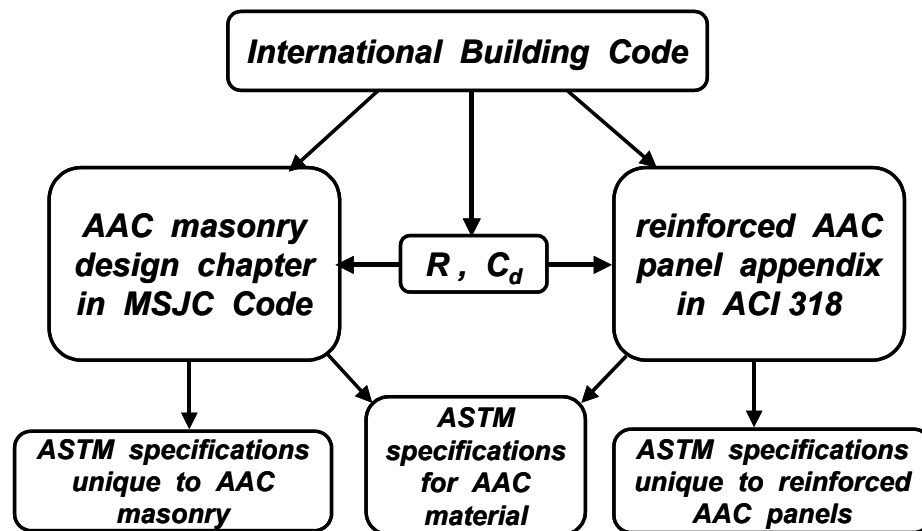


*Figure 1.1 Objectives of program for developing draft design provisions for AAC at The University of Texas at Austin (Klingner, et al., 2003)*

To develop the necessary technical justification for the draft design provisions, some existing test data were used. In addition, a testing program to establish basic material characteristics was begun at The University of Alabama at Birmingham, and a research program to develop design provisions, investigate seismic performance, and propose  $R$  and  $C_d$  factors for seismic design was begun at The University of Texas at Austin.

At the University of Texas at Austin, tests were conducted on AAC shear walls and on a two-story assemblages were used to develop design provisions for AAC masonry elements and structures in a format compatible with MSJC design provisions (Tanner, 2003), and to propose  $R$  and  $C_d$  factors for seismic design of AAC structures (Varela, 2003).

Within that overall scope of work, the objective of this thesis was to synthesize basic material data on AAC from various sources, and to use those synthesized data to develop design provisions for reinforced AAC panels that would be consistent with ACI 318 – 02, and that would be consistent in outcome with provisions developed in the same research program for AAC masonry. In each case, the provisions were accompanied by commentary, and also by a “super-commentary,” or technical justification. The “super-commentary” for reinforced AAC panels was intended to part of a draft guide developed by ACI Subcommittee 523A<sup>1</sup>.

#### **1.4 OBJECTIVE OF THIS THESIS**

The overall objective of this thesis is to evaluate and synthesize available data from The University of Texas at Austin, the University of Alabama at Birmingham, and other sources, to make those synthesized data available for use by others in refining previously developed design provisions for AAC shear walls, and to use those synthesized data to develop the draft design provisions and the associated technical justification for reinforced AAC panels.

#### **1.5 ORGANIZATION OF THIS THESIS**

This thesis is organized as follows: Chapter 2 explains the background of available data; Chapter 3 presents an evaluation and synthesis of available data on

---

<sup>1</sup> Draft document prepared by ACI Subcommittee 523A, under consideration by ACI Committee 523, July 2003.

mechanical characteristics of AAC; Chapter 4 contains proposed draft design provisions for AAC floor panels; and Chapter 5 presents the summary, conclusions and recommendations of this thesis.

Three Appendices are also included:

- o Appendix A presents the draft design provisions for reinforced AAC shear walls and floor diaphragms. This appendix was adapted by Tanner from similar draft provisions developed by her for AAC masonry (Tanner, 2003).
- o Appendix B contains the current draft of the *ACI 523.5R-xx Guide for Using Autoclaved Aerated Concrete Panels*;
- o Appendix C contains the proposed design provisions and commentary; and
- o Appendix D contains complementary sections to Chapters 3 and 4.

## **CHAPTER 2**

### **Background of Available Data on AAC**

#### **2.1 INTRODUCTION**

In this chapter, available data on material behavior of AAC are discussed. First, criteria for evaluation; the data are reviewed. Then, using those criteria, data in each category are critically evaluated and synthesized.

#### **2.2 CRITERIA FOR DATA EVALUATION**

This section contains a discussion of the criteria used to evaluate available data on the structural behavior of AAC elements.

##### **2.2.1 Consistency of Data**

Consistency of data is a requirement for reliable determination of nominal capacities. Internal consistency of data within any particular laboratory was considered acceptable if the coefficient of variation did not exceed 20%, and linear regressions had  $R^2$  values not less than 0.8. External consistency within data from different laboratories was considered acceptable if the coefficients of variations did not exceed 40%, and the linear regressions had  $R^2$  values not less than 0.7. Acceptable internal or external consistency, as applicable, is also used in Chapter 3 to qualify data that were used to develop mathematical relationships to predict the physical behavior of AAC.

### **2.2.2 Completeness of Data**

Completeness of data is a requirement for a useful integration of data from different sources. Information from different sources should be available for all variables involved in a proposed relationship for predicting material behavior.

## **2.3 AVAILABLE DATA**

The data on AAC behavior that were used in the preparation of this thesis include public-domain references and internal reports. The public domain references are Fouad et al. (2002), Tanner (2003) and Varela (2003). The internal reports are cited by footnotes as they are used.

In this section, each of those data sources is discussed in detail, and the corresponding data are presented, summarized and evaluated.

### **2.3.1 Data from Hebel – Germany**

Twelve AAC masonry shear-wall specimens were tested by Hebel in Germany<sup>2</sup>. Results from Hebel tests were combined with results from nine specimens tested in UT Austin, to develop design equations for predicting web-shear cracking capacity of shear walls with mortared and un-mortared head joints (Appendix A, Section A.1.1). Hebel data were essential to address the case of shear walls with un-mortared head joints, because all UT Austin specimens were built with mortared head joints.

---

<sup>2</sup> Personal communication, Violandi Vratsanou, Hebel AG, Germany, November 2000



### **2.3.2 Data from The University of Alabama at Birmingham (UAB)**

The University of Alabama at Birmingham (UAB) tested AAC masonry units and reinforced panels from three different manufacturers (Hebel, Ytong and Contec) and grades (PAAC-2, PAAC-3 and PAAC-4), under the sponsorship of the Autoclaved Aerated Concrete Products Association (AACPA). These grades and their significance are discussed in Appendix B of this thesis.

Tests performed on AAC masonry units included compressive strength, flexural tensile strength, flexural tensile strength with thin-bed and thick-bed mortar joints, modulus of elasticity, and freeze-thaw durability. For reinforced AAC panels, tests were conducted on floor panels, lintels, and vertical wall panels.

Results from UAB tests were submitted to the AACPA in February 2002 (Fouad et al., 2002), in the form of a 500-page report that compiles results from 25 different tests conducted on 697 specimens. That report was intended to be preliminary; it does not address issues of completeness or consistency, and has no conclusions.

As is explained in this thesis, the UAB test results were found to be internally very consistent and could usefully be combined with data from UT Austin to develop equations for predicting key mechanical properties of ACC (Chapter 3) and design provisions for AAC floor panels (Chapter 4).

Consistency between UAB and UT Austin data was not always very good, however. Reasons for those inconsistencies were identified and the design equations for reinforced ACC shear walls (Appendix A) and masonry shear walls (Tanner, 2003) were updated and refined as a result of the integration of UAB and UT Austin data.

### **2.3.3 Data from Construction Technology Laboratories (CTL)**

In 1999, tests were performed by Construction Technology Laboratories (CTL) to evaluate the performance of reinforced floor and wall panels manufactured by AACOA<sup>3</sup>. The CTL tests on wall panels were not useful for the objectives of this thesis, because failure was by crushing of AAC and results were similar to those obtained for compression specimens. Data from CTL tests on six reinforced AAC floor panels were used in Chapter 4, Section 4.5.4 to predict shear capacity and failure mechanisms.

CTL also performed tests on mechanical properties of AAC. Results of tests on compressive strength tests on cubes and prisms, and flexural bond strength tests of two blocks bonded with thick bed mortar were not used, because the densities and moisture contents were not controlled. A modulus of elasticity test conducted by CTL produced a single data point, which was combined with other data from UT Austin and UAB to develop a correlation between modulus of elasticity and compressive strength (Chapter 3, Section 3.3.3).

### **2.3.4 Data from The University of Texas at Arlington**

The Construction Research Center of The University of Texas at Arlington evaluated the performance of Ytong AAC block assemblages with respect to modulus of rupture (ASTM E72) and diagonal tensile strength (ASTM E519).

From 1996 to 1999, four sets of tests were conducted at UT Arlington on different types of AAC masonry units, in different strength grades, following ASTM test methods. A compilation of reports on those four sets of tests was

---

<sup>3</sup> Internal Report by CTL to ACCOA: *Structural Tests on AAC Reinforced Panels Manufactured by Aerated Concrete Corporation of America (ACCOA)*, July 1999.

obtained from Ytong<sup>4</sup>. Results from the UT Arlington tests are internally very consistent.

The main conclusion from those UT Arlington tests is that the capacity of AAC assemblages in flexure (ASTM E72) and in diagonal tension (ASTM E519) is generally controlled by the AAC material itself, rather than the strength of the mortar joint. This behavior is in contrast to that of conventional masonry, whose flexural and diagonal tensile strength are generally controlled by the bond between units and mortar.

The observations contained in the synthesized UT Arlington reports further confirm the conclusions presented in Chapter 3, Section 3.6 (tensile bond strength between AAC and thin-bed mortar) and Section 3.7 (shear bond strength between AAC and thin-bed mortar).

Values for modulus of rupture and shear strength obtained by UT Arlington were consistently lower (about two-thirds, on average) than the combined results from UT Austin and UAB. This significant difference is attributed to the use of different test standards, preparation of specimens, and lack of control over compressive strengths.

Compressive strengths, densities, and moisture contents were not controlled for tested materials. UT Arlington used compressive strengths and densities reported by the manufacturer.

Based on the criteria set for in Section 2.1, UT Arlington data were not integrated with UT Austin and UAB data in Chapter 3.

---

<sup>4</sup> Personal communication, Ronald E. Barnett, Ytong Florida, Ltd., USA, June 2000.

### **2.3.5 Data from The University of Texas at Austin**

Under the AAC research carried out at Ferguson Structural Engineering Laboratory at UT Austin, 17 shear walls and one two-story assemblage were tested to develop design provisions for AAC masonry shear walls (Tanner, 2003 and Varela, 2003). Data from those tests were later used to develop design provisions for reinforced AAC masonry shear walls (Appendix A). Internal consistency of these tests is very good.

Originally, the University of Alabama at Birmingham was expected to provide information on key mechanical properties of AAC, as the result of an experimental testing program that was underway there since 1999. Because results from UAB were not available until 2002, however, researchers at UT Austin decided to conduct independent density tests on blocks, compressive strength and modulus of elasticity tests on 4 x 8 in. (102 x 203 mm) cores, splitting tensile strength (ASTM C1006) tests on blocks, and direct shear tests on three-block assemblages. Internal consistency of those UT Austin tests is good, and those results were combined with UAB data to develop equations for predicting key mechanical properties of ACC (Chapter 3).

# **CHAPTER 3**

## **Evaluation and Synthesis of Available Data on Mechanical Properties of AAC**

### **3.1 GENERAL**

In this chapter, relationships for predicting the mechanical properties of AAC are developed. Those relationships are later used in the proposed design provisions (Chapter 4 and Appendices A and B), and proposed code design provisions and commentary (Appendix C). Sections 3.3.2, 3.4.2, 3.4.3 were developed jointly by Tanner and the author. The evaluation and synthesis of available data also include four additional sections developed by Tanner (Tanner, 2003), which are presented in Appendix D, Section D1.

### **3.2 COMPRESSIVE STRENGTH OF AAC**

#### **3.2.1 Available Information regarding Compressive Strength**

The following sources of information are available:

- a) Manufacturer-reported compressive strengths (102 mm cubes) and manufacturer-reported densities for Matrix Shipment 1; manufacturer-reported compressive strength for Ytong Shipment 2, assumed to be obtained according to ASTM C1386 (Tanner, 2003 and Varela, 2003).

- b) Results from UAB compressive strength tests on 4-in. (102 mm) cubes for three grades from three different manufacturers (Hebel, Ytong and Contec), conducted according to ASTM C1386 (Fouad et al., 2002). UAB reported the moisture content (MC) of the AAC when those strengths were evaluated, and the dry density of the AAC from which those strengths were obtained. Using that information, it was possible to calculate the “1386 density” of the AAC (what the density would have been at the UAB-reported moisture content, which always fell within the 5 - 15% range required by C1386). This information was found to be internally very consistent.
  
- c) Results from UT Austin compressive strength tests for 6 sets of cores from different manufacturer shipments (aspect ratio of 2:1) (Tanner, 2003 and Varela, 2003). The dry density of the cores is available and the density within 3 days of testing is available for 5 groups of specimens. Internal consistency for UT Austin data points corrected to a calculated MC of 10% is not very good, because the moisture content was not tightly controlled. The external consistency between combined data from UAB and UT Austin is good.

### **3.2.2 Discussion of Results for Compressive Strength of AAC**

Results for the compressive strength and density for UT Austin and UAB data are presented in Table 3.1. ASTM C1386 gives requirements for average and minimum compressive strengths for 4-in. (102 mm) cubes tested in the dry condition (Figure 3.1). A high percentage of the data points fall below the

average requirements, and a few tests fall below the minimum compressive strength requirements.

This issue must be addressed by the Autoclaved Aerated Concrete Products Association (AACPA). The relationship between compressive strength and density is very important for demonstrating the consistency and reliability of AAC. It is less important for actual design, which is usually not controlled by compressive strength.

For the case of UT Austin specimens, to compare with the tests performed at UAB (Figure 3.2), the dry density has been converted to a density corresponding to a 10% MC by multiplying it by 1.1. The value of 10% was selected because it is at the middle of the range of moisture contents permitted by ASTM C1386 (5% to 15%).

**Table 3.1 Summary of results for compressive strength and density from UAB and UT Austin**

Data Source	Manufacturer's Specifications Material	Materials' Density			Measured Compressive Strength $f_{AAC}$ (psi)
		Dry Density $\rho_{dry}$ (pcf)	Measured Density at test (pcf)	Calculated Density at MC=10% (pcf)	
UAB	Hebel-HG1	24	25.9	26.4	280
	Hebel-HG2	30	32.4	33.0	560
	Hebel-HG3	38	41.0	41.8	910
	Ytong-YG1	27	29.3	29.7	330
	Ytong-YG2	35	38.0	38.5	630
	Ytong-YG3	41	44.5	45.1	400
	Contec-CG1	29	31.9	31.9	320
	Contec-CG2	32	35.2	35.2	450
	Contec-CG3	36	39.6	39.6	690
UT	Contec-1	39.9	NA	NA	781
	Contec-2	35.9	37.6	39.5	1040
	Babb-1	40.2	44.1	44.2	1140
	Hebel-2	39.5	40.0	43.5	1330
	Ytong-2	34.3	39.1	37.7	650
	Babb-2	33.5	35.6	36.9	496



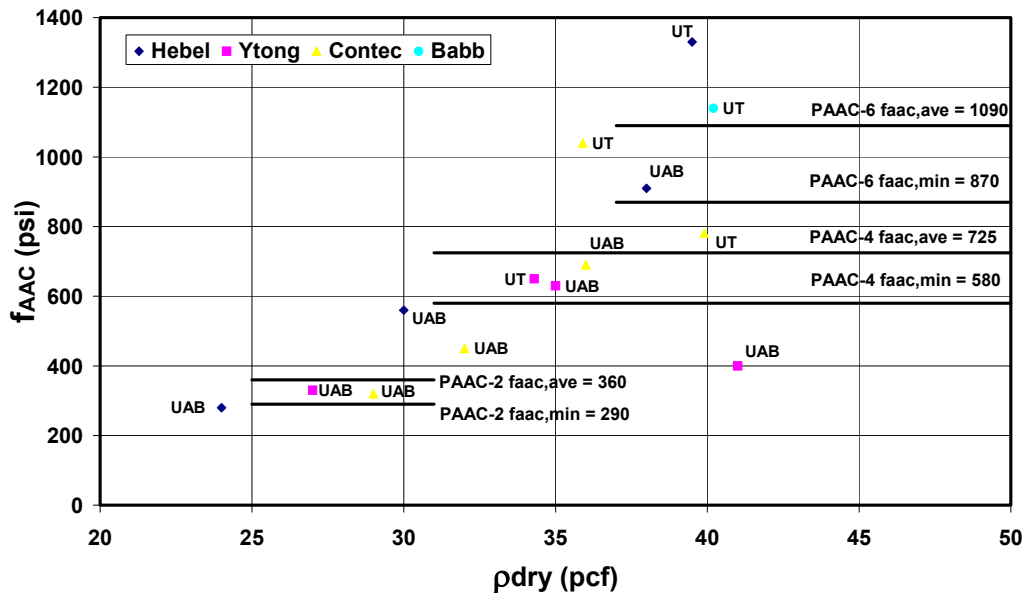


Figure 3.1 Compressive strength versus dry density with ASTM C1386 requirements

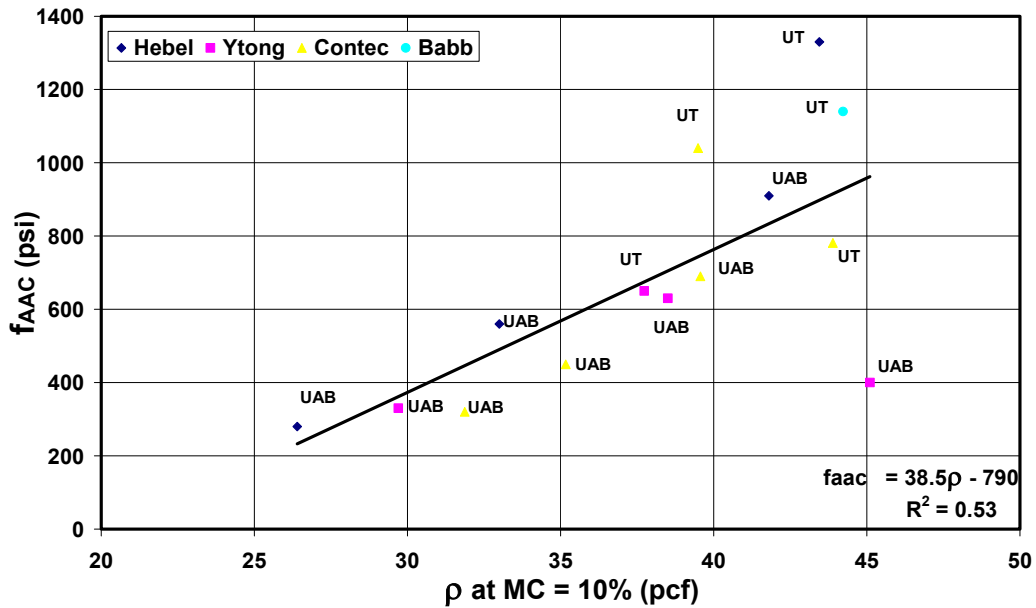


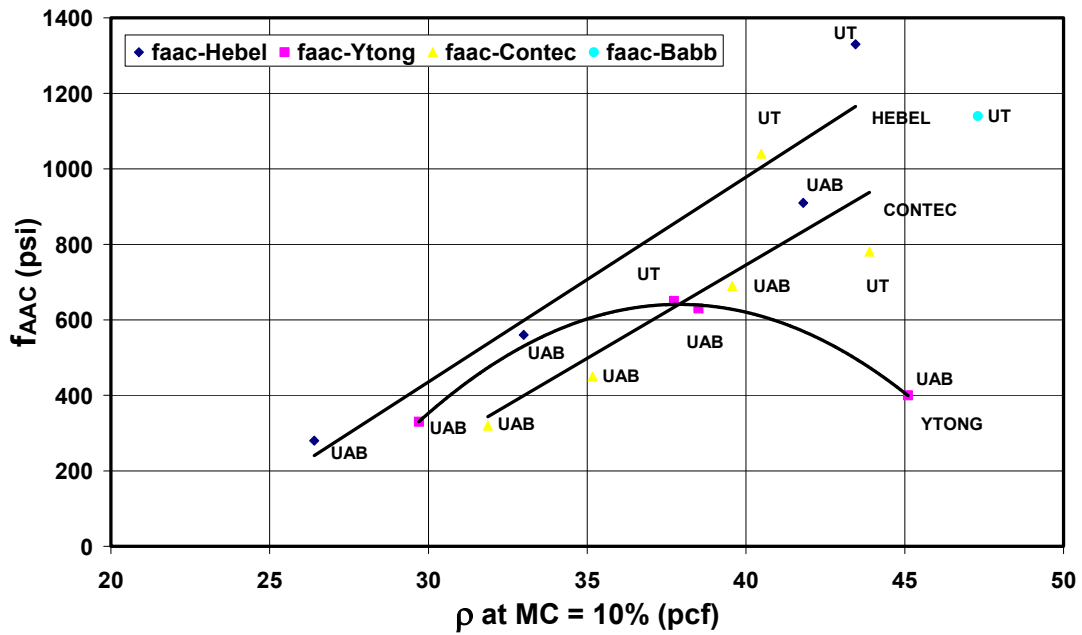
Figure 3.2 Compressive strength versus calculated density corresponding to a 10% moisture content for tests performed at UT Austin and UAB

Figure 3.2 indicates that the UT Austin data fall within or slightly above the trend of data obtained at UAB. The linear regression for this data corresponds to a R-squared value of 0.53. The correlation coefficient could be improved to 0.78 by eliminating data for tests on Ytong Grade 3 AAC. This may not be a good idea, however, because this class of material (high-density) is consistently low in compressive strength, modulus of rupture and shear strength (Figure 3.14 through Figure 3.16, Figure 3.21, and Figure 3.23). This suggests that for Ytong material, as density increases, these mechanical properties of AAC increase, reach a maximum, and then decrease. This nonlinear tendency cannot be verified for other manufacturers using UAB data, because there are no UAB data for high-strength material from other manufacturers. This nonlinear tendency cannot be verified using data from UT Austin, because UT Austin did not test the high-strength Ytong material.

In general the regressions of material strengths versus density for individual manufacturers have been linear or parabolic (Figure 3.3). If results for the Ytong Grade 3 material are considered anomalous, such results can be discarded. If the results are considered reliable, however, it is un-conservative to use a linear relationship with density. Since the compressive strength, tensile strength and shear strength vary in the same way, one independent variable could be selected, and the other two expressed in terms of that independent variable. The compressive strength is a logical choice for that independent variable, because it is calculated routinely. In addition, for traditional reinforced concrete design other material properties are presented in terms of compressive strength. The result of this choice is presented in Figure 3.17 through Figure 3.19. The change in correlation coefficient for these graphs is presented in Table 3.2.

Excluding Ytong G3 increases the correlation coefficient by 30% to 70% when the modulus of rupture is expressed in terms of density; excluding Ytong G3 has almost no effect on the correlation coefficient when the modulus of rupture is expressed as a function of the compressive strength. This is because the compressive and tensile strengths for Ytong G3 diverge similarly with respect to density, and thus the relationship between tensile strength and compressive strength is preserved. For Ytong G3, for design purposes it is more suitable to express the modulus of rupture in terms of compressive strength, rather than as a function of density. If the modulus of rupture were based on a linear relationship with density, the design could be unsafe.

An additional advantage of expressing other material properties in terms of the compressive strength is the elimination of the effect of moisture content as a variable in the relationships among properties, because all properties vary similarly with moisture content (Section 3.3.2).



**Figure 3.3** Variation of compressive strength versus calculated density at a moisture content of 10%

**Table 3.2** Change in correlation coefficients for compressive strength and modulus of rupture tests

Type of test / Direction of stresses relative to material rise	All Data versus Density $\rho$ at MC = 10%	Ytong G3 excluded versus Density $\rho$ at MC = 10%	All Data versus $f_{AAC}$	Ytong G3 excluded versus $f_{AAC}$
Compressive strength / parallel	0.53	0.78	NA	NA
Modulus of rupture Method 1 / parallel	0.19	0.34	0.35	0.31
Modulus of rupture Method 1 / perpendicular	0.45	0.77	0.75	0.74
Modulus of rupture Method 2 / parallel	0.65	0.85	0.89	0.89

### 3.3 STRESS-STRAIN BEHAVIOR AND MODULUS OF ELASTICITY OF AAC

#### 3.3.1 Information regarding Modulus of Elasticity

The following sources of information are available:

- a) In tests at UAB (Fouad et al., 2002), the stress-strain behavior of 4-in. by 4-in. by 12-in. prisms (102 mm by 102 mm by 305 mm) was measured, and was reported E for different grades. At UAB, low strength AAC from one manufacturer, and intermediate strength from two other manufacturers, was tested. No high-strength AAC was tested.
- b) At UT Austin (Tanner, 2003 and Varela, 2003), the stress-strain behavior was measured using of 2:1 cores for 6 shipments from 4 manufacturers. Data are very consistent and sometimes include descending-branch behavior, and thus can be used to support the use of an equivalent rectangular stress block.
- c) Tests performed at Construction Technology Laboratories for ACCOA<sup>5</sup>. Compression tests were performed on four 4-in. by 8-in. (102 mm by 203 mm) cores to determine the compressive strength and modulus of elasticity. Strains are reported up to a stress of  $0.4f_{AAC}$ . This group of tests represents a single material class.

---

<sup>5</sup> Internal Report by CTL to ACCOA: *Structural Tests on AAC Reinforced Panels Manufactured by Aerated Concrete Corporation of America (ACCOA)*, July 1999.

### 3.3.2 Discussion of Results for Modulus of Elasticity of AAC

At UAB, tests were performed on prisms with two orientations: load applied parallel to the direction of rise; and load applied perpendicular to the direction of rise (Figure 3.4). All specimens were conditioned to moisture contents between 8 to 15%.

At UT Austin, tests were performed on 4-in. x 8-in. (102 x 203 mm) cores with the load applied perpendicular to the direction of rise (Figure 3.4). The relationship between modulus and compressive strength obtained from UT-Austin data is consistent. The UT Austin specimens were cured in a laboratory environment and weighed within 3 days of testing. The moisture content varied from 1.3 % to 14.1 %. This variability could have resulted from coring the specimens at different times.

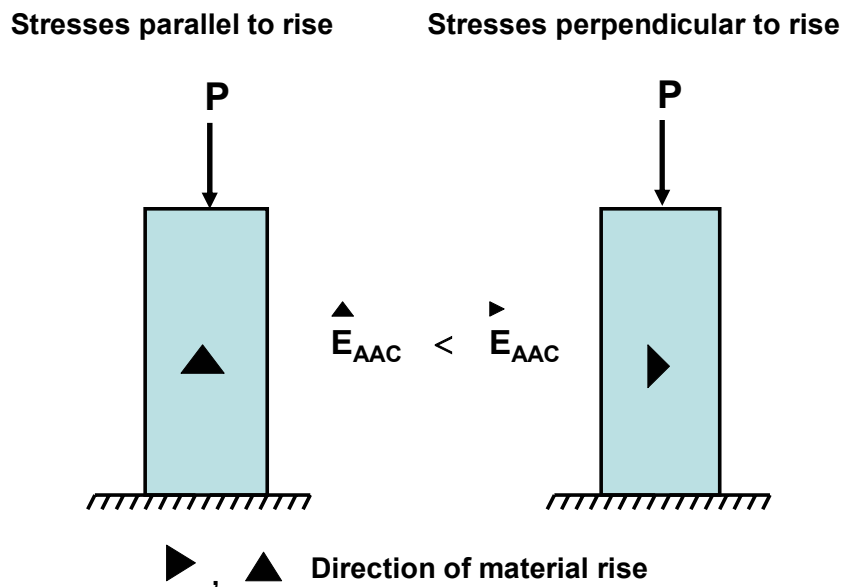


**Figure 3.4** *Direction-of-rise convention for specimens tested by UT Austin and UAB for Modulus of Elasticity*

The relationship between modulus and density obtained from UT Austin data (Figure 3.5) is not consistent, because moisture content was obtained from compressive strength specimens and not from the specimens used to obtain the modulus of elasticity.

Contec Shipment 1 specimens were not weighed, so a calculated density corresponding to a 10% moisture content is used. The results of modulus of elasticity tests for load perpendicular to the direction of rise for tests at UAB, CTL and UT Austin are presented in Table 3.3. The results for UAB tests for load parallel to the direction of rise are presented in Table 3.4.

**Table 3.3** *Modulus of elasticity for load perpendicular to the direction of rise for tests at UAB and UT Austin*

Data Source	Manufacturer	Dry Density (pcf)	MC (%)	Measured Density (pcf)	Measured E, ksi	COV (%) for E	Measured $f_{AAC}$ , psi	COV (%) for $f_{AAC}$
UAB	Hebel	24	8.2	26.0	186	39.5	290	15
	Ytong	35	12	39.2	310	4.9	600	5.3
	Contec	32	13.6	36.4	294	4.9	570	11.5
UT Austin	Contec 1	42.3	5	46.5	323	7.9	781	5.6
	Contec 2	35.9	4.7	37.6	424	2.7	1040	4.7
	Babb 1	39.9	10.4	44.1	462	7.1	1140	3.8
	Hebel 2	39.5	1.3	40.0	511	9.3	1330	6.6
	Ytong 2	34.3	14.1	39.1	269	3.4	650	6.8
	Babb 2	35	16.6	40.8	271	11.7	496	6
CTL	ACCOA	NA	NA	NA	460	13.6	913	5.6

**Table 3.4 Modulus of elasticity for load parallel to the direction of rise for UAB**

<b>Manufacturer</b>	<b>Dry Density (pcf)</b>	<b>MC (%)</b>	<b>Measured Density at Test (pcf)</b>	<b>E (ksi)</b>	<b>COV (%)</b>	<b>f<sub>AAC</sub></b>	<b>COV (%)</b>
Hebel	24	8.2	26.0	139	18	177	17.3
Ytong	35	12	39.2	278	29	467	13
Contec	32	13.6	36.4	271	9	450	12

Modulus of elasticity shows poor correlation with ASTM C 1386 density (Figure 3.5). Modulus data from UAB for load applied parallel and perpendicular to the direction of rise (Figure 3.6) indicate good internal correlation due to tightly controlled moisture contents. The modulus of elasticity is 25 to 50 ksi higher for loading perpendicular to the direction of rise. Figure 3.7 shows the modulus of elasticity versus compressive strength.

A linear regression gives Equation (3.1), with a correlation coefficient ( $R^2$ ) of 0.97. It is proposed to determine modulus of elasticity as a nonlinear function of the compressive strength, as shown in Equation (3.2). Tests performed at CTL for ACCOA give results similar to data from UAB and UT Austin (Figure 3.7), further supporting the proposed Equation (3.2).

It is believed that the variable moisture contents of the UT Austin tests caused similar divergence of the modulus of elasticity and compressive strength. Since the results were obtained in the same test, no difference in moisture content exists for both values.



$$E = 0.3f_{AAC} + 105 \quad \text{Equation (3.1)}$$

$$E = 6500 f_{AAC}^{0.6} \quad \text{Equation (3.2)}$$

$f_{AAC}$  and E in psi

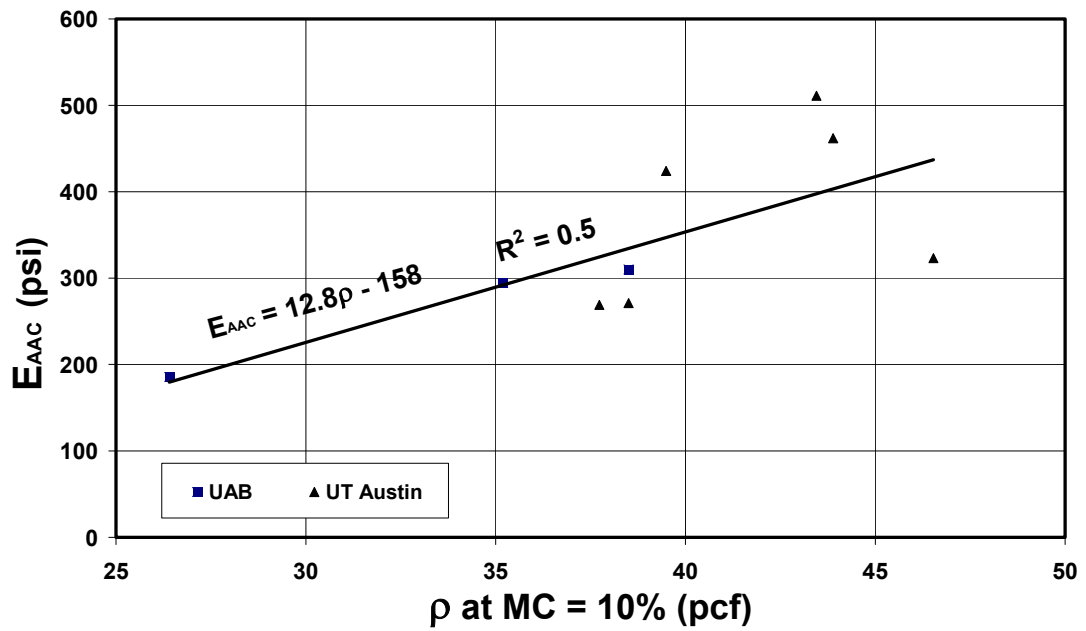


*Figure 3.5 Modulus of elasticity versus calculated density at 10% moisture content for load perpendicular to the direction of rise in UAB and UT Austin*

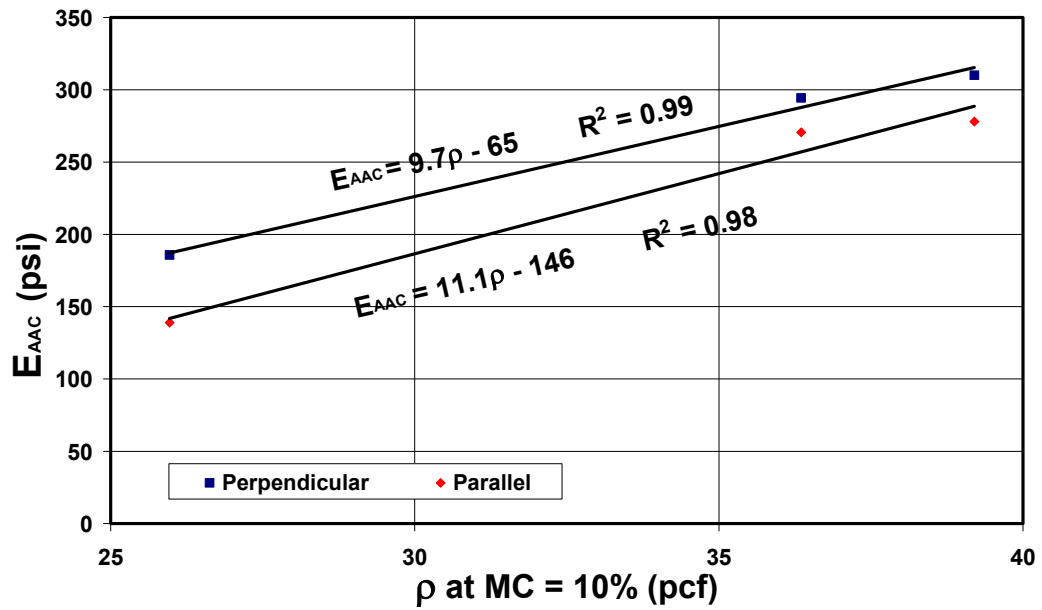


Figure 3.6 Modulus of elasticity versus calculated density at 10% moisture content for all tests performed at UAB

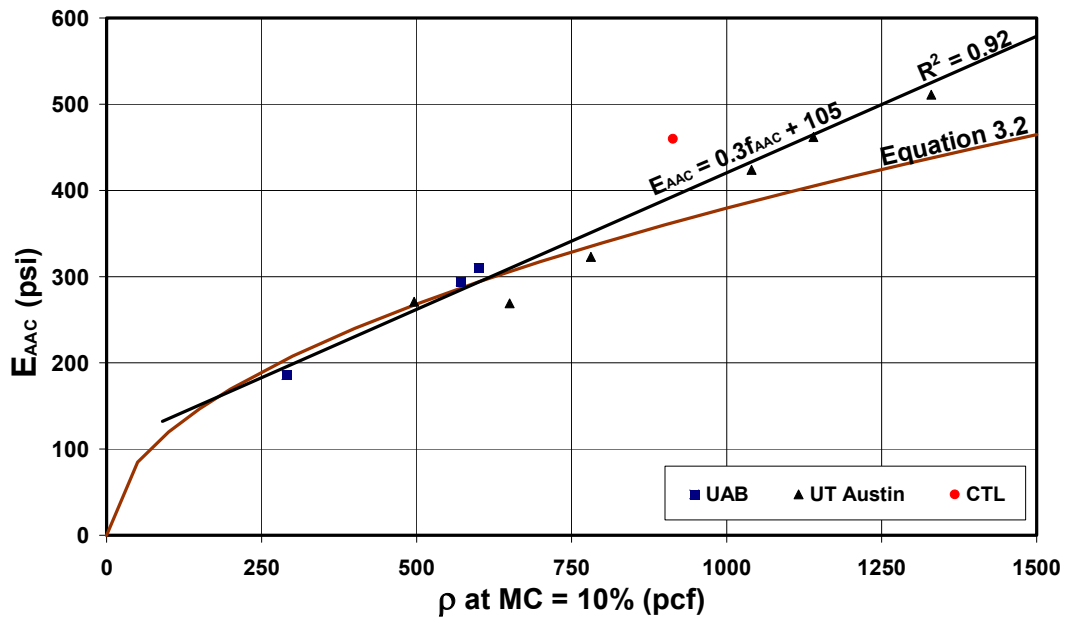


Figure 3.7 Modulus of elasticity versus compressive strength for loading parallel to the direction of rise at UAB and UT Austin

### **3.4 TENSILE STRENGTH OF AAC**

#### **3.4.1 Information regarding Tensile Strength of AAC**

The following sources of information are available:

- a) At UT Austin (Tanner, 2003 and Varela, 2003), information on splitting tensile strength of AAC was determined using ASTM C1006, versus measured density at the time of test. In most but not all cases, the moisture contents at which those densities were measured were within the range of 5% to 15% as permitted by ASTM C1386. More important, the moisture contents corresponded to those in the UT Austin's AAC shear walls at time of test. There are 8 data points, and internal correlation is good for a wide range of densities.
  
- b) UAB (Fouad et al., 2002) reported modulus of rupture versus dry density from two methods. They also report moisture content, making it possible to calculate the density of the material at time of test. Their "Method 1" is a RILEM method involving mid-point loading with an a/d ratio of 1.25 (Figure 3.8). Some "Method 1" tests were performed with specimens oriented so that flexural tensile stresses acted parallel to the direction of rise; others, so that stresses acted perpendicular to the direction of rise (Figure 3.10). "Method 2" is a modified ASTM C78 method with two third-point loads and an a/d ratio of 1.75 (Figure 3.9). "Method 2" tests were performed with specimens oriented so that flexural tensile stresses acted parallel to the direction of rise. Modulus of rupture data were reported by UAB in their report to the AACPA; some of those data (all

corresponding to “Method 2”) had been previously reported in an internal document<sup>6</sup>.

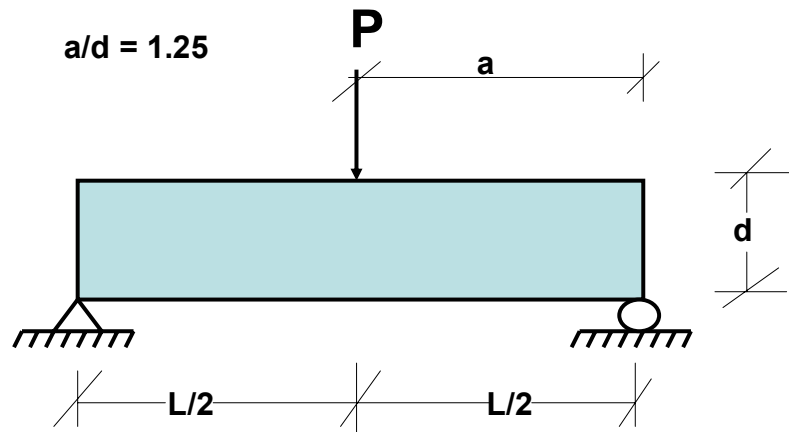


**Figure 3.8** UAB test set up for Modulus of Rupture, “Method 1”

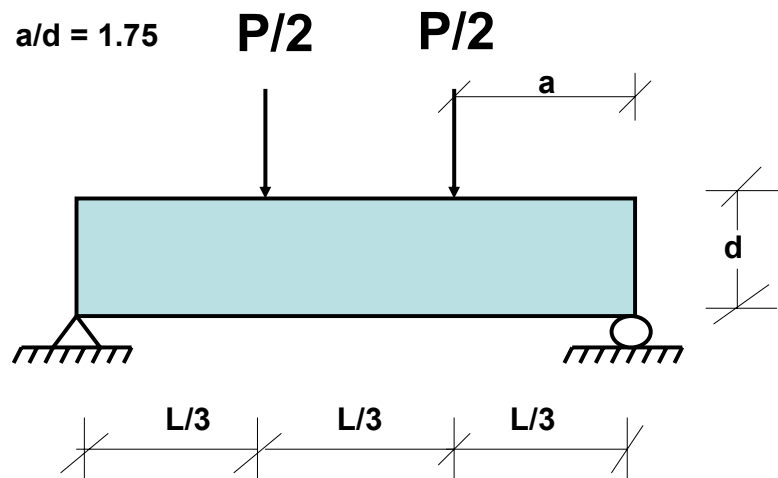


**Figure 3.9** UAB test set up for Modulus of Rupture, “Method 2”

---

<sup>6</sup> Internal report by Fouad H. Fouad, Physical and Mechanical properties of AAC produced in the United States, August 10, 2000.

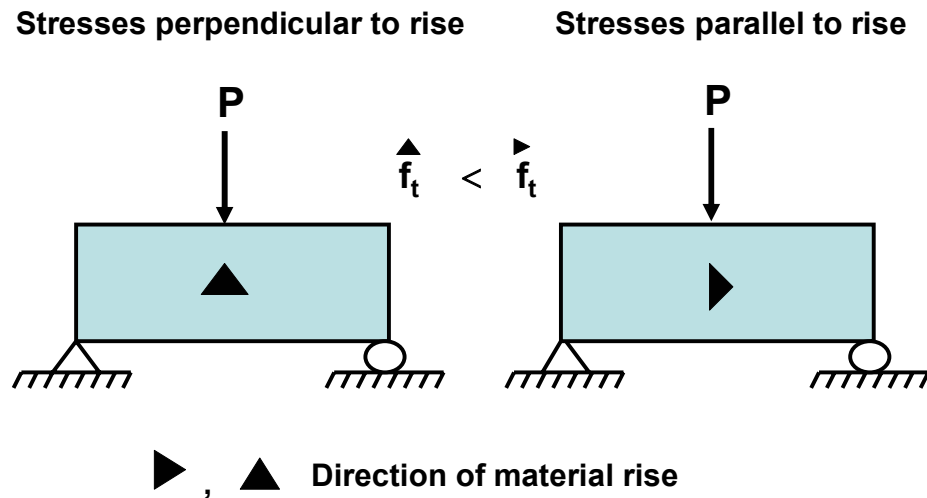


*Figure 3.10 Direction-of-rise convention for specimens tested by UAB for Modulus of Rupture (Method 1)*

### 3.4.2 Discussion regarding Splitting Tensile Strength of AAC

Data for splitting tensile strength of material were obtained at UT Austin from each AAC shipment, using specimens oriented so that splitting tensile stresses acted parallel to the direction of rise. Data on field density of each shipment were also obtained. In most cases, densities were determined within one day of when splitting tensile strengths were determined. In a few cases, the difference in time was as great as 4 months. This is not believed to be significant, however, because those times were more than a year after the production date of the material. Eight data points are available, each representing a series of 4 to 8 specimens tested according to ASTM C1006. The collected data are presented in Table 3.5, and a graph of the relationship between tensile strength and field density (Figure 3.11), shows a linear relationship, with a good R-squared value of 0.84. Equation (3.3) was originally proposed for determining the splitting tensile

strength as a function of the densities measured under field conditions at UT Austin. With the exception of Hebel Shipment 2 and Contec Shipment 2 Test a, the moisture contents in Table 3.5 fall within 4.1 and 16.6. Because those moisture contents generally fall in the 5% to 15% range permitted by ASTM C1386, the corresponding densities are referred to here as “1386 densities.” For design of reinforced AAC panels and also for design of AAC masonry, density-dependent material characteristics are sometimes described in terms of that “1386 density” as well.

$$f_t = 2\rho_{1386} - 10.3$$

Equation (3.3)

$\rho_{1386}$  in pcf,  $f_t$  in psi

There are two data points for Contec Shipment 2. The splitting tensile strength, field density and dry density for the first data point (Contec 2a) were used in preparing the technical submittal to the MSJC in late 2001. After those data were submitted, it was found that the field and dry densities corresponded to a calculated moisture content less than zero. This value is physically impossible, so the tests were repeated (Contec 2b). Later, a calculation error was found in the field density originally reported for Contec 2a. That value is still regarded as suspicious, however, because the corresponding moisture content is 45%. For this reason, values for Contec 2b only (and not Contec 2a) are shown in Figure 3.11.

Finally, Babb Shipment 2 is not included in the linear regression of Figure 3.11 because the splitting tensile strength appeared to be anomalous. Further investigation revealed a low compressive strength for that material. This is potentially a material similar to Ytong G3. The relationship between splitting

tensile strength and compressive strength is presented in Figure 3.12. The linear regression of Equation (3.4) has a correlation coefficient ( $R^2$ ) value of 0.93.

Equation (3.5) relates the splitting tensile strength and the square root of the compressive strength; such exponential correlation is as good as the linear regression presented in Equation (3.4). Equation (3.5) is also consistent with the ACI 318-02 expression for tensile strength.

**Table 3.5**      *Results of C1006 splitting tensile strength tests performed at UT Austin*

Shipment	Average $f_t$ psi (MPa)	COV (%)	Measured Density pcf (kg/cm <sup>3</sup> )	Dry Density pcf (kg/cm <sup>3</sup> )	Moisture Content (%)	Average $f_{AAC}$ psi (MPa)
Contec 1	71.2 (0.49)	10.5	42.3 (2.62)	39.9 (2.47)	6.0	781 (5.4)
Ytong 1	55.3 (0.38)	14.2	32.8 (2.03)	31.5 (1.95)	4.1	517 (3.6)
Ytong 2	62.7 (0.43)	4	38.7 (2.40)	34.0 (2.11)	13.8	650 (4.5)
Hebel 2	88.4 (0.61)	5.2	48.9 (3.03)	39.5 (2.45)	23.8	1330 (9.2)
Contec 2b	74.6 (0.51)	1.8	37.9 (2.35)	35.9 (2.23)	5.6	1040 (7.2)
Babb 1	84.7 (0.58)	10.1	45.2 (2.80)	39.9 (2.47)	13.3	1140 (7.9)
Babb 2a	52.5 (0.36)	12.7	42.6 (2.64)	34.5 (2.14)	23.5	495 (3.4)
Babb 2b	45.0 (0.31)	14.9	40.8 (2.53)	35.0 (2.17)	16.6	495 (3.4)
Contec 2a	54.0 (0.37)	6.8	52.2 (3.24)	35.9 (2.23)	45.4	1040 (7.2)

$$f_t = 0.05f_{AAC} + 30 \quad \text{Equation (3.4)}$$

$f_t$  and  $f_{AAC}$  in psi

$$f_t = 2.4\sqrt{f_{AAC}} \quad \text{Equation (3.5)}$$

$f_t$  and  $f_{AAC}$  in psi

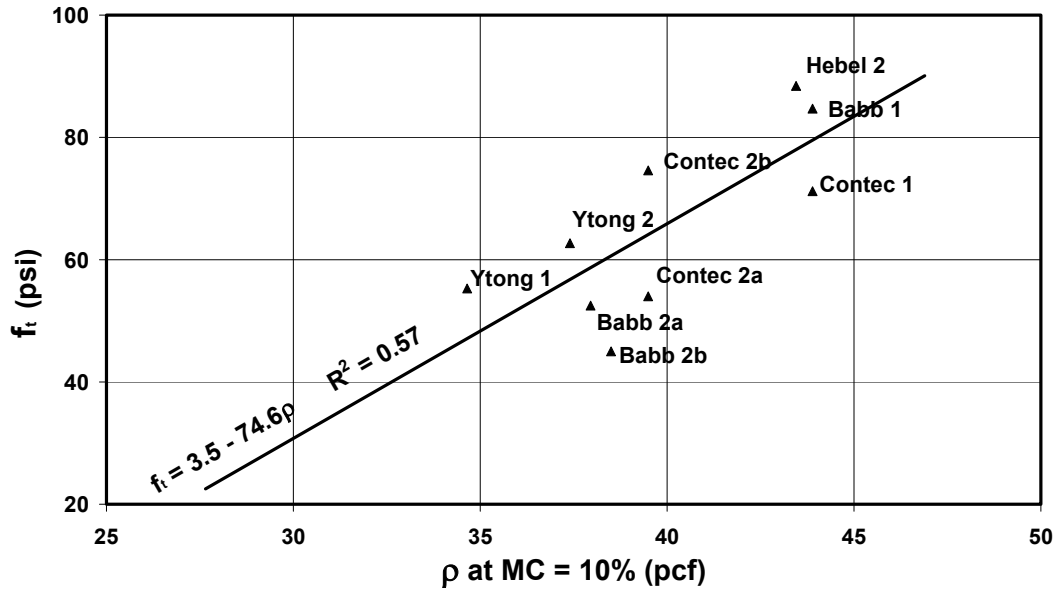


Figure 3.11 Splitting tensile strength versus density

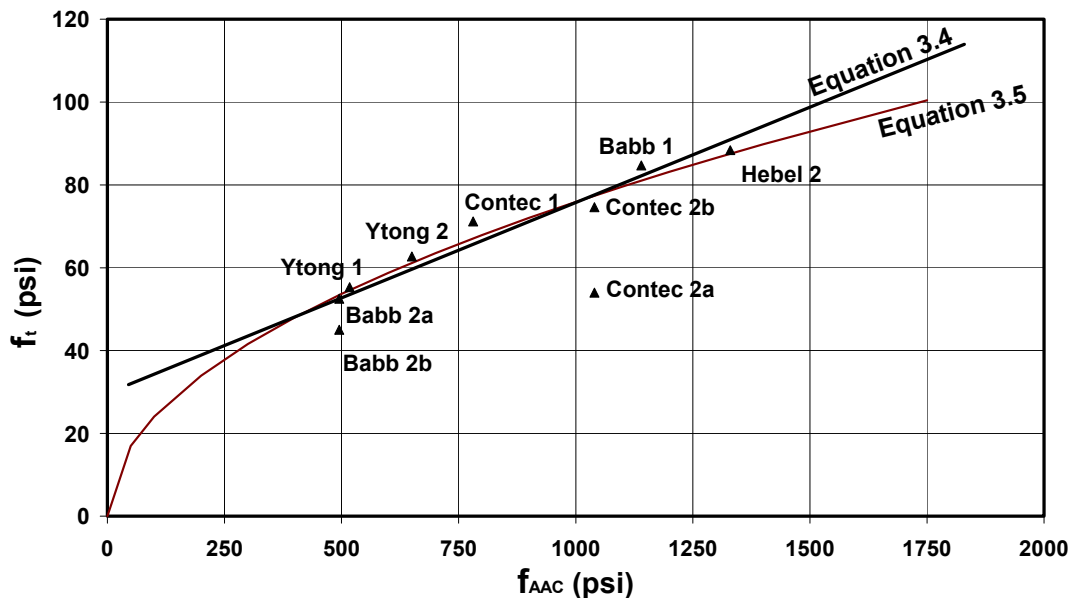


Figure 3.12 Splitting tensile strength versus compressive strength



The Dutch standard NEN 3838<sup>7</sup> provides a linear relationship to calculate the design tensile strength  $f_t'$  as a function of the specified compressive strength ( $f_{AAC}'$ ), which is given by Equation (3.6).

$$f_t' = 0.08125 f_{AAC}' \quad \text{Equation (3.6)}$$

To compare the result of Equation (3.6) with UT Austin relationship between  $f_t$  and  $f_{AAC}$  (Equation (3.5)), measured values for  $f_t$  are multiplied by the capacity reduction factor of ACI 318-99 for shear ( $\phi = 0.85$ ), and the specified compressive strength ( $f_{AAC}'$ ) is taken equal to  $f_{AAC}$ .

Equation (3.5) reduced by  $\phi = 0.85$ , and Equation (3.6) are plotted in Figure 3.13 together with UT Austin data. While both equations provides good estimates for  $f_t'$ , the Dutch equation is un-conservative for high-strength AAC. Therefore, Equation (3.5) is the most suitable relationship between  $f_t$  and  $f_{AAC}$ .

---

<sup>7</sup> NEN 3838 Gas concrete products and constructions, 1987. NNI (Nederlands Normalisatie-Instituut), Delft.

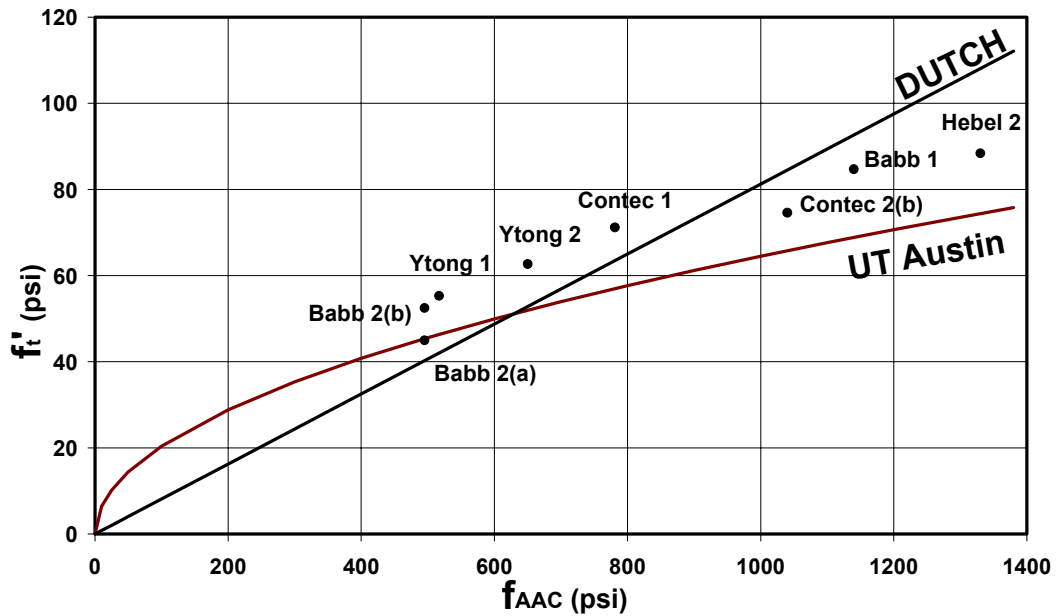


*Figure 3.13 Comparison between Dutch Standards and UT Austin relationships for specified design tensile strength ( $f_t'$ ) versus compressive strength ( $f_{AAC}$ )*

### 3.4.3 Discussion of Relationship between Modulus of Rupture and Splitting Tensile Strength

At UT Austin, a relationship between splitting tensile strength and modulus of rupture was determined, using splitting tensile data from UT Austin tests (Tanner, 2003 and Varela, 2003) and modulus of rupture data from UAB tests (Fouad et al., 2002). In so doing, it was necessary to consider the effects of moisture content on tensile strength. In their final report to the AACPA, UAB did report moisture contents for their modulus of rupture tests, and also dry densities; those dry densities were converted by UT Austin to the corresponding densities at

a moisture content of 10%, a convenient single value that quite well represented the range of moisture contents (8% to 12%) reported by UAB.

Although moisture contents were not recorded at UT Austin, for their splitting tensile tests, those moisture contents were subsequently estimated based on specimens stored under similar environmental conditions in the laboratory. Those specimens had moisture contents averaging about 10%.

Table 3.6 shows values of modulus of rupture reported by UAB for different classes and corresponding oven-dry densities of AAC. Using a moisture content of 10% as explained above, the corresponding density for those specimens is calculated. Using Equation (3.3), the splitting tensile strength of those specimens at that same density is also calculated. The average ratio between the reported modulus of rupture and the calculated splitting tensile strength is 2.26, with a COV of 19.1%. For design purposes, a ratio of 2.0 is proposed (Equation (3.7)).

$$f_r = 2 \cdot f_t \quad \text{Equation (3.7)}$$

$$f_r = 2.26 \cdot f_t \quad \text{Equation (3.8)}$$

**Table 3.6 Ratios between measured modulus of rupture at C1386 density and splitting tensile strength estimated using oven-dry density for different classes of AAC**

Oven-dry density pcf (kg/m <sup>3</sup> )	Calculated density at 10% MC pcf (kg/m <sup>3</sup> )	Calculated $f_t$ at 10% MC psi (MPa)	Measured $f_r$ at ~10% MC psi (MPa)	$f_r / f_t$
32.0 (2.0)	35.2 (2.2)	60.2 (0.41)	123.0 (0.85)	2.04
38.0 (2.4)	41.8 (2.6)	73.4 (0.51)	202.0 (1.39)	2.75
42.0 (2.6)	46.2 (2.9)	82.2 (0.57)	162.0 (1.12)	1.97

#### **3.4.4 Discussion regarding Modulus of Rupture of AAC using Combined UAB and UT Austin Data**

In this section, results from modulus of rupture tests performed at UAB are compared to results from splitting tensile tests performed at UT Austin. For purposes of this comparison, the latter are multiplied by the average value of 2.26, developed as explained above and used in Equation (3.8).

Modulus of rupture results from UAB are presented separately for “Method 1” and “Method 2” (Table 3.7 and Table 3.8) and compared in Figure 3.14 through Figure 3.19 to the corresponding calculated modulus of rupture results (factor of 2.26), from splitting tensile tests at UT Austin. The test setups for “Method 1” and “Method 2,” and the essential differences between those methods, are explained in Section 3.4.1. The best single linear regression occurs with results from “Method 2.” This is reasonable. First, the relationship of Equation (3.8) was derived based on “Method 2” tests; second, the flexural tensile stresses act parallel to the direction of rise in both the C1006 tests and the “Method 2” tests.

**Table 3.7 Modulus of Rupture – UAB Method 1**

Manufacturer's Specifications		Tensile stresses parallel to the direction of rise			Tensile stresses perpendicular to the direction of rise			Measured Compressive Strength $f_{AAC}$ (psi)
Material	$\rho$ (pcf)	Measured Density (pcf)	Calculated Density at MC=10% (pcf)	Modulus of Rupture, $f_r$ (psi)	Measured Density (pcf)	Calculated Density at MC=10% (pcf)	Modulus of Rupture, $f_r$ (psi)	
Hebel-HG1	25	26.02	26.4	115	26.4	26.4	96	280
Hebel-HG2	32	33.00	33.0	208	32.5	33.0	167	560
Hebel-HG3	38	42.10	41.8	331	42.6	41.8	211	910
Ytong-YG1	25	29.48	29.7	113	29.8	29.7	87	330
Ytong-YG2	31	39.06	38.5	217	39.0	38.5	177	630
Ytong-YG3	40	45.39	45.1	115	44.7	45.1	106	400
Contec-CG1	25	31.96	31.9	135	31.7	31.9	131	320
Contec-CG2	32	34.56	35.2	174	35.4	35.2	159	450
Contec-CG3	38	39.46	39.6	225	36.3	39.6	157	690

**Table 3.8 Modulus of Rupture – UAB Method 2**

Manufacturer's Specifications		Tensile stresses parallel to the direction of rise			Measured Compressive Strength $f_{AAC}$ (psi)
Material	$\rho$ (pcf)	Measured Density (pcf)	Calculated Density at MC=10% (pcf)	Modulus of Rupture, $f_r$ (psi)	
Hebel-HG1	25	26.02	26.4	115	280
Hebel-HG2	32	33.00	33.0	208	560
Hebel-HG3	38	42.10	41.8	331	910
Ytong-YG1	25	29.48	29.7	113	330
Ytong-YG2	31	39.06	38.5	217	630
Ytong-YG3	40	45.39	45.1	115	400
Contec-CG1	25	31.96	31.9	135	320
Contec-CG2	32	34.56	35.2	174	450
Contec-CG3	38	39.46	39.6	225	690

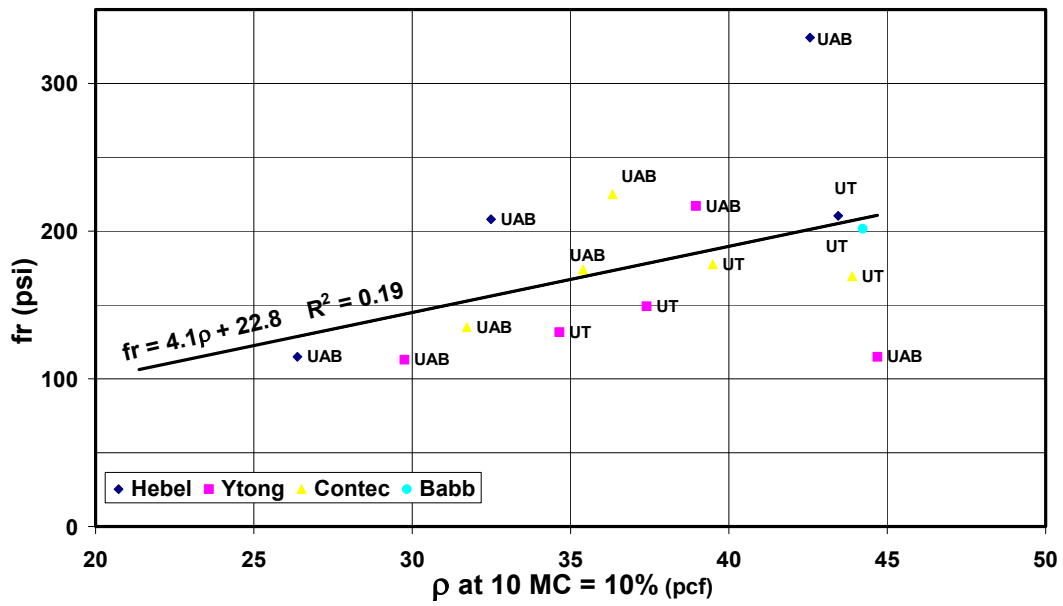


Figure 3.14 Modulus of rupture versus density for Method 1  
(stresses parallel to the direction of rise)

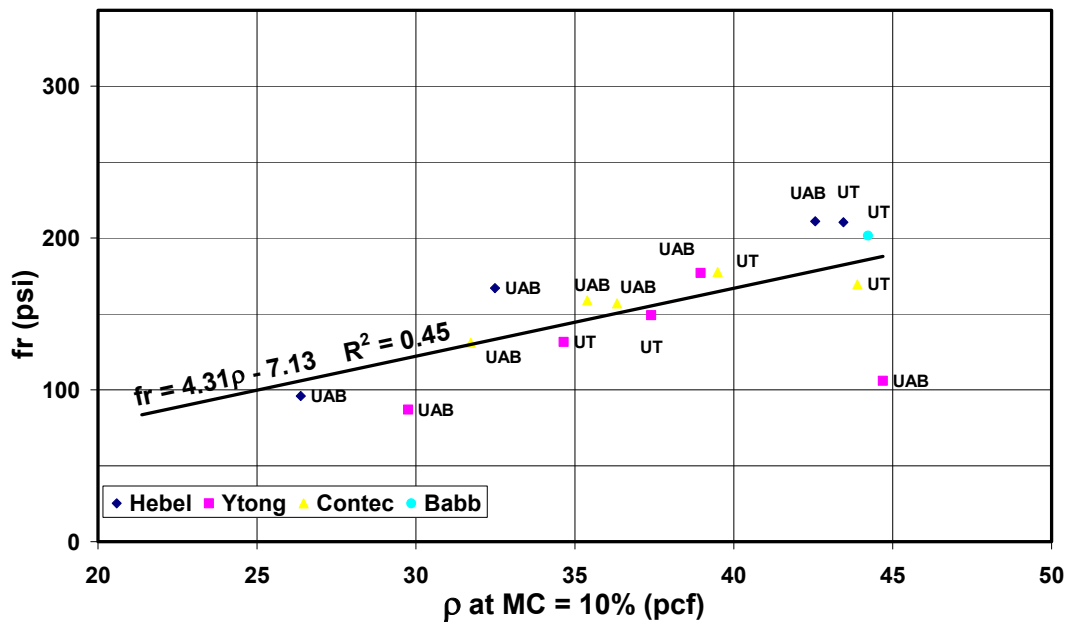
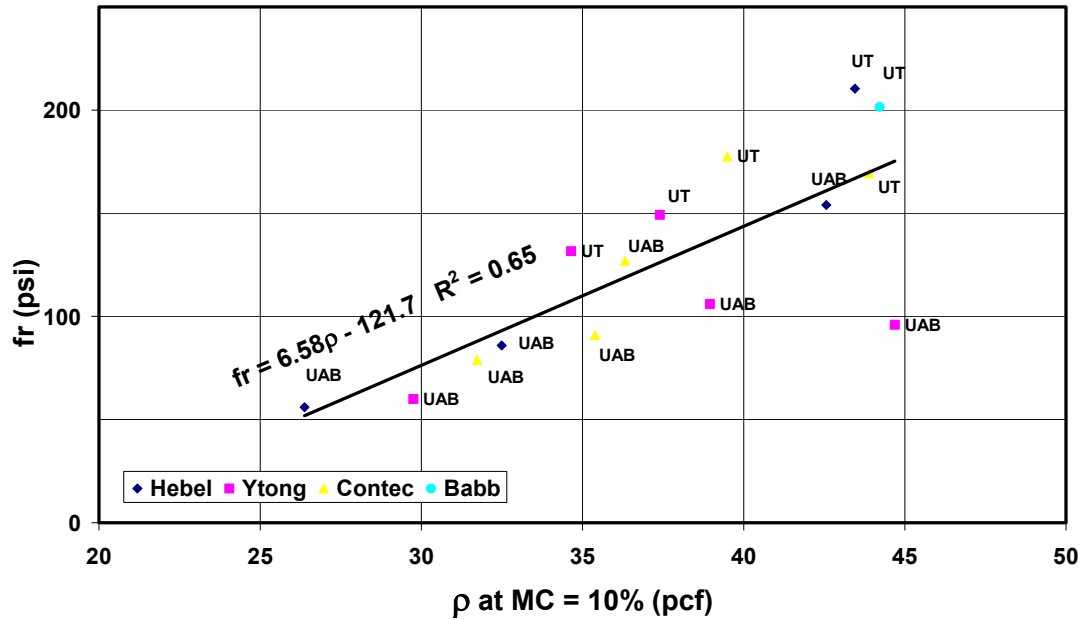


Figure 3.15 Modulus of rupture versus density for Method 1  
(stresses perpendicular to the direction of rise)



**Figure 3.16** Modulus of rupture versus density for Method 2 (stresses parallel to the direction of rise)

Regression lines are calculated and presented in Figure 3.14 through Figure 3.19 for all data available from UT and UAB. Figure 3.17 through Figure 3.19 also contain the RILEM relationship between modulus of rupture and compressive strength expressed in Equation (3.9).

$$f_r = 0.27 + 0.21 \cdot f_{AAC}$$

Equation (3.9)

$f_{AAC}, f_r$  in  $\text{N/mm}^2$

For data from UT and UAB, the RILEM equation approximates the observed relationship for “Method 1,” with stresses parallel to the direction of rise; it is un-conservative for “Method 1” with stresses perpendicular to the direction of rise, and also for “Method 2.”

Modulus of rupture data from UAB tests using “Method 1” with flexural tensile stresses oriented parallel to the direction of rise are approximately 1.25 times the corresponding results for modulus of rupture tests with flexural tensile stresses oriented perpendicular to the direction of rise. It can be concluded that AAC is stronger in flexural tension when tested so that the flexural stresses are oriented parallel to the direction of rise.

Modulus of rupture data from UAB tests according to “Method 1” are almost twice as high as those obtained using “Method 2” when tensile stresses act parallel to the direction of rise. This is due to the  $a/d$  relationship used in those tests. Specimens tested under Method 1 failed predominantly in flexure, while those tested under Method 2 failed in a combination of flexure and shear.



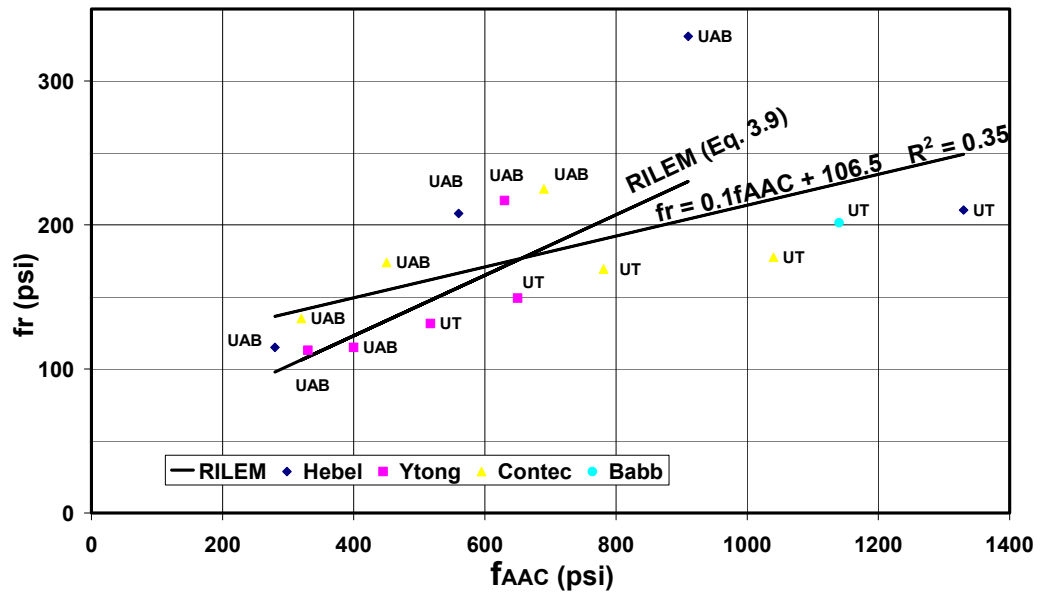


Figure 3.17 Modulus of rupture versus compressive strength for Method 1 (stresses parallel to direction of rise)

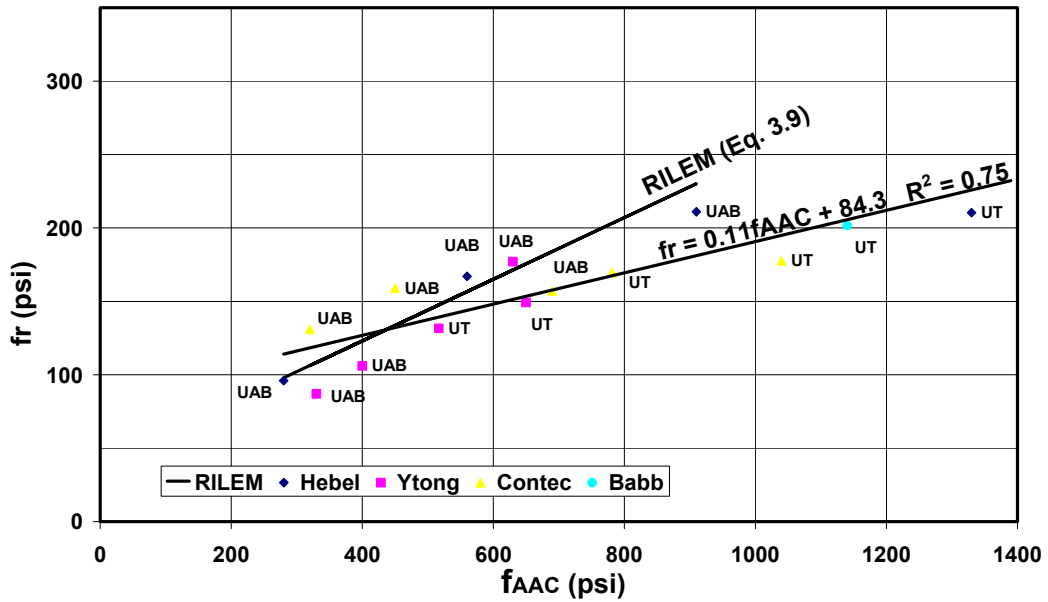
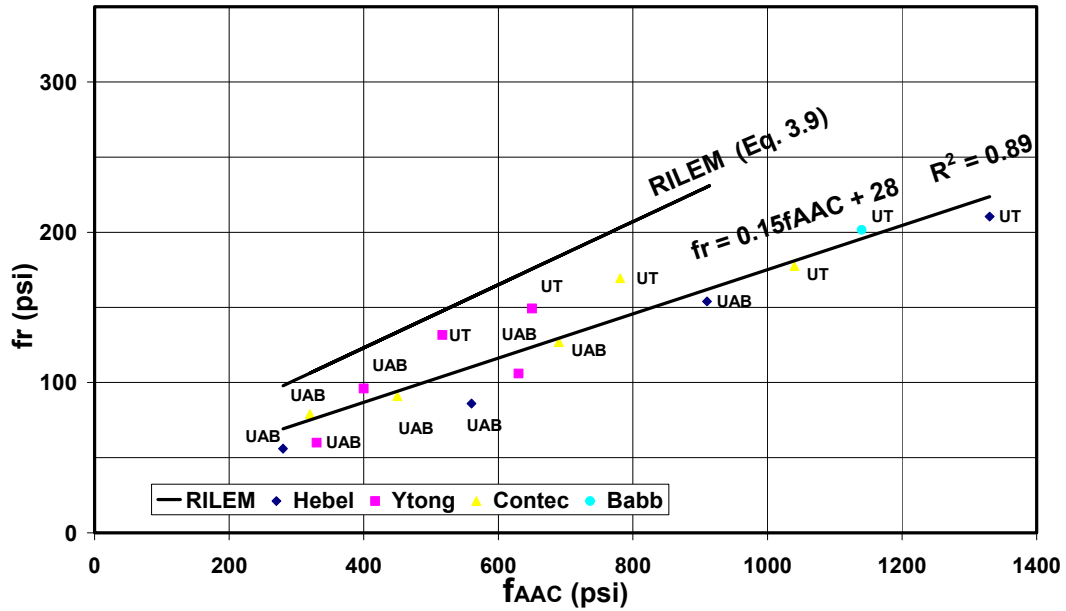


Figure 3.18 Modulus of rupture versus compressive strength for Method 1 (stresses perpendicular to direction of rise)



**Figure 3.19** Modulus of rupture versus compressive strength for Method 2 (stresses parallel to the direction of rise)

### 3.4.5 Relationship between Modulus of Rupture ( $f_r$ ) and Compressive Strength ( $f_{AAC}$ )

As proposed in Equation (3.7), the modulus of rupture ( $f_r$ ) can be expressed as twice the splitting tensile strength ( $f_t$ ). Substituting Equation (3.7) into Equation (3.5), Equation (3.10) is obtained giving the modulus of rupture as a function of the compressive strength.

$$f_r = 4.8\sqrt{f_{AAC}}$$

$f_{AAC}, f_r$  in psi

Equation (3.10)

As discussed in Section 3.4.4, the best correlation between ( $f_r$ ) and ( $f_{AAC}$ ) for combined data from UAB and UT Austin occurs for Method 2. Figure 3.20 shows UAB and UT Austin data for Method 2, along with RILEM relationship (Equation (3.9)), UT-Austin Equation (3.10), and the relationship proposed by Dutch Standard NEN 3838 (Equation (3.11)).

$$f_r' = 0.15 f_{AAC}'$$

Equation (3.11)

$f_{AAC}', f_r'$  in psi

While RILEM relationship overestimates  $f_r$ , the Dutch relationship underestimates it for the whole range of values of  $f_{AAC}$ . Equation (3.10), proposed by UT Austin provides the best estimates for low- and medium-strength materials, and becomes conservative for high-strength materials.

It should be noted that the Dutch Equation (3.11) is a design equation that has a security factor built in, while the RILEM Equation (3.9) and UT Austin Equation (3.10) do not. The Dutch Equation seems to be a good lower bound for the whole set of data presented in Figure 3.20.

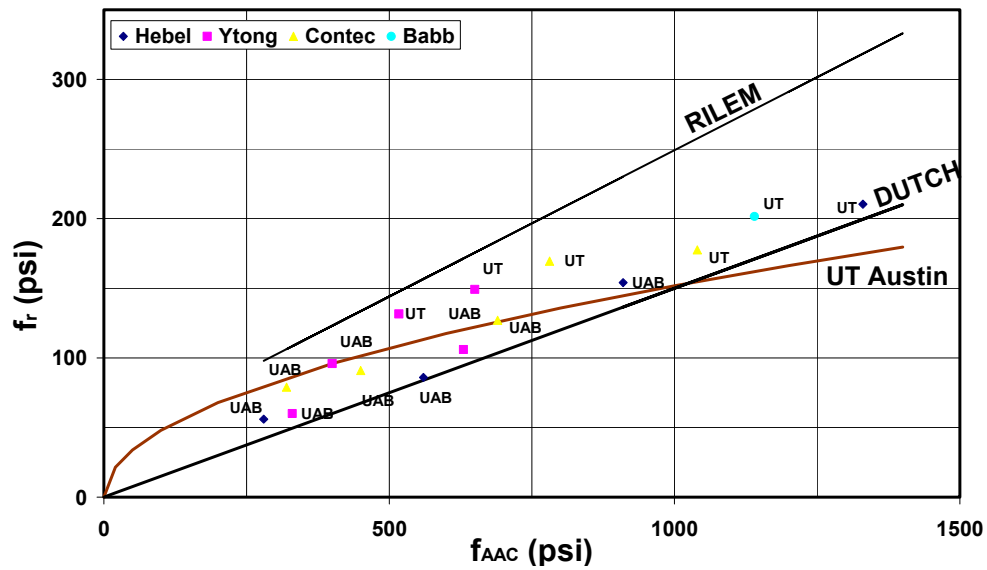


Figure 3.20 Relationship between  $f_r$  and  $f_{AAC}$  based on UAB and UT Austin data (Method 2)

### 3.5 TENSILE BOND BETWEEN AAC AND BEDDING MORTAR

#### 3.5.1 Information regarding Tensile Bond between AAC and Bedding Mortar

- a) Flexural cracking was observed in 11 shear-wall specimens tested at UT Austin (Tanner, 2003 and Varela, 2003). In all cases, these flexural cracks formed between the AAC and the masonry leveling bed (Type S), indicating tensile bond failure between the two materials. The tensile bond strength was back-calculated based on these results.
- b) Modulus of rupture tests were performed at UAB (Fouad et al., 2002) on specimens with masonry mortar (ASTM C270, Type M and S). The tests

also include results from adding thin-bed mortar to the Type M and S mortars (ASTM C270) to increase the bond strength.

### **3.5.2 Discussion regarding Tensile Bond Strength for Masonry Mortar using Combined UAB and UT Austin Data**

This section presents a combined summary of data from UAB and UT Austin. UAB reported tensile bond strengths of 13 and 15 psi for mortar meeting ASTM C270 Type M and S, respectively. The bond strengths were improved to 43 and 47 psi by adding thin-bed mortar to the C270 mortar in a 1:1 proportion. Those strengths are lower than the average reported at UT Austin (73.3 psi). In the shear-wall specimens at UT Austin, each panel was cleaned and pre-wetted prior to placing the panel on the leveling mortar. No preparatory measures are reported by UAB. The difference in bond strength implies that construction practices are important. If a higher value of bond strength is to be used, the construction practices must be carefully defined.

## **3.6 TENSILE BOND BETWEEN AAC AND THIN-BED MORTAR**

### **3.6.1 Information regarding Tensile Bond between AAC and Thin-bed Mortar**

The following sources of information are available:

- a) Modulus of rupture tests were performed on specimens with thin mortar joints at UAB (Fouad et al., 2002).

- b) Flexure-dominated shear-wall specimens tested at UT Austin exhibited flexural cracking at the joints before cracking in the AAC material (Tanner, 2003 and Varela, 2003).

### 3.6.2 Discussion of Results regarding Tensile Bond between AAC and Thin-bed Mortar

UAB (Fouad et al., 2002) had conducted tests to evaluate modulus of rupture in AAC specimens with thin-bed mortar joints, based on Method 2. Data is presented in Table 3.9.

**Table 3.9** *Modulus of Rupture of AAC specimens with thin-bed mortar joints (UAB, Method 2)*

Manufacturers Specifications		Tensile stresses parallel to the direction of rise	
Material	$\rho$ (pcf)	Measured Density $\rho_{1386}$ (pcf)	Modulus of Rupture, $f_r$ (psi)
Hebel-HG1	25	25.7	60
Ytong-YG1	25	28.9	71
Ytong-YG2	31	39.6	85
Ytong-YG3	40	44.0	39
Contec-CG1	25	31.3	80
Contec-CG2	32	34.7	87
Contec-CG3	38	39.2	101

Modulus of rupture tests from UAB on specimens with thin mortar joints showed tensile bond failures of the AAC material for low-strength material only. As the strength of the AAC increased, failure was governed by the tensile bond strength of the thin-bed mortar. If the failure is governed by the material the slope would be the same as the modulus of rupture. Figure 3.21 and Figure 3.22 show, however, that as the density increases the failure is governed by the thin-bed

mortar joint. The limit tensile bond strength is 80 psi. for materials with  $f_{AAC}$  less than 700 psi. For materials with  $f_{AAC}$  less than 450 psi, the AAC unit failure governs, regardless of the type of mortar used and the extent of polymer modification by the addition of thin-bed mortar (Fouad et al., 2002).

Flexure-dominated shear-wall specimens tested at UT Austin (Tanner, 2003 and Varela, 2003) exhibited flexural shear cracking that initiated in the bed joints. In horizontal panel construction (Shear Wall Specimens 13, 14a and 14b) the flexural portion of the crack formed at the bed joint. In vertical panel construction for flexure-dominated shear wall specimens modular blocks are oriented vertically at the end of each wall. In some cases these are modular blocks with a core, (Shear Wall Specimens 15a and 15b); in other cases are U-blocks (Shear Wall Specimen 16). In each test, the flexural portion of flexure-shear cracks formed at the horizontal joints between modular blocks, rather than in the AAC material.

The requirement that the tensile bond behavior of AAC be governed by the material itself, rather than the mortar, is crucial to the development of design equations, testing requirements, and maximum limitations on the spacing of prescriptive reinforcement. It is absolutely essential to verify that with currently specified mortars, tensile bond strength is governed by the AAC material itself.

A reduced flexural capacity for AAC elements, as can be limited by failure of the material in flexural bond, was considered by Tanner (2003) in the development of design formulas for capacities of AAC shear walls (Appendix A).

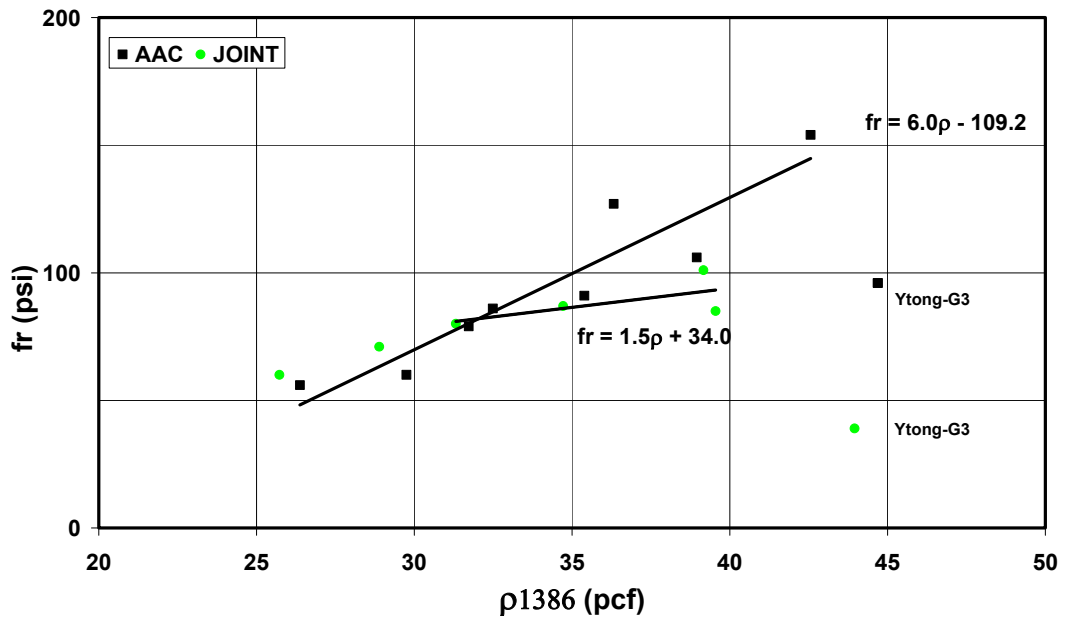


Figure 3.21 Tensile bond strength versus density

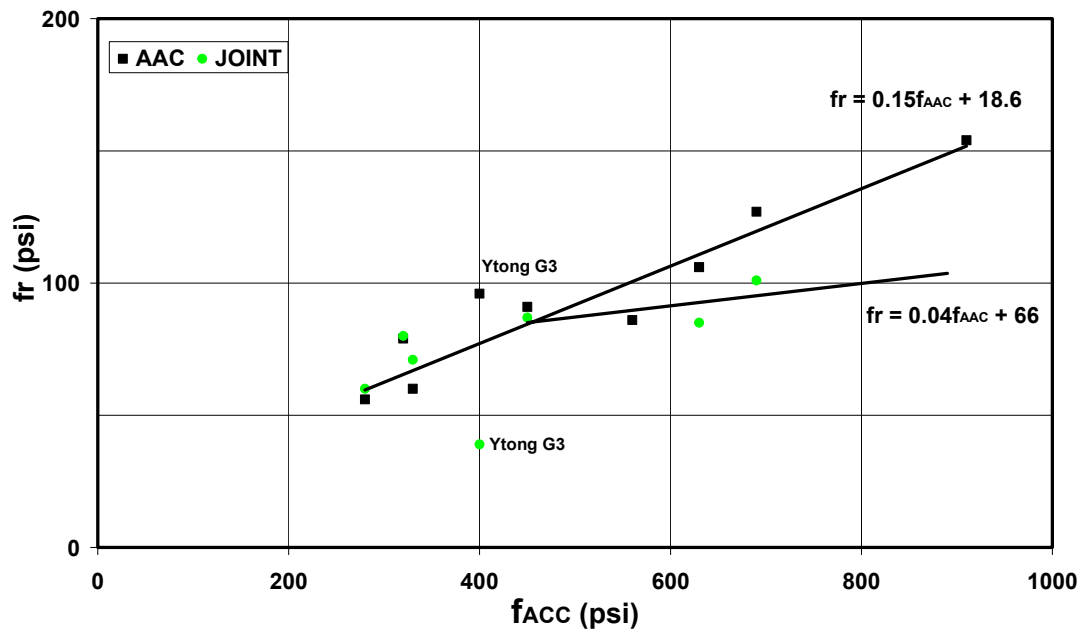


Figure 3.22 Tensile bond strength versus compressive strength



### **3.7 SHEAR BOND BETWEEN AAC AND THIN-BED MORTAR**

#### **3.7.1 Information regarding Shear Bond between AAC and Thin-bed Mortar**

The following sources of information are available:

- a) Modified direct shear tests from UAB (essentially zero moment, high shear) on specimens with thin mortar joints showed some shear bond failures in the mortar itself, and other shear bond failures in the AAC material (Fouad et al., 2002).
- b) Direct shear tests from UT Austin on AAC elements connected by thin-bed mortar also show some shear bond failures in the mortar itself, and other shear bond failures in the AAC material (Tanner, 2003 and Varela, 2003).

#### **3.7.2 Discussion of Results regarding Shear Bond between AAC and Thin-bed Mortar**

UAB conducted tests to evaluate the shear strength in AAC units with and without thin-bed mortar joints. They used a modified ASTM C78 method with two-point loads applied near supports and an  $a/d$  ratio of 8.7.

Data obtained by UAB for AAC specimens tested in shear with and without thin-bed mortar joints are compared in terms of shear strength ( $f_v$ ) versus

compressive strength ( $f_{AAC}$ ) and density ( $\rho_{1386}$ ). Results are shown in Figure 3.23 and Figure 3.24, where the shear strength tests on specimens without and with joints are referred as AAC and JOINT respectively.

Data for the shear strength in AAC units and specimens with thin-bed mortar joints are presented in Table 3.10. Comparison of results between AAC specimens with and without thin-bed mortar leads to the following conclusions:

- a) The shear bond strength in the unit-mortar joint becomes the controlling mechanism of failure for all the AAC materials tested by UAB, regardless of their compressive strength or density.
- b) The use of high versus moderate polymer modification does not influence shear bond capacity.
- c) The shear strengths of AAC specimens with and without thin-bed mortar joints increase as the compressive strength and density of the material increase. Best-fit lines from tests on thin-bed mortar joints and AAC are almost parallel, showing that the shear strength of the AAC is almost 10 psi greater than that of the joints at any compressive strength or density of the material. Therefore, joint shear failures are related to the strength of the AAC material itself, and not to the mortar bond strength.

**Table 3.10 Shear Tests on AAC with and without thin-bed mortar - UAB**

**Method**

Manufacturers Specifications		Specimens without thin-bed mortar joints		Specimens with thin-bed mortar joints	
Material	$\rho$ (pcf)	Measured Density $\rho_{1386}$ (pcf)	Shear Strength, $f_v$ (psi)	Measured Density $\rho_{1386}$ (pcf)	Shear Strength, $f_v$ (psi)
Hebel-HG1	25	26.6	54	27.3	47
Ytong-YG1	25	29.0	50	28.7	49
Ytong-YG2	31	38.2	78	40.3	72
Ytong-YG3	40	46.5	80	44.9	64
Contec-CG1	25	31.4	81	32.9	51
Contec-CG2	32	34.7	79	37.0	66
Contec-CG3	38	40.5	100	40.0	84

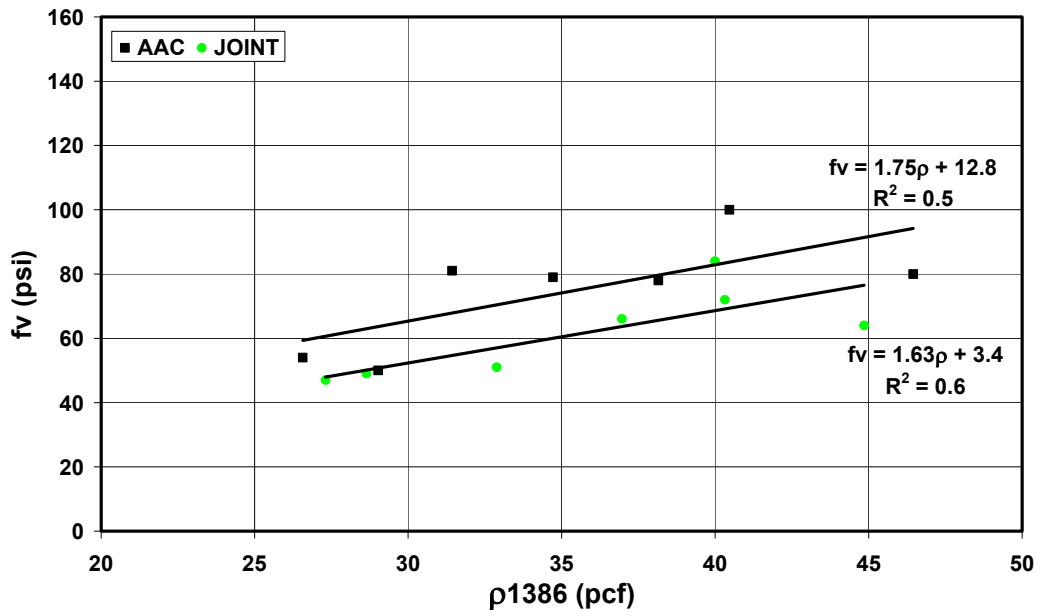


Figure 3.23 Shear strength of AAC units and thin-bed mortar versus density

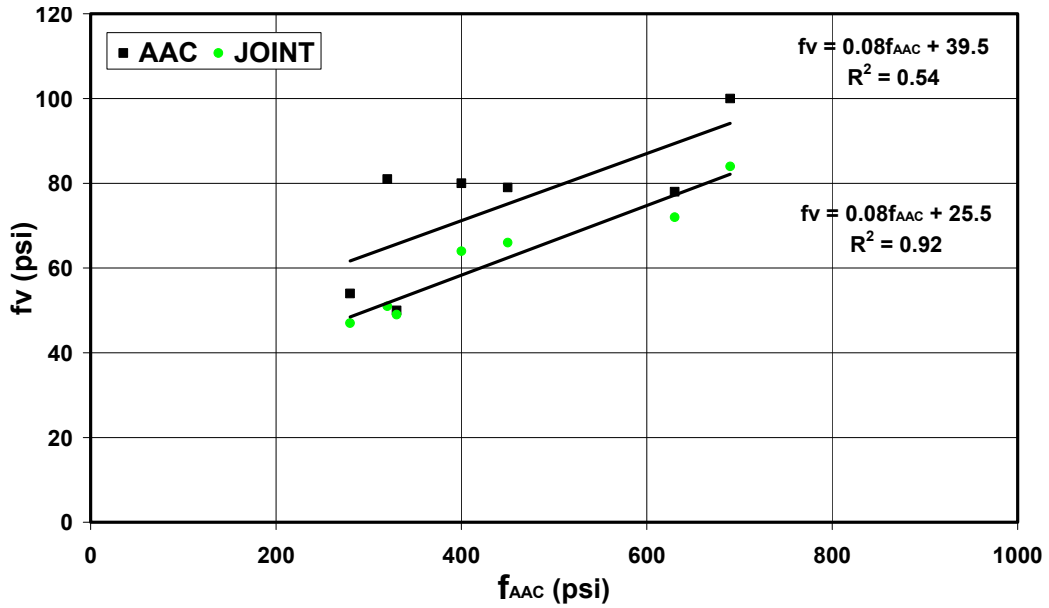


Figure 3.24 Shear strength of AAC units and thin-bed mortar versus compressive strength

UT Austin conducted 11 direct shear tests on AAC specimens with thin-bed mortar joints. The average shear strength was 64 psi, with a COV of 44%. In some failed specimens, crushing of the material due to compression of a piece of the inner part of the bearing blocks can be observed, and is attributed to the eccentricity of the reactions acting on the bottom of the specimens (Appendix D, Figure D.8 and Figure D.9). Flexural cracks were also found on the outer side of the bearing blocks resulting from the eccentricity of reacting forces and tensile stresses due to Poisson effects. The eccentric reaction might produce local moments at the joint surfaces, decreasing the tested shear strength. Probably because of this, the UT Austin results may underestimate the shear strength of thin-bed mortar joints. Using the probable compressive strengths of the UT Austin specimens, their shear strengths predicted using the linear regression from UAB tests would have been between 80 and 100 psi.

The requirement that the shear-bond behavior of AAC be governed by the material itself, rather than the mortar, is crucial to the development of design equations, testing requirements, and maximum limitations on the spacing of prescriptive reinforcement. It is absolutely essential to verify that with currently specified mortars, shear bond strength is governed by the AAC material itself.

### **3.8 DIRECT SHEAR STRENGTH OF AAC**

UAB (Fouad et al. 2002), conducted direct shear tests (at essentially zero moment and high shear) on plain AAC specimens. One group of specimens was oven-dried to a MC ranging from 8% to 12%. A second group of specimens was air-dried to a MC ranging from 15% to 25%. Data from such groups are referred as AAC-oven dry (MC=10%) and AAC-air dry (MC=20%) respectively.

Researchers at UAB tested air-dried specimens to confirm that the shear strength of oven-dried specimens can be less than that of otherwise identical air-dried specimens because of micro-cracking produced by oven-drying. There are no shear tests on reinforced AAC elements.

The relationship between direct shear strength ( $f_v$ ) and compressive strength ( $f_{AAC}$ ) is shown in Figure 3.25, in which two points ( $f_{AAC} = 560$  psi and 910 psi) show a significant decrease in shear strength from air-dried to oven-dried specimens. Because those points may be influenced by micro-cracking, it is debatable whether or not they should be included in the data analysis. The linear relationship  $f_v = 0.1 \cdot f_{AAC}$  provides results slightly above the 5% lower fractile of the complete set of data. To avoid un-necessary conservatism, points presumed to be influenced by micro-cracking are excluded from the proposed relationship between  $f_v$  and  $f_{AAC}$  presented in Equation (3.12).

$$f_v = 0.15 \cdot f_{AAC}$$

$f_{AAC}$  and  $f_v$  in psi

Equation (3.12)

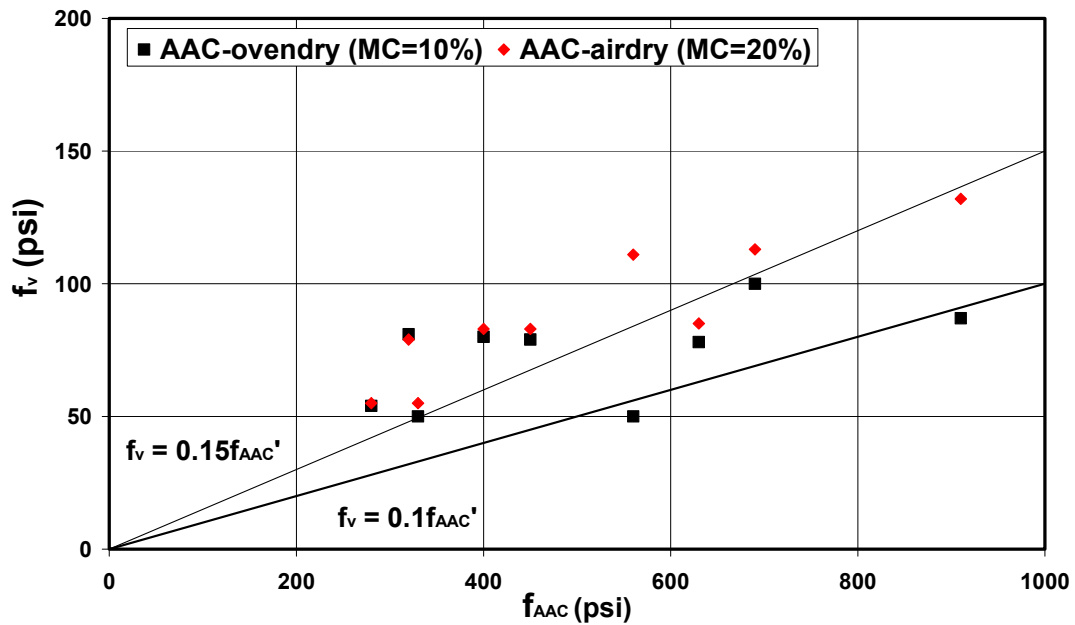


*Figure 3.25 Relationship between direct shear strength ( $f_v$ ) and compressive strength ( $f_{AAC}$ )*

### 3.9 FREEZE-THAW RESISTANCE OF AAC

Although tests were performed at UAB (Fouad et al., 2002), this information is not required for structural design provisions.

### 3.10 VARIATION IN THE COMPRESSIVE STRENGTH OF AAC WITH MOISTURE CONTENT

Many tests were conducted at UAB (Fouad et al., 2002) to investigate the effects of moisture-content variations in the compressive strength. This issue has been resolved with the approval of ASTM C1386. Compressive strengths are evaluated at “1386 density” (moisture content of 5%-15% by weight).

## **CHAPTER 4**

### **Design Provisions for Reinforced AAC Floor Panels**

#### **4.1 ORGANIZATION OF WORK ON DESIGN PROVISIONS FOR REINFORCED AAC PANELS**

Table 4.1 summarizes the organization of primary responsibility for development of design provisions for AAC elements.

Based on tests conducted at UT Austin and elsewhere, Tanner (2003) and Varela (2003) developed design formulas for capacities of AAC shear walls as governed by flexure, shear, and interface shear. Based on tests conducted at UAB (Fouad et al., 2002), the author developed design formulas for flexure, one-way shear and anchorage for floor panels. Those design formulas and their technical basis are discussed in this chapter.



**Table 4.1**      *Organization of primary responsibility for development of design provisions for AAC elements*

<b>Description of Task</b>	<b>Where Presented</b>	<b>Responsible Individual(s)</b>
technical justification for design provisions for AAC shear walls and floor diaphragms	Appendix A	Tanner Varela
technical justification for design provisions for reinforced AAC floor panels	this chapter	Argudo
proposed design provisions and commentary for AAC shear walls, floor diaphragms and floor panels	Tanner (2003) Varela (2003) Appendix C	Tanner Varela Argudo
development of $R$ and $C_d$ factors for the seismic design of AAC structures	Varela (2003)	Varela

#### **4.2 APPROACH FOR DEVELOPING DESIGN PROVISIONS**

Design provisions consistent in approach, organization and style to existing ACI 318-02 provisions are required to encourage professionals in the United States and other countries already familiar with ACI 318 to use reinforced AAC panels. In this Chapter, Section 4.3.2 was developed jointly by Tanner and the author. The Design Provisions for Reinforced AAC Floor Panels also include one additional section entitled “Discussion regarding Anchorage Behavior of Tensile Reinforcement for Shear Walls Tested at UT Austin,” which was developed by Tanner (Tanner, 2003) and is presented in Appendix D, Section D.2.

### **4.3 BOND STRENGTH BETWEEN FACTORY-INSTALLED WIRE REINFORCEMENT AND AAC**

#### **4.3.1 Information regarding Bond Strength between Welded Wire Reinforcement and AAC**

The following sources of information are available:

- a) Out-of-plane bending tests on reinforced panels at UAB show some bond failures. It was possible to back-calculate average bond strengths.
- b) Shear wall tests at UT Austin (Tanner, 2003 and Varela, 2003) show some cases in which shear capacity after cracking was apparently limited by bond transfer between wire reinforcement and AAC. Based on that, average bond strengths calculated at UT Austin are compared with the derived UAB bond strengths as discussed in a subsequent section.

#### **4.3.2 Discussion regarding Anchorage Failure of Tensile Reinforcement for UAB Panel Tests**

Of the 12 reinforced floor panels tested at UAB, 3 were reported by UAB to fail in the anchorage zone. In this section, this behavior is discussed, a mathematical model is proposed, and the implications of that model are presented.

The basic behavior of welded wire fabric within a matrix of AAC is approached using flexural theory. In Figure 4.1, a free-body diagram of the outer quarter of the panel span is presented, and the resistance mechanism based on

bearing of the cross wires against the AAC is shown in Figure 4.2. The internal lever arm in the panel is taken as the distance between the layers of welded wire mesh. Due to the low compressive strength of AAC, this arm is slightly shorter than the traditional value of  $0.9d$  often assumed in design of conventional reinforced concrete.

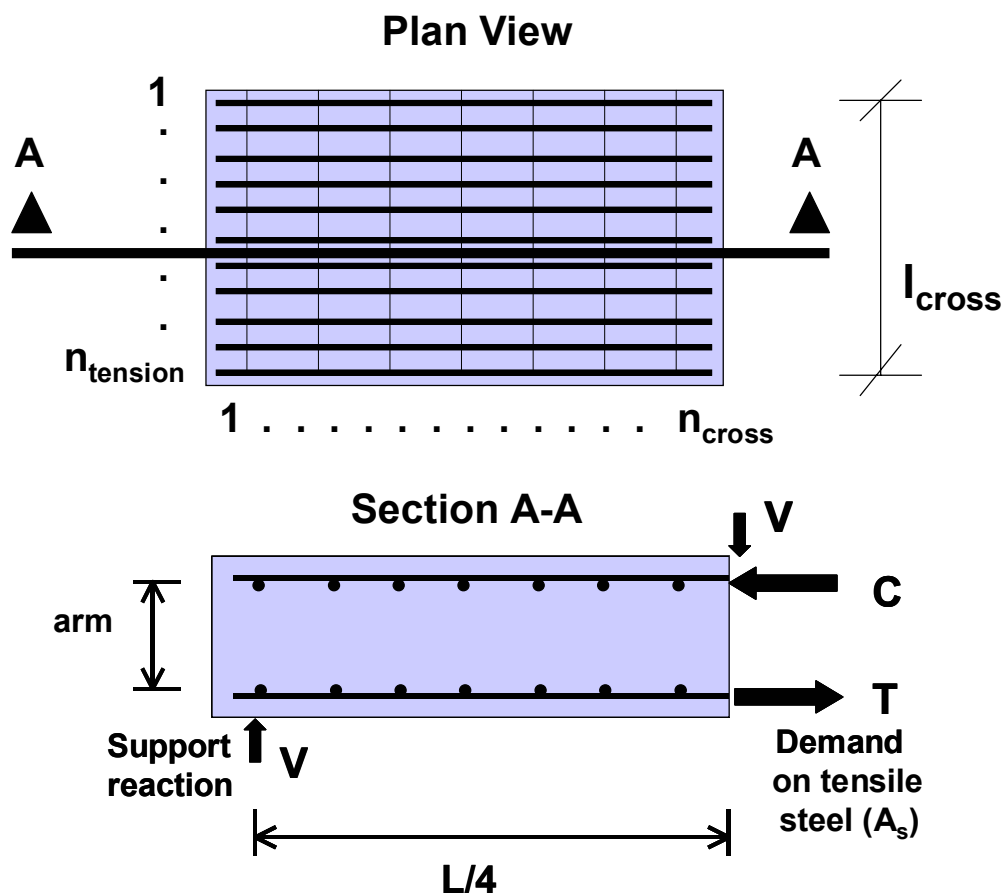
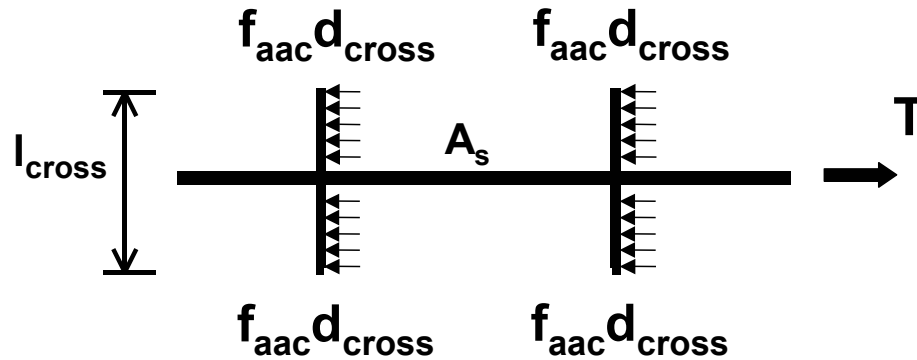


Figure 4.1 Free-body diagram of panel section



**Figure 4.2** *Resistance mechanism based on cross-wires functioning in bearing*

As shown in Figure 4.2, the tensile force in the tensile reinforcement is limited by the bearing capacity of the AAC under the cross-wires. The demand on the tensile layer of steel and the bond resistance of the reinforcement based on bearing of the cross-wires are presented by Equation (4.1) and Equation (4.2) respectively. In the capacity equation,  $n_{cross}$  refers to the number of cross wires,  $l_{cross}$  refers to the length of the cross wires, and  $d_{cross}$  refers to their diameter. Possible additional frictional resistance at the support reaction is calculated as the product of the support reaction times a coefficient of friction of 0.5, selected based on engineering judgment. In Table 4.2, this resistance is compared to the capacity. In eight of twelve cases failure is predicted. Results are summarized in Table 4.2.

$$T_{demand} = VL/(4 \cdot arm) \quad \text{Equation (4.1)}$$

$$T_{capacity} = n_{cross} d_{cross} \cdot l_{cross} \cdot f_{AAC} \quad \text{Equation (4.2)}$$

The implications of this prediction are important. Equation (4.3) relates the average bond stress ( $u_{ave}$ ) to the change in the force in the wire ( $\Delta T$ ). The term  $d_b$  is the diameter of the tensile reinforcement, and  $dx$  is the length  $L/4$ .

**Table 4.2 Comparison of anchorage demand to anchorage resistance for reinforced panels tested at UAB**

Specimen	Pmax (kips)	Arm (in.)	Tensile demand on wires (kips) Equation (4.1)	n of bars	Capacity based on bearing (kips) Equation (4.2)	Additional frictional resistance at support (kips)	Capacity / Demand	Failure predicted ?	Failure observed ?
1 YF 6-24-12.5 A	3.9	4.5	16.1	6	15.9	1.9	1.11	No	No
2 YF 6-24-12.5 A	4.0	4.5	16.6	6	15.9	2.0	1.04	No	No
1 YF 8-24-16.5 A	4.2	6.5	16.1	6	15.9	2.1	1.12	No	No
2 YF 8-24-16.5 A	4.2	6.5	16.1	6	15.9	2.1	1.12	No	No
1 YF 6-24-12.5 B	4.6	4.5	19.0	6	15.9	2.3	0.96	Yes	No
2 YF 6-24-12.5 B	4.5	4.5	18.9	6	15.9	2.3	0.96	Yes	No
1 YF 8-24-16.5 B	5.8	6.5	22.1	6	15.9	2.9	0.85	Yes	No
2 YF 8-24-16.5 B	6.3	6.5	24.2	6	15.9	3.2	0.79	Yes	No
1 YF 6-24-12.5 C	6.1	4.5	25.5	6	15.9	3.1	0.75	Yes	Yes
2 YF 6-24-12.5 C	5.9	4.5	24.6	6	15.9	3.0	0.77	Yes	Yes
1 YF 8-24-16.5 C	8.1	6.5	30.8	6	15.9	4.0	0.65	Yes	Yes
2 YF 8-24-16.5 C	8.0	6.5	30.4	6	15.9	4.0	0.65	Yes	No

$$\frac{\Delta T}{dx} = u_{ave} d_b \pi \quad \text{Equation (4.3)}$$

$$\frac{V}{n_{tension} \pi d_b \text{arm}} = u_{ave} \quad \text{Equation (4.4)}$$

By substituting Equation (4.2) into Equation (4.3) a relationship between shear and average bond stress can be expressed in terms of shear (Equation (4.4)), where  $n_{tension}$  is the number of longitudinal wires. If the average bond stress is proportional to shear, then so is the bearing stress of the cross-wires on the AAC.

For a case of uniform shear, as in the UAB panel tests subject to quarter-point bending, the bearing stress on AAC is uniform. The panel capacity associated with this limit state can be predicted based on local crushing of the AAC under the cross-wires. The maximum force in the tensile reinforcement will cause local crushing of the cross wire bearing against the AAC at the full compressive strength. As load is increased, cross-wires not fully bearing on the AAC will begin to exert more bearing stress. By such redistribution, the load can increase until all cross-wires participate evenly.

In the case of non-uniform shear in a section, the cross-wires near the support will be most highly stressed first, as the shear is maximum there. As the AAC crushes in bearing, the bearing stress on the adjacent cross-wires will increase. For a given detail, if the bond stress is uniform, the required tensile force in the reinforcement can be determined based on equilibrium, and the available resistance can be predicted to avoid anchorage failure.

### **4.3.3 Design Proposal for Anchorage Capacity**

Equation (4.1) and Equation (4.2) in Section 4.3.2 were proposed for predicting the capacity, as governed by anchorage failure, for the panels tested at UAB. In that case, the shear force and the variation of the tensile force ( $dT_{demand}/dx$ ) were uniform within the shear span ( $L/4$ ), making it possible to

calculate the minimum number of equally spaced cross-wires ( $n_{cross}$ ) required to avoid anchorage (bond) failure.

Equation (4.1) and Equation (4.2) are generalized and rewritten as Equation (4.5) and Equation (4.6) for a beam subjected to distributed loads and variable shear along its length.

$$\frac{d\Gamma_{demand}(x)}{dx} = \frac{dM(x)}{dx} \cdot \frac{1}{arm} = \frac{V(x)}{arm} \quad \text{Equation (4.5)}$$

$$\frac{d\Gamma_{capacity}(x)}{dx} = \frac{dn_{cross}(x)}{dx} \cdot d_{cross} \cdot l_{cross} \cdot f_{AAC} \quad \text{Equation (4.6)}$$

Equating Equation (4.5) and Equation (4.6) results in Equation (4.7), which gives the number of cross-wires per unit length required to resist the tensile force in the longitudinal reinforcement, as a function of the shear in the panel and its cross-sectional geometry.

$$\frac{dn_{cross}(x)}{dx} = \frac{V(x)}{arm \cdot d_{cross} \cdot l_{cross} \cdot f_{AAC}} \quad \text{Equation (4.7)}$$

For design purpose, it is not recommended to compute the number of cross wires ( $n_{cross}$ ) as a variable of the length of the beam. Instead, the minimum cross-wire spacing ( $s_{min}$ ) or alternatively, the minimum number of equally spaced cross wires ( $n_{cross,min}$ ) corresponding to the maximum shear force ( $V_{max}$ ) in a certain shear span  $a$  can be computed by Equation (4.8) and Equation (4.9).

$$s_{\min} = \frac{V_{\max}}{0.85d \cdot d_{\text{cross}} \cdot l_{\text{cross}} \cdot f_{\text{AAC}}} \quad \text{Equation (4.8)}$$

$$n_{\text{cross},\min} = \frac{V_{\max}}{0.85d \cdot d_{\text{cross}} \cdot l_{\text{cross}} \cdot f_{\text{AAC}}} \cdot a \quad \text{Equation (4.9)}$$

For a simply supported floor panel with uniformly distributed load, the variation of the tensile force ( $dT_{\text{demand}}/dx$ ) becomes critical at the supports and to a distance  $L/6$  from them, requiring the longitudinal reinforcement to be anchored by the cross wires. Substituting  $a = L/6$  and taking the lever arm as  $0.85d$ , Equation (4.9) can be rewritten as:

$$n_{\text{cross},\min} = \frac{V_{\max} \cdot L}{5.1 \cdot d \cdot d_{\text{cross}} \cdot l_{\text{cross}} \cdot f_{\text{AAC}}}, \quad \text{Equation (4.10)}$$

to a distance  $L/6$  from supports

Between  $L/6$  and  $L/2$  from each support, a minimum number of cross-wires needs to be specified to permit redistribution of bearing stresses along the length of the panel. Therefore, for those intermediate zones it is recommended to use the same the number of cross wires at twice the spacing calculated for the anchorage zones ( $L/6$  from each support).

Finally, a capacity-reduction factor ( $\phi=0.75$ ) should be introduced to modify the above equations for design (Equation (4.11)).



$$V_{\max} = \frac{V_u}{\phi} = \frac{V_u}{0.75} \quad \text{Equation (4.11)}$$

#### 4.4 FLEXURAL DESIGN OF AAC BEAM ELEMENTS

##### 4.4.1 Nominal Flexural Capacity ( $M_n$ )

Nominal flexural capacity ( $M_n$ ) can be calculated using conventional assumptions of plane sections, strain compatibility, stress-strain relationships, and equilibrium. The compressive zone is determined based on a bi-linear stress-strain relationship, using a maximum useful compressive strain in the AAC of 0.003, and an equivalent rectangular stress block whose height is  $0.85f'_{AAC}$ , and whose depth is  $\beta_1c$ , where  $\beta_1 = 0.67$ .

Using these relationships, very good agreement was found at UT Austin between experimentally derived and analytically determined nominal moment capacities ( $M_n$ ) for UAB panels failing predominantly in flexure (Panels 1-2 YF 6-24-12.5 A and 1-2 YF 8-24-16.5 A).

The design flexural capacity ( $\phi M_n$ ) is obtained by multiplying  $M_n$  by a capacity-reduction factor  $\phi$ .

##### 4.4.2 Minimum Flexural Reinforcement Ratio

Selection of the minimum reinforcement ratio ( $\rho_{min}$ ) for AAC flexural elements is based on the objective that the nominal flexural capacity ( $M_n$ ) be equal to at least twice the cracking moment ( $M_{cr}$ ). For a rectangular section,  $M_n$

and  $M_{cr}$  are approximately defined by Equation (4.12) and Equation (4.13).

Assuming that  $I_t = 1.5I_g$ , and  $\left(d - \frac{a}{2}\right) = 0.7h$ .

$$M_n = A_s f_y \left(d - \frac{a}{2}\right) = 0.7 h A_s f_y \quad \text{Equation (4.12)}$$

$$M_{cr} = f_r S = f_r \left(\frac{I_t}{y_t}\right) = 4.8 \sqrt{f_{AAC}'} \left(1.5 \frac{b_w h^3}{\frac{h}{2}}\right) = 1.2 \sqrt{f_{AAC}'} b_w h^2;$$

thus:

$$2M_{cr} = 2.4 \sqrt{f_{AAC}'} b_w h^2 \quad \text{Equation (4.13)}$$

Equating Equation (4.12) and Equation (4.13), assuming that  $h = 1.15d$  and solving for  $A_s/b_w d$ , the minimum reinforcement ratio ( $\rho_{min}$ ) is found and is given by Equation (4.14).

$$\begin{aligned} 0.7 h A_s f_y &= 2.4 \sqrt{f_{AAC}'} b_w h^2 \\ A_s &= 3.5 \frac{\sqrt{f_{AAC}'}}{f_y} b_w h = 3.5 \frac{\sqrt{f_{AAC}'}}{f_y} b_w (1.15d) \\ \rho_{min} &= \frac{4 \sqrt{f_{AAC}'}}{f_y} \end{aligned} \quad \begin{array}{l} \text{Equation (4.14)} \\ f_{AAC}' \text{ and } f_y \text{ in psi} \end{array}$$

#### **4.4.3 Flexural Design of Tension- and Compression-Controlled AAC Elements under ACI 318-02**

Following Section 10.3 of ACI 318-02, AAC flexural elements can be designed as compression-controlled or tension-controlled sections. For compression-controlled sections with longitudinal reinforcement with specified  $f_y = 80$  ksi, the compression-controlled strain limit can be set equal to 0.0027.

Section 9.3.2 of ACI-318-02 should be applied using a capacity-reduction factor of  $\phi = 0.65$  for compression-controlled sections, of  $\phi = 0.9$  for tension-controlled sections, and equal to a linear interpolation between 0.65 and 0.90 when the strain in the extreme tensile reinforcement ( $\epsilon_t$ ) is between 0.0027 and 0.005.

Under ACI-318-02, the requirement for a maximum longitudinal reinforcement ratio equal to  $0.75\rho_b$  for compression-controlled sections can be relaxed if appropriate capacity-reduction factors are used.

#### **4.5 CONTROL OF DEFLECTIONS**

Deflections experimentally measured by UAB (Foad et al., 2002) were found by UT Austin researchers to be consistently higher (by a factor of 1.25 to 1.8) than those calculated using the effective moment of inertia ( $I_e$ ) given by Equations 9-8 and 9-9 of ACI 318-02. Because those equations are implicitly linked to Table 9.5 (a) of ACI 318-02, both that table and the deflection-calculation equations need to be modified for use with AAC elements.

The minimum-thickness requirements of Table 9.5(a) of ACI 318-02 can be used for reinforced AAC elements, if the following constraints are applied:

- 1) Footnote (a) to Table 9.5(a) of ACI 318-02 should be applied. It specifies that for structural lightweight concrete having unit weight in the range 90-120 pcf, the minimum thickness shall be multiplied by  $(1.65 - 0.005w_c)$ , where  $w_c$  is the unit weight in pcf. The footnote is applicable, because AAC is comparable to lightweight concrete in terms of its flexural stiffness. For the reinforced AAC panels tested at UAB, the corresponding factor from Footnote (a) to Table 9.5(a) is 1.47, making the ratios of calculated to observed deflections all comfortably above unity.
  
- 2) Footnote (b) to Table 9.5(a) of ACI 318-02 requires that for  $f_y$  other than 60,000 psi, calculated deflection values be multiplied by  $(0.4 + f_y/100,000)$ . This requirement is believed not to apply to AAC, because the bond between smooth wire and AAC differs considerably from the bond between deformed reinforcement and conventional concrete. Also, the specified yield strength of AAC reinforcement ( $f_y = 80,000$  psi) would correspond to a factor of 1.2, which would result in an over-estimate of deflections if the RILEM effective inertia were used.

The deflection-calculation provisions of Section 9.5.2.2 and 9.5.2.3 of ACI 318-02 can be applied to reinforced AAC elements, with the following modifications:

- 1) Short-term deflections should be calculated using an effective flexural stiffness ( $EI_e$ ) corresponding to the unfactored moment ( $M_a$ ). The effective flexural stiffness ( $EI_e$ ) should be obtained by linear interpolation between the cracking point ( $M_{cr}, \phi_{cr}$ ) and the yielding points ( $M_y, \phi_y$ ) on a bilinear moment-curvature diagram. This procedure is recommended by RILEM (1993). The short-term deflections so obtained should then be multiplied by the factor from Footnote (a) of Table 9.5(a). When this approach is used, calculated deflections are 0.9 to 1.2 times the experimentally observed values.
  
- 2) For calculation of additional long-term deflections resulting from creep and shrinkage of AAC flexural members, Section 9.5.2.5 of ACI 318-02 is not applicable because the reinforcement ratio for compressive reinforcement ( $\rho'$ ) is generally much smaller for AAC than for reinforced concrete. To calculate total deflections, including long-term deflections, a simplified approach based on RILEM specifications can be adopted. Total deflections can be calculated using an effective modulus of elasticity ( $E_{AAC}'$ ) equal to the modulus of elasticity ( $E_{AAC}$ ) divided by 1.5.

## **4.6 SHEAR DESIGN OF AAC BEAM ELEMENTS**

### **4.6.1 Shear Capacity of AAC ( $V_{AAC}$ )**

For reinforced concrete beams without shear reinforcement, the mean diagonal tensile strength ( $f_t$ ) can be taken equal to  $6\sqrt{f_c'}$  (US customary units). Equation (11-5) of ACI 318-02 uses a nominal unit strength in shear that decreases from  $3.5\sqrt{f_c'}$  for low ratios of shear span to depth, to  $1.9\sqrt{f_c'}$  for high

ratios. For simplicity, Equation (11-3) can be used, with a corresponding unit strength of  $2\sqrt{f'_c}$ . That unit strength is one-third of the mean diagonal tensile strength.

On that basis, Equations (11-3) and (11-4) of ACI 318-02 can be rewritten in terms of the splitting tensile strength ( $f_t$ ) for use with AAC elements. The corresponding shear capacity ( $V_{AAC}$ ) is given by Equation (4.15) for members subjected to shear and flexure only, and by Equation (4.16) for members subjected to axial compression as well.

$$V_{AAC} = \frac{f_t}{3} b_w d \quad \text{Equation (4.15)}$$

$$V_{AAC} = \frac{f_t}{3} \left( 1 + \frac{N_u}{2000 A_g} \right) b_w d \quad \text{Equation (4.16)}$$

Substituting Equation (3.5) into Equation (4.15) and Equation (4.16), Equation (4.17) and Equation (4.18) are obtained as follows:

$$V_{AAC} = 0.8 \sqrt{f_{AAC}} b_w d \quad \text{Equation (4.17)}$$

$V_{AAC}$  in lb,  $f_{AAC}$  in psi

$$V_{AAC} = 0.8 \sqrt{f_{AAC}} \left( 1 + \frac{N_u}{2000 A_g} \right) b_w d \quad \text{Equation (4.18)}$$

$V_{AAC}$  in lb,  $f_{AAC}$  in psi

#### 4.6.2 Shear Strength provided by Shear Reinforcement ( $V_s$ )

Shear strength provided by shear reinforcement ( $V_s$ ) can be calculated using Section 11.5 of ACI 318-02, with the following qualifications:

- a) Vertical or inclined wires designed to provide shear strength need to be welded to the longitudinal reinforcement; and
- b) The maximum usable shear strength provided by each shear reinforcement bar ( $V_{sb}$ ) is limited by the bearing capacity of the AAC on the longitudinal reinforcement. Equation (4.19) shall be verified.

$$V_{sb} \leq d_{long} \cdot s \cdot f_{AAC} \qquad \text{Equation (4.19)}$$

Where:  $d_{long}$  is the diameter of longitudinal reinforcement,  $s$  is shear reinforcement spacing along the beam axis and  $f_{AAC}$  is the compressive strength of AAC.

#### 4.6.3 Design Shear Capacity ( $\phi V_n$ )

The nominal shear capacity ( $V_n$ ) is equal to the sum of the nominal shear capacity of AAC ( $V_{AAC}$ ) and the shear strength provided by the shear reinforcement ( $V_s$ ). The design shear capacity ( $\phi V_n$ ) is obtained by multiplying the nominal shear capacity  $V_n$  by a capacity-reduction factor  $\phi = 0.75$ .

#### **4.6.4 Predicted Shear Capacities of Reinforced AAC Floor Panels Tested at UAB and CTL**

In Table 4.3, observed (Fouad et al., 2002) and predicted capacities are shown for UAB Panel Types B and C (8 of 12), as governed by shear, by flexure, and by anchorage. Shear capacities are calculated using Equation (4.17); flexural capacities are calculated as explained in Section 4.4.1; and anchorage capacities are computed as the summation of the resistance from bearing and the resistance from friction, as in Table 4.2. Ratios of capacity / demand can be used to predict governing failure modes. Failures in those panels were predicted to occur by a combination of shear and anchorage failure. Many panels in Table 4.3 show capacity / demand ratios close to or less than 1.0 for shear and for anchorage. In some cases, experimental observations at UAB agreed with these predictions. In other cases, the nature of the observed failure mode was not specified.

The same procedure was followed for the panels manufactured by ACCOA and tested by Construction Technology Laboratories (CTL) in 1999<sup>8</sup>. Results are presented in Table 4.4.

---

<sup>8</sup> Internal Report by CTL to ACCOA: *Structural Tests on AAC Reinforced Panels Manufactured by Aerated Concrete Corporation of America (ACCOA)*, July 1999.



**Table 4.3** *Summary of predicted and observed modes of failure for floor panels tested at UAB*

Specimen	Shear		Flexure		Anchorage		Reported failure mode (UAB)	Predicted failure mode (UT Austin)
	V <sub>AAC</sub> observed (kips)	V <sub>AAC</sub> predicted (ksi)	M <sub>n</sub> observed (kip-in.)	M <sub>n</sub> predicted (kip-in.)	T demand (kips)	T capacity (kips)		
1 YF 6-24-12.5 A	2.06	2.2	80.7	80.9	16.1	17.8	Not Specified	Flexure
2 YF 6-24-12.5 A	2.12	2.2	83.1	80.9	16.6	17.9		
1 YF 8-24-16.5 A	2.37	3.0	119.4	119.1	16.1	18.0		Flexure
2 YF 8-24-16.5 A	2.38	3.0	119.4	119.1	16.1	18.0		
1 YF 6-24-12.5 B	2.40	2.2	93.6	116.8	19.0	18.2		Shear/Anchorage
2 YF 6-24-12.5 B	2.39	2.2	93.3	116.8	18.9	18.2		
1 YF 8-24-16.5 B	3.16	3.0	158.3	174.1	22.1	18.8		Shear/Anchorage
2 YF 8-24-16.5 B	3.43	3.0	171.7	174.1	24.2	19.1		
1 YF 6-24-12.5 C	3.19	2.2	123.1	178.3	25.5	19.0	Anchorage	Shear/Anchorage
2 YF 6-24-12.5 C	3.08	2.2	118.9	178.3	24.6	18.9		
1 YF 8-24-16.5 C	4.43	3.0	214.5	284.9	30.8	19.9	Anchorage	Shear/Anchorage
2 YF 8-24-16.5 C	4.24	3.0	211.8	284.9	30.4	19.9	Not Specified	

**Table 4.4** *Summary of predicted and observed modes of failure in ACCOA panels*

Specimen	Shear		Flexure		Anchorage		Reported failure mode (CTL)	Predicted failure mode (UT Austin)
	V <sub>AAC</sub> observed (kips)	V <sub>AAC</sub> predicted (ksi)	M <sub>n</sub> observed (kip-in.)	M <sub>n</sub> predicted (kip-in.)	T demand (kips)	T capacity (kips)		
S1-8-24-15	3.84	3.24	158.8	153.0	25.4	19.8	Shear	Flexure/Shear/Anchorage
S2-8-24-15	3.62	3.24	149.9	153.0	24.0	19.6		Shear/Anchorage
S3-8-24-15	3.18	3.24	131.5	153.0	21.0	19.1		Anchorage
WT1-8-24-14	3.08	3.24	136.6	153.0	21.9	19.0		
WT2-8-24-14	3.31	3.24	146.8	153.0	23.5	19.3		Shear/Anchorage
WT3-8-24-14	2.57	3.24	113.9	153.0	18.2	18.5		Shear

## 4.7 DESIGN EXAMPLE OF AN AAC FLOOR PANEL

### 4.7.1 Design data

Figure 4.3 shows a simply supported AAC floor panel to be designed according to design provisions set for in Sections 4.3 through 4.6. Material properties, uniform gravity loads, and geometry are given as follows:

Dead load  $w_d = 80$  psf, and Live load  $w_l = 40$  psf

AAC Floor panel type PAAC-4:

$f'_{AAC} = 580$  psi and  $w_c = 45$  lbs / ft<sup>3</sup>, per ASTM C1386

$f_y = 80,000$  psi (wires),  $E_s = 29,000$  ksi, and  $A_{S\#7wire} = 0.06$  in.<sup>2</sup>

Diameter of longitudinal wires, 7 mm

Diameter of cross wires, 5 mm

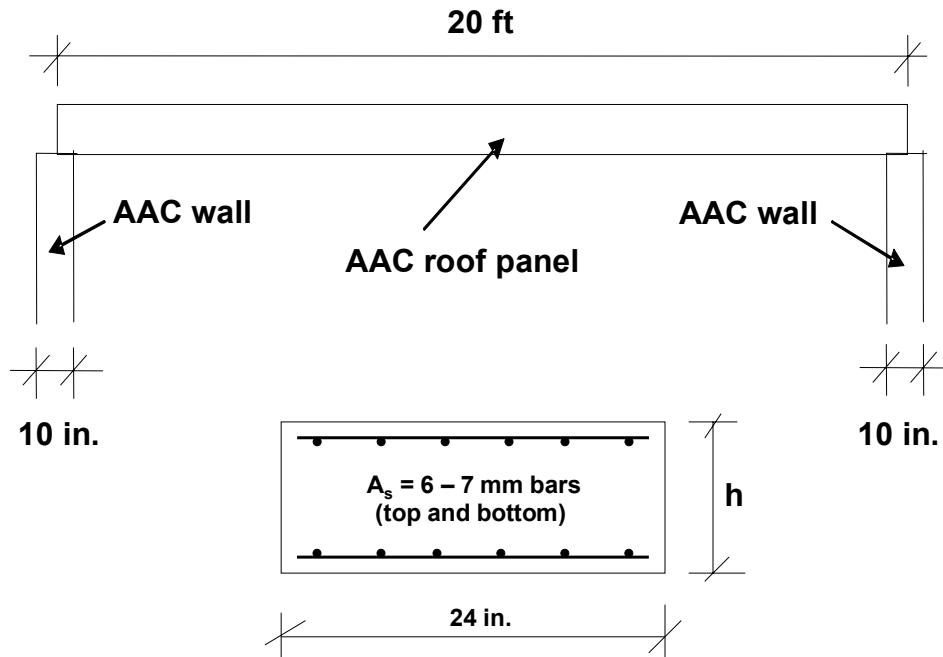


Figure 4.3 Simply supported AAC floor panel

#### 4.7.2 Control of Deflections

This panel is 20 ft long. Long-span panels, over 16 ft clear span, can be controlled by deflections. Therefore, the minimum thickness (h) that can be used to avoid calculation of deflections is computed following Section 4.5.

$$h = \frac{l_n}{20}(1.65 - 0.005w_c) = \frac{240-10}{20}(1.65 - 0.005(45)) = 16.4 \text{ in.} \quad \text{Say } h = 16 \text{ in.}$$

To optimize the design for  $h < 16$  in., deflections would need to be calculated rigorously.

Key mechanical properties of AAC need to be determined following provisions set for in Chapter 3, as follows:

Modulus of elasticity of AAC

$$E_{AAC} = 6.5(f'_{AAC})^{0.6} = 6.5(580)^{0.6} = 296 \text{ Ksi}$$

Reduced modulus of elasticity of AAC:

$$E'_{AAC} = \frac{E_{AAC}}{1.5} = \frac{296}{1.5} = 197 \text{ Ksi}$$

Splitting tensile strength of AAC:

$$f_t = 2.4\sqrt{f'_{AAC}} = 2.4\sqrt{580} = 57.8 \text{ psi}$$

Modulus of rupture of AAC:

$$f_r = 2f_t = 2(57.8) = 115.6 \text{ psi}$$

Modular ratio (modulus of elasticity of wire to reduced modulus of elasticity of AAC):

$$\eta = \frac{E_s}{E'_{AAC}} = \frac{29,000}{197} = 147$$

i) Try if  $h = 10$  in. satisfies Section 4.5 specifications:

Find the transformed moment of inertia ( $I_t$ ) for un-cracked section and cracking moment ( $M_{cr}$ ). Assume top and bottom cover  $r = 7/8$  in.

$$A_{st} = \eta A_s = 147(6)(0.06) = 53 \text{ in.}^2$$

$$I_t = \frac{b_w h^3}{12} + 2 A_{st} \left( \frac{h}{2} - r - \frac{d_b}{2} \right)^2 = \frac{24(10)^3}{12} + 2(53)(5 - 0.438 - 0.15)^2 = 4063 \text{ in.}^4$$

$$M_{cr} = \frac{f_r I_t}{\frac{h}{2}} = \frac{115.6(4063)}{\frac{10}{2}} = 94,000 \text{ lbs - in.}$$

Calculate un-factored uniformed distributed load and bending moment at mid-span of floor panel:

$$w_a = (80 + 40) \left( \frac{24}{12} \right) \left( \frac{1}{12} \right) = 20 \frac{\text{lbs}}{\text{in}}$$

$$M_a = \frac{w_a l_n^2}{8} = \frac{20(230)^2}{8} = 132,250 \text{ lbs - in.}$$

Since  $M_a = 132,250 \text{ lbs-in.} > M_{cr} = 94,000 \text{ lbs-in.}$ , the section will crack.

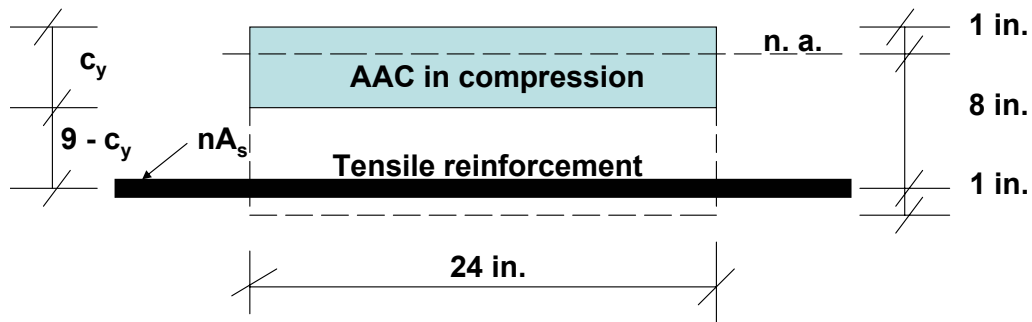


**Figure 4.4 Cracked transformed section ( $h = 10$  in.)**

For the cracked section analysis Figure 4.4, determine position of neutral axis ( $c_y$ ) neglecting the contribution of compressive steel, calculate the yielding moment ( $M_y$ ), and the cracked transformed moment of inertia ( $M_{cr}$ ), as follows:

From equilibrium:

$$53(9 - c_y) - \left(\frac{24}{2}\right)c_y^2 = 0$$

Position of neutral axis,  $c_y = 4.47$  in.

$$I_{cr} = \frac{24(4.47)^3}{3} + 53(9 - 4.47)^2 = 1,800 \text{ in.}^4$$

Determine moment at yielding of longitudinal cross-wires:

$$M_y = E'_{AAC} I_{cr} \left( \frac{F_y}{E_s} \right) = 197(1,000)(1,800) \left( \frac{80}{29,000} \right) \left( \frac{29,000}{9 - 4.47} \right) = 216,300 \text{ lbs - in.}$$

Determine curvature at cracking ( $\phi_{cr}$ ) and yielding of the cross wires ( $\phi_y$ ) and the curvature ( $\phi_a$ ) at  $M_a$ . Use linear interpolation to calculate  $\phi_a$ :

$$\phi_{cr} = \left( \frac{M_{cr}}{E'_{AAC} I_t} \right) = \left( \frac{94,000}{197(1000)(4060)} \right) = 0.000116 \frac{1}{in.}$$

$$\phi_y = \left( \frac{M_y}{E'_{AAC} I_{cr}} \right) = \left( \frac{216,300}{197(1,000)(1,800)} \right) = 0.000609 \frac{1}{in.}$$

$$\phi_a = \phi_{cr} + \left( \frac{M_a - M_{cr}}{M_y - M_{cr}} \right) (\phi_y - \phi_{cr})$$

$$\phi_a = 0.000116 + \left( \frac{132,250 - 94,000}{216,300 - 94,000} \right) (0.000609 - 0.000116) = 0.00027 \frac{1}{in.}$$

Calculate equivalent stiffness at service conditions ( $M_a, \phi_a$ ) and long-term deflections assuming that the full load is sustained for more than 5 years:

$$E'_{AAC} I_e = \frac{M_a}{\phi_a} = \frac{132,250}{0.00027} = 490 E6 \text{ lbs} - in.^2$$

$$\delta_{long-term} = 1.425 \left( \frac{5 w_a L_n^4}{384 E'_{AAC} I_e} \right) = 1.425 \left( \frac{5(20)(230)^4}{384(490 E6)} \right) = 2.1 in.$$

Where  $1.452 = (1.65 - 0.005w_c)$  is the magnification factor that comes from the application of footnote (a) in Table 9.5(a) of ACI 318-02.

Compare computed deflection to  $\delta_{max}$

$$\delta_{max} = \frac{L}{240} = \frac{240}{240} = 1 in.$$

$$\delta_{long-term} = 2.1 in. > \delta_{max} = 1 in. \quad \text{Not Good}$$

i) Try if  $h = 12$  in. satisfies Section 4.5 specifications:

Determine transformed moment of inertia and cracking moment:

$$I_t = \frac{b_w h^3}{12} + 2 A_{st} \left( \frac{h}{2} - r - \frac{d_b}{2} \right)^2 = \frac{24(12)^3}{12} + 2(53)(6 - 0.438 - 0.15)^2 = 6570 \text{ in.}^4$$

$$M_{cr} = \frac{f_r I_t}{\frac{h}{2}} = \frac{115.6(6570)}{\frac{12}{2}} = 126,600 \text{ lbs-in.}$$

Since  $M_a = 132,250$  lbs-in.  $>$   $M_{cr} = 126,600$  lbs-in., therefore need to calculate yielding moment. Determine position of neutral axis and cracked transformed moment of inertia:

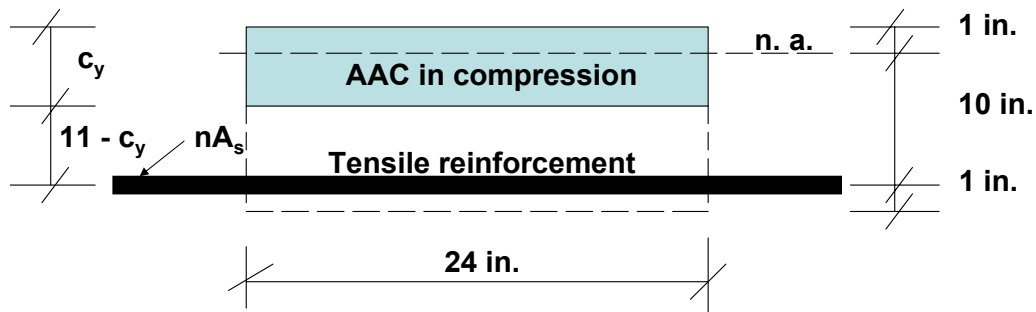


**Figure 4.5 Cracked transformed section ( $h = 12$  in.)**

From equilibrium:

$$53(11 - c_y) - \left( \frac{24}{2} \right) c_y^2 = 0$$

Position of neutral axis,  $c_y = 5.1$  in.

$$I_{cr} = \frac{24(5.1)^3}{3} + 53(11 - 5.1)^2 = 2,900 \text{ in.}^4$$

Determine moment at yielding of longitudinal cross-wires:

$$M_y = E'_{AAC} I_{cr} \left( \frac{\frac{F_y}{E_s}}{d - c} \right) = 197 (1,000)(2,900) \left( \frac{80}{11 - 5.1} \right) = 267,100 \text{ lbs - in.}$$

Determine curvature at cracking and yielding of the cross wires and curvature at  $M_a$ :

$$\phi_{cr} = \left( \frac{M_{cr}}{E'_{AAC} I_t} \right) = \left( \frac{126,600}{197 (1000)(6570)} \right) = 0.000098 \frac{1}{in.}$$

$$\phi_y = \left( \frac{M_y}{E'_{AAC} I_{cr}} \right) = \left( \frac{267,100}{197 (1,000)(2,900)} \right) = 0.00047 \frac{1}{in.}$$

$$\phi_a = \phi_{cr} + \left( \frac{M_a - M_{cr}}{M_y - M_{cr}} \right) (\phi_y - \phi_{cr})$$

$$\phi_a = 0.000098 + \left( \frac{132,250 - 126,600}{267,100 - 126,600} \right) (0.00047 - 0.000098) = 0.000113 \frac{1}{in.}$$

Calculate equivalent stiffness and long-term deflections:

$$E'_{AAC} I_e = \frac{M_a}{\phi_a} = \frac{132,250}{0.000113} = 1170 E6 \text{ lbs - in.}^2$$

$$\delta_{long-term} = 1.425 \left( \frac{5 w_a l_n^4}{384 E'_{AAC} I_e} \right) = 1.425 \left( \frac{5 (20)(230)^4}{384 (1170 E6)} \right) = 0.89 \text{ in.}$$

$$\delta_{max} = \frac{L}{240} = \frac{240}{240} = 1 \text{ in.}$$

Since  $\delta_{long-term} = 0.89 \text{ in.} < \delta_{max.} = 1 \text{ in.}$ ; therefore  $h = 12 \text{ in.}$  is OK.



### 4.7.3 Shear capacity

Determine factored loads and maximum shear for a panel  $b = 2$  ft wide:

$$w_u = 1.2(80) + 1.6(40) = 160 \text{ psf}$$

$$V_u = \frac{b w_u L}{2} = \frac{2(160)20}{2} = 3,200 \text{ lbs}$$

Determine shear capacity of floor panel:

$$\phi V_{AAC} = \phi 0.8 \sqrt{f_{AAC}} b d = 0.75(0.8) \sqrt{580}(24)(11) = 3,815 \text{ lbs}$$

$$\phi V_{AAC} = 3,815 \text{ lbs} > V_u = 3,200 \text{ lbs} \quad \text{OK}$$

### 4.7.4 Anchorage

Determine minimum number of cross-wires needed at panel ends ( $L/6$  from ends):

$$\frac{L}{6} = \frac{240}{6} = 40 \text{ in.}$$

$$V_{\max} = \frac{V_u}{\phi} = \frac{3,200}{0.75} = 4,270 \text{ lbs}$$

$$n_{\text{cross},\min} = \frac{V_{\max} L}{5.1 d d_{\text{cross}} l_{\text{cross}} f'_{AAC}} = \frac{4,270(240)}{5.1(11) \left( \frac{5}{10(2.54)} \right) (22)(580)} = 7.15$$

Use  $n_{\text{cross}} = 8$  for edges ( $L/6$ ). Spacing of cross-wires at edges would be:

$$S_{\min} = \frac{39}{8} = 4.9 \text{ in.}$$

Use 8 cross-wires spaced evenly. One cross-wire (5 mm diameter) every 5 in. in the first 40 in. from panel ends. In the intermediate zone ( $2L/3$ ) use 1 cross wire (5 mm diameter) every 10 in (twice  $S_{\min}$ ).

#### 4.7.5 Flexural capacity

Determine factored bending moment at mid-span of the panel ( $b = 2$  ft):

$$M_u = \frac{b w_u L^2}{(12 \text{ in/ft}) 8} = \frac{2(160) 240^2}{(12) 8} = 192,000 \text{ lbs} - \text{in.}$$

Check if minimum reinforcement ratio is satisfied for  $h = 12$  in.

$$\rho_{\min} = \frac{4 \sqrt{f'_{AAC}}}{f_y} = \frac{4 \sqrt{580}}{80,000} = 0.0012$$

$$\rho = \frac{A_s}{b_w d} = \frac{0.36}{24(11)} = 0.0014$$

$\rho = 0.0014 > \rho_{\min} = 0.0012$  is OK.

Stress in the tensile reinforcement can be limited by the bearing capacity of AAC over cross-wires. Equilibrium shall be checked as follows:

Total number of cross wires ( $n_{cross}$ ) in ( $L/2$ ) = 16

(8 in edge  $L/6$  and 8 in interior  $L/3$ )

$$A_s f_s = n_{cross} l_{cross} f_{AAC} ' d_{cross}$$

$$f_s = \frac{n_{cross}}{A_s} l_{cross} f_{AAC} ' d_{cross} = \frac{16}{6(0.06 \text{ in}^2)} (22 \text{ in})(0.58 \text{ Ksi})(0.2 \text{ in}) = 113.4 \text{ Ksi}$$

Since  $f_s > f_y$ , then longitudinal reinforcement will yield before bearing failure occurs in the AAC. This ductile mechanism is desirable.

Determine flexural capacity of floor panel at yielding of longitudinal steel:

$$T = A_s f_y = 0.36 (80) = 28.8 \text{ kips}$$

$$T = C = 0.85 f'_{AAC} a b_w = 0.85 (0.58)(a)(24) = 28.8$$

Solving for a, then a = 2.43 in.

Check strains in tensile reinforcement:

Assume position of neutral axis  $c = a/0.67 = 2.43/0.67 = 3.63$  in.

$$\epsilon_s = 0.003 \frac{d - c}{c} = 0.003 \frac{11 - 3.63}{3.63} = 0.0061$$

This section is tension controlled. Use a strength reduction factor of 0.9

$$M_n = T \left( d - \frac{a}{2} \right) = 28.8 \left( 11 - \frac{3.63}{2} \right) = 282.2 \text{ kip-in}$$

$$\phi M_n = 0.9(282.2) = 254 \text{ kip-in.}$$

$$\phi M_n = 254,000 \text{ lbs-in.} > M_u = 192,000 \text{ lbs-in.} \quad \text{OK}$$

#### 4.7.6 Wall-panel connection, shear force on bearing critical section

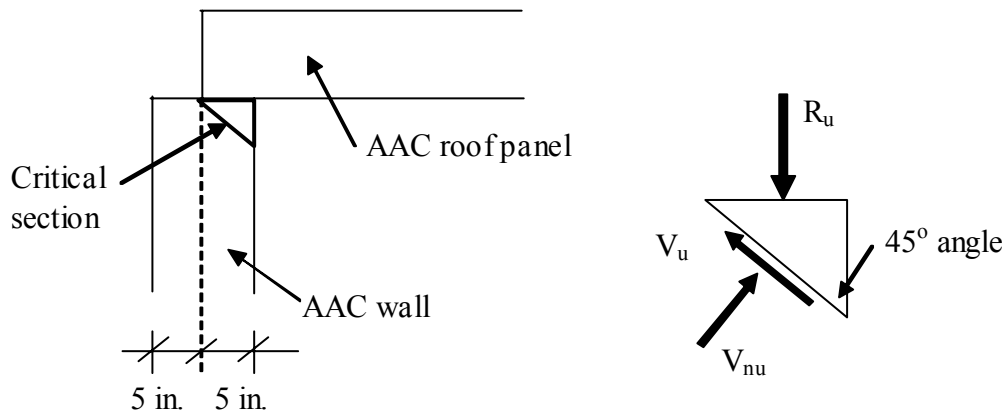


**Figure 4.6** Detail of panel bearing area

Determine vertical reaction on wall in a 1 in. strip (Figure 4.6). Use factored loads:

$$R_u = \frac{w_u}{12} \frac{L}{2} \frac{1}{12} = \frac{160}{12} \frac{240}{2} \frac{1}{12} = 133.3 \frac{\text{lbs}}{\text{in.}}$$

$$V_u = \frac{R_u \sqrt{2}}{2} = \frac{133.3 \sqrt{2}}{2} = 94.2 \frac{\text{lbs}}{\text{in.}}$$

Determine shear capacity:

$$f_v = 0.15 f'_{AAC} = 0.15 (580) = 87 \text{ psi}$$

$$\phi V_n = \phi f_v A_d = 0.75 (87) \sqrt{5^2 + 5^2} (1) = 461 \frac{\text{lbs}}{\text{in.}}$$

$$\phi V_n = 461 \frac{\text{lbs}}{\text{in.}} > V_u = 94.2 \frac{\text{lbs}}{\text{in.}} \quad \text{OK}$$

## **CHAPTER 5**

### **Summary, Conclusions and Recommendations**

#### **5.1 SUMMARY**

The objective of this thesis was to evaluate and synthesize data from various sources regarding the mechanical behavior of autoclaved aerated concrete (AAC), and to integrate those data in a consistent and coherent fashion, for use by others to refine previously developed design formulas for AAC shear walls, and for use by the author to develop design provisions and their technical justification for reinforced AAC floor panels. That objective was accomplished.

#### **5.2 CONCLUSIONS**

##### **5.2.1 Available data are sufficient to develop design provisions for reinforced AAC panels**

Available data regarding the mechanical characteristics of AAC are sufficiently consistent for use in developing design provisions. Using the relationships developed here for AAC material properties, AAC floor panels and lintels constructed with factory-installed reinforcement can be designed as beams, following the design provisions proposed in Chapter 4. AAC walls constructed with wall panels with factory-installed reinforcement and grouted cells with deformed reinforcement in grouted cores can be designed as reinforced elements, following the proposed design provisions in Appendix A.

### **5.2.2 Use of specified compressive strength as key independent variable**

The most consistent expressions for tensile strength, shear strength, and modulus of AAC were obtained in terms of the specified compressive strength,  $f_{AAC}'$ . That specified compressive strength is linked to the strength classes in which AAC is produced. Use of specified compressive strength rather than density as the key independent variable, eliminates the effects of normal variation in moisture content of AAC.

### **5.2.3 Quality assurance for compressive strength is essential**

Because the specified compressive strength,  $f_{AAC}'$ , is fundamental for calculating element capacities, it is vital to verify that specified strengths represent an acceptable lower fractile of tested strengths. This verification should be conducted by manufacturers as part of production quality assurance, and should also be checked regularly by independent third-party testing.

### **5.2.4 Flexural and shear strength of the material can be controlled by the tensile bond capacity at the interface between AAC and the mortar**

In diagonal tension tests (ASTM E519) and flexural capacity tests (ASTM E72) conducted at UT Arlington; modulus of rupture tests (Section 3.6) and direct shear tests (Section 3.7) conducted at UAB on specimens with thin mortar joints; and in shear-wall tests conducted at UT Austin, failure of AAC block assemblages was observed to be controlled by the tensile capacity of the AAC material for low-strength AAC, and by the tensile bond capacity at the interface between AAC and the mortar for high-strength AAC. Low strength AAC

materials ( $f_{AAC}' \leq 450$  psi) tend to fail in diagonal tension through the block, and medium- to high-strength AAC materials ( $f_{AAC}' > 450$  psi) tended to fail in tensile bond at the interface between AAC and mortar. This general observation was independent of the extent of polymer modification of the mortar.

### **5.2.5 Good construction practices can significantly increase the tensile bond capacity at the interface between AAC and the mortar**

Because the proposed design provisions for AAC elements and structures are based on the monolithic behavior requirement (strength controlled by AAC material rather than thin-bed mortar joints), it is vital to ensure that this requirement is satisfied in practice. Good construction practices, including pre-wetting of the block surface, were found by UT Austin to increase bond strength so that failure would be governed by the strength of the AAC material. In addition, AAC manufacturers should regularly verify the performance of their recommended thin-bed mortars in this regard. That verification should be checked by independent third-party testing. Finally, work should be continue on the development of ASTM specifications for thin-bed mortar, and those specifications should include requirements for tensile bond strength.

## **5.3 RECOMMENDATIONS FOR FUTURE RESEARCH WORK**

Although significant progress has been achieved by the AAC research at UT Austin and elsewhere to characterize the behavior of AAC material and of reinforced AAC elements and assemblies, additional work would be useful in the following areas:

- 1) Creep for different AAC material sources and manufacturers, and drying shrinkage of the material as functions of moisture content;
- 2) Effects of long-term loading and creep on the tensile, shear and compressive strengths of AAC elements;
- 3) Effects of different raw materials and manufacturing processes on the statistical variability of AAC material strengths;
- 4) Additional techniques for enhancing the ductility of AAC elements;
- 5) Effects of elevated ambient temperatures (above 50 °C) on creep of AAC material;
- 6) Long-term durability of corrosion-resistant coatings on factory-installed reinforcement;
- 7) Fracture toughness as related to the cyclic behavior of direct mechanical connections to AAC;
- 8) Feasibility of pre-stressed AAC elements for particular applications;
- 9) Continued examination of the field performance of AAC elements and structures designed using provisions based on the synthesized data of this thesis.



## APPENDIX A

### Design Provisions for Reinforced AAC Shear Walls and Floor Diaphragms

#### A.1 DESIGN OF AAC SHEAR WALLS

A suite of 14 AAC shear wall specimens, with aspect ratios (height of the point of load application divided by the plan length) from 0.6 to 3, has been tested at the University of Texas at Austin. The behavior of each shear wall may be shear or flexure dominated. The shear-dominated specimens were heavily reinforced in flexure using external reinforcement. The flexure-dominated specimens were lightly reinforced in flexure. The test setup is shown in Figure A.1.

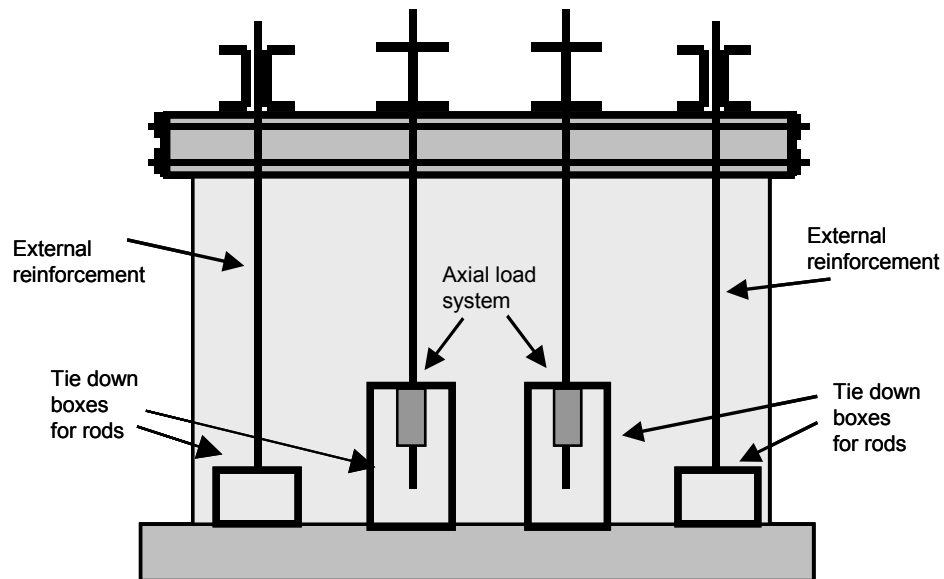


*Figure A.1 Test set up for shear wall specimens (UT Austin)*

Physical details for each specimen are presented in Table A.1. The number after the supplier's name identifies in which shipment the AAC material arrived.

**Table A.1 Details of shear wall specimens tested at UT Austin**

Specimen	Failure Mode	AAC units	Material supplier	Length in. (m)	Height in. (m)	Thickness in. (m)	Aspect Ratio	Interior Vertical Reinforcement
1	Shear	Horiz. Panels	Contec 1	240 (6.1)	154 (3.9)	8 (0.2)	0.64	No
2	Shear	Vert. Panels	Ytong 1	240 (6.1)	154 (3.9)	8 (0.2)	0.64	No
3	Shear	Blocks	Ytong 2	240 (6.1)	151 (3.8)	8 (0.2)	0.63	No
4	Shear	Horiz. Panels	Matrix 1	240 (6.1)	154 (3.9)	8 (0.2)	0.64	#5 (16 mm) at 48 in. (1.2 m)
5	Shear	Blocks	Contec 2	240 (6.1)	151 (3.8)	8 (0.2)	0.63	No
7	Shear	Blocks	Ytong 2	144 (3.7)	151 (3.8)	8 (0.2)	1.05	No
9	Shear	Horiz. Panels	Matrix 1	96 (2.4)	154 (3.9)	8 (0.2)	1.60	No
11	Shear	Blocks	Contec 2	48 (1.2)	151 (3.8)	8 (0.2)	3.15	No
13	Flexure	Horizontal Panels	Ytong 1	72 (2.1)	154 (3.9)	8 (0.2)	2.13	# 5 (16 mm) 12 in. (0.6 m) from ends
14a	Flexure	Horizontal Panels	Babb 1	56 (1.4)	154 (3.9)	10 (0.3)	3.2	# 5 (16 mm) 4 in. (0.1 m) from ends
14b	Flexure	Horizontal Panels	Babb 1	56 (1.4)	154 (3.9)	10 (0.3)	3.2	# 5 (16 mm) 4 in. (0.1 m) from ends
15a	Flexure	Vertical Panels with End Blocks	Babb 1	112 (2.8)	154 (3.9)	10 (0.3)	1.4	# 5 (16 mm) 8 in. (0.2 m) from ends
15b	Flexure	Vertical Panels with End Blocks	Babb 1	112 (2.8)	154 (3.9)	10 (0.3)	1.4	# 5 (16 mm) 8 in. (0.2 m) from ends
16	Flexure	Vertical Panels with U End Blocks	Babb 1	112 (2.8)	154 (3.9)	10 (0.3)	1.4	# 5 (16 mm) 8 in. (0.2 m) from ends
17	Flexure	Vertical Panels with U End Blocks	Babb 2	112 (2.8)	154 (3.9)	10 (0.3)	1.4	# 5 (16 mm) 8 in. (0.2 m) from ends

Results from a suite of 12 shear-wall tests performed by Hebel (Germany) provide additional information<sup>1</sup>. Each of those walls measured 8.2 ft (2.5 m)

<sup>1</sup> Personal communication, Violandi Vratanou, Hebel AG, Germany, November 2000

long, 8.2 ft (2.5 m) tall and 9.5 in. (0.24 m) thick. The aspect ratio of each specimen is 1.0. The test set up is shown in Figure A.2. Additional physical details for each Hebel specimen are presented in Table A.2.

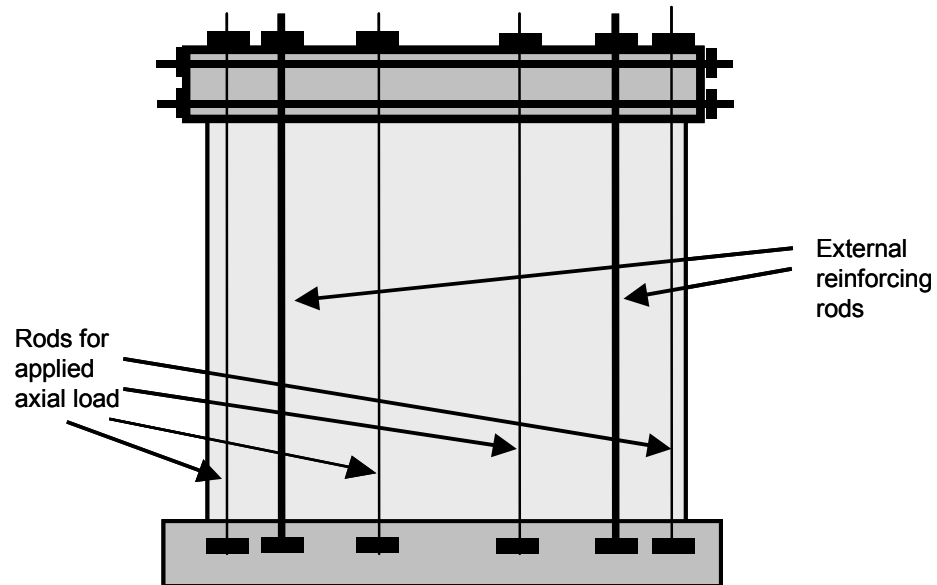


**Figure A.2** Test setup for shear wall specimens at Hebel (Germany)

**Table A.2** Details of shear wall specimens tested by Hebel (Germany)

Specimen	AAC Units	Mortared Head Joints	Type of Running Bond
3.3	Blocks	No	one-half
3.2	Blocks	No	one-half
3.4	Blocks	No	one-half
3.5	Blocks	No	one-fifth
3.6	Blocks	Yes	one-fifth
4.3	Blocks	No	one-half
4.4	Blocks	No	one-half
4.1	Blocks	No	one-half
4.5	Blocks	No	one-fifth
4.6	Blocks	No	one-fifth
4.7	Blocks	Yes	one-fifth
4.8	Blocks	Yes	one-fifth

In the Hebel tests, axial load was applied using uniformly spaced, external post-tensioning rods. This axial load was monitored and was kept constant. Two additional 1 in. (25 mm) diameter rods on each side of the wall, with initial pre-tension less than 0.5 kip (2 kN), were used as external reinforcement. As the wall displaces laterally in its own plane, tensile forces increase in the external reinforcement on the tension side. The rods on the compressive side of the wall are not initially post-tensioned, so the force in them does not decrease as the force in the tension rods increases. Increasing the force in the tension rods without decreasing the force in the compression rods is equivalent to applying an additional compressive axial load to the wall. Therefore, the axial load in the Hebel specimens changed as the lateral load changed. The axial load used to evaluate the behavior of the Hebel specimens at each state is the initial axial load (including weight of loading equipment) plus the summation of tensile forces in the rods at that state.

### **A.1.1 Web-shear Cracking**

Using additional data points determined at UT Austin between November 2001 and August 2002, the relationship between splitting tensile strength and “1386 density” presented in Equation (A.1) has been replaced by  $f_t = 2.4 \sqrt{f'_{AAC}}$ . As discussed in this section, that difference in splitting tensile strength is less a few percent, and the actual change in computed values of  $V_{AAC}$  is quite small.

This section is dedicated to explaining the changes. The form of the equation for  $V_{AAC}$  will stay the same, with only slight changes in the external coefficients. In the following section, the derivation of the equation for web-shear cracking is reviewed.

$$V_{AAC} = 0.9 \ell_w t \sqrt{f'_{AAC}} \sqrt{1 + \frac{P_u}{2.4 \sqrt{f'_{AAC}} \ell_w t}} \quad \text{Equation (A.1)}$$

$$V_{AAC} = 0.6 \ell_w t \sqrt{f'_{AAC}} \sqrt{1 + \frac{P_u}{2.4 \sqrt{f'_{AAC}} \ell_w t}} \quad \text{Equation (A.2)}$$

$$V_{AAC} = 0.37 \ell_w t f_t \sqrt{1 + \frac{P_u}{f_t \ell_w t}} \quad \text{Equation (A.3)}$$

$$V_{AAC} = 0.25 \ell_w t f_t \sqrt{1 + \frac{P_u}{f_t \ell_w t}} \quad \text{Equation (A.4)}$$

This inclined crack forms when the principal tensile stress in the web exceeds the tensile strength of the AAC. That principal stress is given by Equation (A.5), in which the normal stress in the wall is  $n$  and the maximum shear stress in the center of the web is  $v$ .

$$f_t = \sqrt{\left[\left(\frac{n}{2}\right)^2 + (v^2)\right]} - \frac{n}{2} \quad \text{where} \quad v = \frac{3V}{2l_w t} \quad \text{and} \quad n = \frac{P}{l_w t} \quad \text{Equation (A.5)}$$

Substituting the equations for shear stress and axial stress into the above equation, and solving for the shear, the corresponding shear capacity is given by Equation (A.6):

$$V_{AAC} = \frac{2l_w t}{3} f_t \cdot \left[1 + \left(\frac{P}{f_t l_w t}\right)\right]^{0.5} \quad \text{Equation (A.6)}$$

For reinforced concrete shear walls, ACI 318-02 uses a conservative (low) diagonal tensile capacity of  $4\sqrt{f'_c}$  (US customary units) to develop a conservative, semi-empirical equation for shear capacity as governed by web-shear cracking (ACI 318-02).

Web-shear cracking was observed in all AAC shear-wall specimens tested at The University of Texas at Austin except Shear Wall Specimen 2 (constructed of vertical panels). In addition, the tests performed by Hebel (Germany) provide corroborating data on shear strength as controlled by web-shear cracking. The observed and predicted web-shear cracking capacities based on Equation (A.6) are presented in Table A.3 and Table A.4 for fully and partially mortared specimens respectively.

**Table A.3** *Initial predictions of capacity as governed by web-shear cracking for fully mortared specimens*

Specimen	Axial load, P kips (kN)	Observed $V_{AAC}$ kips (kN)	Predicted $V_{AAC}$ kips (kN)	Observed $V_{AAC}$ / Predicted $V_{AAC}$
1 (UT)	156.0 (694)	164.2 (730)	127.7 (568)	1.29
3 (UT)	120.0 (534)	81.3 (362)	111.4 (495)	0.73
4 (UT)	120.0 (534)	110.5 (492)	132.5 (589)	0.83
5 (UT)	60.0 (267)	62.2 (277)	117.4 (522)	0.53
7 (UT)	80.0 (356)	57.4 (255)	68.7 (305)	0.84
9 (UT)	30.0 (267)	37.7 (168)	55.9 (249)	0.67
11 (UT)	25.0 (111)	15.6 (69)	26.9 (120)	0.58
Assemblage (UT)	25.0 (111)	52.0 (231)	96.7 (430)	0.54
3.6 (Hebel)	36.8 (164)	27.7 (123)	39.3 (175)	0.71
4.7 (Hebel)	62.4 (277)	46.7 (208)	57.7 (256)	0.81
4.8 (Hebel)	178.2 (792)	61.5 (273)	80.3 (357)	0.77
			Mean	0.70
			COV (%)	16.8

**Table A.4** *Initial predictions of capacity as governed by web-shear cracking for partially mortared specimens*

Specimen	Axial load, P kips (kN)	Observed $V_{AAC}$ kips (kN)	Predicted $V_{AAC}$ kips (kN)	Observed $V_{AAC}$ / Predicted $V_{AAC}$
3.3 (Hebel)	60.0 (267)	18.3 (81)	36.2 (161)	0.50
3.2 (Hebel)	26.2 (116)	20.6 (92)	42.0 (187)	0.49
3.4 (Hebel)	49.7 (221)	24.4 (109)	52.2 (232)	0.47
3.5 (Hebel)	89.8 (399)	18.2 (81)	36.7 (163)	0.49
4.3 (Hebel)	30.3 (135)	23.7 (105)	49.4 (220)	0.48
4.4 (Hebel)	30.3 (135)	32.1 (143)	62.7 (279)	0.51
4.1 (Hebel)	85.5 (380)	25.1 (112)	76.7 (341)	0.33
4.5 (Hebel)	153.9 (685)	21.3 (95)	48.5 (216)	0.44
4.6 (Hebel)	33.5 (149)	29.9 (133)	74.5 (331)	0.40
			Mean	0.46
			COV (%)	13.1

The shear strength of the AAC shear-wall specimens was initially predicted using Equation (A.6). The ratios of observed to predicted capacities, shown in Table A.3, indicate that the ratio of observed strength to predicted strength of Shear Wall Specimen 1 (UT Austin) is significantly greater than for the other specimens, and can be considered an anomaly with respect to the rest of the tests. The remaining specimens show lower observed than predicted strengths, indicating that Equation (A.6) is unconservative.

To further evaluate the effects of mortared head joints, the AAC shear-walls tested at UT Austin and by Hebel (Germany) are divided into two groups: those with fully mortared head joints, and those with unmortared head joints. The range of ratios of observed  $V_{AAC}$  to predicted  $V_{AAC}$  is 0.54 to 0.1.29 for the fully mortared specimens, and 0.33 to 0.51 for the partially mortared specimens. For the specimens with fully mortared head joints, the mean ratio of observed to predicted  $V_{AAC}$  is 0.70, with a coefficient of variation of 17%. For the specimens with unmortared head joints, corresponding values are 0.46 and 13%.

These data can be plotted in Figure A.3 and Figure A.4. In each figure, the mean ratio of observed capacity to that predicted using the theoretical Equation (A.6) is represented by a solid horizontal line. Also plotted on each figure is the normal distribution with the same mean and COV as the test data. The lower 10% fractile of that distribution, shown by a dashed horizontal line, has a value of 0.55 for the fully mortared specimens and 0.38 for the partially mortared ones.

Equation (A.6) was therefore reduced so that it would correspond to the lower 10% fractiles of the ratios of observed to predicted capacities. In carrying out that reduction, fully mortared and partially mortared specimens were considered separately. Equation (A.6) was multiplied by 0.55 to obtain proposed Equation (A.1) for fully mortared specimens. In the same way, Equation (A.6) was multiplied by 0.38 to obtain proposed Equation (A.2) for partially mortared specimens.

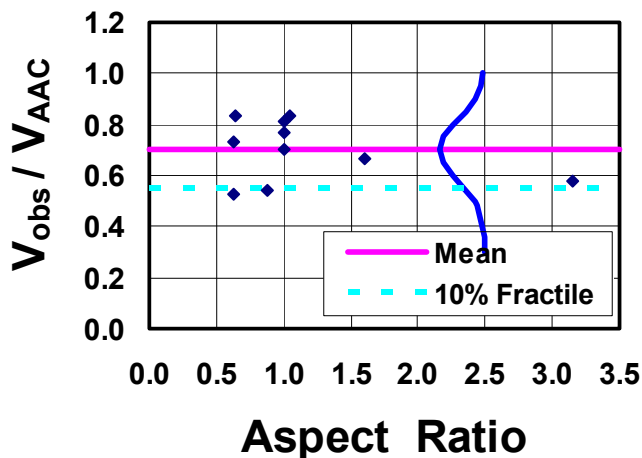


*Figure A.3 Ratios of observed to predicted (Equation (A.6)) web-shear cracking capacities for AAC shear-wall specimens with fully mortared head joints*



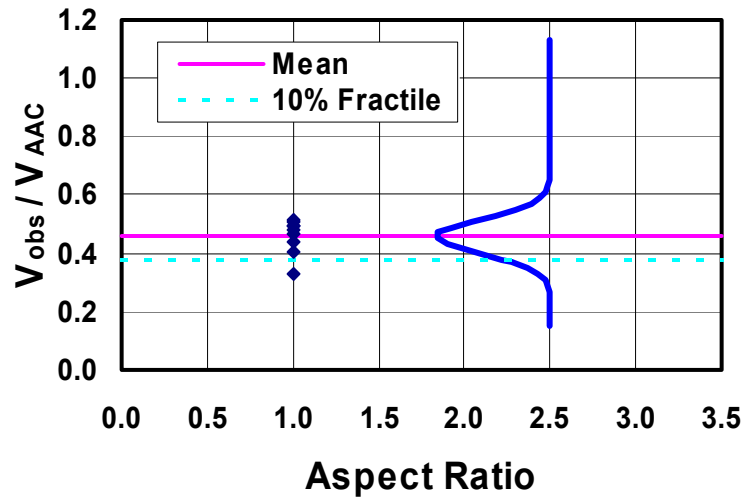


**Figure A.4** Ratios of observed to predicted (Equation (A.6)) web-shear cracking capacities for AAC shear-wall specimens with partially mortared head joints

The predicted  $V_{AAC}$  using Equation (A.1) and Equation (A.2) are presented in Table A.5 and

Table A.6 for all specimens that exhibited web-shear cracking. Ratios of observed  $V_{AAC}$  versus predicted  $V_{AAC}$  using Equation (A.1) and Equation (A.2) based on the tested compressive strength are presented in Figure A.5. In that figure, a solid diagonal line represents perfect agreement between observed and predicted shear capacities. The proposed equations are very close, or have slight errors in the direction of conservatism, for the specimens tested. If the ACI 318-02 equation for web shear cracking is used directly for AAC (substituting  $f_{AAC}$  for  $f_c$ ), the predicted capacity is greater than that observed, and hence unconservative. This is also true if the ACI 318-02 equation for web shear cracking is used with equivalent expressions for the tensile strength of concrete and for AAC. The web-shear cracking capacity will be further reduced by using the specified

compressive strength rather than the tested compressive strength. These results for the specimens tested at UT Austin are presented in Figure A.5. The one data point where the observed  $V_{AAC}$  falls below the predicted  $V_{AAC}$  is the Two-story Assemblage Specimen where the tested compressive strength fell below the specified compressive strength.

**Table A.5 Prediction of capacity as governed by web-shear cracking for fully mortared specimens (Equation (A.1)) using tested compressive strength**

Specimen	Axial load, P kips (kN)	Observed $V_{AAC}$ kips (kN)	Predicted $V_{AAC}$ kips (kN)	Observed $V_{AAC}$ / Predicted $V_{AAC}$
1 (UT)	156.0 (694)	164.2 (730)	70 (312)	2.34
3 (UT)	120.0 (534)	81.3 (362)	61 (273)	1.33
4 (UT)	120.0 (534)	110.5 (492)	73 (324)	1.52
5 (UT)	60.0 (267)	62.2 (277)	65 (287)	0.96
7 (UT)	80.0 (356)	57.4 (255)	38 (168)	1.52
9 (UT)	30.0 (267)	37.7 (168)	31 (137)	1.22
11 (UT)	25.0 (111)	15.6 (69)	15 (66)	1.05
Assemblage (UT)	26.0 (116)	52.0 (231)	53 (237)	0.98
3.6 (Hebel)	36.8 (164)	27.7 (123)	22 (96)	1.28
4.7 (Hebel)	62.4 (277)	46.7 (208)	32 (141)	1.47
4.8 (Hebel)	178.2 (792)	61.5 (273)	44 (197)	1.39
			Mean	1.27
			COV (%)	16.8

**Table A.6 Prediction of capacity as governed by web-shear cracking for unmortared head joints (Equation (A.2)) using tested compressive strength**

Specimen	Axial load, P kips (kN)	Observed $V_{AAC}$ kips (kN)	Predicted $V_{AAC}$ kips (kN)	Observed $V_{AAC}$ / Predicted $V_{AAC}$
3.3 (Hebel)	26.2 (116)	18.3 (81)	14 (61)	1.33
3.2 (Hebel)	49.7 (221)	20.6 (92)	16 (71)	1.29
3.4 (Hebel)	89.8 (399)	24.4 (109)	20 (88)	1.23
3.5 (Hebel)	26.6 (118)	18.2 (81)	14 (62)	1.30
4.3 (Hebel)	30.3 (135)	23.7 (105)	19 (84)	1.26
4.4 (Hebel)	85.5 (380)	32.1 (143)	24 (106)	1.35
4.1 (Hebel)	153.9 (685)	25.1 (112)	29 (130)	0.86
4.5 (Hebel)	33.5 (149)	21.3 (95)	18 (82)	1.15
4.6 (Hebel)	158.1 (703)	29.9 (133)	28 (126)	1.06
			Mean	1.21
			COV (%)	13.1

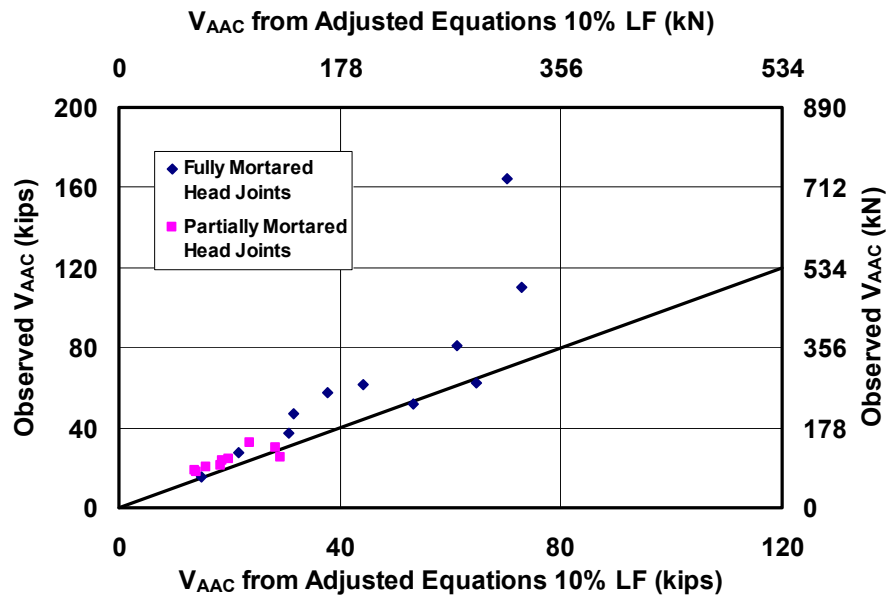


*Figure A.5 Observed versus predicted capacities as governed by web-shear cracking (Equation (A.1) and Equation (A.2)) using tested compressive strength*

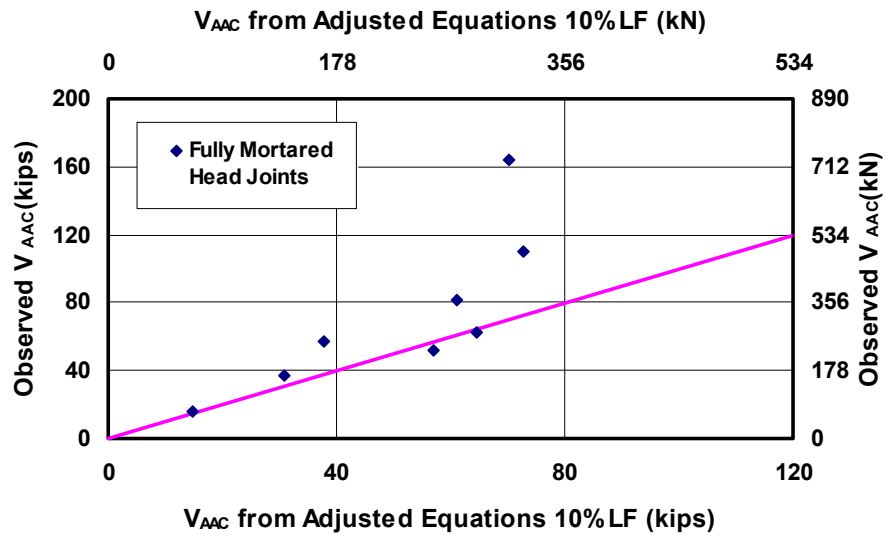


*Figure A.6 Observed versus predicted capacities as governed by web-shear cracking (Equation (A.1)) and Equation (A.2)) using specified compressive strength*

### A.1.2 Flexure-Shear Cracking for AAC Shear Walls

A flexure-shear crack begins as a horizontal crack at a height of about one-half the plan length of the wall ( $l_w$ ) above the base of the wall, and then propagates diagonally through the center of the wall, as shown in Figure A.7.

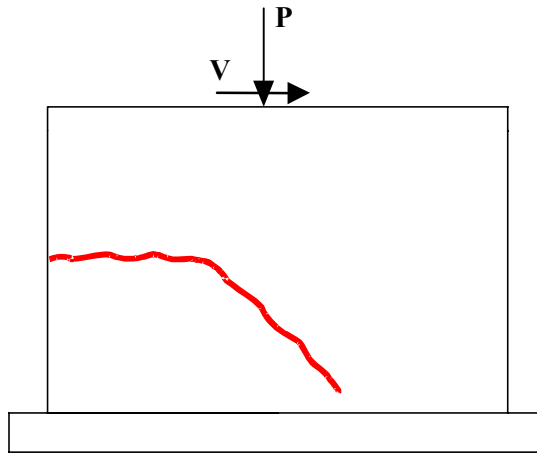


*Figure A.7 Flexure-shear cracking*

The formation of this crack is governed by the flexural tensile stress in the wall (Equation (A.7)).

$$\sigma = \frac{M}{S_x} \pm \frac{N}{A_n} \quad \text{Equation (A.7)}$$

Based on experiments with reinforced concrete shear walls, the controlling horizontal crack develops at a height of about  $l_w/2$ . Therefore, the moment at the crack,  $M_{\text{flcr}}$  is:

$$M_{flcr} = M - \frac{Vl_w}{2} \quad \text{Equation (A.8)}$$

where M is the moment at the base. Equation (A.9) presents the base shear at the formation of the flexural portion of the flexure-shear crack:

$$V_{flcr} = \frac{S_x \left( f_r + \frac{N}{l_w t} \right)}{\frac{M}{V} - \frac{l_w}{2}} \quad \text{Equation (A.9)}$$

ACI 318-02 uses a conservative (low) flexural tensile strength of  $6\sqrt{f'_c}$  (US customary units) substituted into Equation (A.9); experiments have shown an additional force of  $0.6\sqrt{f'_c} \cdot td$  is required to develop the crack. Therefore, ACI 318-02 uses Equation (A.10) for the flexure-shear cracking capacity.

$$V_c = \left[ 0.6\sqrt{f'_c} + \frac{l_w \left( 1.25\sqrt{f'_c} + 0.21 \frac{N}{l_w t} \right)}{\frac{M}{V} - \frac{l_w}{2}} \right] \cdot td \quad \text{Equation (A.10)}$$

Flexure-shear cracking was not observed in the 8 shear-dominated shear wall specimens tested at UT Austin because the exterior unbonded reinforcement (threaded rods) prevents vertical tensile stresses from forming at the base of the wall after flexural cracking (see Figure A.1). Flexure-shear cracking was

observed in the 6 flexure-dominated shear wall specimens. In every case the flexural portion of the flexure-shear crack formed first in the horizontal joint.

Based on the location of the flexural crack, the predicted load can be determined based on Equation (A.9) (see Table A.7). For AAC the modulus of rupture was calculated using  $f_r = 2 \cdot f_t$ , and the tested splitting tensile strength. This value was used in Equation (A.9). For flexure-dominated shear wall specimens, with the exception of Shear Wall Specimen 14a, the ratio of observed load versus predicted load ranges from 0.6 to 1.3. The mean ratio is 0.86 with a COV of 36%.

The observed load is lower than the predicted load because the failure occurred in the joint between the AAC and the thin-bed mortar rather than in the AAC material itself. A relationship for the tensile bond strength  $f_{\text{bond}}$  between AAC and thin-bed mortar was determined based on tests performed at UAB was presented in Section 3.6.2. Equation (A.11) presents the tensile bond strength for AAC densities greater than 32 pcf ( $2 \text{ kg/m}^3$ ). This indicates that for mid- to high-density AAC the tensile bond strength,  $f_{\text{bond}}$ , will be lower than the modulus of rupture. The tensile bond strength of the material in the flexure-dominated specimens except Shear Wall Specimen 13, is 94 psi (0.7 MPa) based on a density of 39.9 pcf ( $2.5 \text{ kg/m}^3$ ). Shear Wall Specimen 13 had a density below the limit of 32 pcf; therefore the modulus of rupture will govern the formation of a flexure-shear crack. The results of using the tensile bond strength rather than the modulus of rupture in Equation (A.9) for the remaining specimens are presented in Table A.8. With the exception of Shear Wall Specimen 14a, the ratios of observed to predicted strength range from 1.0 to 1.3 with a mean of 1.15 and a COV of 6.5%.

Shear Wall Specimen 14a exhibited flexural cracks at the base of the wall prior to testing. These cracks are presumed to have occurred while moving the top of the wall (out-of-plane) approximately 1 in. (25 mm) to the east to align the rams and loading beam. This would be expected to cause premature out-of-plane flexural cracks on the west side of the wall, which is where the first flexure-shear cracks did in fact occur.

$$f_{bond} = 1.5 \cdot \rho + 34$$

Equation (A.11)

$\rho$  in lb/ft<sup>3</sup>, and  $f_{bond}$  in lb/in.<sup>2</sup>

$$f_{bond} = 0.04 \cdot f_{AAC} + 66$$

Equation (A.12)

$f_{AAC}$  and  $f_{bond}$  in lb/in.<sup>2</sup>

**Table A.7 Results for flexure-shear cracking of AAC flexure-dominated shear wall specimens**

Specimen	$f_r$	N kips (kN)	Tested $V_{ncr}$ North kips (kN)	Predicted $V_{ncr}$ North Kips (kN)	Tested $V_{ncr}$ South kips (kN)	Predicted $V_{ncr}$ South kips (kN)	Observed $V_{ncr}$ /Predicted $V_{ncr}$ North Kips (kN)	Observed $V_{ncr}$ /Predicted $V_{ncr}$ North kips (kN)
13	110 (0.8)	25 (111)	9.6 (43)	8.2 (36)	10.1 (45)	8.0 (36)	1.18	1.26
14a	178 (1.2)	5 (22)	N/A	N/A	2.8 (12)	7.4 (33)	N/A	0.38
14b	178 (1.2)	5 (22)	4.9 (22)	7.4 (33)	4.6 (20)	7.4 (33)	0.66	0.62
15a	178 (1.2)	25 (111)	21.5 (96)	31.9 (142)	24.0 (107)	39.1 (174)	0.71	0.61
15b	178 (1.2)	25 (111)	20.0 (89)	-17.9 (-80)	17.5 (78)	17.1 (76)	0.66	0.60
16	178 (1.2)	25 (111)	-24.0 (-107)	31.9 (142)	21.8 (97)	32.4 (144)	0.75	0.67
							Mean	0.86
							COV (%)	36.1



**Table A.8 Results for flexure-shear cracking of AAC flexure-dominated shear wall specimens using tensile bond strength of material**

Specimen	$f_{bond}$	P kips (kN)	Tested $V_{flcr}$ North kips (kN)	Predicted $V_{flcr}$ North Kips (kN)	Tested $V_{flcr}$ South kips (kN)	Predicted $V_{flcr}$ South kips (kN)	Observed $V_{flcr}$ /Predicted $V_{flcr}$ North Kips (kN)	Observed $V_{flcr}$ /Predicted $V_{flcr}$ North kips (kN)
13	110 (0.8)	25 (111)	9.6 (43)	8.2 (36)	10.1 (45)	8.0 (36)	1.18	1.26
14a	94 (0.7)	5 (22)	N/A	N/A	2.8 (12)	4.1 (18)	N/A	0.68
14b	94 (0.7)	5 (22)	4.9 (22)	4.1 (18)	4.6 (20)	4.1 (18)	1.19	1.11
15a	94 (0.7)	25 (111)	21.5 (96)	18.7 (83)	24.0 (107)	22.9 (102)	1.15	1.05
15b	94 (0.7)	25 (111)	20.0 (89)	-17.9 (-80)	17.5 (78)	17.1 (76)	1.12	1.02
16	94 (0.7)	25 (111)	24.0 (107)	18.7 (83)	21.8 (97)	19.0 (84)	1.28	1.15
							Mean	1.15
							COV (%)	6.5

The predictions of Table A.8 can be repeated with the equivalent equation in terms of compressive strength using Equation (A.12). The resulting average ratio of observed  $V_{flcr}$  to predicted  $V_{flcr}$  is 1.1, with a COV of 14%.

The formation of flexural cracks did not cause a decrease in strength or stiffness of the specimens. Examples of the hysteretic behavior are shown in Figure A.8 through Figure A.12. In each case at least one load cycle was completed before a significant loss of stiffness was observed. Furthermore, the vertical reinforcement was sufficient to carry the load after flexure-shear cracking occurred. Based on these conclusions, no limiting design equations are proposed for flexure-shear cracking.

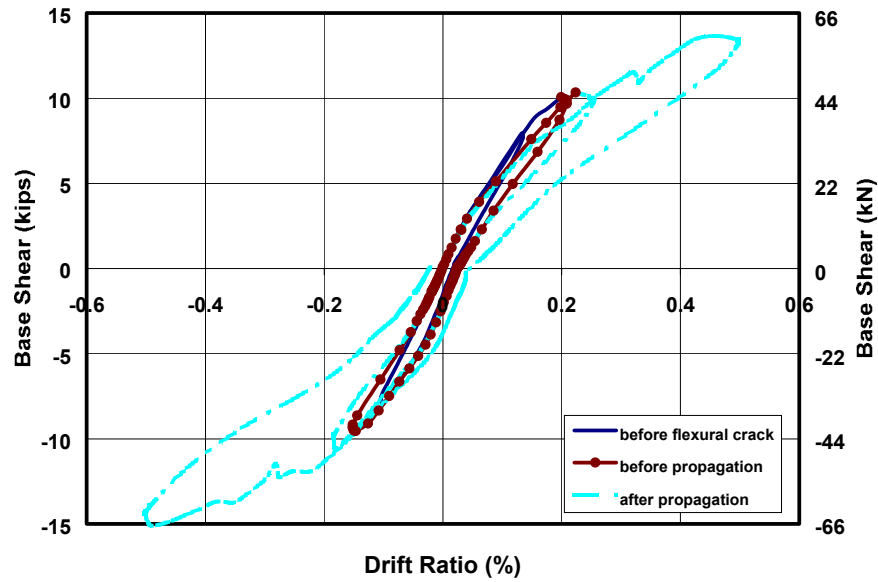


*Figure A.8 Hysteretic behavior of Shear Wall Specimen 13 before and after flexure-shear cracking*

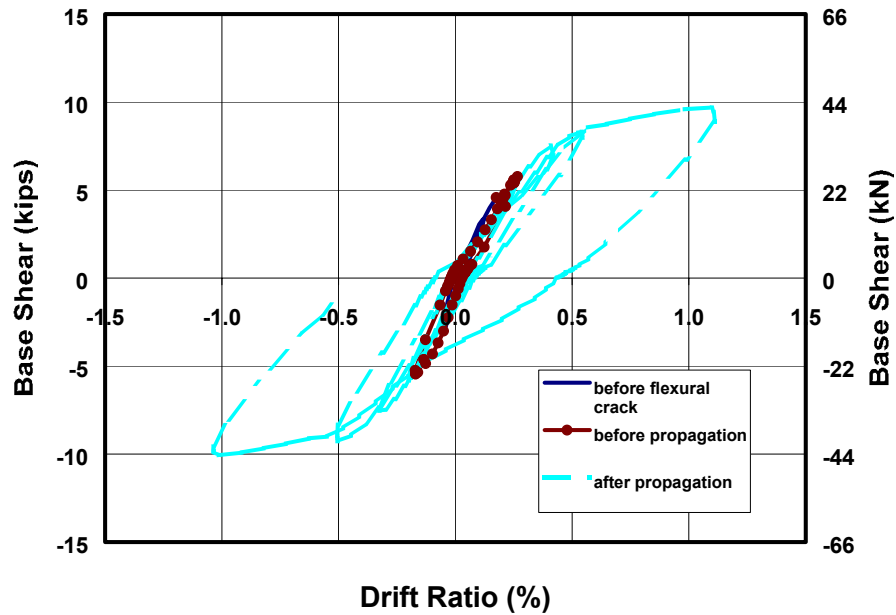


*Figure A.9 Hysteretic behavior of Shear Wall Specimen 14b before and after flexure-shear cracking*

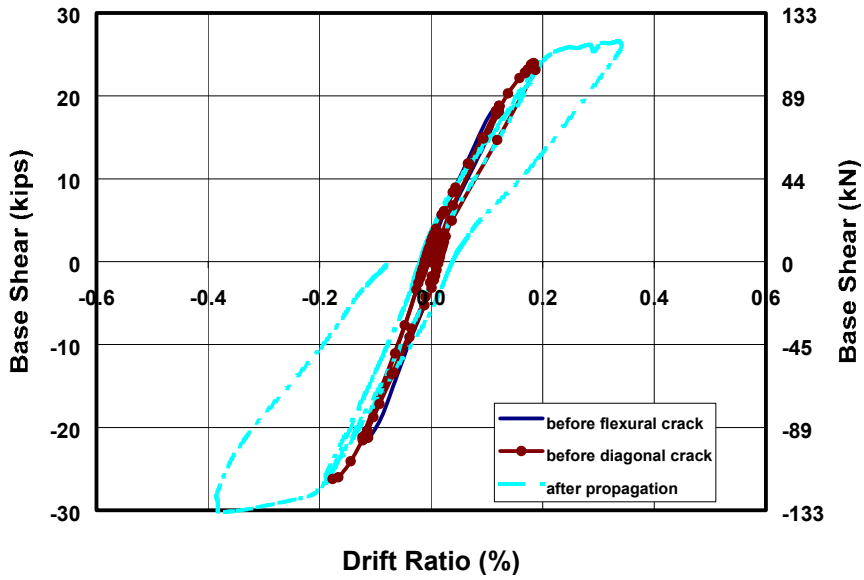


*Figure A.10 Hysteretic behavior of Shear Wall Specimen 15a before and after flexure-shear cracking*

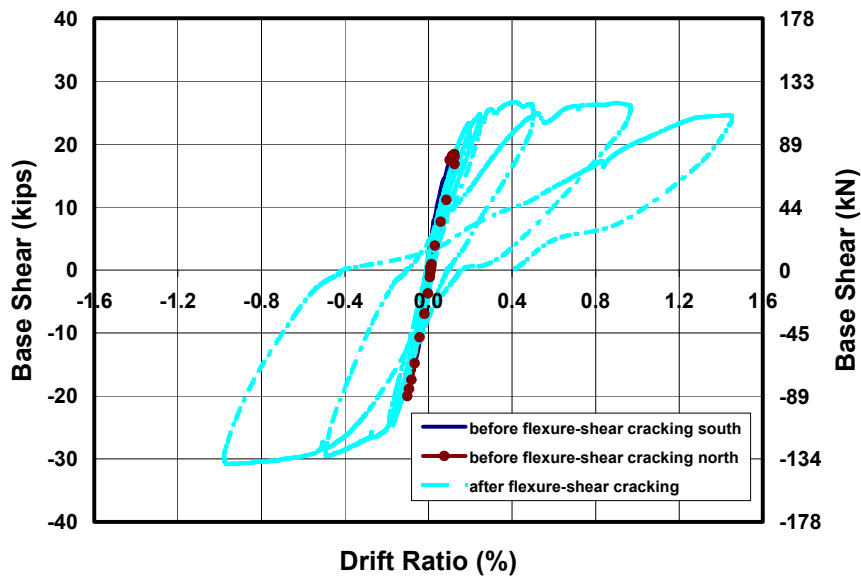


*Figure A.11 Hysteretic behavior of Shear Wall Specimen 15b before and after flexure-shear cracking*

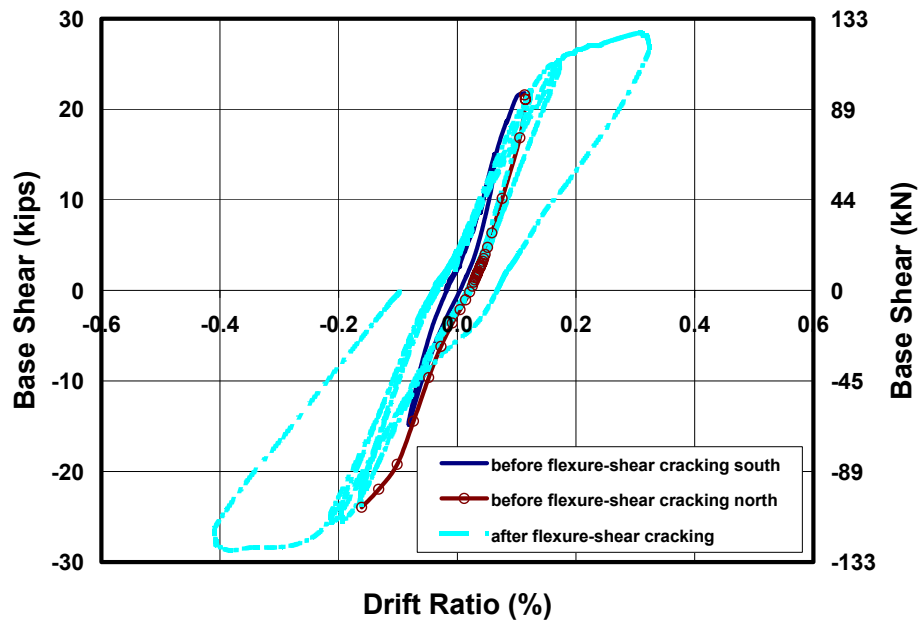


*Figure A.12 Hysteretic behavior of Shear Wall Specimen 16 before and after flexure-shear cracking*

### A.1.3 Crushing of the Diagonal Strut

An AAC shear wall can transfer load through the formation of a diagonal strut. The resultant of the applied lateral load and vertical forces acting on a wall is transferred along a diagonal strip in the wall (Figure A.13). The compressive force transferred along the diagonal strut is equilibrated at the base of the wall by the frictional resistance and by the vertical component of the compressive force in the diagonal strut. AAC shear walls with high axial loads can fail by crushing of this diagonal strut.

Crushing of the diagonal strut will occur in an AAC shear wall when the compressive stress in the strut exceeds the compressive strength of the AAC. Figure A.14 shows the external forces acting on an AAC shear wall due to in-plane shear and axial load.

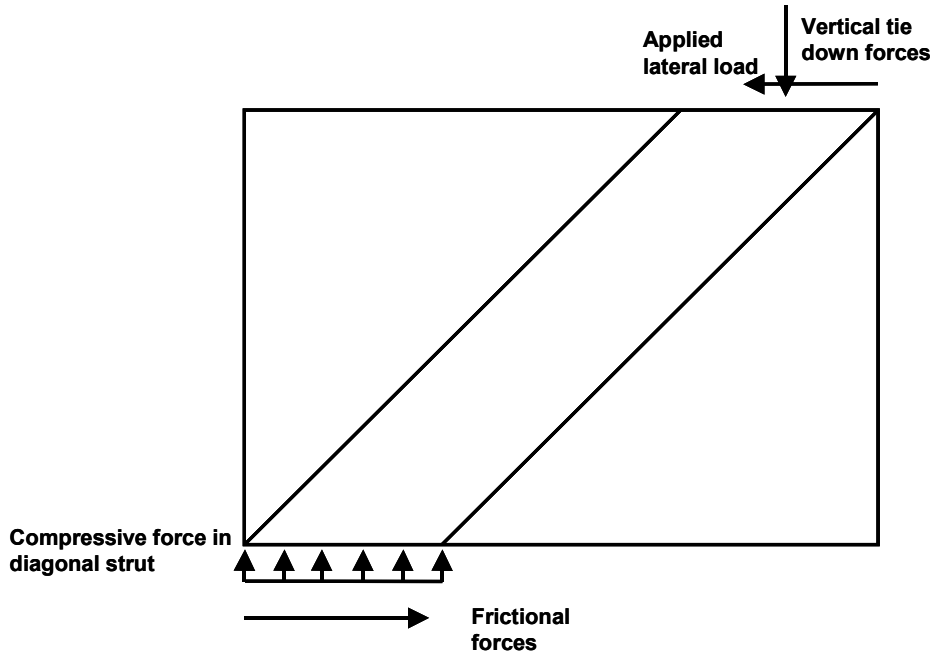


*Figure A.13 Diagonal compressive strut in an AAC shear wall*

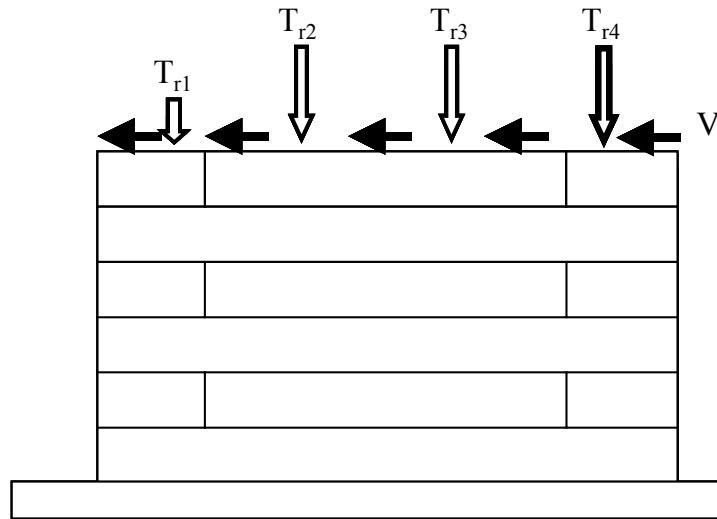


*Figure A.14 External forces acting on an AAC shear wall*

Diagonal crushing can be predicted using a strut-and-tie model consisting of two elements: a diagonal compression strut ( $F_{\text{strut}}$ ); and a tension tie-down force ( $T$ ). The compressive force in the diagonal strut is the resultant of the vertical tie-down forces and the applied horizontal load. Because the system is statically determinate, the vertical component is the summation of the force in the tie-down rods, and the horizontal component is the applied lateral load ( $V$ ).

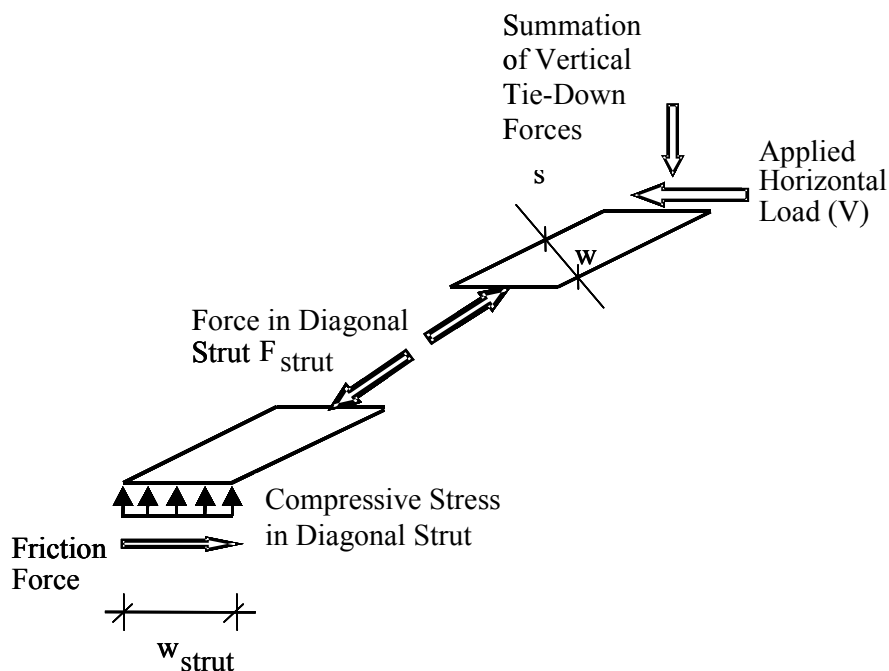


**Figure A.15** Forces acting on diagonal strut in an AAC shear wall

Equation (A.19) represents the horizontal force ( $V$ ) at crushing based on equilibrium of horizontal forces at the base of the diagonal strut. The derivation can be shown in Equation (A.13) to Equation (A.18). The limiting force in the diagonal strut is based on a uniform compressive stress acting over the smallest area of the strut, as shown in Equation (A.13). The maximum applied lateral load

is related by geometry to the force in the strut. Likewise, the minimum width of the strut can be related to the horizontal width of the diagonal strut. By substitution, the lateral load of Equation (A.19) can be expressed in terms of the wall geometry and horizontal width of the strut (see Equation (A.16) and Equation (A.17)).

$$F_{strut} = w t f_{AAC} \quad \text{Equation (A.13)}$$

$$V_{ds} = F_{strut} \cos(\theta) \quad \text{Equation (A.14)}$$

$$w = \sin(\theta) w_{strut} \quad \text{Equation (A.15)}$$

$$\quad \text{Equation (A.16)}$$

$$\cos(\theta) = \frac{l_w - w_{strut}}{\left[ h^2 + (l_w - w_{strut})^2 \right]^{0.5}}, \sin(\theta) = \frac{h}{\left[ h^2 + (l_w - w_{strut})^2 \right]^{0.5}} \quad \text{Equation (A.17)}$$

$$V_{ds} = w_{strut} \cdot t \cdot f_{AAC} \cos(\theta) \sin(\theta) \quad \text{Equation (A.18)}$$

$$V_{ds} = f_{AAC} \cdot t \cdot w_{strut} \left[ \frac{h \cdot (l_w - w_{strut})}{\left[ h^2 + (l_w - w_{strut})^2 \right]} \right] \quad \text{Equation (A.19)}$$

Shear Wall Specimen 1 (UT Austin) confirmed this proposed model for crushing of the diagonal strut. Minor spalling occurred at the toe at a load of 152 kips (676 kN), and major spalling, at a load of 167.6 kips (745 kN). The observed horizontal width of the diagonal strut was approximately one-quarter of the plan length. Using Equation (A.19), crushing of the diagonal strut for Shear Wall Specimen 1 was predicted at a lateral load of 185.1 kips (823 kN). The ultimate

load was 90% of the load predicted by the model for crushing of the diagonal strut. Since, the model for crushing of the diagonal strut was unconservative in this case, it is multiplied by a factor of 0.9. Equation (A.20) incorporates this factor and a width of the compression strut of  $0.25l_w$ . The results of the predicted lateral load at crushing of the diagonal strut, for an assumed strut width of one-quarter of the plan length, are presented along with the ultimate lateral load in Table A.9.

$$V_{AAC} = 0.17 \frac{f_{AAC} \cdot h \cdot l_w^2}{h^2 + \left(\frac{3}{4}l_w\right)^2} \quad \text{Equation (A.20)}$$

**Table A.9** *Predicted shear wall capacities as governed by crushing of the diagonal strut*

Specimen	$V_{ds}$ kips (kN)	$0.9V_{ds}$ kips (kN)	Maximum V kips (kN)	$0.9 V_{ds} -$ Maximum V	Maximum V / $0.9 V_{ds}$
1	185 (824)	167 (741)	168 (745)	-1 (-4)	1.01
3	154 (683)	138 (615)	118 (526)	20 (89)	0.86
4	315 (1403)	284 (1262)	126 (561)	158 (701)	0.44
5	246 (1093)	221 (984)	85 (377)	136 (607)	0.38
7	89 (394)	80 (355)	59 (263)	21 (91)	0.74
9	98 (436)	88 (392)	42 (189)	46 (204)	0.48
11	23 (100)	20 (90)	17 (74)	4 (16)	0.82
13	21 (93)	19 (84)	22.5 (100)	-4 (-16)	1.19
14a	36 (162)	33 (146)	9.9 (44)	23 (102)	0.30
14b	36 (162)	33 (146)	10.1 (45)	23 (101)	0.31
15a	121 (537)	109 (483)	30.1 (134)	79 (350)	0.28
15b	121 (537)	109 (483)	30.9 (137)	78 (346)	0.28
16	121 (537)	109 (483)	35.2 (157)	73 (327)	0.32

In the remaining shear wall specimens crushing of the diagonal strut was avoided by limiting the axial load. The validity of Equation (A.20) was indirectly determined by avoiding crushing. In Shear Wall Specimen 13, the maximum



lateral load was higher than the proposed equation for the design provisions without observing crushing of a diagonal strut. One reason for the discrepancy is that the assumed width of the diagonal strut of one-quarter of the plan length of the wall is no longer valid. The aspect ratio of Shear Wall Specimen 13 is 2. Since the model was adequate for walls with aspect ratios less than 2, that aspect ratio is used as an upper limit to the proposed Code equation.

#### **A.1.4 Sliding Shear Capacity**

An AAC shear wall of horizontal panels or masonry-type blocks exhibits a bed-joint crack when the shear stress on the bed joints exceeds the interface shear capacity,  $v$  (Figure A.18). An AAC shear wall subject to sliding shear across a horizontal bed joint is presented in (Figure A.16). After the crack forms the shear is resisted by the vertical reinforcement and frictional forces due to the axial load.

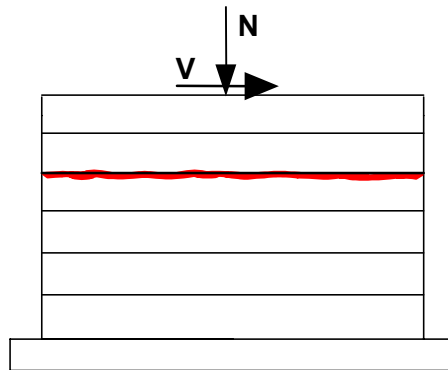


**Figure A.16** *Formation of bed-joint crack in an AAC shear wall with horizontal panels*

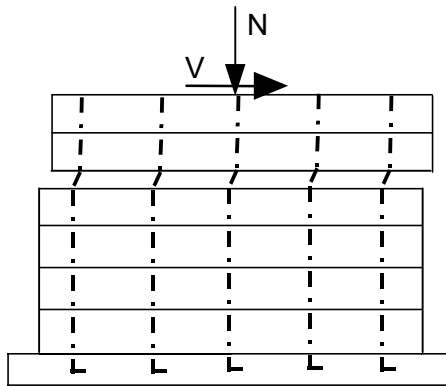


**Figure A.17 Sliding shear mechanism in an AAC shear wall with horizontal panels**

After the crack forms, some resistance will be provided by shear friction across the bed joints:

$$V_{ss} = \mu(A_v f_s + N) \quad \text{Equation (A.21)}$$

Sliding shear resistance is the product of the coefficient of friction across an interface, and the force acting perpendicular to that interface. This mechanism is referred to in ACI 318 as “shear friction.” This resistance can come from reinforcement crossing the interface and applied axial load.

In the traditional “shear friction” mechanism, sliding over a rough joint causes one section of the crack to lift upwards; this results in yielding of the vertical reinforcement, which provides additional clamping force. Under reversed cyclic loading of AAC, the roughness of the bed joints can decrease, and resistance to sliding shear is provided by dowel action of reinforcement crossing the bed joints. This contribution to  $V_{ss}$  is the area of the reinforcement

perpendicular to the crack and the shear resistance of the bars,  $0.6f_y$ . This contribution to the sliding shear mechanism is shown in Figure A.19.

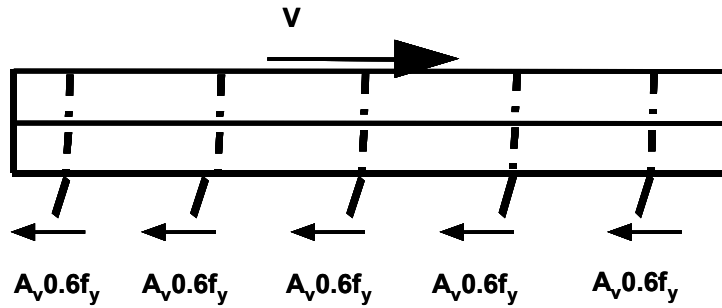


**Figure A.18** *Internal lateral forces generated by dowel action along plane of sliding shear mechanism*

Frictional resistance is the second component of resistance due to sliding shear. Figure A.19 is a free-body diagram showing the horizontal equilibrium due to frictional forces.

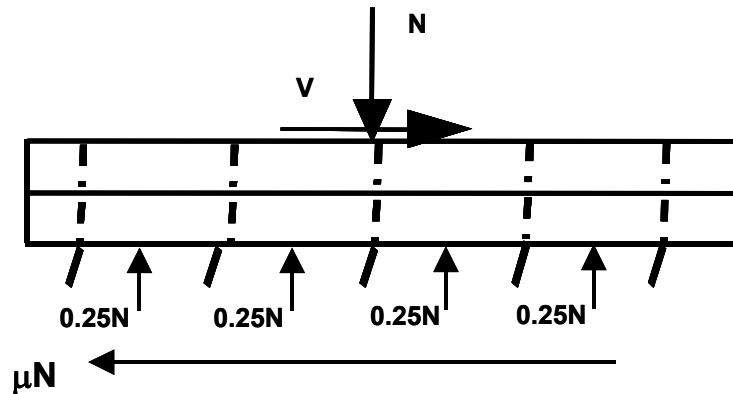


**Figure A.19** *Internal lateral forces generated by friction along plane of sliding for sliding shear mechanism*

$$V_{ss} = \mu N + 0.6A_s f_y \quad \text{Equation (A.22)}$$

In subsequent specimens, the clamping force  $N$  was determined such that the shear capacity will be limited by web-shear cracking or flexure-shear cracking, rather than bed-joint sliding. Sliding shear was avoided in 12 out of the remaining 14 specimens; it was observed in Shear Wall Specimen 4 and the Two-story Assemblage Specimen. Since the specimens were designed to avoid sliding shear, sufficient dowels were placed to ensure that  $V_{ss}$  was significantly greater than  $V_{AAC}$ . In four specimens,  $V_{max}$  was greater than  $V_{AAC}$ . Shear Wall Specimen 3 and Shear Wall Specimen 5 were both overdesigned in sliding shear. The load did not reach the sliding shear capacity because the specimen capacities were limited by distributed web-shear cracking. Shear Wall Specimen 4 and the Two-story Assemblage Specimen can be used to determine the effectiveness of Equation (A.22).

The hysteretic behavior for the Two-story Assemblage Specimen is shown in Figure A.20. The total base shear and sliding shear capacity for the specimen versus Load Point is presented in Figure A.21. The design sliding shear capacity is presented for the contribution of axial load and dowels (Equation (A.22)) and the contribution of axial load only. A coefficient of friction of 1.0 was used since the sliding plane occurred between the vertical panels and the leveling bed mortar. The entire axial load was applied through gravity, therefore, the axial load remained constant throughout the test. In this specimen the longitudinal steel and dowels contribute significantly to the capacity for several cycles. Damage around the dowels began at Load Point 677 and continued throughout the test. Each loading cycle was accompanied by increasing damage. The cumulative damage at each cycle is accompanied by a continually decreasing base shear, as shown in load points above 800 in Figure A.21.

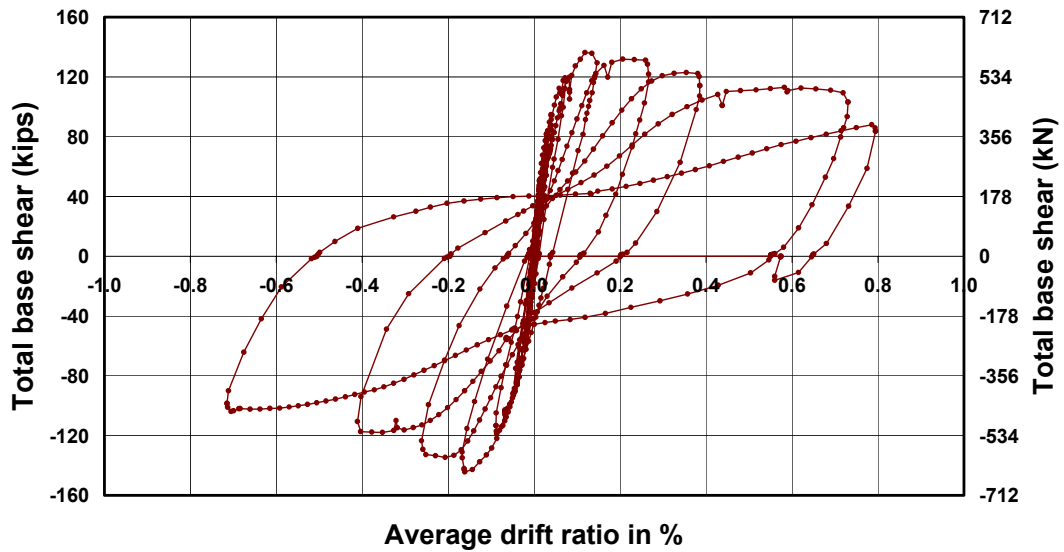


*Figure A.20 Hysteretic behavior of Two-story Assemblage Specimen*

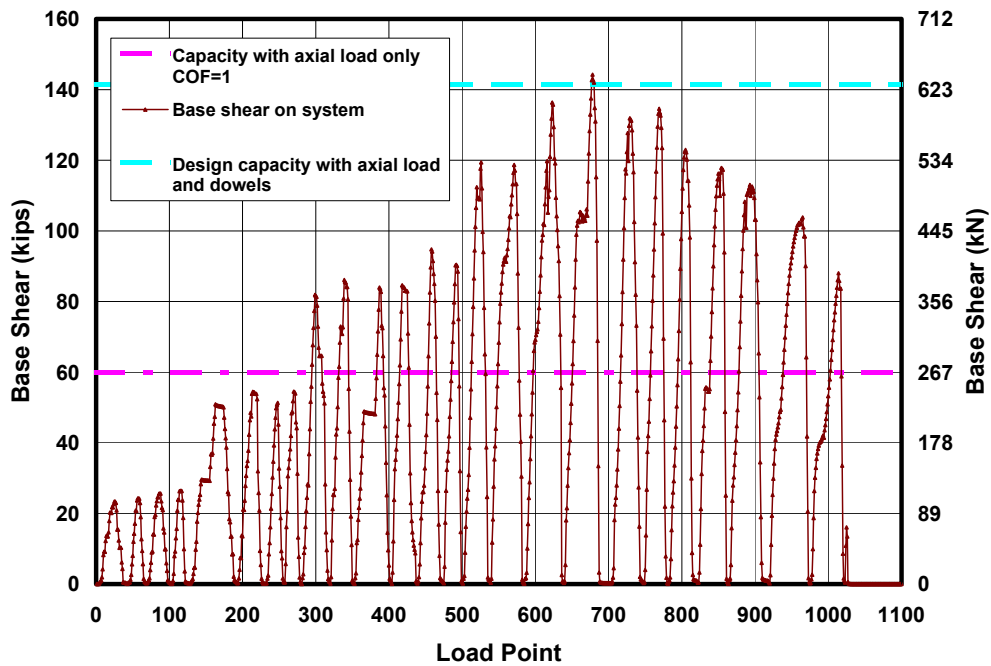


*Figure A.21 Base shear and sliding shear capacity versus Load Point for Two-story Assemblage Specimen*

Sliding was observed in two adjacent panels in Shear Wall Specimen 4. A horizontal crack formed along the bed joint between the second and third courses. This crack formed in three stages, corresponding to Load Points 634, 717 and 764. The final crack propagation occurred after the maximum base shear was reached. A graph of base shear versus Load Point for Shear Wall Specimen 4 is shown in Figure A.22. Since the sliding occurred between panels, a coefficient of friction of 0.8 was used to predict the capacity. The applied base shear increased beyond the sliding shear resistance for the level of axial load that was applied to the specimen. Several diagonal cracks formed at the compression toes of the walls. Spalling between these cracks occurred at Load Point 871.

The axial load consisted of three portions: gravity load from loading equipment; load applied through the load maintainer; and post-tensioning force in the rods. The pressure in the load maintainer system was checked during testing. It did not change, nor did the contribution of axial load due to gravity. Any decrease in axial load would therefore have to have occurred due to a loss of post-tensioning. This was observed in the spalling of the compression toe that occurred at Load Point 871. The loss of post-tensioning decreased the applied axial load and thus decreased the sliding shear capacity.

The measured axial load capacity of Figure A.23 includes the unchanged axial load and the measured force in the external rods. As the base shear increases, a slight increase is also observed in the axial load (see Load Point 1080 through 1110). This is the increase in load in the axial rods caused by the in-plane rotation of the wall about its compression toe. At later load points, at points of zero base shear the force in the rods decreases due to toe crushing. This can be observed in the difference between measured axial loads at two points where the

base shear is zero. For example, at Load Point 830 the measured axial load is 91 kips (405 kN); at Load Point 890 it decreases to 87 kips (387 kN); and at Load Point 960 it further decreases to 82 kips (365 kN).

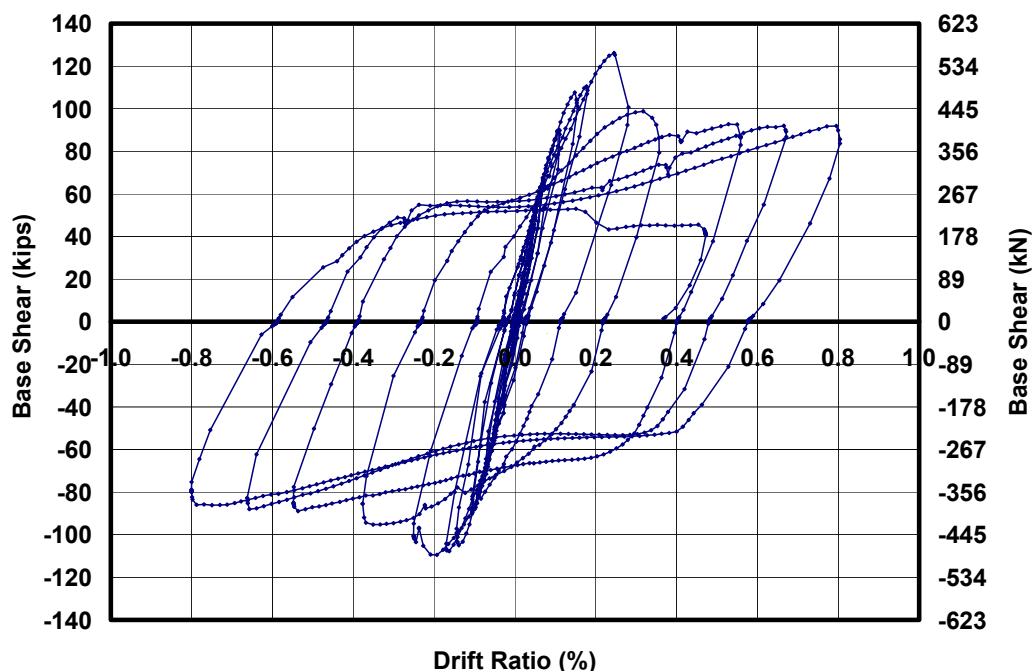


**Figure A.22** *Hysteretic behavior of Shear Wall Specimen 4*

For load points beyond 700 the base shear capacity decreases. This was also observed in the Two-story Assemblage Specimen. This is a further indication that as damage increases the effectiveness of the dowel action decreases. As the damage increases, the resistance provided by bearing on the dowel is reduced. For this reason, the proposed code language conservatively neglects the contribution of the dowels as shown in Equation (A.23).

$$V_{ss} = \mu N \quad \text{Equation (A.23)}$$

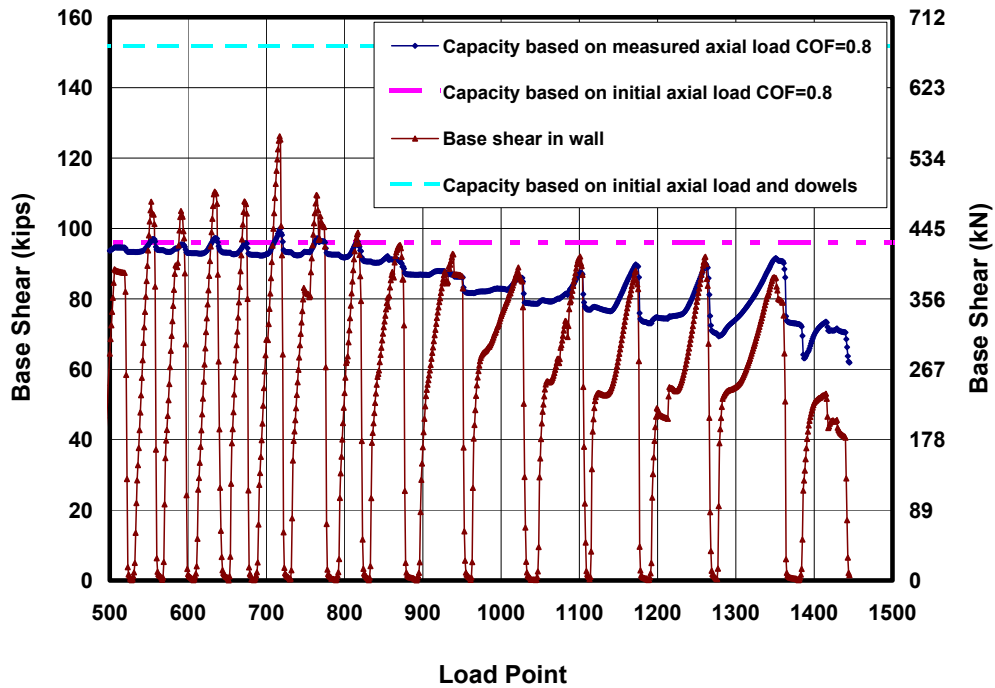


**Figure A.23** *Base shear and sliding shear capacity versus Load Point for Two-Story AAC Assbemblage Specimen*

Structures with small axial load may have low sliding shear capacity. In these cases the interface shear strength between AAC and thin-bed mortar may be used. Based on the direct shear tests performed at UT Austin, the average interface shear strength between AAC and thin-bed mortar was 64 psi (441 kPa), with a COV of 44%. A lower 5 % fractile is proposed, for design, reducing the interface shear strength to 17 psi (117 kPa). This value is conservative compared to test results of 45 psi (310 kPa) to 82 psi (565 kPa).



The measured axial load in Figure A.23 does not include the tensile forces in the internal reinforcement. Although those forces were not measured, they can be estimated based on flexural calculations. The wall instrumentation indicates that the longitudinal reinforcement in the wall had yielded at the bed joint where sliding occurred. When the lateral load is removed and the bed-joint gap closes, the bars will be subject to compression. Based on an assumed debonded bar length, the compressive forces can be estimated. The solid blue line in Figure A.24 shows the revised axial load considering compressive stresses in longitudinal reinforcement.

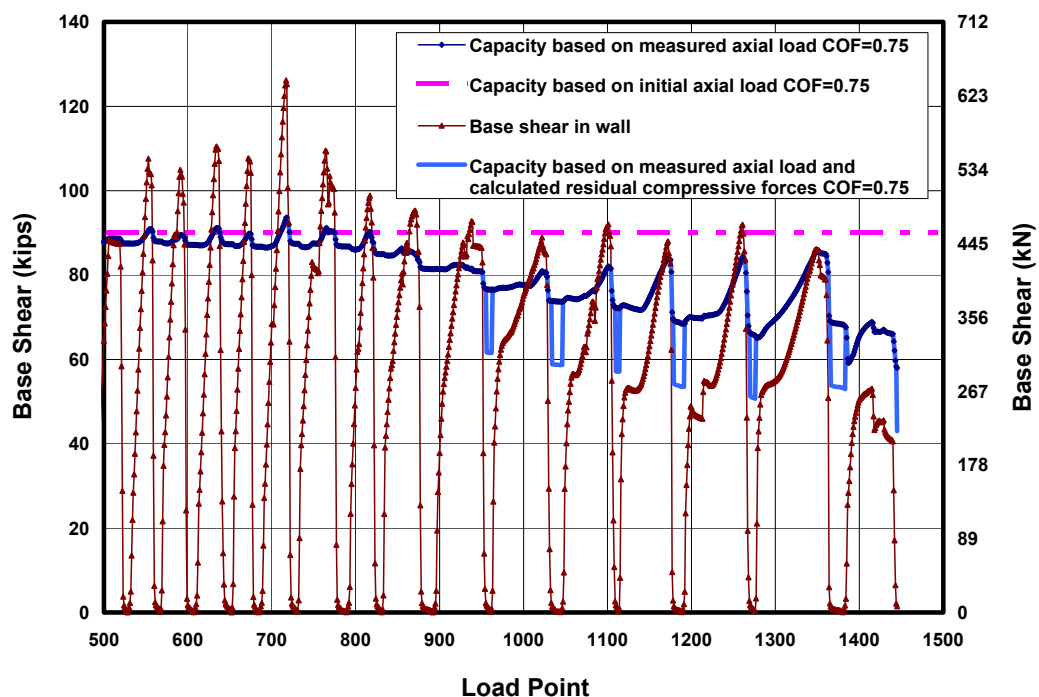


**Figure A.24** *Base shear and reduced sliding shear capacity versus Load Point for Two-story Assemblage Specimen*

### A.1.5 Nominal Flexural Capacity

The nominal flexural capacity of AAC shear walls can be determined based on equilibrium of a cross section. Using the proposed design provisions, the nominal flexural capacity of AAC shear walls can be predicted using conventional flexural theory. The compressive zone is determined based on a linear strain relationship, using a maximum useful compressive strain in the AAC of 0.003 (RILEM 1993 and Section 4.3.1), and an equivalent rectangular stress block whose height is  $0.85f'_{AAC}$  (or  $0.85f'_m$ ), and whose depth is  $\beta_1c$ , where  $\beta_1 = 0.67$  (Figure A.25). The value of  $\beta_1$  is selected to maintain equilibrium between the equivalent stress block and a triangular compressive stress distribution based on tested stress-strain results of Section 3.6.1.

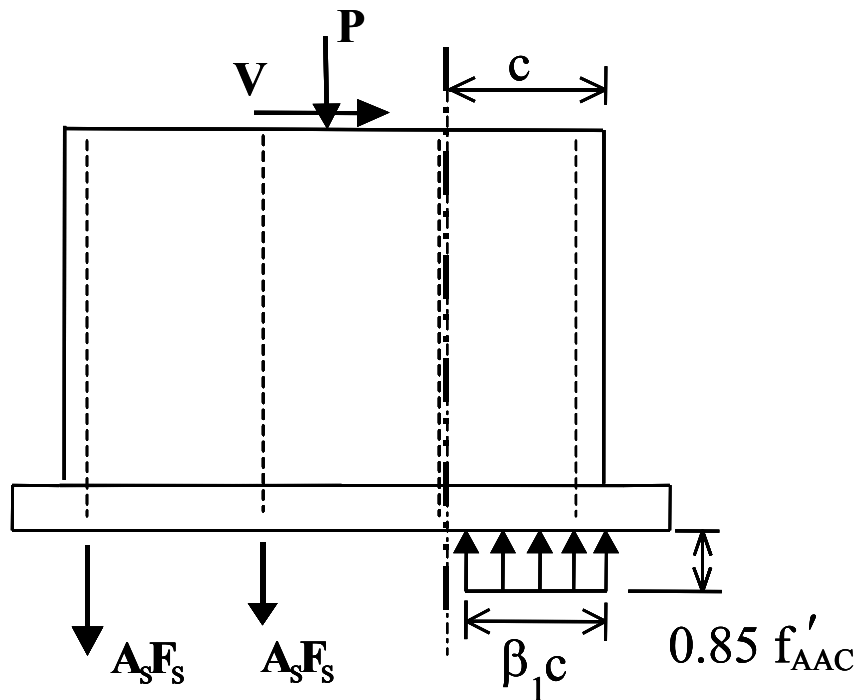


Figure A.25 Equilibrium of an AAC shear wall at nominal flexural capacity

Observed versus predicted nominal flexural capacities can be compared for flexure-dominated Shear Wall Specimen 14a, 14b, 15a and 15b. During the test of Shear Wall Specimen 13 and Shear Wall Specimen 16, the actuators used to apply the constant axial load inadvertently reached the end of their travel. As increasing lateral drifts were applied, axial load on the wall inadvertently increased. To successfully interpret those test results, the probable axial load applied to the walls was back-calculated from the predicted flexural capacity, removing those two tests from consideration for verifying observed versus predicted flexural capacity.

The nominal flexural capacity was calculated using a steel yield strength of 75 ksi (490 MPa), based on mill reports, along with the assumptions of 8.8.2. The ratios of observed to predicted strength range from 1.11 to 1.29, with an average of 1.19 and a COV of 5.8%. A refined analysis was performed considering strain hardening using RCCOLA (RCCOLA). The effect of strain hardening will increase the nominal flexural capacity as shown in the results of Table A.11. With this refinement the range of observed to predicted nominal flexural capacity ranges from 0.95 to 1.13. The average is 1.03 with a COV of 6.2%.

**Table A.10** *Observed versus predicted nominal shear capacities based on nominal flexural capacity*

Specimen	Predicted $V_{Mn}$ kips (kN)	Observed $V_{Mn}$ South kips (kN)	Observed $V_{Mn}$ North kips (kN)	Observed / Predicted $V_{Mn}$ South	Observed / Predicted $V_{Mn}$ North
14a	8.5 (38)	9.4 (42)	NA	1.11	NA
14b	8.5 (38)	9.9 (44)	10.1 (45)	1.16	1.19
15a	23.9 (106)	28.8 (128)	30.1 (134)	1.21	1.26
15b	23.9 (106)	26.7 (119)	30.9 (137)	1.12	1.29
Average					1.19
COV (%)					5.8

**Table A.11** *Observed versus predicted nominal shear capacities based on nominal flexural capacity with strain hardening included*

Specimen	Predicted $V_{Mn}$ kips (kN)	Observed $V_{Mn}$ South kips (kN)	Observed $V_{Mn}$ North kips (kN)	Observed / Predicted $V_{Mn}$ South	Observed / Predicted $V_{Mn}$ North
14a	9.9 (44)	9.4 (42)	NA	0.95	NA
14b	9.9 (44)	9.9 (44)	10.1 (45)	1.00	1.02
15a	27.4 (122)	28.8 (128)	30.1 (134)	1.05	1.10
15b	27.4 (122)	26.7 (119)	30.9 (137)	0.97	1.13
Average					1.03
COV (%)					6.2

## A.2 SPECIAL PROVISIONS FOR VERTICAL PANEL CONSTRUCTION

AAC panels oriented vertically have potential planes of failure along continuous head joints. These cracks may be attributed to shrinkage or weak joints, where the thin-bed mortar is not in contact with both panel faces. The presence of vertical cracks can change the behavior of a shear wall specimen. The observance of this behavior in Shear Wall Specimen 2 will be discussed then

theoretical and design methodologies will be presented in Sections A.2.1 and A.2.2.

In Shear Wall Specimen 2, two vertical cracks formed prior to testing. Shortly after flexural cracks formed another two vertical cracks formed and separated the wall into smaller sections. The initial cracks are indicated by gray lines and the cracks formed during testing are indicated by black lines in Figure A.26. The first diagonal crack formed at a load of 55.6 kips (247 kN). As the load increased, additional vertical and diagonal cracks formed in the specimen (Figure A.27).

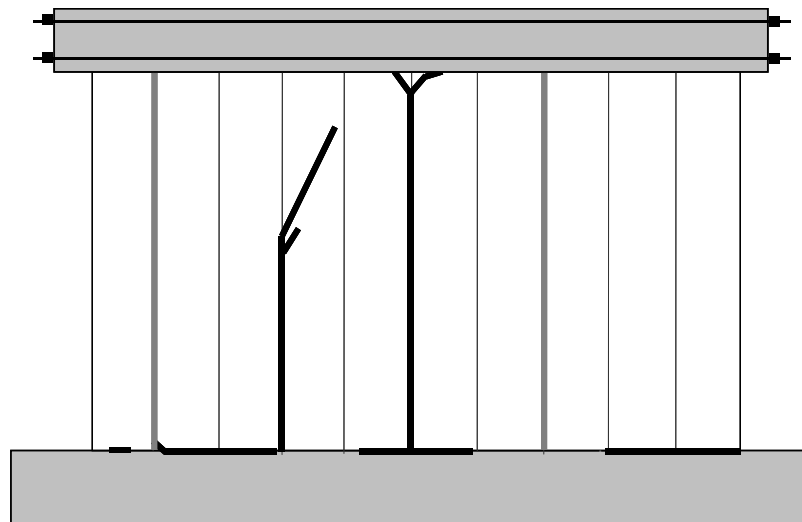


**Figure A.26** *Formation of first diagonal crack in Shear Wall Specimen 2*

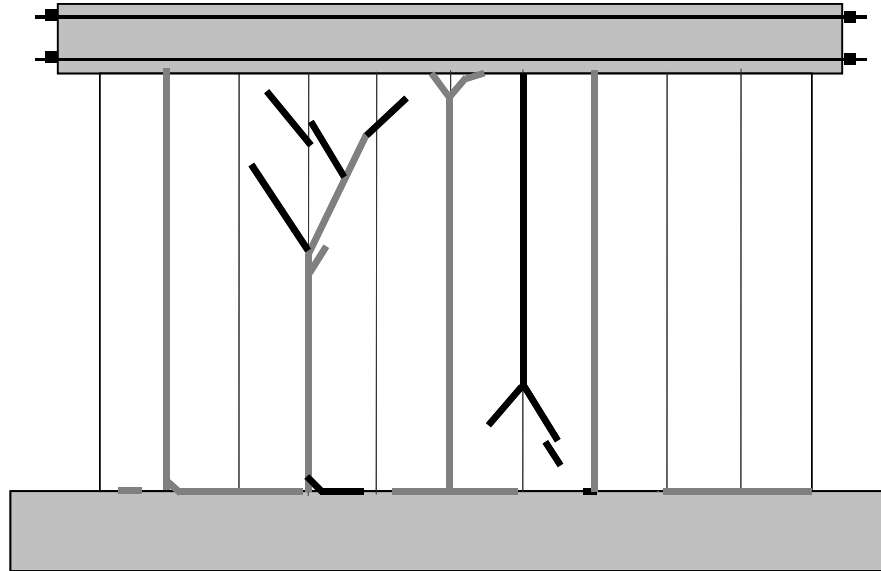


*Figure A.27 Formation of additional cracks in Shear Wall Specimen 2*

### **A.2.1 Prediction of Flexural and Shear Capacities for AAC Shear Walls with Vertically Oriented Panels**

In the case of monolithic behavior, the wall behaves as a cantilever (see Figure A.28). In the case of individual panels, the stiffness of the loading beam is large compared to a single panel, and the loading beam restrains the wall at the top (Figure A.29). If the wall behaves monolithically, the shear capacity will remain the same as presented in Section A.1, and the flexural design will be conventional. If the panels are separated by vertical cracks at the head joints, however, the behavior will change. That is the subject of this section.

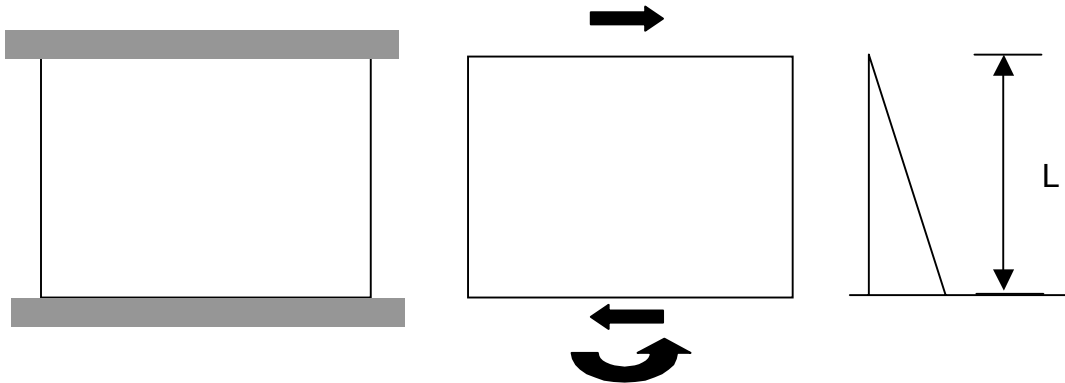


**Figure A.28** Behavior of monolithic AAC shear wall

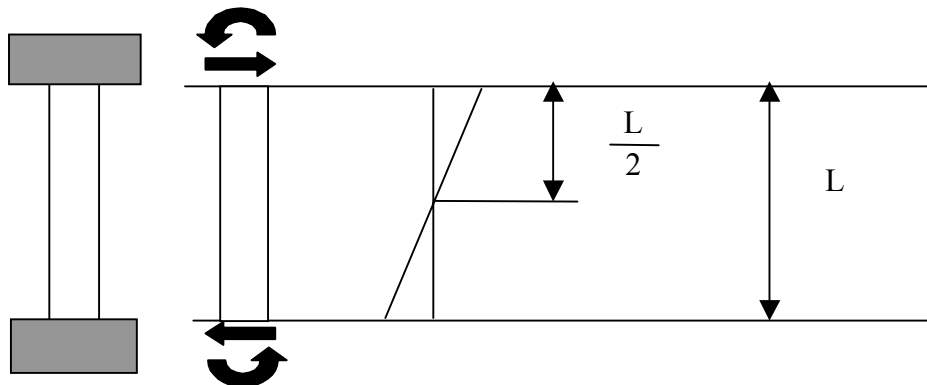


**Figure A.29** Behavior of individual panel for an AAC shear wall

The most critical case would be panels with vertical cracks at every section. The flexural capacity can be predicted based on the sum of the capacity of the individual panels. An interaction diagram for a single panel can be calculated and the flexural capacity of each panel can be determined based on the axial load in the respective panel; a value that depends on the forces acting on the wall. The lateral load will produce a series of axial loads in each panel that vary linearly based on the wall geometry. The applied axial load per panel will be the total axial load divided by the number of panels (see Figure A.30).

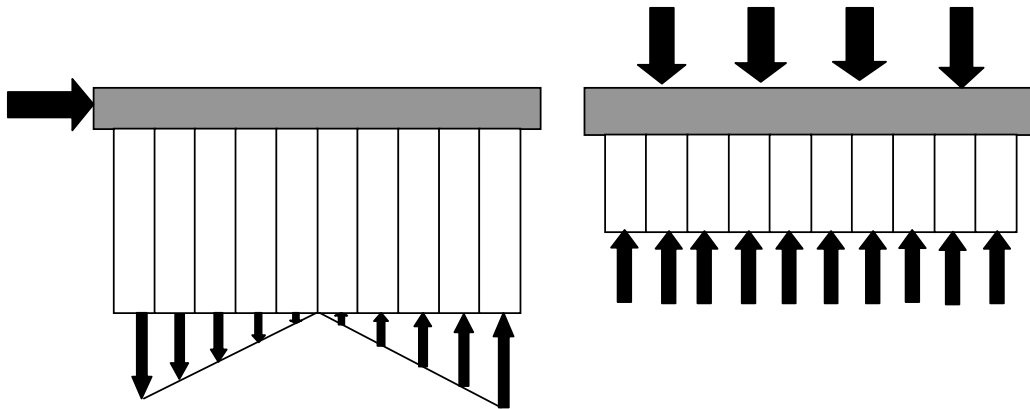


**Figure A.30** *Distribution of axial loads for laterally loaded condition and axially loaded condition*

If the net axial load applied to each panel is within the straight-line portion of the interaction diagram for a single panel, the total wall capacity will be the capacity at the axial load in a single panel, multiplied by the number of panels:

$$V_{wall} = \Sigma V_{panels} \quad \text{Equation (A.24)}$$

$$M_{wall} = \Sigma M_{panels} \quad \text{Equation (A.25)}$$

If the wall behaves as individual panels, the aspect ratio of piece becomes large; each panel behaves as a beam subject to compressive and lateral loads. The shear capacity in this condition can be predicted using the shear equations for beams presented in Section 4.5.



### **A.2.2 Verification of Shear Capacity for Vertical-Panel Shear Walls Tested at UT Austin**

The application of the individual panel design equations and the monolithic wall equations for Shear Wall Specimen 2 is presented in Figure A.31. The base shear at which cracking occurred was 55 kips (245 kN), and the maximum base shear was 92 kips (410 kN). Both are presented in the figure. The design equations are much more conservative than the wall behavior.

Several conditions can increase the performance of a head joint between vertical panels:

- a) Cleaning and wetting the panel face prior to application of the thin-bed mortar improves the adhesion.
- b) Applying mortar to both faces of the vertical joint improves the mortar coverage at the joint.
- c) Clamping adjacent panels applies pressure and improves the joint quality.

In Shear Wall Specimen 2 the panel faces were prepared and pressure was applied perpendicular to the joint, parallel to the plane of the wall. Initially, the joints were not mortared on both faces. After a lack of coverage was observed in several joints, the panel was removed, cleaned and re-installed with mortar applied to both faces of the joint. This procedure was applied thereafter. The joint was clamped at the base (using one clamp on each wall face) and at the top (using one clamp at the centerline of the wall).

In the remaining specimens constructed of vertical panels (Shear Wall Specimens 15, 16 and the Two-story Assemblage Specimen), vertical cracks were not observed. In each case the three previous construction recommendations were used. Pressure was applied to the joint using 4 clamps, one clamp on each wall face, both at the bottom and top of the wall.

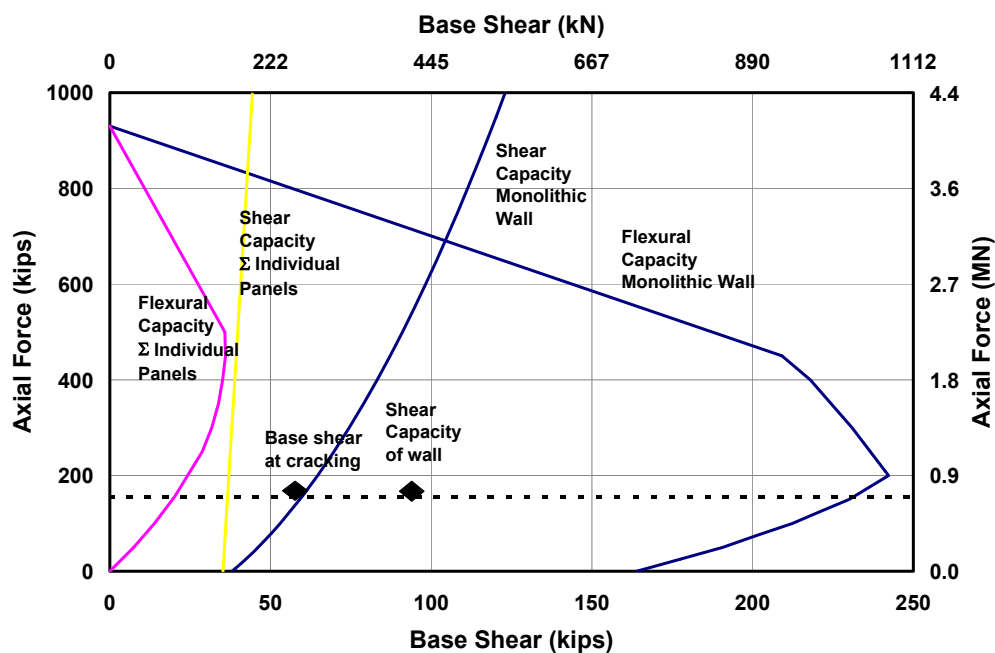


**Figure A.31** Base shear capacity for Shear Wall Specimen 2 considering individual panel behavior and monolithic wall behavior

In these specimens, vertical cracks at the joints were not observed until the end of the test when the wall stiffness was reduced due to prior cracks. Furthermore, the cracks left at least three panels joined together. For this construction type, the proposed design recommendation is to relax the individual panel requirements to groups of three panels connected together. The changes to the flexure and shear design capacities are presented in Figure A.32. Equation

(A.3) to predict web-shear cracking was used for panel groups with an aspect ratio less than 2.

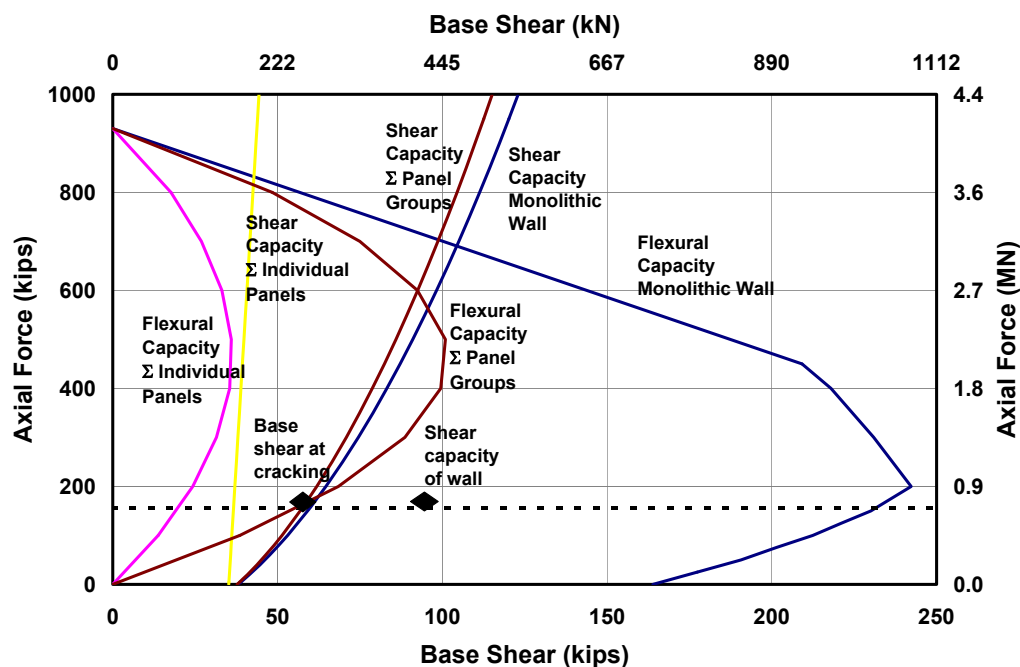


**Figure A.32** Base shear capacity for Shear Wall Specimen 2 considering individual panel behavior, behavior of panel groups and monolithic wall behavior

### A.2.3 Special Provisions to Avoid Longitudinal Cracking at the Location of Vertical Reinforcement

In each of the flexure-dominated specimens vertical (longitudinal) cracks formed along the grouted cores and the surrounding AAC. In the following sections the observed load at which these cracks formed is presented, along with two analyses to determine if the cracks occurred before yielding of the flexural reinforcement. The effect of these longitudinal cracks is presented, followed by design recommendations intended to prevent their formation.

#### A.2.4 Formation of Cracks along Longitudinal Bars in AAC Shear Walls

The base shears at which cracks formed along longitudinal reinforcement formed are presented in Table A.12. The base shear at which the first and second cracks formed along the vertical reinforcement is presented in Column 2 of that table. No second observed vertical crack data are presented for Shear Wall Specimen 14a, because that wall was tested in one direction only. The base shear at the expected flexural capacity (nominal capacity increased by steel overstrength) is presented in Column 3.

**Table A.12** *Ratio of base shear at formation of vertical cracks to base shear at expected flexural capacity (including overstrength) in the flexure-dominated shear wall specimens*

AAC Shear Wall Specimen	Base shear at first and second observed vertical crack, kips (kN)	Base shear at expected flexural capacity ( $f_s=1.25f_y$ ) $V_{max}$ kips (kN)	Ratio of base shear at observed crack to $V_{max}$ ( $f_s=1.25f_y$ )
13	13.6 (60) – first 15.6 (69) - second	13.0 (58)	1.05 – first 1.20 – second
14a	6.9 (31) – first NA – second	8.3 (37)	0.83 – first NA – second
14b	7.0 (31) – first 9.8 (44) - second	8.3 (37)	0.84 – first 1.18 – second
15a	26.5 (118) – first 27.3 (128) - second	23.8 (106)	1.11 – first 1.15 – second
15b	17.5 (78) – first 24.5 (109) - second	23.8 (106)	0.74 – first 1.03 – second
16	24.0 (107)– first 28.0 (125) - second	25.5 (113)	0.94 – first 1.10 – second

The ratios of base shear at the observed crack to the base shear at the expected flexural capacity range from 0.74 to 1.20, with an average of 1.02 and a COV of 16%. Longitudinal cracks were observed in three specimens at 74% to 84% of the expected flexural capacity. The ratios of base shear at cracking to expected flexural capacity, along with a corresponding normal distribution, are shown in Figure A.33. As shown in that figure, it is highly probable that an AAC

shear wall will reach between 74% and 84% of its expected flexural capacity in a moderate to strong earthquake, and therefore highly probable that such longitudinal cracks would form.

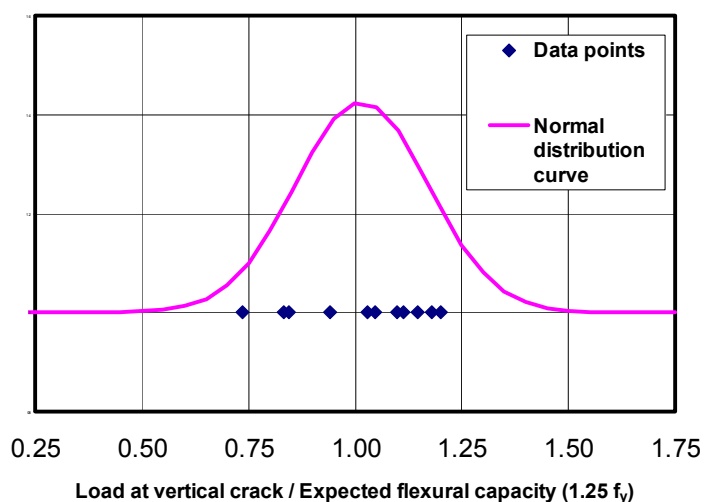


**Figure A.33** *Ratio of base shear at observed longitudinal crack to base shear at expected flexural capacity ( $f_s=1.25 f_y$ )*

For lower base shears, a similar analysis can be performed. The results of Table A.12 are reproduced based on nominal moment capacity (rather than expected), and are presented in Table A.13. In this case the ratios of base shear at longitudinal cracking to base shear at nominal capacity range from 0.84 to 1.42, with an average of 1.2 and a COV of 15.5%. These data are illustrated graphically in Figure A.34. The ratio of 1.0 between base shear at longitudinal cracking to base shear at nominal flexural capacity, corresponds to a 16% lower fractile. A 5% lower fractile corresponds to a ratio of 0.88. Based on these results, 5% of shear walls would exhibit longitudinal cracking at the factored nominal flexural capacity. To further determine if vertical cracks would occur at service loads, analyses were performed to determine if the cracks formed prior to yielding, and are presented in the following section.

**Table A.13** *Ratio of base shear at observed vertical cracking to the nominal flexural capacity (without overstrength) in flexure-dominated AAC shear wall specimens*

Specimen	Base shear at first and second observed vertical crack kips (kN)	Base shear at design flexural capacity $V_{Mn}$ kips (kN)	Ratio of base shear at first observed crack to $V_{Mn}$
13	13.6 (60) – first 15.6 (69) - second	11.4 (51)	1.19 – first 1.37 – second
14a	6.9 (31) – first NA – second	6.9 (31)	1.00 – first NA – second
14b	7.0 (31) – first 9.8 (44) - second	6.9 (31)	1.01 – first 1.41 – second
15a	26.5 (118) – first 27.3 (128) - second	20.9 (93)	1.27 – first 1.31 – second
15b	17.5 (78) – first 24.5 (109) - second	20.9 (93)	0.84 – first 1.17 – second
16	24.0 (107) – first 28.0 (125) - second	22.2 (99)	1.08 – first 1.26 – second

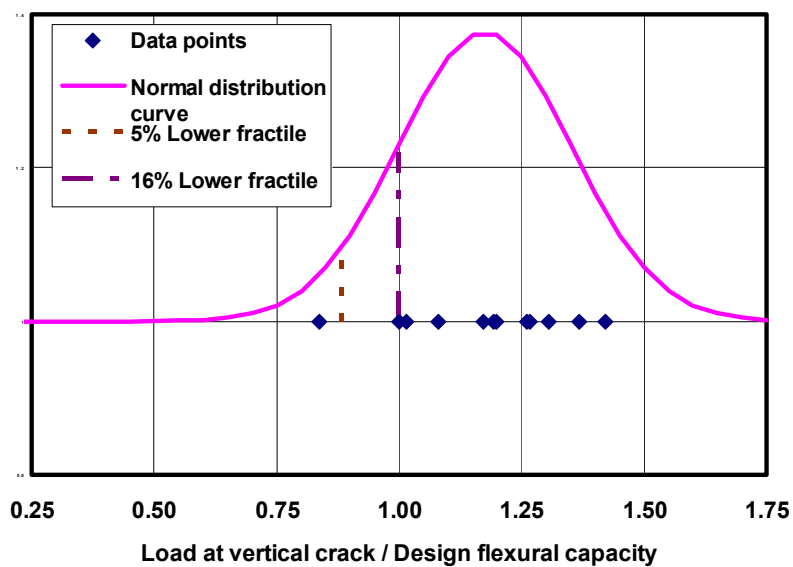


**Figure A.34** *Ratio of base shear at observed longitudinal crack to base shear at nominal flexural capacity without overstrength*

### **A.2.5 Analysis to Determine if Longitudinal Cracks Formed Prior to Yielding**

Additional analysis was performed to determine if longitudinal cracks formed before or after the vertical reinforcement yielded. If the vertical cracks formed prior to yielding, then those cracks might also be present in walls at factored design loads. If the vertical cracks formed after yielding, it can be assumed that they would occur only during overloading beyond the nominal capacity.

Strain was measured by three strain gages on the longitudinal reinforcement at each end of the wall. If one strain gage indicated strains beyond yield and another strain gage indicated strains near but not exceeding yield, this was assumed to denote yielding. The base shear and load points at the formation of longitudinal cracks in each specimen, while loading to the south and to the north, are recorded in Column 2 of Table A.14. In Shear Wall Specimen 13, strain gage data were not available; for this reason, in Column 2 both the South and North loading directions are labeled “NA.” The base shear and load points at the yielding of the flexural reinforcement are presented in Column 3. Since load points are assigned in ascending order, the first event (either longitudinal cracking or yielding of longitudinal reinforcement) has the lowest-numbered load point. The event that occurred first for each loading direction is presented in Column 4. If the load-point numbers did not vary by more than 5, it was assumed that longitudinal cracking occurred simultaneously with yielding of flexural reinforcement, and was therefore associated with that yielding. For example, in Shear Wall Specimen 14a while loading to the south, longitudinal cracking was observed at Load Point 542, and the longitudinal reinforcement was determined to have yielded at Load Point 539. Since these load points do not vary by more than

5, it was concluded that the longitudinal cracking and yielding of the reinforcement occurred simultaneously, as indicated in Column 4. Finally, the ratio of base shear at longitudinal cracking to base shear at yielding is presented in Column 5.

**Table A.14** *Estimation of order of vertical cracking and yielding of longitudinal reinforcement, based on strain gages*

Specimen	Base shear at observed vertical crack, loading south and loading north, Kips (kN) Load point	Base shear at yielding of flexural reinforcement, loading south and loading north, kips (kN) Load point	Estimated order of yielding of reinforcement and longitudinal cracking	Ratio of base shear at formation of longitudinal crack of base shear at yielding of flexural reinforcement
13	13.6 (60) LP 1023 – S 15.6 (69) LP 1232 - N	NA – S NA – N	NA – S NA – N	NA – S NA – N
14a	6.9 (31) LP 542 – S NA – N	6.2 (27.6) LP 539 – S NA – N	Together – S NA – N	1.1 – S NA – N
14b	7.0 (31) LP 326 – S 9.8 (25) LP 487 - N	7.5 (33) LP 327 – S 8.9 (40) LP 410 – N	Together – S Yielding – N	0.9 – S 1.1 – N
15a	28.8 (128) LP 437 – S 27.3 (121) LP 528 – N	22.1 (98) LP 299 – S 26.0 (116) LP 333 – N	Yielding – S Yielding – N	1.3 – S 1.1 – N
15b	17.5 (78) LP 202 – S 24.5 (109) LP 338 – N	23.7 (102) LP 363 – S 24.5 (109) LP 340 – N	Cracking – S Together – N	0.7 – S 1.0 – N
16	28.0 (125) LP 716 – S 24.0 (107) LP 426 - N	27.0 (120) LP 704 – S 26.8 (119) LP 754 – N	Yielding – S Cracking – N	1.0 – S 0.9 – N

In four cases, yielding occurred before longitudinal cracking; and in two cases, it occurred afterwards. In the remaining cases these events probably occurred simultaneously. In both cases where the flexural reinforcement yielded after longitudinal cracks were observed, the ratio of base shear at formation of longitudinal cracking to base shear at yielding was also less than 1. This further supports the conclusion that if #5 bars are used in 3-in. grouted cores, longitudinal cracks may form prior to yielding of the flexural reinforcement. The ratio of base shear at longitudinal cracking to base shear at yielding is less than 1.25 for all of the specimens, which indicates that longitudinal cracks will probably form prior



to reaching the nominal flexural capacity considering a strain hardening factor of 1.25. This analysis does not consider the height at which the vertical crack formed. If the crack formed at a height of 48 in. (1.2 m) the stress in the reinforcement could be significantly below yield. The impact of crack height is considered in a separate analysis.

An additional analysis was performed to estimate the stress in the flexural reinforcement at longitudinal cracking, using elastic flexural stresses calculated based on a cracked transformed section (Table A.15). The applied base shear was converted to an applied moment at the location of the crack by multiplying by the height of the wall minus the crack height. The stress in the longitudinal tensile reinforcement was computed using Equation (A.26). The contributions from the axial load are not presented in Table A.15 because they were less than 2 ksi (14 MPa). The distance from the neutral axis to the centroid of the tensile reinforcement is denoted by  $y_{As}$ ; the modular ratio between steel and AAC is denoted by  $n$ ; and the cracked transformed moment of inertia is denoted by  $I_{ctr}$ . The results indicate that in 6 of the 11 cases, calculated stresses at longitudinal cracking exceeded the expected yield strength of 75 ksi (10.9 GPa). This indicates that approximately half of the vertical cracks occurred prior to or simultaneously with yielding of the flexural reinforcement.

$$\sigma_{As} = \frac{My_{As}n}{I_{ctr}} - \frac{Pn}{A_{tr}} \quad \text{Equation (A.26)}$$

**Table A.15** *Calculated stresses in tensile reinforcement based on elastic theory for vertical cracks on the south and north sides of the specimen*

Specimen	Base shear at observed vertical crack, loading south and loading north kips (kN)	Height of the vertical crack in. (m)	Cracked transformed moment of inertia in. <sup>4</sup> (m <sup>4</sup> )	yAs, distance from the area of tensile steel to the neutral axis in. (m)	Calculated stress in tensile reinforcement for first observed vertical crack ksi (GPa)
13	13.6 (60) – S 15.6 (69) – N	24 (0.6) – S 24 (0.6) – N	64900 (0.027)	45 (1.1)	96 (0.67) – S 111 (0.79) – N
14a	6.9 (31) – S NA – N	48 (1.2) – S NA – N	46100 (0.019)	39 (1.0)	49 (0.35) – S NA – N
14b	7.0 (31) – S 9.8 (44) – N	24 (0.6) – S 48 (1.2) – N	46100 (0.019)	39 (1.0)	61 (0.44) – S 70 (0.50) – N
15a	28.8 (128) – S 27.3 (121) – N	48 (1.2) – S 0 (0) – N	226800 (0.094)	86 (2.2)	91 (0.65) – S 127 (0.90) – N
15b	17.5 (78) – S 24.5 (109) – N	12 (0.3) – S 24 (0.6) – N	226800 (0.094)	86 (2.2)	74 (0.53) – S 95 (0.68) – N
16	28.0 (125) – S 24.0 (107) – N	0 (0) – S 24 (0.6) – N	309100 (0.129)	94 (2.4)	104 (0.73) – S 75 (0.54) – N

### A.2.6 Implications of the Formation of Longitudinal Cracks

The above evaluations show that longitudinal cracks are highly probable in real AAC shear walls subject to lateral loads. This section is devoted to explaining the probable consequences of those cracks and providing design recommendations for preventing them.

Cracks along reinforcement in a grouted core are inherently undesirable, because they provide an opportunity for air and water to enter the core, and thereby increase the probability of corrosion of that reinforcement. Longitudinal cracks along the height of the wall, combined with horizontal cracks, can cause the end blocks to spall and crush sooner than in otherwise identical walls without longitudinal cracks (Figure A.35). Longitudinal cracks can also lead to buckling of the longitudinal reinforcement in the compression toe (Figure A.36).



**Figure A.35** *Loss of end block on compression toe in Shear Wall Specimen 16*

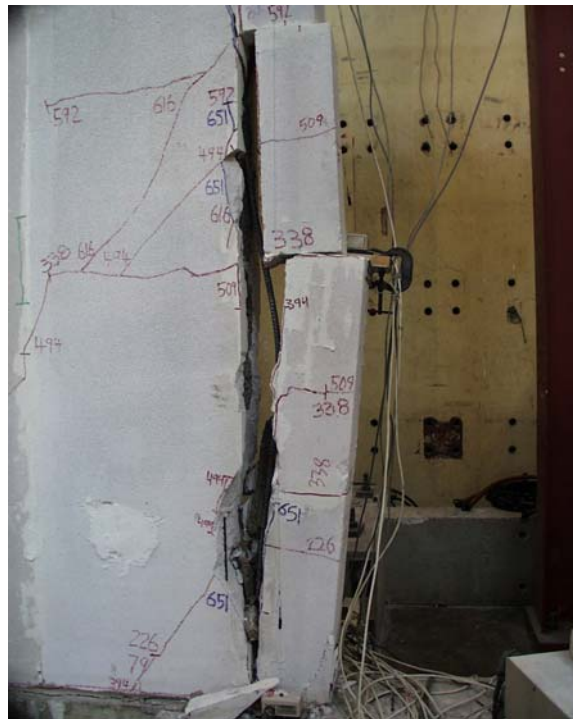


**Figure A.36** *Loss of end blocks and buckling of compression reinforcement in Shear Wall Specimen 15b*

As the load is reversed, the previously buckled longitudinal reinforcement may fracture, effectively reducing the wall's flexural capacity to zero. Examples of the undesirable consequences of loss of the compression toe are shown by Shear Wall Specimen 15b and Shear Wall Specimen 16.

Resistance to cracks along longitudinal reinforcement could be increased. Longitudinal splitting cracks could be prevented by increasing the size of grouted core or decreasing the bar diameter. This is equivalent to limiting the ratio of area of the longitudinal reinforcement to area of core (area ratio).

The area ratio of a #5 (17 mm) bar in a 3-in. (76 mm) diameter grouted core (4.4%) was observed to produce splitting along longitudinal bars in plastic hinge zones. This is inherently undesirable for AAC shear walls. Such cracking not been observed with #4 bars in 3-in. grouted cores, even at splices. A #4 (12 mm) bar in a 3 in. (76 mm) core corresponds to an area ratio of 2.8%. For that reason, the proposed design provisions for AAC masonry and reinforced AAC panels limit the maximum ratio of the area of reinforcement to the area of the grouted core containing that reinforcement, to 3% in plastic hinge zones.

#### **A.2.7 Analysis of Maximum Permissible Area Ratio if Longitudinal Reinforcement Remains Elastic**

Area ratios of reinforcement up to 4.5% are permitted, provided that radial (splitting) stresses can be limited by limiting the bond stress, which in turn means limiting the shear. The formation of radial stresses is explained in Section 8.8 of this dissertation, and briefly reviewed here.

After the initial adhesion between the reinforcement and concrete is broken, load is transferred from deformed reinforcement to the surrounding concrete or grout by the deformations (lugs). The axial component of the force transferred by the lugs to a vertical core is the difference in force ( $\Delta T$ ) in a section of vertical reinforcement (Figure A.37). The associated radial component of that force also acts on the surrounding grout (Figure A.37). The resultant forces generally act at about 45 degrees to the axis of the reinforcement, so that the resultants of the radial and axial component of the forces are equal. The radial forces generated per length of the bar equal the change in force in the bar over that same length. The pressure generated by the radial forces in the longitudinal bar can be determined by dividing the radial forces by the product of the circumference of the deformed bar and the length of the section of the bar,  $\Delta x$ , as shown in Figure A.37. The diameter of the longitudinal bar is denoted by  $d_{\text{bar}}$ .

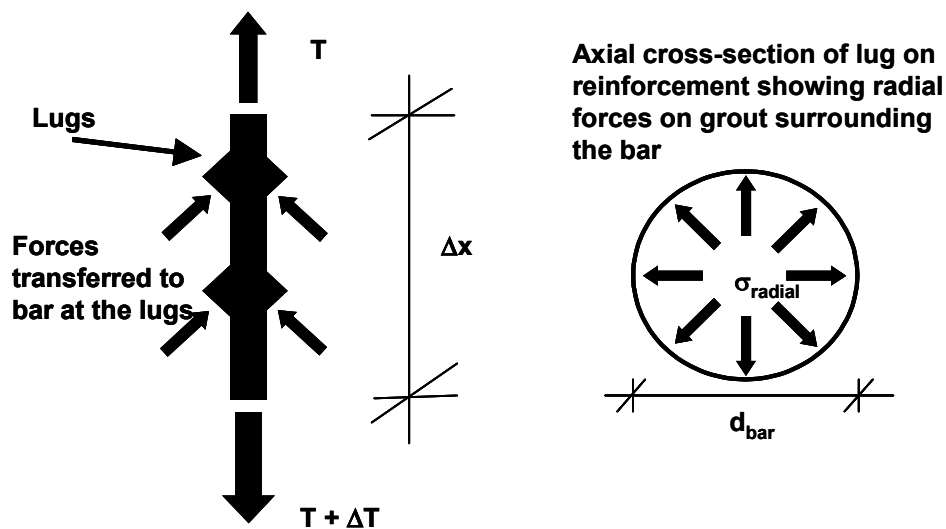


**Figure A.37** Free-body diagram of longitudinal bar with all load transferred through lugs and pressure generated in the surrounding grout

For design convenience the bond stress can be expressed as a function of shear as shown in Equation (A.27). This relationship is valid in cases where the bond between grout and reinforcement remains intact. Generally bond is broken after the reinforcement yields, therefore this development does not apply to cases where a plastic hinge may form. For practical reasons this analysis based on Equation (A.27) is limited to out-of-plane loading. Since the resultant force acting on the lugs acts at about 45 degrees, the radial stresses,  $\sigma_{radial}$  are also equal to the bond stress,  $u$ , as shown in Equation (A.28).

$$u = \frac{\Delta T}{\pi d_{bar} \cdot \Delta x} = \frac{\Delta M}{jd \cdot \pi d_{bar} \cdot \Delta x} = \frac{V}{jd \cdot \pi d_{bar}} \quad \text{Equation (A.27)}$$

$$\sigma_{radial} = u = \frac{V}{jd \cdot \pi d_{bar}} \quad \text{Equation (A.28)}$$

These radial forces cause splitting tensile stresses along a section through the wall at the center of the grouted core. Because the AAC has only about 15% of the splitting tensile strength of the grout, its tensile strength is neglected. A uniform distribution of splitting stresses across any section through the diameter of the grout core is assumed as shown in Figure A.38a. Since the radial stresses are symmetric about the centerline of the core (Figure A.38a), the net resultant of those radial stresses perpendicular to the centerline is zero. The splitting tensile stresses are resisted by the splitting tensile capacity of a section of grout, whose area is the length of grout shown in Figure A.38b, multiplied by the length of a section  $\Delta x$ . The resistance to the splitting tensile stresses is expressed in Equation (A.29). The resistance is increased by increasing the diameter of the core, decreasing the diameter of the bar, or increasing the tensile strength of the grout.

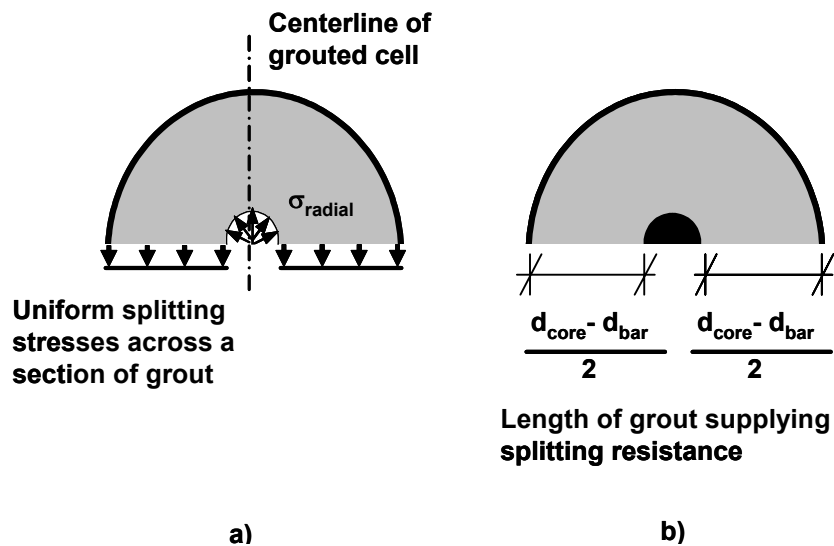


**Figure A.38** Stresses generated perpendicular to a cut along the diameter of a grouted cell

$$F_{resistance} = f_t (d_{core} - d_{bar}) \Delta x \quad \text{Equation (A.29)}$$

The uniform splitting stress across a section of grout as shown in Figure A.38a is calculated by integration. Figure A.39a shows the radial stress acting at the interface between the bar and grout. The vertical component of stress which corresponds to a uniform splitting stress is calculated using geometry for a differential section of the arc,  $ds$  (Figure A.39b). Integrating this expression for the vertical component of force between angles of 0 and  $\pi$  yields the expression for the total force generated by the splitting stress shown in Equation (A.30). If the resultant of the uniform splitting tensile stress is set equal to the total force supplied by the resistance of the grout (Figure A.38), Equation (A.31) is generated. The splitting tensile strength,  $f_t$ , is expressed in terms of the bond stress in Equation (A.32).

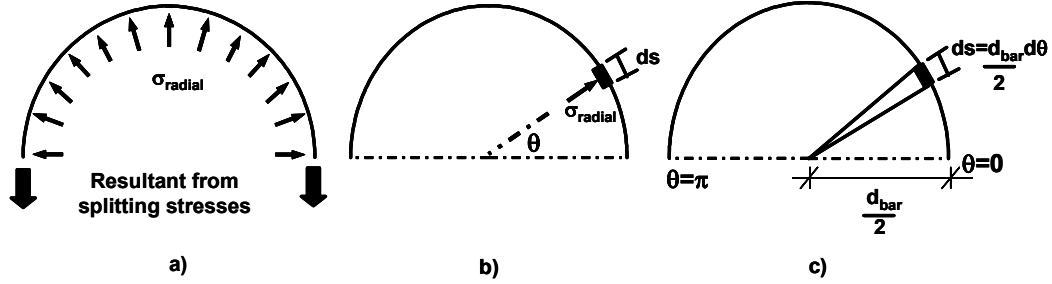


**Figure A.39** Calculation of force corresponding to the splitting tensile stresses across a section of grout

$$F_{splitting} = \int_0^{\pi} \sigma_{radial} \Delta x \sin \theta \cdot ds = \int_0^{\pi} \sigma_{radial} \Delta x \sin \theta \cdot \frac{d_{bar}}{2} d\theta = \sigma_{radial} d_{bar} \Delta x \quad \text{Equation (A.30)}$$

$$f_t (d_{core} - d_{bar}) \Delta x = \sigma_{radial} d_{bar} \Delta x \quad \text{Equation (A.31)}$$

$$f_{t, reqd} = \frac{\sigma_{radial} d_{bar}}{(d_{core} - d_{bar})} = \frac{u d_{bar}}{(d_{core} - d_{bar})} = \frac{V d_{bar}}{j d \cdot d_{bar} \cdot (d_{core} - d_{bar})} \quad \text{Equation (A.32)}$$

Based on this analysis, for reinforcement in the elastic stress range, the acting splitting tensile stress can be calculated. In such a case the area ratio of longitudinal steel may be increased beyond the proposed value of 3% for the design provisions of Section A.2.8. These proposed design provisions permit area ratios of longitudinal steel to grouted core up to 4.5%, provided that the splitting tensile stress generated in the core (Equation (A.32)) is less than the available splitting tensile strength. A detailed example of these calculations is presented in a design example involving walls subject to out-of-plane loading (Appendix B). The proposed design provisions in ACI 318-02 Code language are as follows:



**12.1.3** – *The maximum ratio of vertical reinforcement to area of a grouted cell shall be 3%. It shall be permitted to use ratios of vertical reinforcement up to 4.5% if the reinforcement remains elastic throughout its entire length and the available splitting tensile strength of the grout is greater than the acting splitting tensile strength as defined by Equation (12-xx)*

$$f_t = \frac{Vd_{bar}}{jd \cdot d_{bar} \cdot (d_{core} - d_{bar})} \quad \text{Equation (12-xx)}$$

*The splitting tensile strength of the grout shall be taken as  $4\sqrt{f'_g}$ . If  $f'_g$  is not specified it shall be permitted to be taken as 2000 psi.*

### **A.2.8 Analysis of the Maximum Permissible Area Ratio in a Plastic Hinge Zone**

If the reinforcement is located in a plastic hinge zone, compatibility of strains no longer exists between the reinforcement and the surrounding grout, and the splitting tensile stress cannot be determined using Equation (A.32). Based on the cracking observed along the flexural reinforcement in the flexure-dominated specimens (Section A.2.4), the proposed design provisions limit the area ratio to 3% in areas where a plastic hinge may form.

### **A.3 DESIGN OF AAC DIAPHRAGMS**

Lateral loads generated by inertial forces due to movement of a structure must be transferred to the base of the structure. Since mass is concentrated at the floor levels, this load is generated in the diaphragm and must be transferred to the shear walls and to the remainder of the structure. Lateral loads can act in any plan direction, the lateral load may be either parallel or perpendicular to the panel orientation. Each configuration is discussed in the following sections.

### **A.3.1 Shear transfer in floor panels oriented perpendicular to the direction of load**

Plan and elevation views of a diaphragm with floor panels oriented perpendicular to the walls are presented in Figure A.40 and Figure A.41. The shear is transferred from the diaphragm to the shear walls through the reinforcement in the grouted keys that was also anchored into the bond beam at Detail A (Figure A.42).

This configuration was tested in the first story of the Two-story Assemblage Specimen. The maximum applied load at this story of 72.1 kips (321 kN) corresponds to a load of 36.1 kips (160 kN) at each diaphragm to shear wall connection. The shear strength of the reinforcement in the grouted keys working in dowel action is 39.6 kips (176 kN). No distress was observed at the joints, which indicates that load could have also been transferred through adhesion. Although the dowel action was not tested in this specimen, the mechanism has been successfully used in traditional masonry construction.

### **A.3.2 Shear transfer in floor panels oriented parallel to the direction of load**

Shear transfer is critical in the case of panels oriented parallel to the direction of load, due to the lack of continuous reinforcement perpendicular to the applied lateral load. Shear transfer can occur in panels through adhesion or a truss mechanism. These methods are discussed independently in the following sections. The design calculations are presented in Appendix B.

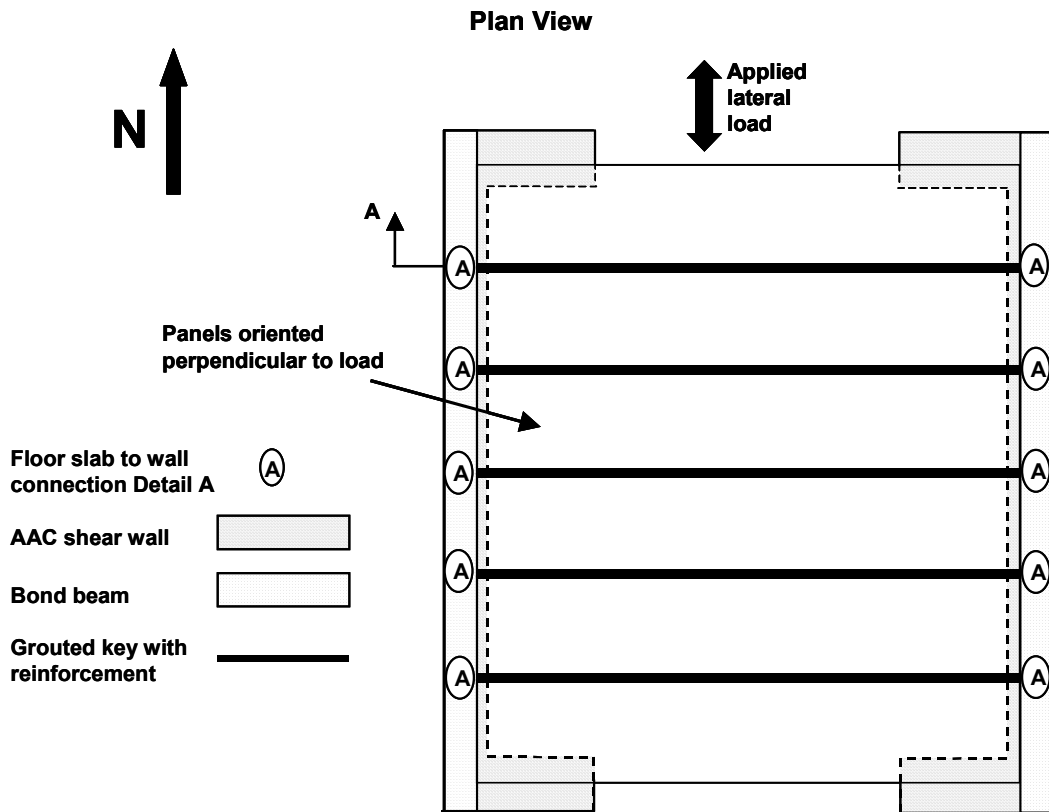


*Figure A.40 Floor plan for panels oriented perpendicular to applied load*

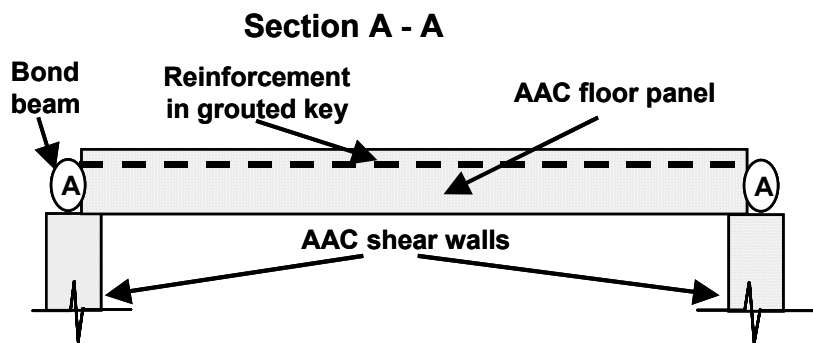


*Figure A.41 Elevation of Section A-A, floor slab-shear wall connection (panels oriented perpendicular to the direction of loading)*

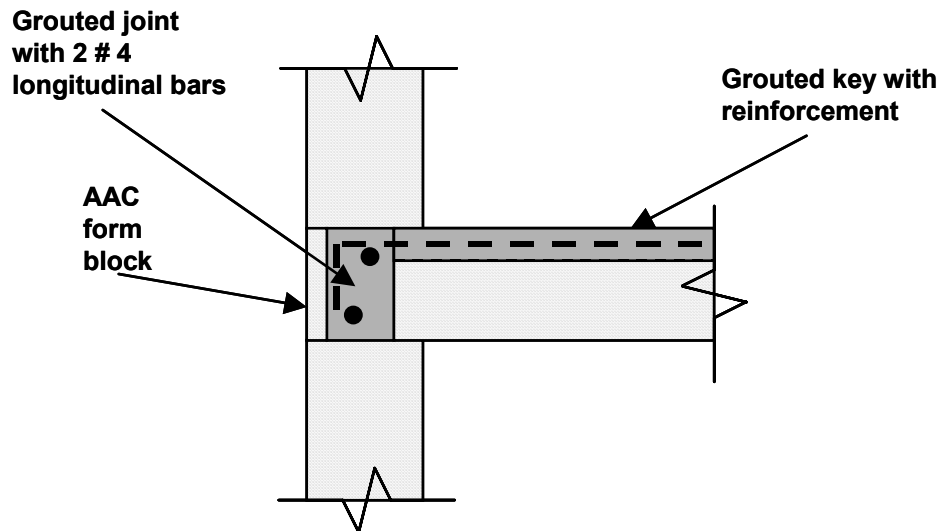


**Figure A.42** *Detail A, anchorage of reinforcement in grouted keys for panels oriented perpendicular to the direction of loading*

### **A.3.3 Shear transfer through adhesion between joints**

The second story of the Two-story Assemblage Specimen, panels oriented parallel to the direction of applied load was designed based on shear transfer through adhesion. The critical paths in the second story floor slab are Section D-D and Section E-E, since no steel crosses this path (Figure A.43). In panel to panel connections, Section D-D, the adhesion depends on both the thin-bed mortar and grouted key adhesion (Figure A.44). In panel to bond beam connections the adhesion depends primarily on grout and a small section of thin-bed mortar (Figure A.45).

The panel to panel joints were constructed by applying thin-bed mortar at the panel joint below the grouted key and clamping adjacent panels. The grouted key was cleaned with compressed air and pre-wet prior to placing grout. The grout was vibrated during placement. The same construction process is proposed for all panel to panel joints. Based on the average shear strengths and the

corresponding lengths of grout and thin-bed mortar the shear capacity is 60.5 kips (270 kN) for each joint, 1.7 times the maximum applied load at each joint of 36.1 kips (160 kN).

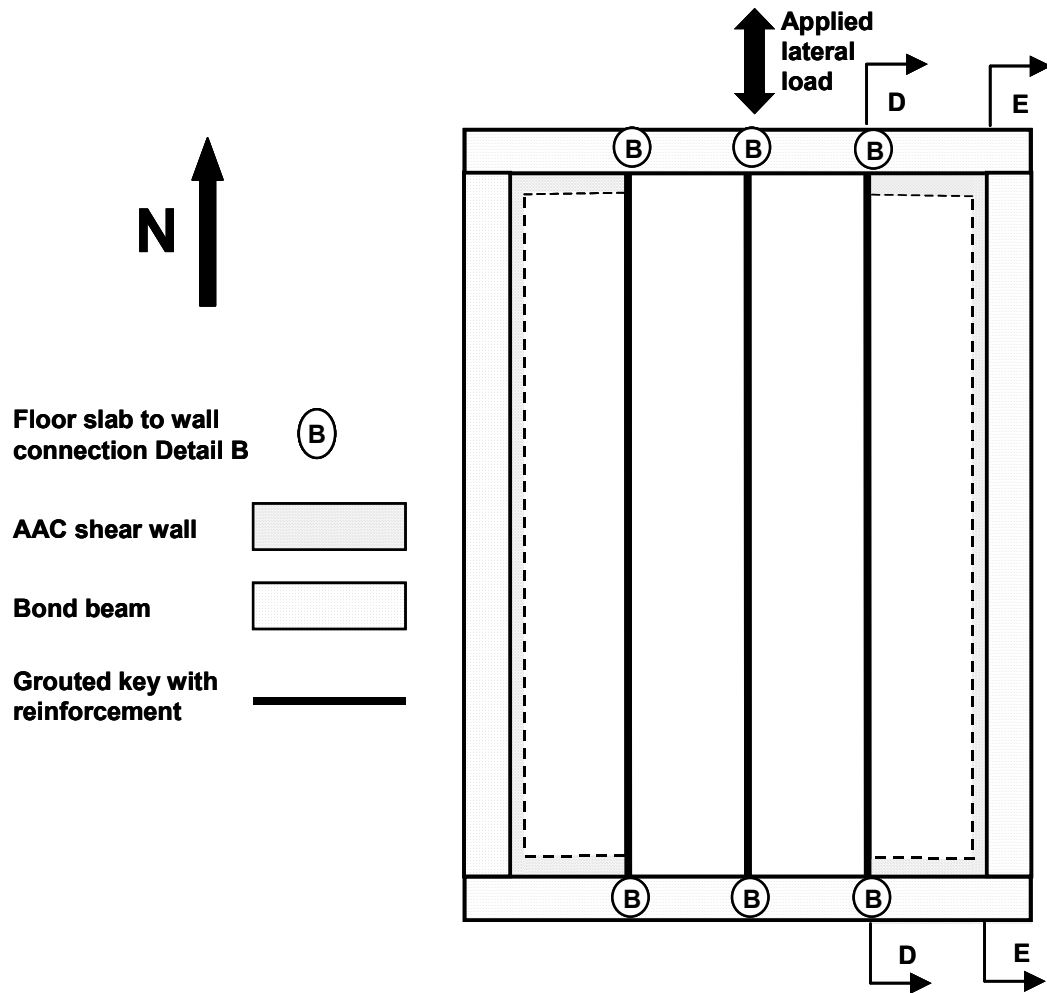


*Figure A.43 Plan view of second story floor panels*

### Section D - D

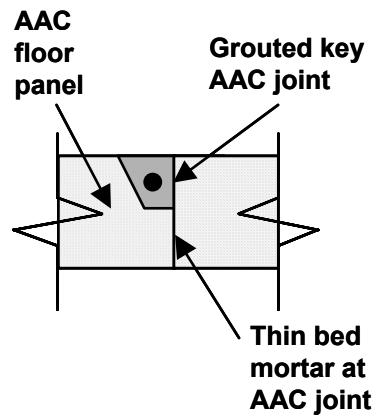


*Figure A.44 Elevation of Section D-D, panel-panel connection*

The panel to bond beam joints were constructed by applying thin-bed mortar at the bed joint between panels and the slab. In some cases a gap existed between the top of the vertical panel and the floor panel due to differences in the height of the leveling bed, which caused different heights at the top of panels. For this reason, the thin-bed mortar area was conservatively neglected. The bond beam was cleaned with compressed air and pre-wet prior to placing grout. The grout was vibrated during placement. The same construction process is proposed for all panel to bond beam joints. Based on the average shear strength of grout and AAC the shear capacity is 69.1 kips (310 kN) for each joint, 1.9 times the maximum applied load per joint of 36.1 kips (160 kN).

The proposed design margin of safety for joints depending on adhesion is 1.5. This factor is introduced as a strength reduction factor of 0.67, applied to the nominal interface shear capacity of AAC joints as governed by adhesion. This comfortable safety factor combined with using a nominal strength based on a

lower fractile of the observed shear strength provides an adequately conservative model for a brittle. Since this failure is brittle, it is limited to Seismic Design Categories A and B.

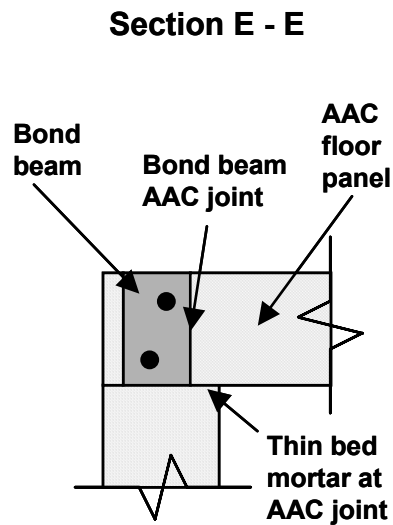


*Figure A.45 Elevation of Section E-E, panel-bond beam connection*

#### **A.3.4 Shear transfer through a truss mechanism**

Shear transfer may also be applied through a truss mechanism, which follows the principles of a strut-and-tie model. Compression is transferred through the panels in the form of struts. The reinforcement in the grouted keys serves as tension ties, which must be tied into the ring beam by 90-degree standard hooks bent around the longitudinal reinforcement in the tension ties and oriented in a vertical plane.

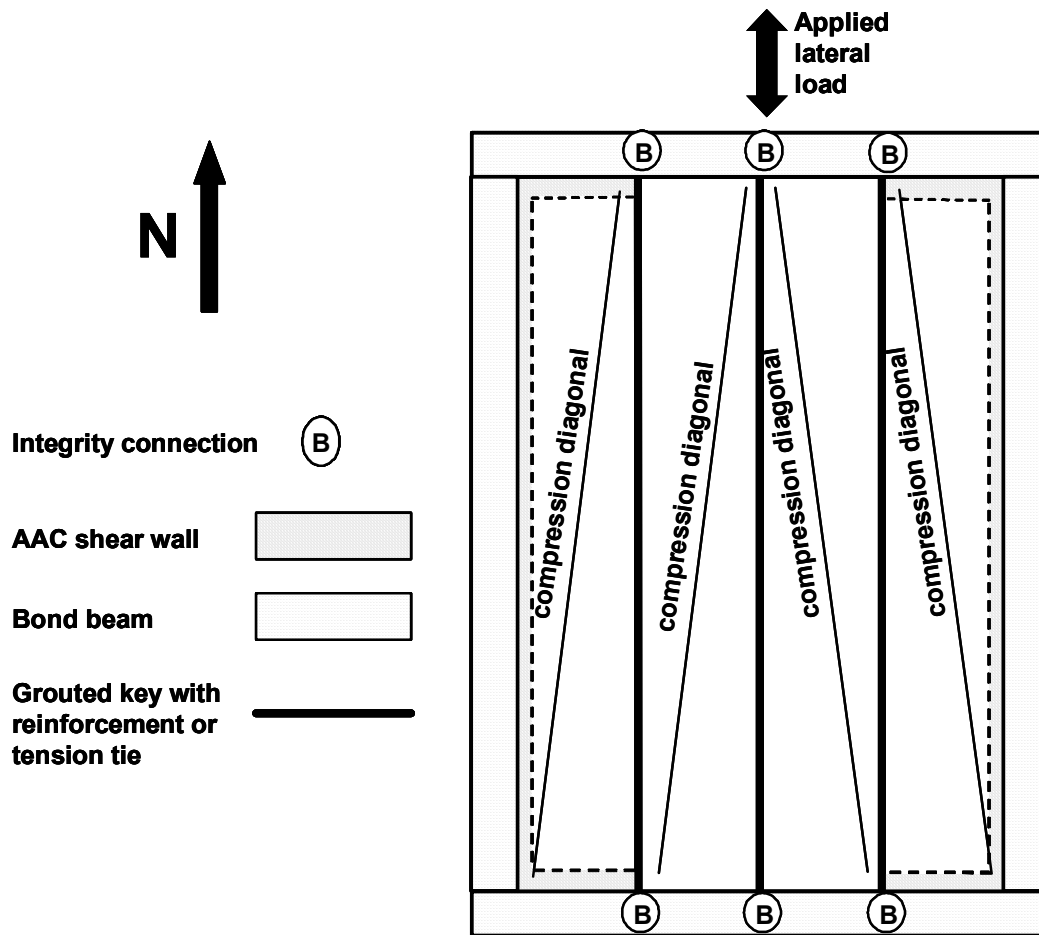


*Figure A.46 Truss mechanism for transferring lateral load parallel to the orientation of the panels*

Using this strut-and-tie model the computed nominal shear capacity of the diaphragm is 22.5 kips (100 kN). This is only 31% of the maximum load carried by the diaphragm in the assemblage test, which suggests that the strut-and-tie model is certainly conservative. If necessary, the nominal capacity calculated using the strut-and-tie model could be increased by increasing the bar size in the grouted key.



The required ratio of reinforcing bar area to cell area need not be limited because splitting cracks between panels will not reduce the strength of the model. Since the compression diagonals do not cross the panel joints, the capacity of the compression struts will not be decreased if the panel joints crack.. The proposed width of the compression strut is 6 in. (153 mm), one-quarter of the panel width. The depth of the strut is the thickness of the panel. The nodal forces will not limit the design in this case because the compressive strength of the grout is approximately 4 times the compressive strength of the AAC.

An alternate strut-and-tie model was initially used to design the diaphragm (Figure A.47). Based on that model, the nominal design capacity was 77.1 kips (343 kN), and the design capacity was 57.9 kips (257 kN). That alternate model is not proposed for design, for the following reasons:

- a) Cracks at the panel interfaces could decrease the capacity of the compression strut; and
- b) Additional steel is required to provide a transverse tension tie at the center of the diaphragm.

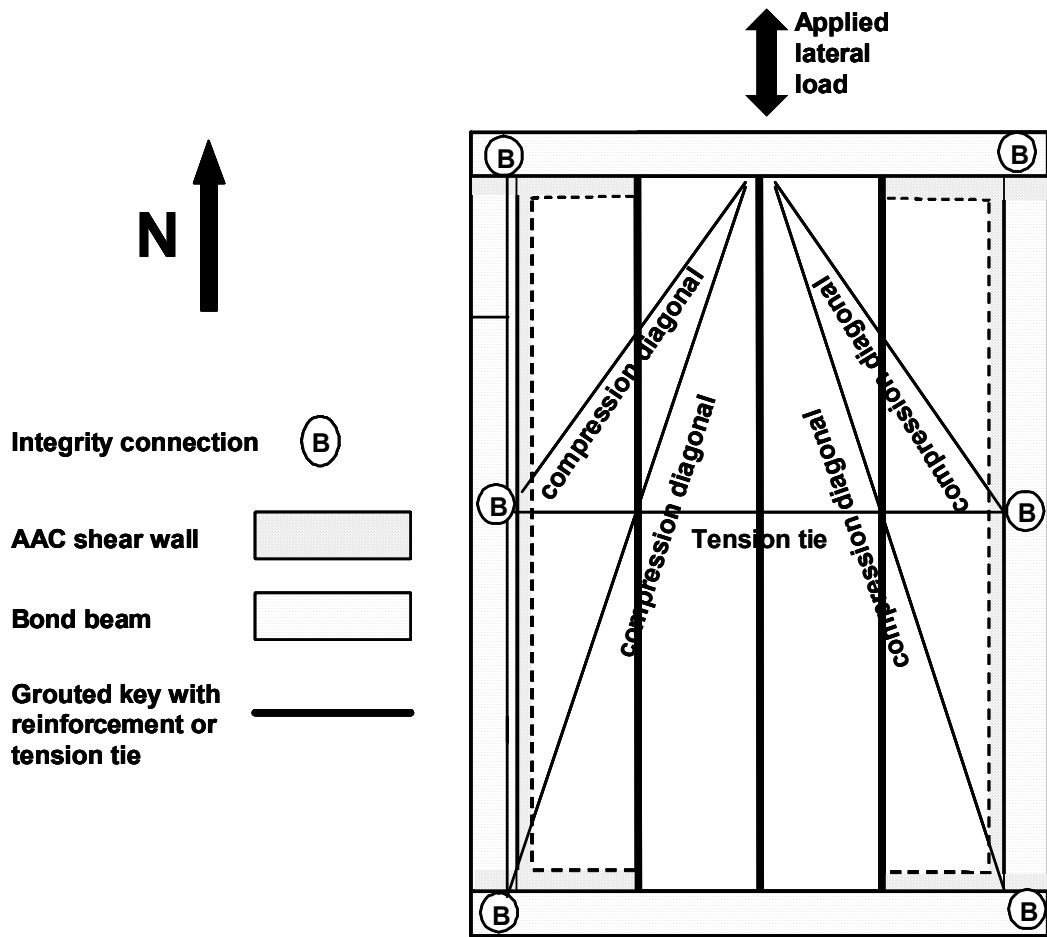


*Figure A.47 Alternate truss mechanism for transferring lateral load parallel to the orientation of the panels (not recommended for design)*

## A.4 DESIGN EXAMPLES

### A.4.1 Design of an AAC shear wall

Design the following two-story AAC shear wall. Material properties, factored loads, and geometry are:

PAAC-5

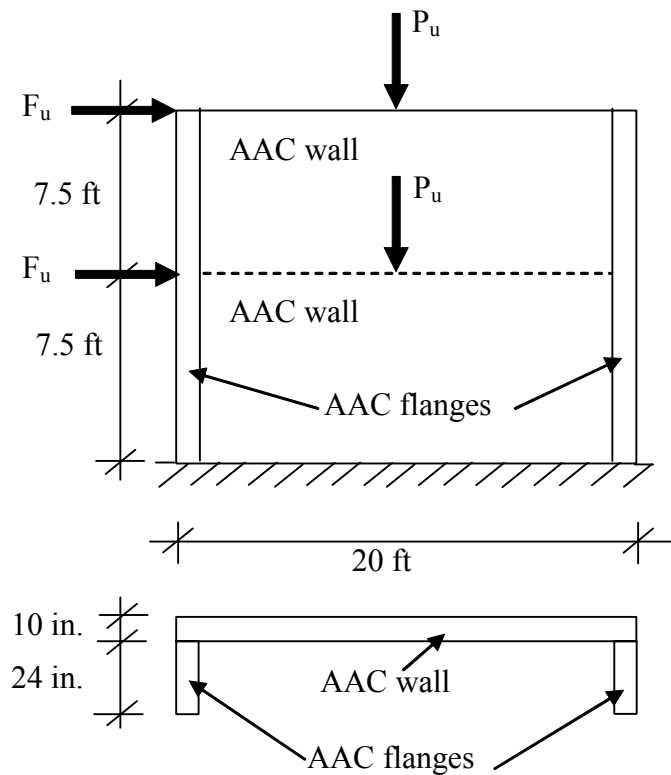
$$f'_{AAC} = 580 \text{ psi}$$

$f_y = 60,000 \text{ psi}$  (flexural reinforcement)

$$E_s = 29,000 \text{ Ksi}$$

Factored axial load at each story,  $P_u = 35,000 \text{ lbs}$

Factored lateral load at each story,  $F_u = 18,000 \text{ lbs}$

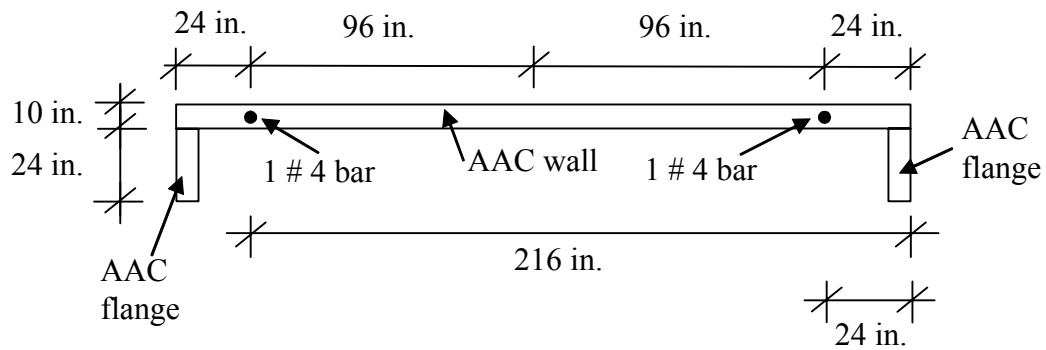


### A.4.1.1 Flexural capacity

Determine factored bending moment at the base of the wall:

$$M_u = 18,000 (15)(12) + 18,000 (7.5)(12) = 4,860,000 \text{ lbs} - \text{in.}$$

Determine flexural capacity at the base of the wall. Assume flexural reinforcement at wall ends only, equal to 1 # 4 bar, located 24 in. from the wall ends.



Calculate forces in bars ( $T_1$  and  $T_2$ ) assuming that both bars are yielding:

$$T_1 = T_2 = A_s f_y = 0.2 (60,000) = 12,000 \text{ lbs}$$

For equilibrium:

$$C = N_u + T_1 + T_2$$

$$N_u = 2 (P_u) = 35,000 + 35,000 = 70,000 \text{ lbs}$$

$$C = 0.85 f'_{AAC} a b$$

$$a = \frac{C}{0.85 f'_{AAC} b} = \frac{70,000 + 12,000 (2)}{0.85 (580) (10 + 24)} = 5.6 \text{ in.}$$

$$M_n = T_1 \left( 216 - \frac{l_w}{2} \right) - T_2 \left( \frac{l_w}{2} - 24 \right) + C \left( \frac{l_w - a}{2} \right)$$

$$M_n = 12,000 \left( 216 - \frac{240}{2} \right) - 12,000 \left( \frac{240}{2} - 24 \right) + 94,000 \left( \frac{240 - 5.6}{2} \right) = 11,020,000 \text{ lbs}$$

$$\phi M_n = 0.9 (11,020,000) = 9,900,000 \text{ lbs}$$

$$\phi M_n = 9,900,000 \text{ lbs-in.} > M_u = 4,860,000 \text{ lbs-in.} \quad \text{OK}$$

Check if right bar ( $T_2$ ) is yielding.

$$c = \frac{a}{\beta_1} = \frac{5.6}{0.67} = 8.4 \text{ in.}$$

$$\varepsilon_2 = \frac{24}{8.4} (\varepsilon_{AAC}) = \frac{24}{8.4} (0.003) = 0.0086$$

$$\varepsilon_y = \frac{f_y}{E_s} = \frac{60,000}{29,000,000} = 0.0021$$

$$\varepsilon_2 = 0.0086 > \varepsilon_y = 0.0021 \quad \text{OK}$$

#### ***A.4.1.2 Shear capacity***

Determine factored shear force and axial force at the base of the wall:

$$V_u = 2 F_u = 2 (18,000) = 36,000 \text{ lbs}$$

$$N_u = 70,000 \text{ lbs}$$

Determine shear capacity at the base of the wall (web shear cracking):

$$\phi V_{AAC} = \phi 0.9 t l_w \sqrt{f'_{AAC}} \sqrt{1 + \frac{N_u}{2.4 \sqrt{f'_{AAC}} t l_w}}$$

$$\phi V_{AAC} = 0.75 (0.9)(10)(240)\sqrt{580} \sqrt{1 + \frac{70,000}{2.4 \sqrt{580} (10)(240)}} = 47,850 \text{ lbs}$$

$$\phi V_{AAC} = 47,850 \text{ lbs} > V_u = 36,000 \text{ lbs} \quad \text{OK}$$

Determine factored shear force and axial force at 7.5 ft from the base of the wall:

$$V_u = F_u = 18,000 \text{ lbs}$$

$$P_u = N_u = 35,000 \text{ lbs}$$

Determine shear capacity at 7.5 ft from the base of the wall (web shear cracking):

$$\phi V_{AAC} = 0.75 (0.9)(10)(240)\sqrt{580} \sqrt{1 + \frac{35,000}{2.4 \sqrt{580} (10)(240)}} = 43,700 \text{ lbs}$$

$$\phi V_{AAC} = 43,700 \text{ lbs} > V_u = 18,000 \text{ lbs} \quad \text{OK}$$

Determine shear capacity of bottom wall (crushing of the diagonal strut):

$$\phi V_{AAC} = 0.75 (0.9) f'_{AAC} t w_{\text{strut}} \frac{h \left( \frac{3l_w}{4} \right)}{h^2 + \left( \frac{3l_w}{4} \right)^2}$$

$$w_{\text{strut}} = \frac{l_w}{4} = \frac{240}{4} = 60 \text{ in}$$

$$\phi V_{AAC} = 0.75 (0.9)(580)(10)(60) \frac{90 \left( \frac{3(240)}{4} \right)}{90^2 + \left( \frac{3(240)}{4} \right)^2} = 93,960 \text{ lbs}$$

$$\phi V_{AAC} = 93,960 \text{ lbs} > V_u = 36,000 \text{ lbs} \quad \text{OK}$$

Determine sliding shear capacity of bottom wall and a thin-bed mortar joint:

$\mu = 1$  at a leveling bed joint

$$\phi V_{ss} = \phi (\mu N_u)$$

Neglect additional force in tensile steel:

$$\phi V_{ss} = 0.75 ( (1)(70,000) ) = 52,500 \text{ lbs}$$

$$\phi V_{ss} = 52,500 \text{ lbs} > V_u = 36,000 \text{ lbs} \quad \text{OK}$$

$\mu = 0.75$  at AAC to AAC joint

$$\phi V_{ss} = \phi (\mu N_u)$$

Neglect additional force in tensile steel.

$$\phi V_{ss} = 0.75 ( (0.75)(70,000) ) = 39,375 \text{ lbs}$$

$$\phi V_{ss} = 39,375 \text{ lbs} > V_u = 36,000 \text{ lbs} \quad \text{OK}$$

#### **A.4.2 Design an AAC Diaphragm**

Design the AAC diaphragm. Assume the following material properties, factored loads, and geometry.

PAAC-5

$$f'_{AAC} = 580 \text{ psi}$$

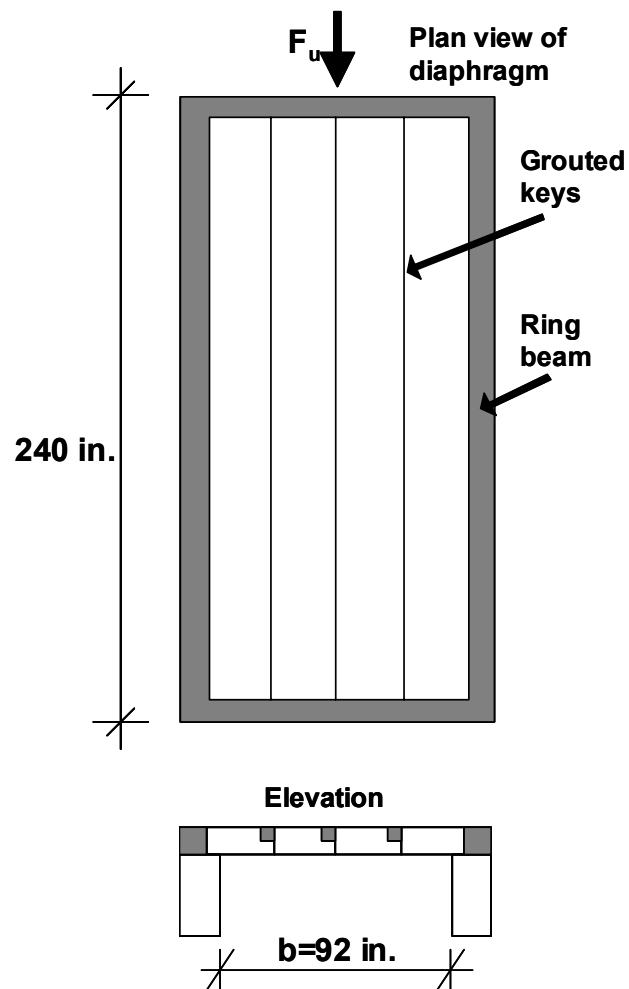
$$f'_{\text{grout}} = 3000 \text{ psi}$$

$$f_y = 60,000 \text{ psi}$$

Factored lateral load at each story,  $F_u = 18,000 \text{ lbs}$

Ring beam reinforcement 2 #5

Grouted key reinforcement 1 #5



Design diaphragm for flexure:



$$M = \frac{F_u l}{4} = \frac{18000 \cdot 92}{4} = 414,000 \text{ bin}$$

$$T = A_s f_y = 2 \cdot 0.2 \cdot 60000 = 24,000 \text{ lb}$$

$$a = \frac{C}{0.85 f'_{grout} b} = \frac{24,000}{0.85 (3000) (92)} = 0.1 \text{ in.}$$

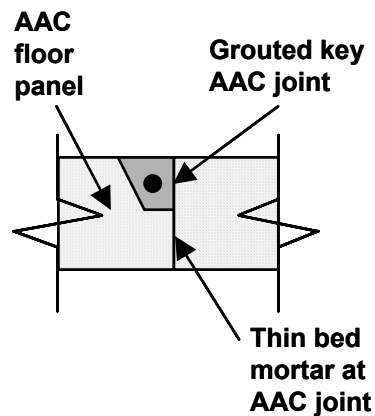
$$D = \text{length of key} - \text{ring beam}/2 - 2\text{U-block thickness} = 240 - 4 - 4$$

$$M_n = A_s f_y \cdot \left(d - \frac{a}{2}\right) = 5518000 \text{ bin} > M_{reqd} = 414,000 \text{ bin} \quad \text{OK}$$

Design diaphragm for shear based on adhesion:

i) Panel to panel joint:

#### Section D - D



The total resistance is the adhesion of the grouted area plus the adhesion of the thin-bed mortar area.

$$b_{grout} = 5 \text{ in.}$$

$$b_{thin-bed} = 3 \text{ in.}$$

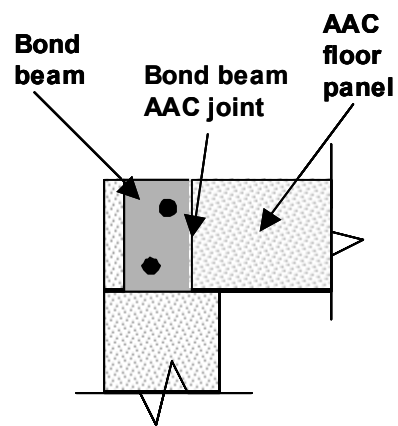
$$V_{grout} = \tau_{grout} \cdot b_{grout} \cdot l = 36 \cdot 5 \cdot 240 = 43,200 \text{ lb}$$

$$V_{thin-bed} = \tau_{thin-bed} \cdot b_{thin-bed} \cdot l = 18 \cdot 3 \cdot 240 = 13,000lb$$

$$V_{total} = V_{grout} + V_{thin-bed} = 55,200lbs$$

$$\phi V_{total} = 0.67 \cdot 55,200 = 36,980lbs > \frac{F_u}{2} = 9,000lbs$$

ii) Panel bond beam joint:



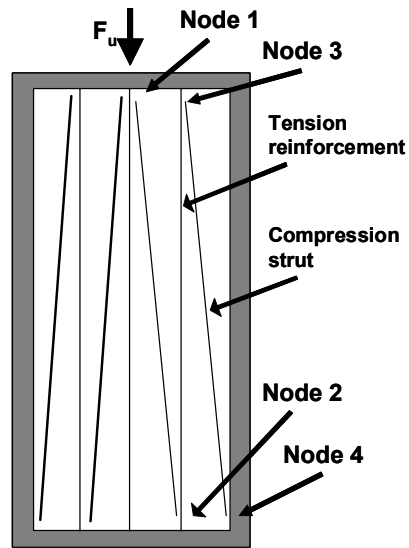
$$b_{grout} = 8 \text{ in.}$$

$$V_{grout} = \tau_{grout} \cdot b_{grout} \cdot l = 36 \cdot 8 \cdot 240 = 69,100lbs$$

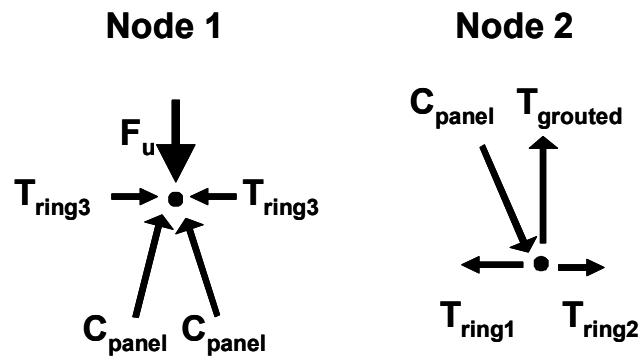
$$\phi V_{total} = 0.67 \cdot 69,100 = 46,300lbs > \frac{F_u}{2} = 9,000lbs$$

Design diaphragm for shear based on truss model:

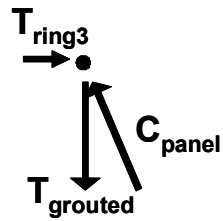
One # 5 bar in each grouted key



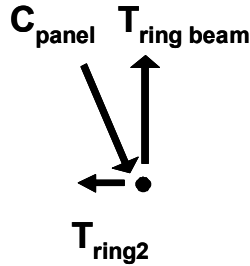
In this model the compression chords act as diagonal compression members.



### Node 3



### Node 4



Based on equilibrium:

C <sub>panel</sub>	= 9,456 lbs
T <sub>gouted</sub> key	= 9,000 lbs
T <sub>ring1</sub>	= 1800 lbs
T <sub>ring2</sub>	= 900 lbs
T <sub>ring3</sub>	= 900 lbs
T <sub>ring beam</sub>	= 9,000 lbs

Check capacity of strut tie and ring beam tie:

Compression strut capacity

W<sub>strut</sub> = 6 in.

T<sub>panel</sub> = 8 in.

$$F_{strut} = 9,456/48 = 197 \text{ psi} < 0.75(0.85f'_{AAC}) = 0.75(0.85)(580) = 370 \text{ psi}$$

OK

Check capacity of tension tie in grouted cell:

$$T_{gouted \text{ key}} = 9,000 \text{ lb} < \phi A_s f_y = 0.75 * 0.31 * 60,000 = 14,000 \text{ lb} \quad \text{OK}$$

The reinforcement ratio limit of 3% required by Section A.2.8 does not apply to horizontal reinforcement.

If tension tie in grouted cell is sufficient the remaining tension ties will also be sufficient, because the area of steel provided is larger.

#### A.4.3 Design an AAC Shear Wall for Out-of-plane loads

PAAC-5

$$f'_{AAC} = 580 \text{ psi}$$

$f_y = 60,000 \text{ psi}$  (flexural reinforcement)

$$E_s = 29,000 \text{ ksi}$$

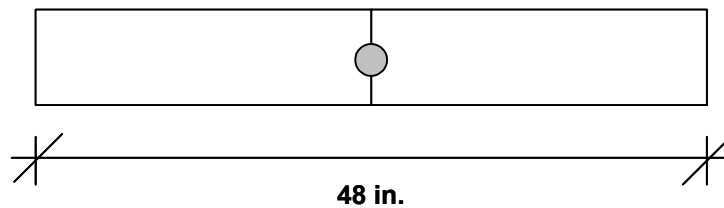
Factored wind load on wall  $p_u = 110 \text{ lbs/ft}^2$

Reinforcement in a 3 in. grouted cell at 4 ft. on center

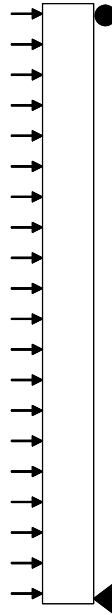
$h = 10 \text{ ft}$

$t = 10 \text{ in.}$

Plan view of 4 ft. section of wall



Elevation of shear wall simply supported at top and bottom



#### A.4.3.1 Flexural capacity

Determine acting moment:

$$w_u = \rho \cdot \text{width} = 110 \text{ lb/ft}^2 \cdot 4 \text{ ft} = 440 \text{ lb/ft}$$

$$M_u = \frac{w l^2}{8} = \frac{440 \cdot (10)^2}{8} = 5,500 \text{ lb-ft} = 66,000 \text{ lb-in.}$$

Try #4 bar:

$$T = A_s f_y = 0.2 \cdot 60,000 = 12,000 \text{ lb}$$

$$a = \frac{T}{0.85 f_{AC} 'b} = \frac{12,000}{0.85 \cdot 580 \cdot 48} = 0.5 \text{ in}$$

$$M_n = A_s \cdot f_y \cdot \left(d - \frac{a}{2}\right) = 12 \cdot \left(5 - \frac{0.5}{2}\right) = 57,000 \text{ lb-in}$$

$$\phi M_n = 0.9 \cdot 57,000 \text{ lb-in} = 51,300 \text{ lb-in} < M_u \quad \text{Not Good}$$

Try #5 bar:

$$T = A_s f_y = 0.31 \cdot 60,000 = 18,600 \text{ lb}$$

$$a = \frac{T}{0.85 f_{AC} 'b} = \frac{18,600}{0.85 \cdot 580 \cdot 48} = 0.8 \text{ in}$$

$$M_n = A_s \cdot f_y \cdot \left(d - \frac{a}{2}\right) = 18.6 \cdot \left(5 - \frac{0.8}{2}\right) = 85,700 \text{ lb-in}$$

$$\phi M_n = 0.9 \cdot 85,700 \text{ lb-in} = 77,130 \text{ lb-in} > M_u \quad \text{O.K.}$$

Check strain limits for this case:

$$c = a / \beta_1 = 0.8 / 0.67 = 1.2$$

$$d = 5$$

$$\epsilon_s = 0.003 \cdot (d - c) / c = 0.0095 > 1.3 \epsilon_y = 1.3 \cdot 1.25 \cdot f_y / E_s = 0.0033$$

Use a #5 bar

$$A_{\text{steel}} / A_{\text{grout}} = 0.31 / 7.1 = 0.044 = 4.4\% > 3\%$$

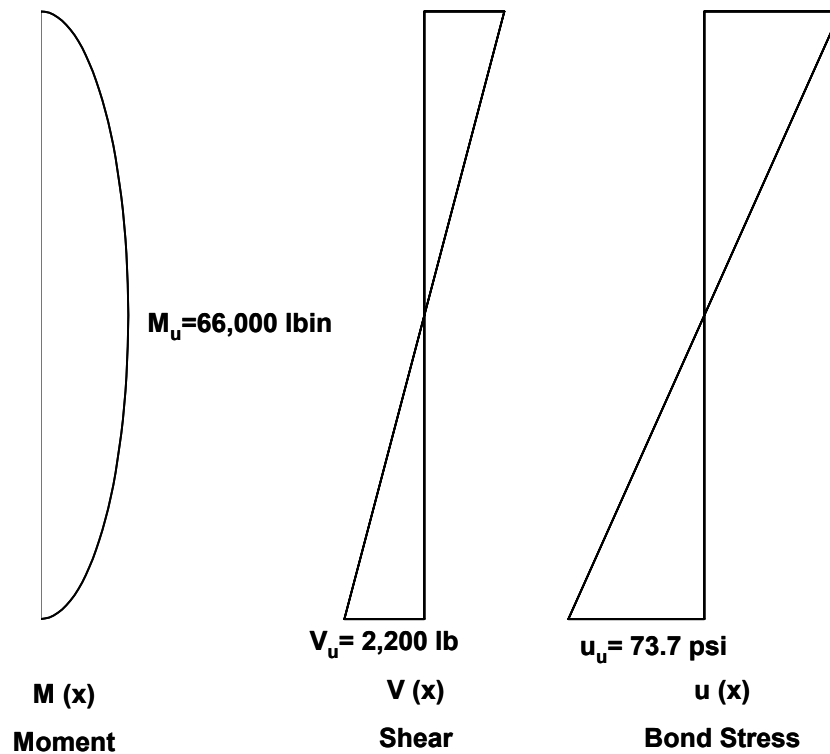
Perform an analysis to check the bond stress. In the case of out-of-plane loads the reinforcement in the wall does not yield and no plastic hinge forms. In this example, the classical bond stress analysis shown in the example can be used.

Check bond stress:

Determine if reinforcement is yielding:

$\phi M_n = 0.9 \cdot 85,700 \text{ lb-in} = 77,130 \text{ lb-in} > M_u = 66,000 \text{ lb-in}$ , reinforcement will not be yielding. Since reinforcement will not be yielding consider case where bond remains intact and express bond stress as a function of shear.

Determine shear and bond stress along the length of the wall. Based on the bond stress determine the splitting tensile stress in the wall and compare to the splitting tensile strength of the grout.



$$V_u = \frac{440 \cdot 10}{2} = 2200 \text{ lbs}$$

$$u_u = \frac{V}{arm \cdot \pi d_{bar}} = \frac{2200}{0.8 \cdot 5 \cdot \pi \cdot 0.625} = 280 \text{ psi}$$

$$f_{treqd} = \frac{u d_{bar}}{(d_{core} - d_{bar})} = \frac{280 \cdot 0.625}{(3 - 0.625)} = 73.7 \text{ psi}$$

$$f_{available} = 4\sqrt{f_g} = 4\sqrt{3000} = 219 \text{ psi}$$



The factored splitting tensile stress is less than the factored tensile strength available. Use  $\phi=0.75$  which corresponds to shear.

$$u_u = 74 \text{ psi} < \phi f_t = 0.75(219) = 164 \text{ psi.}$$

#### ***A.4.3.2 Shear capacity***

Determine factored loads and maximum shear force for a single panel.

$$w_u = 110 \text{ psf}$$

$$V_u = 2 w_u \frac{L}{2} = 2(110) \frac{10}{2} = 1,100 \text{ lbs}$$

Determine shear capacity of floor panel:

$$V_{AAC} = 0.9 \sqrt{f'_{AAC}} A_n + 0.05 P_u = 0.9 \sqrt{580} \cdot 24 \cdot 10 = 5200 \text{ lbs}$$

$$\phi V_{AAC} = 0.75 * (5,200) = 3,900 \text{ lbs} > V_u = 1,100 \text{ lbs} \quad \text{OK}$$

## **APPENDIX B**

### **ACI 523.5R-xx Guide for using Autoclaved Aerated Concrete Panels**

#### **B.1 INTRODUCTION**

##### **B.1.1 Definition of Autoclaved Aerated Concrete**

Autoclaved Aerated Concrete (AAC) is a low-density cementitious product of calcium silicate hydrates in which the low density is obtained by the formation of macroscopic air bubbles, mainly by chemical reactions within the mass during the liquid or plastic phase. The air bubbles are uniformly distributed and are retained in the matrix on setting, hardening, and subsequent curing with high-pressure steam in an autoclave, to produce a cellular structure (Figure B.1). Material specifications for this product are prescribed in ASTM C 1386.



*Figure B.1 Cellular structure of AAC*

### B.1.2 Typical Mechanical and Thermal Characteristics of AAC

In Table B.1, typical mechanical and thermal characteristics of AAC are compared with those of conventional concrete, including conventional concrete made with lightweight aggregates. AAC typically has one-sixth to one-third the density of conventional concrete, and about the same ratio of compressive strength, making it potentially suitable for cladding and infills, and for bearing-wall components of low- to medium-rise structures. Its thermal conductivity is one-sixth or less that of concrete, making it potentially energy-efficient. Its fire rating is slightly longer than that of conventional concrete of the same thickness, making it potentially useful in applications where fire resistance is important. Because of its internal porosity, AAC has very low sound transmission, making it potentially useful acoustically.

*Table B.1 Typical mechanical and thermal characteristics of AAC*

<b>Characteristic</b>	<b>AAC</b>	<b>Conventional Concrete</b>
density, pcf ( $\text{kg/m}^3$ )	25 - 50 (400 - 800)	80 - 150 (1280 - 2400)
compressive strength, $f_c$ , psi (MPa)	360 - 1090 (2.5 - 7.5)	1000 - 10000 (6.9 - 69)
thermal conductivity, Btu- in/ft <sup>2</sup> -hr-F	0.75 - 1.20	6.0 - 10
fire rating, hours	$\leq 8$	$\leq 6$

### **B.1.3 Historical Background of AAC**

AAC was first produced commercially in Sweden, in 1923. Since that time, its production and use have spread to more than 40 countries on all continents, including North America, Central and South America, Europe, the Middle East, the Far East, and Australia. This wide experience has produced many case studies of use in different climates, and under different building codes.

In the US, modern uses of AAC began in 1990, for residential and commercial projects in the southeastern states. US production of plain and reinforced AAC started in 1995 in the southeast, and has since spread to other parts of the country. A nationwide group of AAC manufacturers was formed in 1998 as the Autoclaved Aerated Concrete Products Association. This *Guide* is an effort by the AAC technical community, including manufacturers, designers and researchers, to propose national design guidelines that could later be developed into code provisions.

### **B.1.4 Applications of AAC Panels**

AAC can be used to make unreinforced, masonry-type units, and also factory-reinforced floor panels, roof panels, wall panels, lintels, beams, and other special shapes (Figure B.2). These elements can be used in a variety of applications including residential, commercial and industrial construction. Reinforced wall panels can be used as cladding systems as well as loadbearing and non-loadbearing exterior and interior wall systems. Reinforced floor and roof panels can be efficiently used to provide the horizontal diaphragm system while supporting the necessary gravity loads.

### **B.1.5 Scope and Objectives of this *Guide***

This *Guide* is limited to AAC with a density of 50 lb/ft<sup>3</sup> (800 kg/m<sup>3</sup>) or less. This *Guide* is written for structural designers. It addresses design using factory-reinforced AAC elements. Design of AAC masonry is addressed in other documents.



***Figure B.2 Examples of AAC structural elements***

Design documents produced by ACI technical committees are classified as standards or non-standards. The latter include “guides,” which are intended to present directions for analysis, design, construction, materials, or testing on a general basis. Their language is non-mandatory, permitting the user latitude in judgment concerning particular needs.

The specific objectives of this *Guide* are:

- a) To review the basic characteristics of AAC
- b) To provide a capsule history of structural applications of AAC
- c) To review the fabrication of AAC elements
- d) To recommend structural design procedures for factory-reinforced AAC elements
- e) To recommend construction details for use with factory-reinforced AAC elements

The structural design procedures and construction details recommended here are intended to result in AAC elements with adequate structural capacity, durability, appearance and overall serviceability.

## **B.2 TYPICAL MATERIALS AND MANUFACTURE OF AAC**

### **B.2.1 Materials Used in AAC**

Materials for AAC vary with manufacture and location, and are specified in ASTM C1386. They include some or all of the following:

- a) Fine silica sand (ASTM C33, C144 or C332);
- b) Class F fly ash (ASTM C618) with up to 12% loss on ignition (LOI);
- c) Hydraulic cements (ASTM C150 or C595);
- d) Calcined lime (ASTM C110);
- e) Gypsum (ASTM C22);
- f) Expansive agent, such as finely ground aluminum powder;
- g) Mixing water (clean and free of deleterious substances); and

- h) Reinforcement (ASTM A82), welded to form cages, with corrosion-inhibiting coating.

## B.2.2 Manufacture of AAC

Overall steps in the manufacture of AAC are shown in Figure B.3.

### B.2.2.1 Preparation, Batching and Mixing of Raw Materials

Sand is ground to the required fineness in a ball mill, if necessary, and is stored along with other raw materials. The raw materials are then batched by weight and delivered to the mixer. Measured amounts of water and expansive agent are added to the mixer, and the cementitious slurry is mixed.

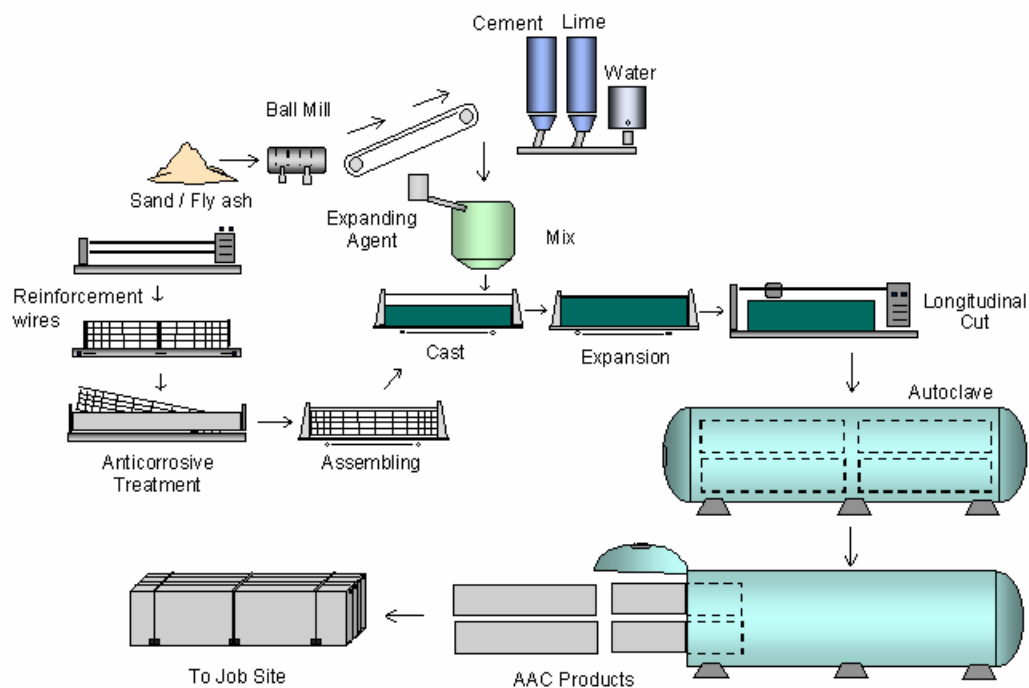


**Figure B.3 Overall steps in manufacture of AAC**

### ***B.2.2.2 Casting, Expansion and Initial Hydration***

Steel molds are prepared to receive the fresh AAC. If reinforced AAC panels are to be produced, steel reinforcing cages are secured within the molds. After mixing, the slurry is poured into the molds. The expansive agent creates small, finely dispersed voids in the fresh mixture, which approximately triples in volume in less than an hour in the molds.

### ***B.2.2.3 Cutting***

Within a few hours after casting, the initial hydration of cementitious compounds in the AAC gives it sufficient strength to hold its shape and support its own weight. The material is removed from the molds (Figure B.4) and fed into a cutting machine, which, using wires, sections the blocks and panels into the required sizes and shapes (Figure B.5). After cutting, the units remain in their original positions in the larger AAC block.



***Figure B.4 Fresh AAC after removal of molds***





**Figure B.5** *Cutting AAC into desired shapes*

#### ***B.2.2.4 Autoclaving***

After cutting, the aerated concrete product is transported to a large autoclave, where the curing process is completed (Figure B.6). Autoclaving is required to achieve the desired structural properties and dimensional stability. The process takes about 8 – 12 hours under a pressure of about 174 psi (12 Bars) and a temperature of about 360 °F (180 °C) depending on the grade of material produced. During autoclaving, the wire-cut units remain in their original positions in the AAC block. After autoclaving, they are separated for packaging.



*Figure B.6 Autoclaving AAC*

#### ***B.2.2.5 Packaging***

AAC units are normally placed on pallets for shipping. Unreinforced units are typically shrink-wrapped, while reinforced elements are banded only, using corner guards to minimize potential localized damage that might be caused by the banding.



*Figure B.7 Packaging of finished AAC units*

#### ***B.2.2.6 AAC Strength Classes***

AAC is produced in different densities and corresponding compressive strengths, in accordance with ASTM C1386 (Precast Autoclaved Aerated Concrete Wall Construction Units) and ASTM C 1452 (Standard Specification for Reinforced Autoclaved Aerated Concrete Elements). Densities and corresponding strengths are described in terms of “strength classes.” In each case, the strength class corresponds to the specified compressive strength in MPa.

**Table B.2** *Material characteristics of AAC in different strength classes*

<b>Strength Class</b>	<b>Specified Compressive Strength lb/in<sup>2</sup> (MPa)</b>	<b>Average Compressive Strength</b>	<b>Nominal Dry Bulk Density lb/ft<sup>3</sup> (kg/m<sup>3</sup>)</b>	<b>Density Limits lb/ft<sup>3</sup> (kg/m<sup>3</sup>)</b>
AAC 2.0	290 (2.0)	360 (2.5)	25 (400) 31 (500)	22 (350) - 28 (450) 28 (450) - 34 (550)
AAC 3.3	478 (3.3)		31 (500) 37 (600)	28 (450) - 34 (550) 34 (550) - 41 (650)
AAC 4.0	580 (4.0)	720 (5.0)	31 (500) 37 (600) 44 (700) 50 (800)	28 (450) - 34 (550) 34 (550) - 41 (650) 41 (650) - 47 (750) 47 (750) - 53 (850)
AAC 4.4	638 (4.4)		37 (600) 44 (700)	34 (550) - 41 (650) 41 (650) - 47 (750)
AAC 6.0	870 (6.0)	1090 (7.5)	44 (700) 50 (800)	41 (650) - 47 (750) 47 (750) - 53 (850)

### **B.2.3 Typical Dimensions of AAC Units**

#### ***B.2.3.1 Plain AAC Wall Units***

Typical dimensions for plain AAC wall units (masonry-type units) are shown in Table B.3.

**Table B.3 Dimensions of plain AAC wall units**

<b>AAC Unit Type</b>	<b>Width, in. (mm)</b>	<b>Height, in. (mm)</b>	<b>Length, in. (mm)</b>
Standard Block	2 - 15 (50 - 375)	8 (200)	24 (610)
Jumbo Block	4 - 15 (100 - 375)	16 - 24 (400 - 610)	24 - 40 (610 - 1050)

**B.2.3.2 Reinforced AAC Units**

Dimensional tolerances, requirements for reinforcement, and other requirements for reinforced AAC panels are specified in ASTM C1452, which also cites C1386. Typical dimensions for reinforced AAC wall units (panels) are shown in Table B.4.

**Table B.4 Dimensions of reinforced AAC wall units**

<b>Product Type</b>	<b>Thickness, in. (mm)</b>	<b>Height or Width, in. (mm)</b>	<b>Typical Length, ft (mm)</b>
Wall Panel	2 -15 (50 - 375)	24 (610)	20 (6090)
Floor Panel	4 -15 (100 - 375)	24 (610)	20 (6090)
Lintel / Beam	4 -15 (100 - 375)	8 - 24 (200 - 610)	20 (6090)

**B.2.4 Dimensional Tolerances**

In accordance with ASTM C1386, dimensional tolerances for plain AAC wall units are 1/8 in. (3 mm) in each dimension. Dimensional tolerances for reinforced elements are given in ASTM C1452, and are listed in Table B.5.

**Table B.5**     *Dimensional tolerances for reinforced AAC units*

<b>Dimension</b>	<b>Floor or Roof Panels, in. (mm)</b>	<b>Wall Panels, in. (mm)</b>
Length	$\pm 0.20 (\pm 5)$	$\pm 0.20 (\pm 5)$
Width	$\pm 0.12 (\pm 3)$	$\pm 0.12 (\pm 3)$
Thickness	$\pm 0.12 (\pm 3)$	$\pm 0.12 (\pm 3)$
Tongue	$\pm 0.12 (\pm 3)$	$\pm 0.12 (\pm 3)$
Groove	$\pm 0.12 (\pm 3)$	$\pm 0.12 (\pm 3)$

### **B.2.5 Identification and Marking of AAC Units**

All reinforced AAC units should bear identifying symbol to include a mark indicating the strength class, production identification code, and position number for reinforced panels. Pallets of unreinforced AAC units should be labeled with strength class, production identification code and size of units.

## **B.3 STRUCTURAL DESIGN OF REINFORCED AAC ELEMENTS**

### **B.3.1 Introductory Remarks regarding Design Provisions**

This document is a guide. Its design provisions are non-mandatory, and are a synthesis of design recommendations from the Autoclaved Aerated Concrete Products Association, and from the results of research conducted at the University of Alabama at Birmingham (UAB), the University of Texas at Austin (UT Austin), and elsewhere.

In this chapter, the proposed design provisions are introduced in narrative form. In Appendix C, more information is presented regarding specific design provisions, and a commentary on those provisions.

The specific design provisions and their associated commentary of Appendix C, are intended to be compatible in organization, numbering and form with the design provisions of ACI 318, in order to facilitate their use by concrete designers, and also to facilitate their future consideration, in mandatory form, by ACI Committee 318. For that reason, the provisions are arranged to refer directly to ACI 318-02. Additions and exceptions are specifically noted. New subcategories are inserted for new design provisions.

Loads for structural design of AAC elements should be taken from appropriate load codes, such as ASCE 7. Understrength factors ( $\Phi$ -factors) for AAC elements depend on the actions under consideration. They reflect the statistical variability of the capacity, and the accuracy of the capacity-calculation formulas. When failure is governed by yield and fracture of tensile reinforcement,  $\Phi$ -factors are justifiably identical to those used for reinforced

concrete. When failure is governed by crushing or diagonal tension of the AAC itself,  $\Phi$ -factors are similar to those used for concrete. They may even be higher, because the factory production of AAC leads to decreased variability in its mechanical characteristics compared to conventional concrete.

The design provisions of this *Guide* are not intended for use with unreinforced, masonry-type units. Design of those units is covered by provisions currently under development within the Masonry Standards Joint Committee.

## **B.3.2 Proposed Design Provisions for Reinforced AAC Panels**

### ***B.3.2.1 Basic Design Assumptions***

The proposed design provisions for reinforced AAC panels are based on the same principles used for strength design of conventional reinforced concrete elements: strain compatibility between AAC and reinforcement (with some modifications as noted below); stress-strain behavior of AAC and reinforcement; and equilibrium. The design strength of AAC in compression is based on a specified design compressive strength,  $f_{AAC}'$ . Compliance with that specified compressive strength is verified by compressive strength testing, using ASTM C1386, when the AAC panels are fabricated. The design strength of AAC in tension is proposed as a function of the specified compressive strength. The design strength of reinforcement in tension is proposed as the specified yield strength.



### ***B.3.2.2 Combinations of Flexure and Axial Load***

AAC panels are designed for combinations of flexural and axial load using principles identical to those for conventional reinforcement. Nominal capacity is computed assuming plane sections; tensile reinforcement is assumed to be yielded; the stress in compressive reinforcement is computed based on its strain and its stress-strain behavior; and the distribution of compressive stress in the AAC is approximated by an equivalent rectangular stress block.

Because reinforced AAC panels usually have equal areas of tensile and compressive reinforcement, flexural capacity is usually “tension-controlled” (in the terminology of ACI 318-02. Sections are under-reinforced (in the terminology of ACI 318-99).

### ***B.3.2.3 Bond and Development of Reinforcement***

Reinforcement in AAC panels consists of welded-wire mesh installed when the panels are produced, and deformed reinforcement installed in 3- to 4- in. grouted cores as the panels are erected.

Bond and development requirements for deformed reinforcement in grout are identical to those used for concrete or masonry construction. Given the small sizes of deformed bars used in AAC construction, bond between the grout and the AAC itself does not govern the bond capacity.

Bond and development requirements for welded-wire fabric embedded in AAC are quite different from those for conventional concrete, however. Because the welded-wire fabric has a corrosion-resistant coating, bond strength between the coated wire and the AAC itself is negligible. Bond strength comes from

bearing of the cross wires against the AAC. For typical cross-wire spacings, local crushing of the AAC under the cross wires can be assumed to redistribute the bearing stresses under the cross wires, leading to a uniform bearing strength of  $f_{AAC}'$  under every cross-wire. Multiplying this stress by the number of cross wires and by the bearing area of each cross-wire gives the maximum force that can be developed in the welded wire fabric (Figure B.8).

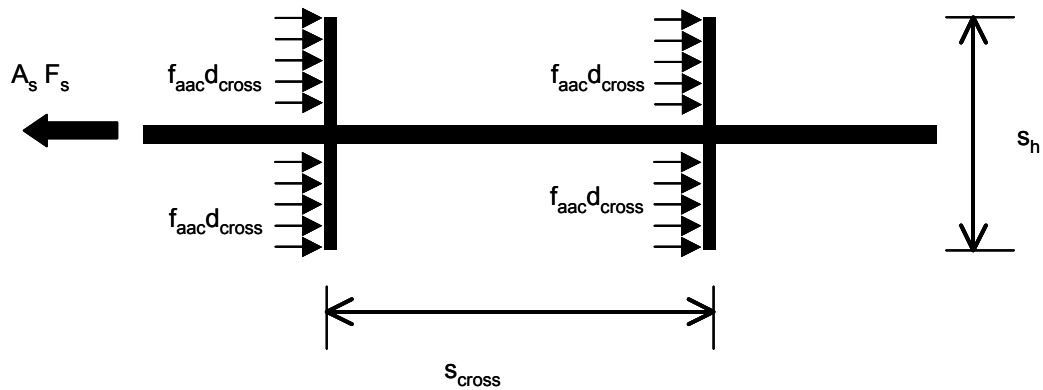


**Figure B.8** Bond mechanism of welded-wire fabric in AAC

This maximum force in the welded-wire mesh can limit the flexural capacity of a reinforced AAC panel.

#### **B.3.2.4 Shear**

As with conventional reinforced concrete elements, the shear resistance of AAC elements is computed as the summation of a shear resistance due to the AAC itself ( $V_{AAC}$ ), and a shear resistance due to reinforcement oriented parallel to the direction of the shear.

The shear resistance due to the AAC itself ( $V_{AAC}$ ) is computed using the web-shear approach of ACI 318-02. The diagonal tension resistance of the AAC is expressed in terms of its specified compressive strength, and principal tensile stresses, including the effects of axial loads, are equated with this strength. This produces an expression for  $V_{AAC}$  in terms of the diagonal tension resistance of the AAC, and the axial load on the element.

The shear resistance due to transverse reinforcement is computed based on the cross-sectional area of the transverse reinforcement crossing a hypothetical 45-degree crack in the AAC. As explained in the previous subsection, it may also be limited by bond and development of the reinforcement.

#### ***B.3.2.5 Bearing***

To prevent local crushing of the AAC, nominal stresses in it are limited to  $f_{AAC}'$ . When AAC floor or roof panels bear on AAC walls, shear failure of the edge of the wall is also possible. This is handled by limiting the shear stress on potential inclined failure surfaces.

## **B.4 HANDLING, ERECTION AND CONSTRUCTION WITH AAC UNITS**

### **B.4.1 Handling of AAC Panels**

AAC panels should be stored on suitably prepared supports, so that they are prevented from warping. They should be carefully placed in their final position without being overstressed or damaged. Instructions from the manufacturer on how to handle the units should be followed. Special equipment is usually used or recommended by the manufacturer to assist in the transportation and erection of the units.

### **B.4.2 Erection of AAC Wall Panels**

AAC panels are lifted and placed using specially designed clamps, and are aligned using alignment bars.

#### ***B.4.2.1 Erection of AAC Cladding Systems***

AAC panels can be used as non-load bearing cladding systems. This application usually involves horizontally oriented panels attached to steel or reinforced concrete frame. Erection of such panels follows these steps:

- a) Ensure that supporting columns are plumb and true.
- b) Set the bottom panel against the supporting columns and over the floor slab or slab on ground, on top of a bed joint of conventional masonry mortar. Make sure that the panel is true and level.

- c) Immediately after placing the first panel, fasten a wall anchor plate to the column (using a dovetail or mechanically locking connector), and nail the plate to the AAC panel. The back face of the panel should be flush with the outer face of the column.
- d) Place subsequent panels on top of the first one. The top and bottom faces of the horizontal wall panels can have either a tongue and groove profile, or a flat profile. Tongue and groove joints do not require mortar. Flat joints are mortared with thin-bed mortar.
- e) Seal horizontal and vertical joints with flexible sealant.

#### ***B.4.2.2 Erection of Vertical AAC Panels for Bearing-Wall Systems***

Vertical AAC panels may also be used as a load-bearing wall system. In such cases, the floor roof systems are usually designed and detailed as horizontal diaphragms to transfer lateral loads to shear walls. The tops of the panels are connected to the floor or roof diaphragms using a cast-in-place reinforced concrete ring beam. This and many other structural details are addressed in the next chapter.

When vertical wall panels are used in this way, they are set on a bedding joint of conventional masonry mortar, with or without a waterproofing admixture. Vertical wall panels are usually mortared together with thin-bed mortar.

### **B.4.3 Erection of AAC Floor and Roof Panels**

AAC floor and roof panels can be erected on concrete, steel or masonry construction. All bearing surfaces should be level and minimum required bearing areas (to prevent local crushing) should be maintained.

As in any precast construction system, care must be exercised in the installation of the first panel to ensure correct alignment of the remaining panels. All floor and roof anchors should be installed prior to placement of the panels, thus streamlining and expediting panel installation.

Most floor and roof panels are connected by keyed joints that are reinforced and filled with grout to lock the panels together and provide diaphragm action to resist lateral loads. A cast-in-place reinforced concrete ring beam is normally placed along the perimeter of the diaphragm, completing the system.

### **B.4.4 Electrical and Plumbing Installations in AAC**

Electrical and plumbing installations in AAC are placed in routed chases. Care should be taken when laying out chases to ensure that the structural integrity of the AAC elements is maintained. Do not cut reinforcing steel or reduce the structural thickness of the AAC elements in critical areas. When analyzing the AAC element is intended to span vertically, horizontal routing should be permitted only in areas with low flexural and compressive stresses. In contrast, when the AAC element is intended to span horizontally, vertical routing should be minimized. When possible, it may be advantageous to provide designated chases for large quantities of conduit or plumbing.

#### **B.4.5 Exterior Finishes for AAC**

Unprotected exterior AAC deteriorates when exposed to cycles of freezing and thawing while saturated. To prevent such freeze-thaw deterioration, and to enhance the aesthetics and abrasion resistance of AAC, exterior finishes should be used. They should be compatible with the underlying AAC in terms of thermal expansion and modulus of elasticity, and should be vapor permeable. Many different types of exterior finishes are available, and the most common are discussed here.

##### ***B.4.5.1 Polymer-Modified Stuccos, Paints or Finish Systems***

Polymer-modified stuccos, paints or finish systems are the most common exterior finish for AAC. They increase the AAC's water-penetration resistance while allowing the passage of water vapor. Heavy acrylic-based paints containing aggregates are also used to increase abrasion resistance. There is generally no need to level the surface, and horizontal and vertical joints may be chamfered as an architectural feature, or may be filled.

##### ***B.4.5.2 Masonry Veneer***

Masonry veneer may be used over AAC panels in much the same way that it is used over other materials. The veneer is attached to the AAC wall using masonry ties. The space between the AAC and the masonry can be left open (forming a drainage wall), or can be filled with mortar.

##### ***B.4.5.3 Finishes for Basement Walls***

When AAC panels are used in contact with moist or saturated soil (for example, in basement walls, the surface in contact with the soil should be coated with a waterproof material or membrane. The interior surface should either remain uncoated, or be coated with a vapor-permeable interior finish.

## **B.4.6 Interior Finishes for AAC Panels**

Interior finishes are used to enhance the aesthetics and durability of AAC. They should be compatible with the underlying AAC in terms of thermal expansion and modulus of elasticity, and should be vapor permeable. Many different types of interior finishes are available, and the most common are discussed here.

### ***B.4.6.1 Interior Plasters***

Interior AAC wall panels may have a thin coat of a mineral-based plaster to achieve a smooth finished surface. Lightweight interior gypsum-based plaster may provide a thicker coating to level and straighten walls, and to provide a base for decorative interior paints or wall finishes. Interior plasters have bonding agents to enhance their adhesion and flexibility, and are commonly installed by either spraying or troweling.

### ***B.4.6.2 Gypsum Board***

When applied to the interior surface of exterior AAC walls, gypsum board should be attached using pressure-treated furring strips. When applied to interior walls, moisture-resistant gypsum board can be applied directly to the AAC surface.

### ***B.4.6.3 High-Durability Finishes for Commercial Applications***

For commercial applications requiring high durability and low maintenance, acrylic-based coatings are often used. Some contain aggregates to enhance abrasion resistance.



#### ***B.4.6.4 Ceramic Tile***

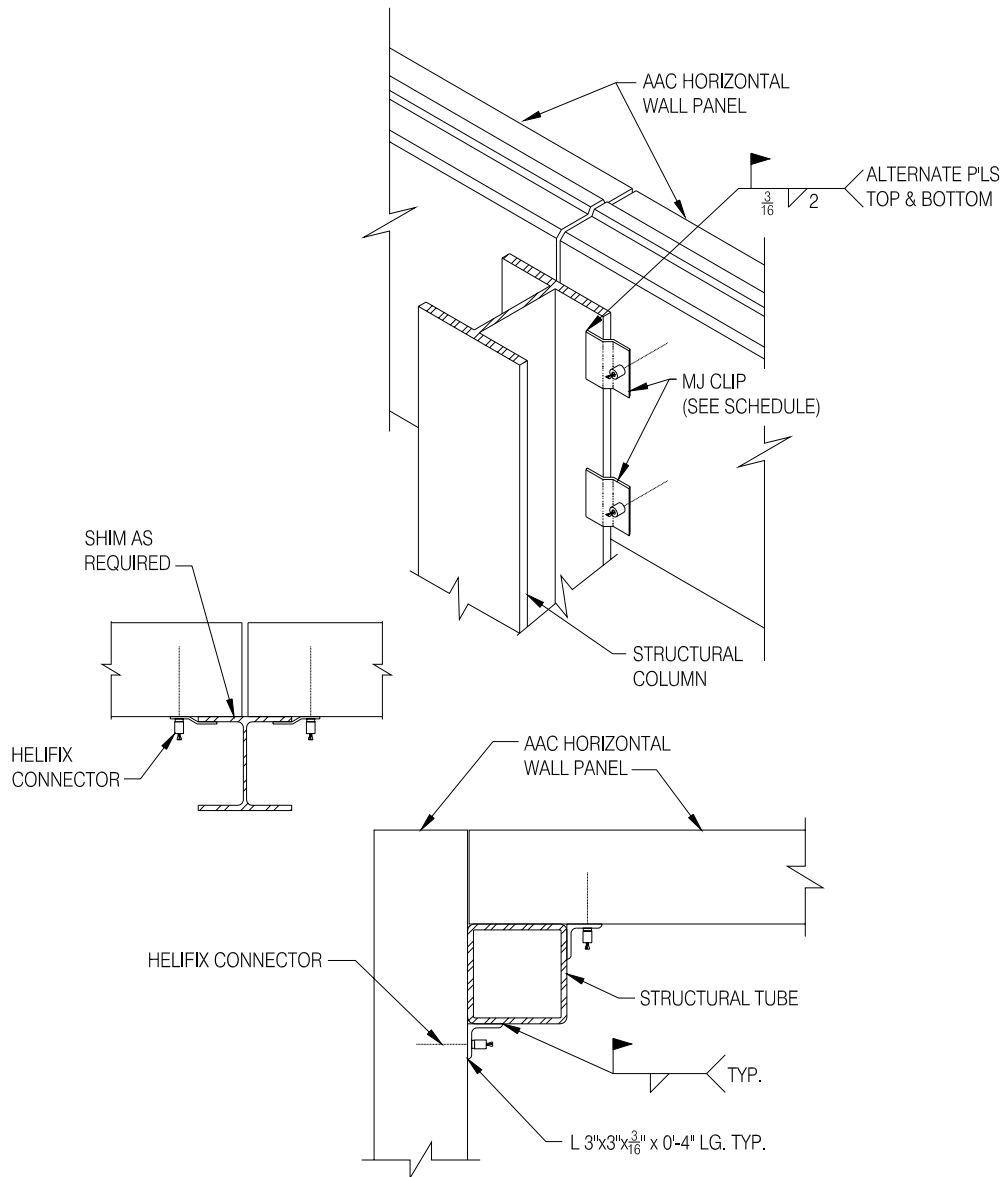
When ceramic wall tile is to be applied over AAC, surface preparation is normally necessary only when the AAC surface requires leveling. In such cases, a portland cement- or gypsum-based parge coat is applied to the AAC surface before setting the ceramic tile. The ceramic tile should then be adhered to the parged wall using either a cement-based thin-set mortar or an organic adhesive. In moist areas such as showers, only a portland cement-based parge coat should be used, and the ceramic tile should be set with cement-based thin-set mortar only.

## **B.5 TYPICAL CONSTRUCTION DETAILS FOR AAC ELEMENTS**

### **B.5.1 Cladding System**

**B.5.1.1**

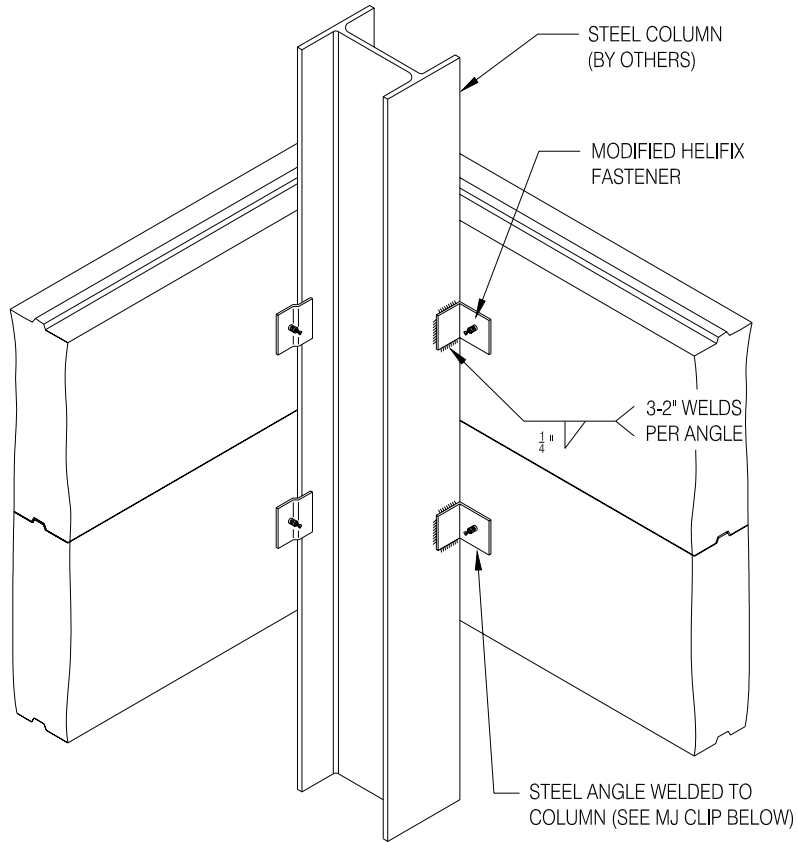
**B.5.1.1.1 Exterior Horizontal Wall Panel at Steel Column**



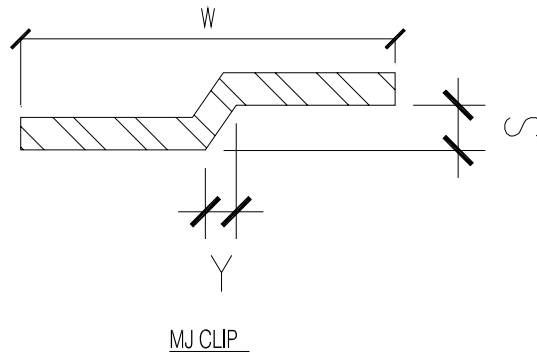
**5.1.1.1 EXTERIOR HORIZONTAL WALL PANEL AT STEEL COLUMN**

1" = 1'-0"

**B.5.1.1.2 Exterior Horizontal Wall Panel at Steel Column**



MJ CLIP DIMENSIONS		
W	S	Y
4"	1/4"	3/4"

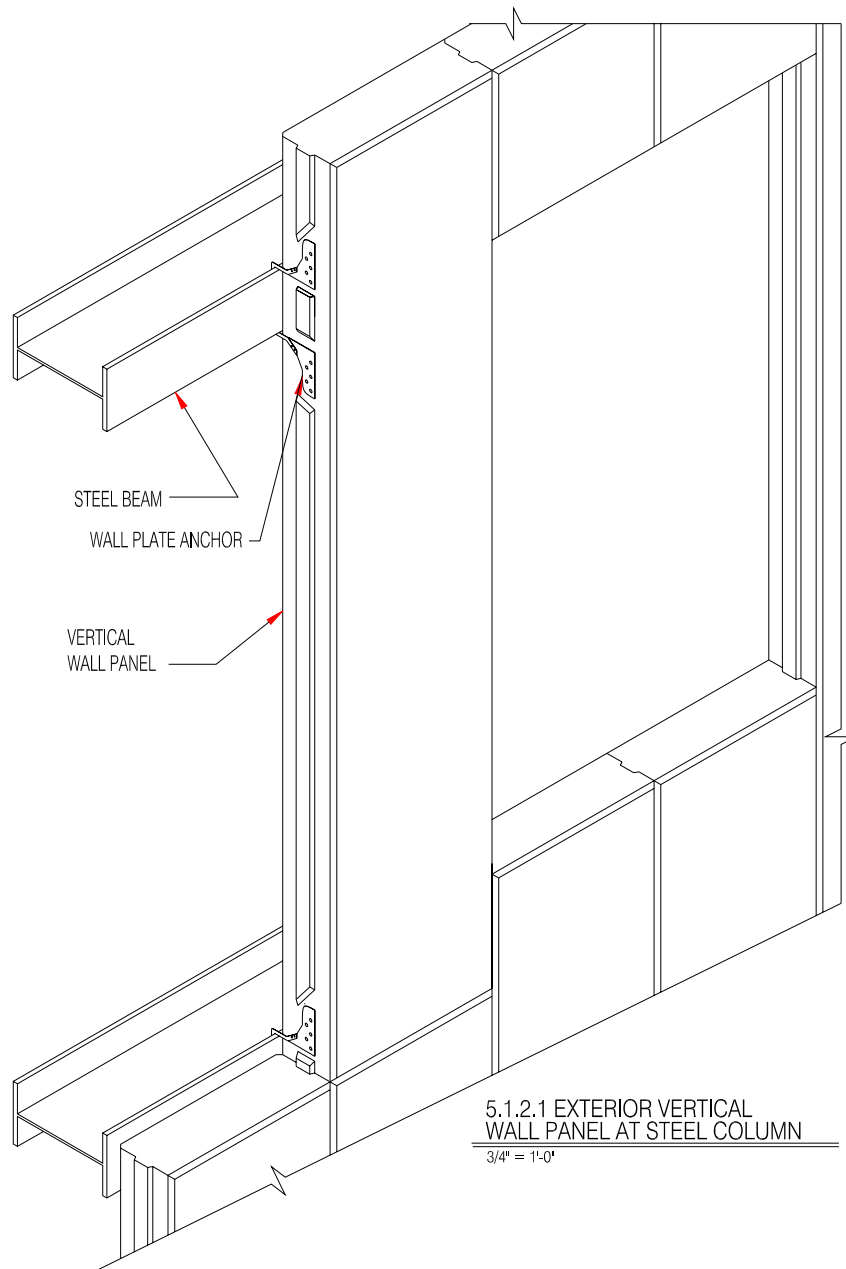


**5.1.1.2 EXTERIOR HORIZONTAL WALL PANEL AT STEEL COLUMN**

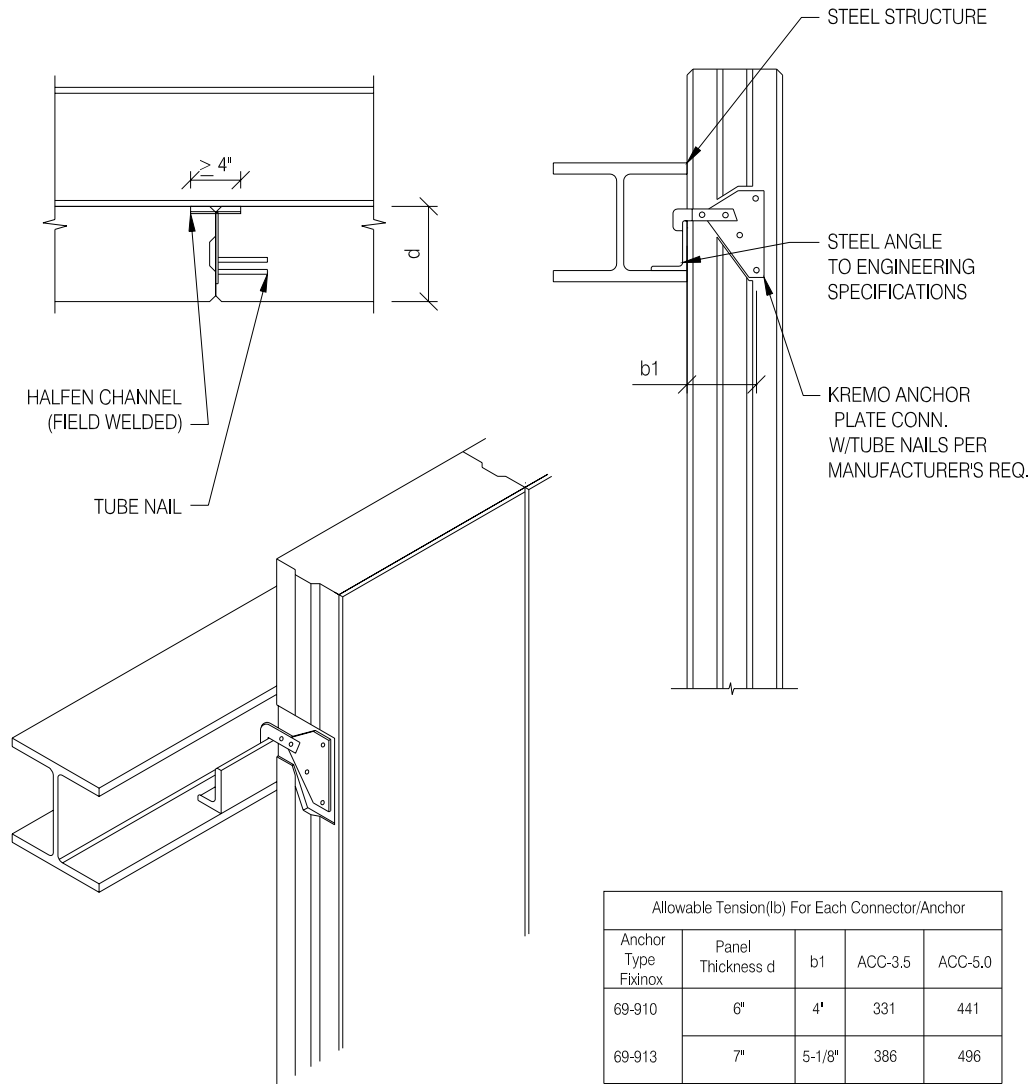
1" = 1'-0"

**B.5.1.2**

**B.5.1.2.1 Exterior Vertical Wall Panel at Steel Beam**



**B.5.1.2.2 Exterior Vertical Wall Panels at Steel Beam**

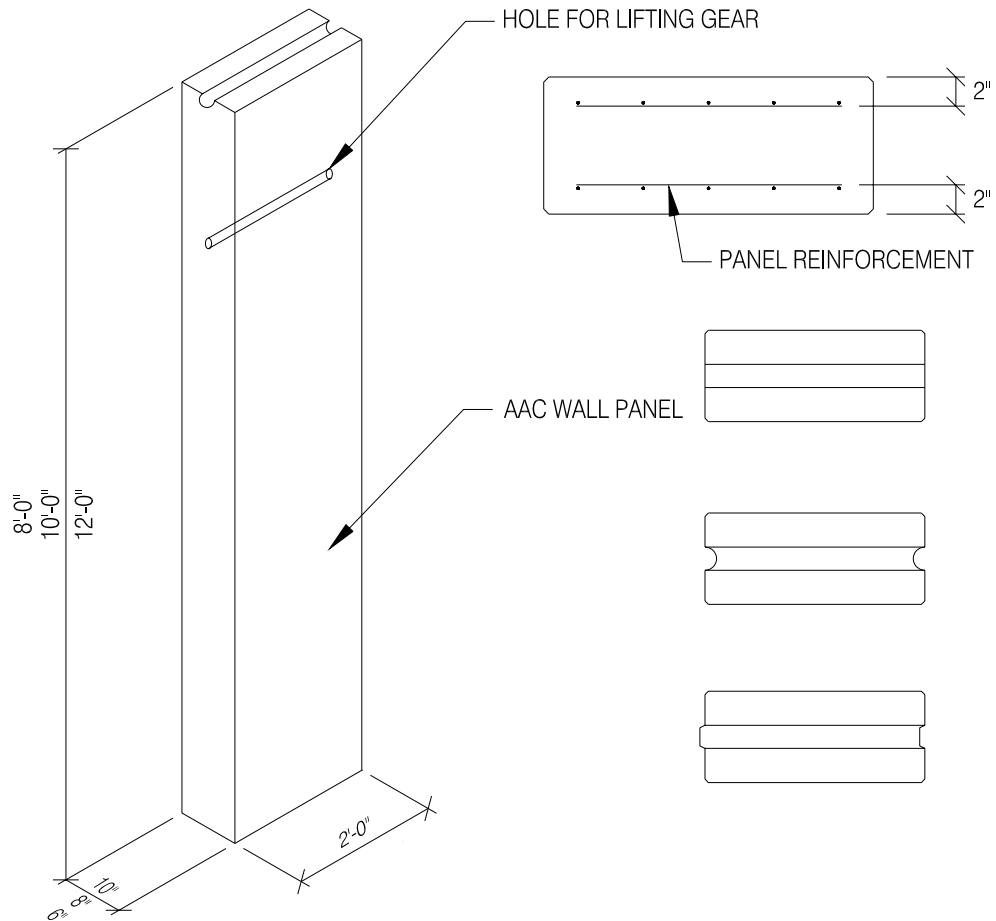


**5.1.2.2 EXTERIOR VERTICAL WALL PANEL AT STEEL BEAM**

1" = 1'-0"

**B.5.1.3**

**B.5.1.3.1 Typical Vertical Wall Panel and Sections**



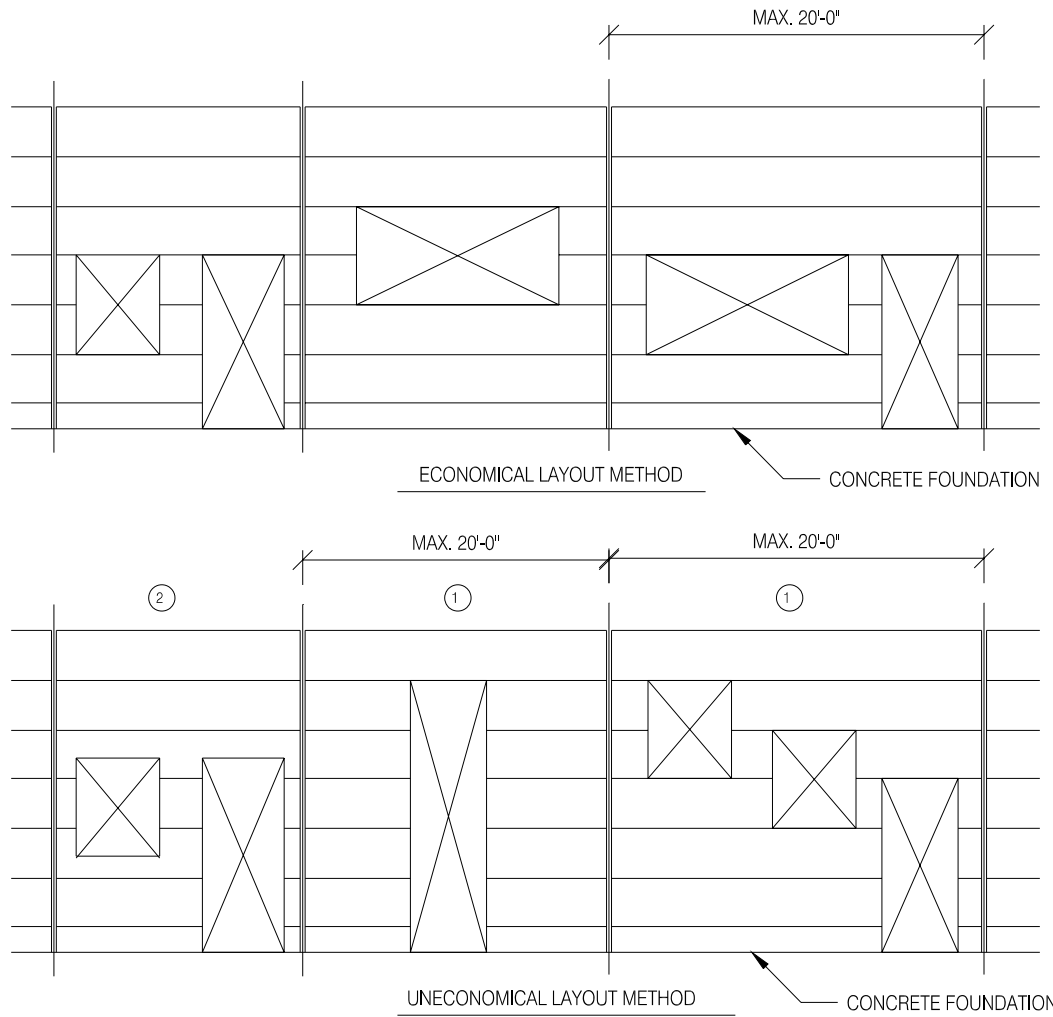
NOTE: CHAMFERED EDGES ARE RECOMMENDED

**5.1.3.1 TYPICAL VERTICAL  
WALL PANEL AND SECTIONS**

1" = 1'-0"

**B.5.1.4**

**B.5.1.4.1 Typical Horizontal Panel Layout**

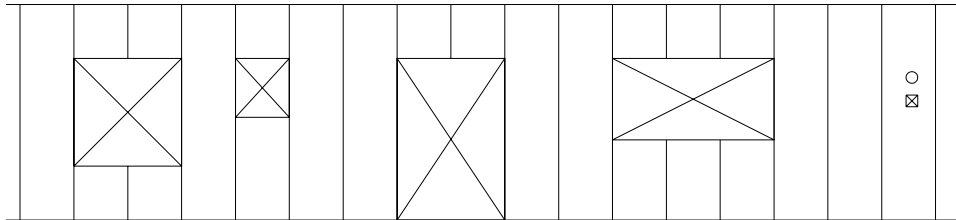


- ① REQUIRES ADDITIONAL STEEL BRACING
- ② REQUIRES ADDITIONAL COST FOR FIELD CUT

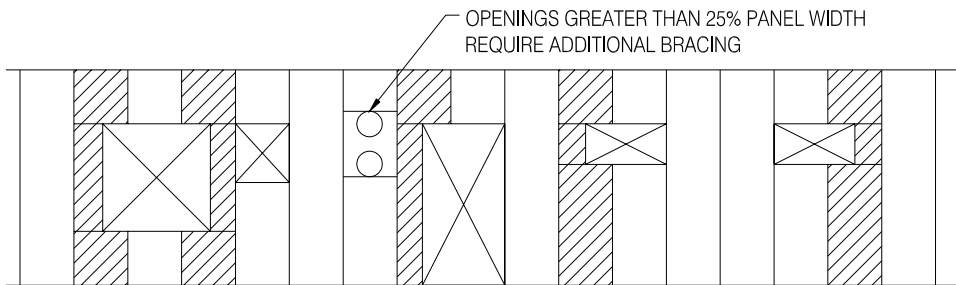
5.1.4.1 TYPICAL HORIZONTAL PANEL LAYOUT  
N.T.S.



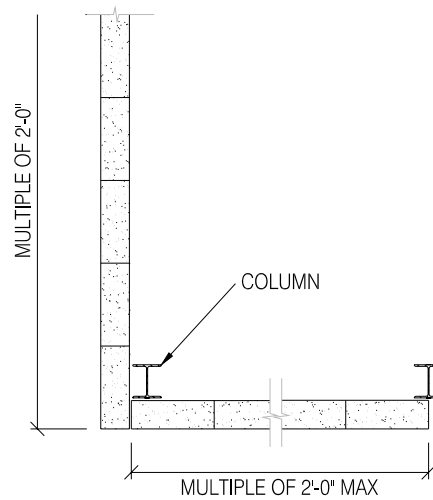
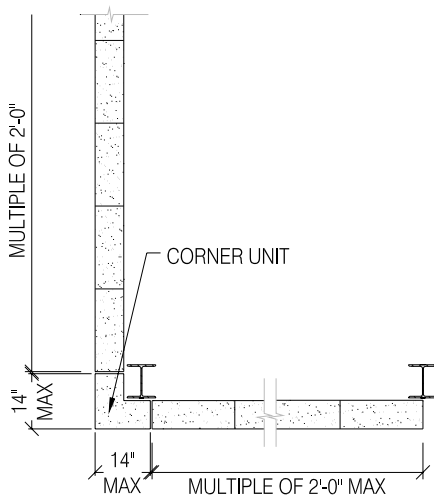
***B.5.1.4.2 Typical Vertical Panel Layout***



ECONOMICAL LAYOUT METHOD



UNECONOMICAL LAYOUT METHOD

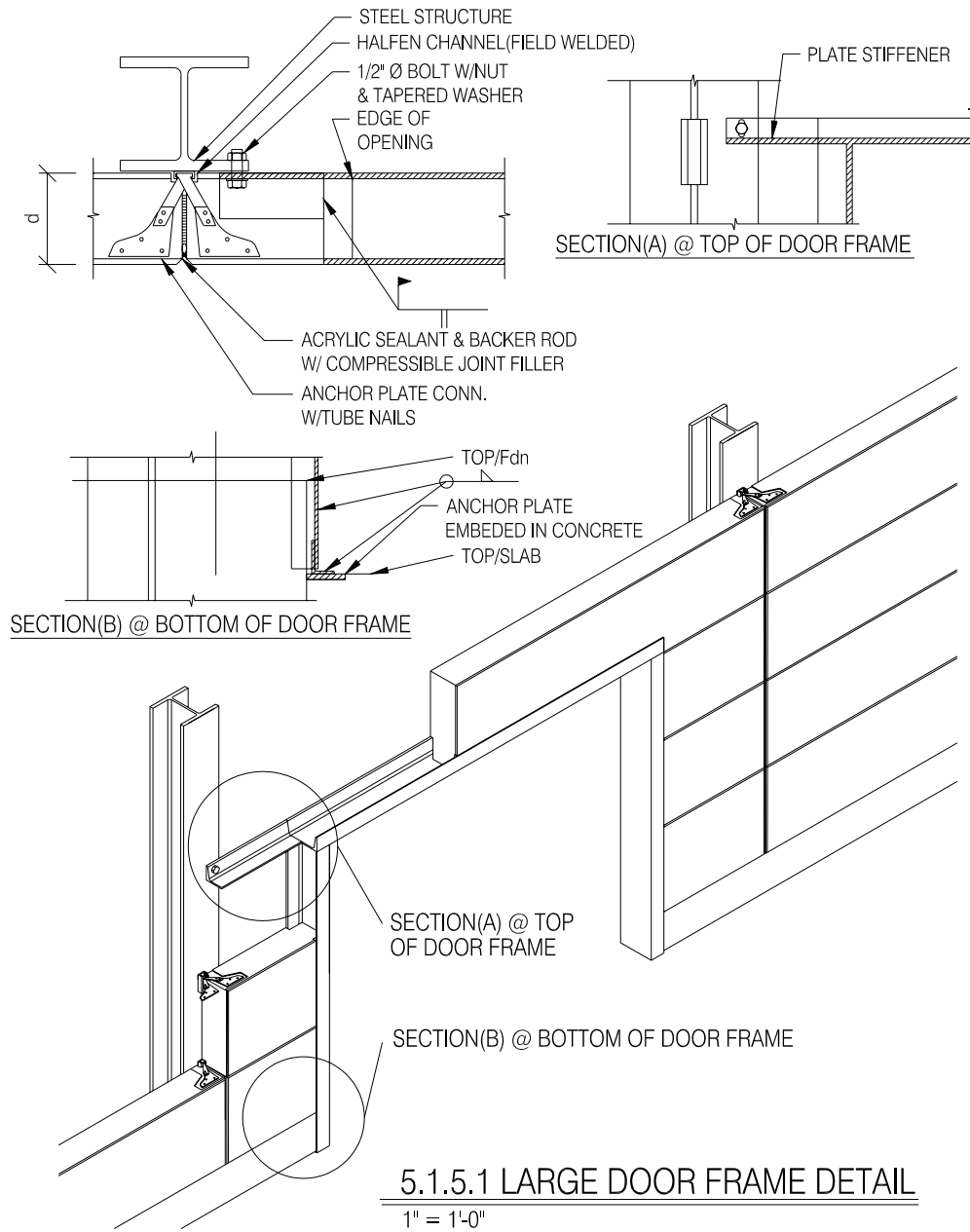


5.1.4.2 TYPICAL VERTICL PANEL LAYOUT

N.T.S.

**B.5.1.5**

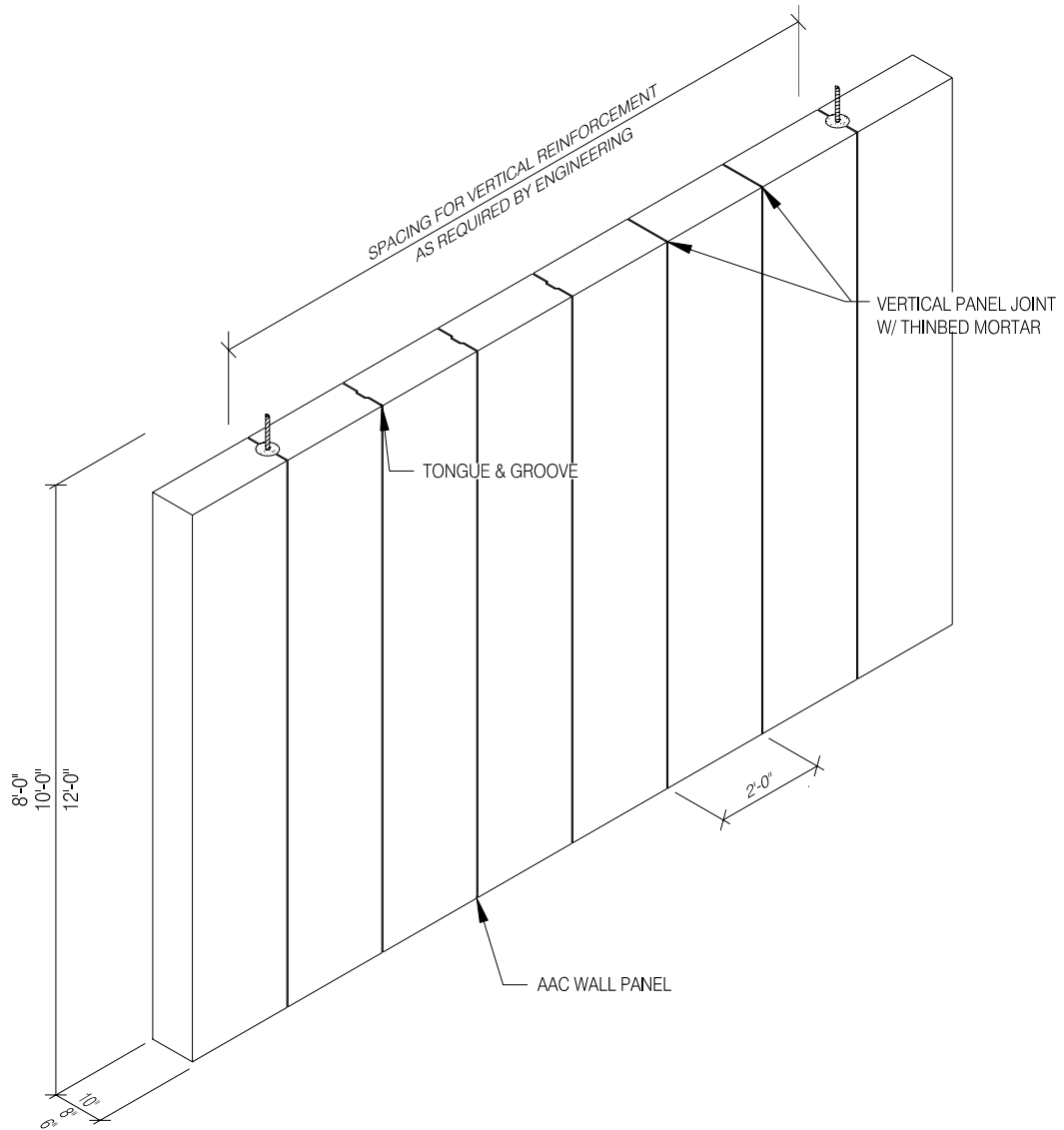
**B.5.1.5.1 Large Door Frame Detail**



## **B.5.2 Load Bearing Vertical Wall Panel Systems**

**B.5.2.1**

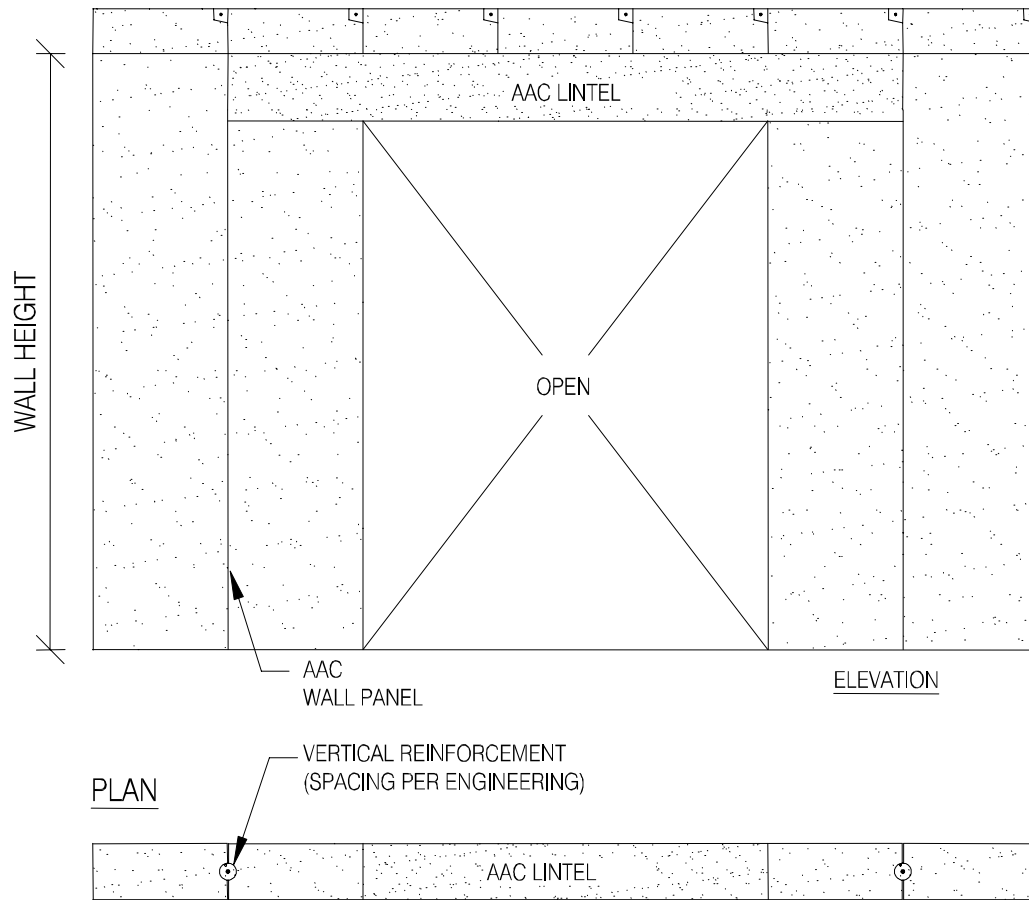
**B.5.2.1.1 Typical Vertical Joint Profile**



**5.2.1.1 TYPICAL VERTICAL JOINT PROFILE**

1" = 1'-0"

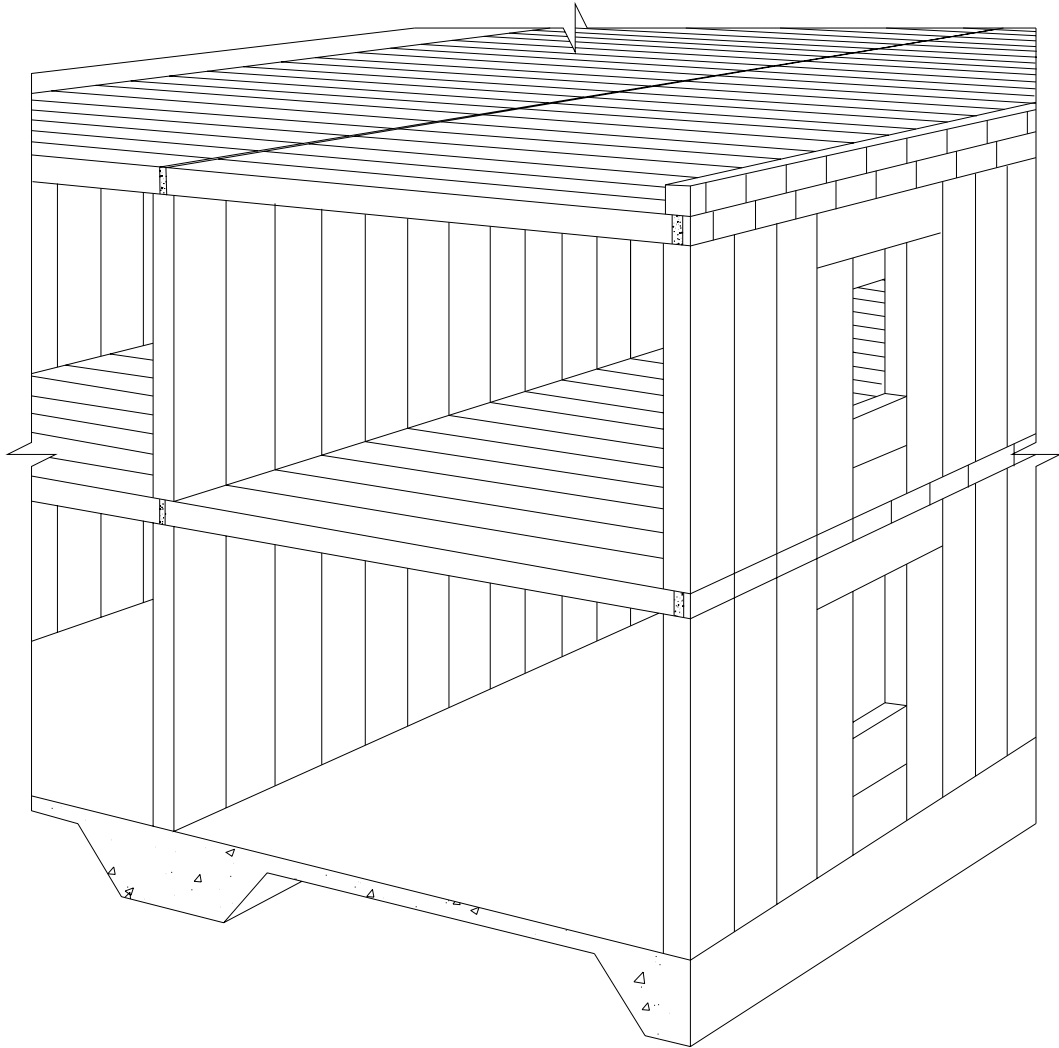
***B.5.2.1.2 Typical Vertical Joint Profile at AAC Lintel***



**5.2.1.2 TYPICAL VERTICAL JOINT PROFILE AT AAC LINTEL**

**B.5.2.2**

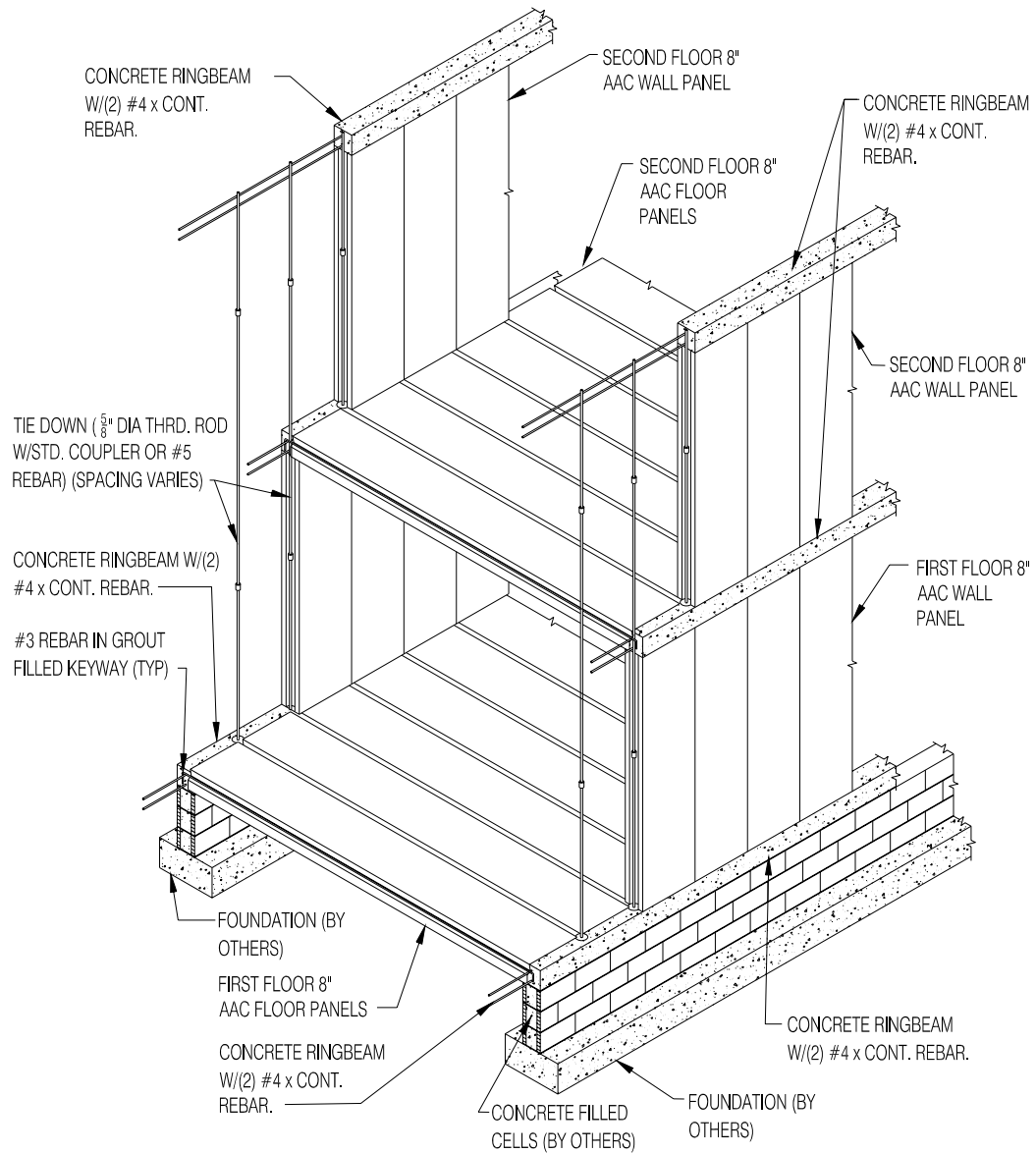
***B.5.2.2.1 Wall Section for Multiple Stories***



5.2.2.1 WALL SECTION FOR MULTIPLE STORIES

1"=1'-0"

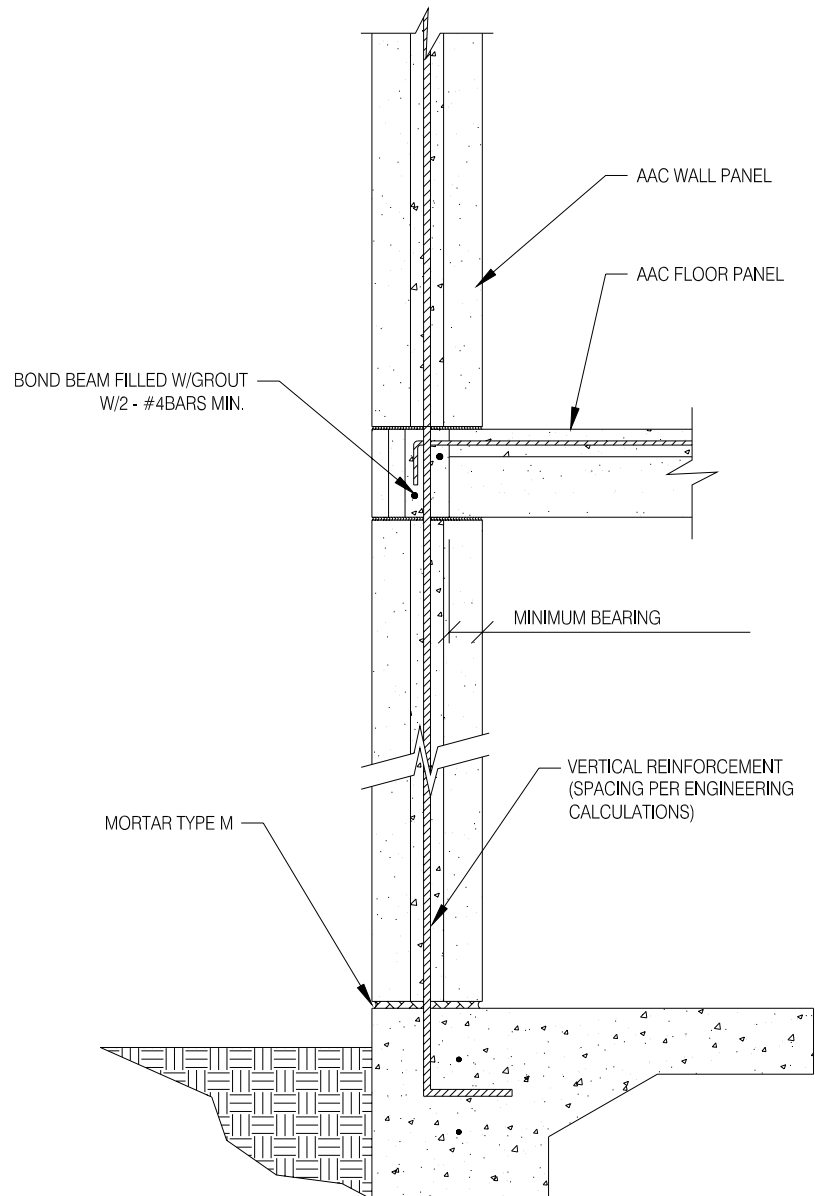
***B.5.2.2.2 Exterior Wall Section for Multiple Stories with Vertical Reinforcement***



**5.2.2.2 EXTERIOR WALL SECTION FOR MULTIPLE STORIES WITH STEEL REINFORCEMENT**

N.T.S.

***B.5.2.2.3 Exterior Wall Section for Multiple Stories with Vertical Reinforcement***



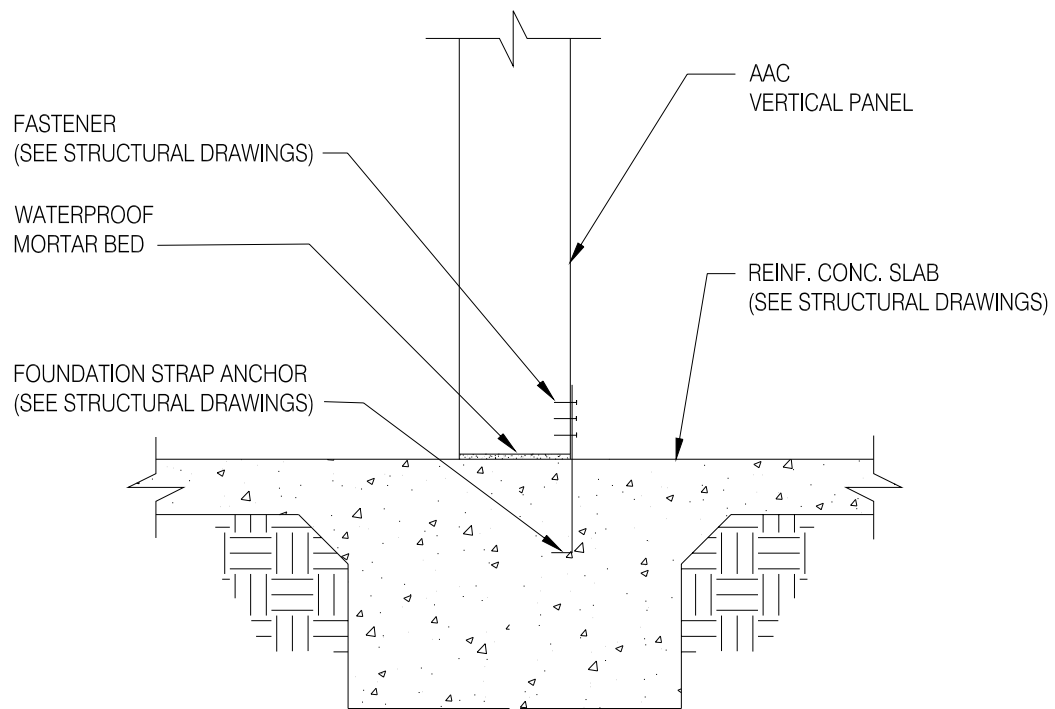
**5.2.2.3 EXTERIOR WALL SECTION AT MULTIPLE  
STORIES WITH VERTICAL REINFORCEMENT**

1" = 1'-0"



**B.5.2.3**

**B.5.2.3.1 Interior Bearing Section at Footing**

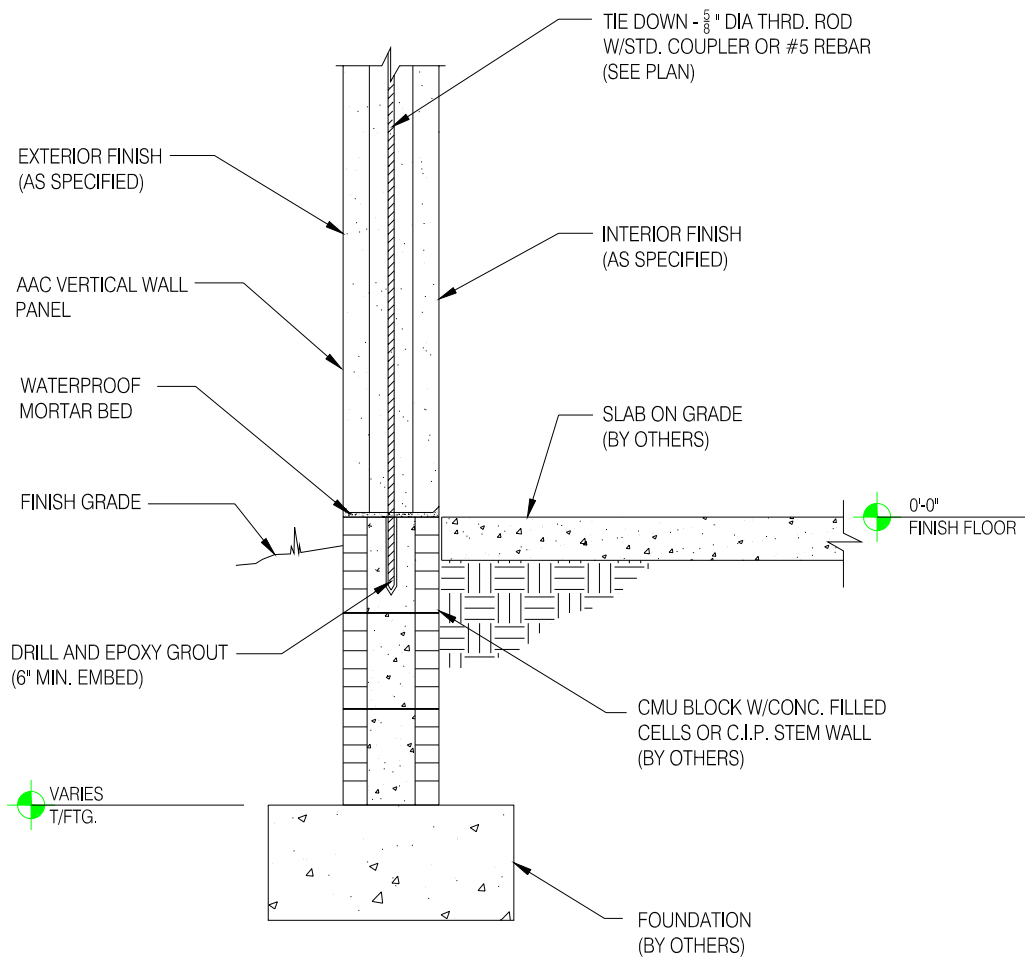


5.2.3.1 INTERIOR BEARING WALL SECTION AT FOOTING

1"=1'-0"

**B.5.2.4**

**B.5.2.4.1 Exterior Wall Panel at CMU Stem Wall and Footing**

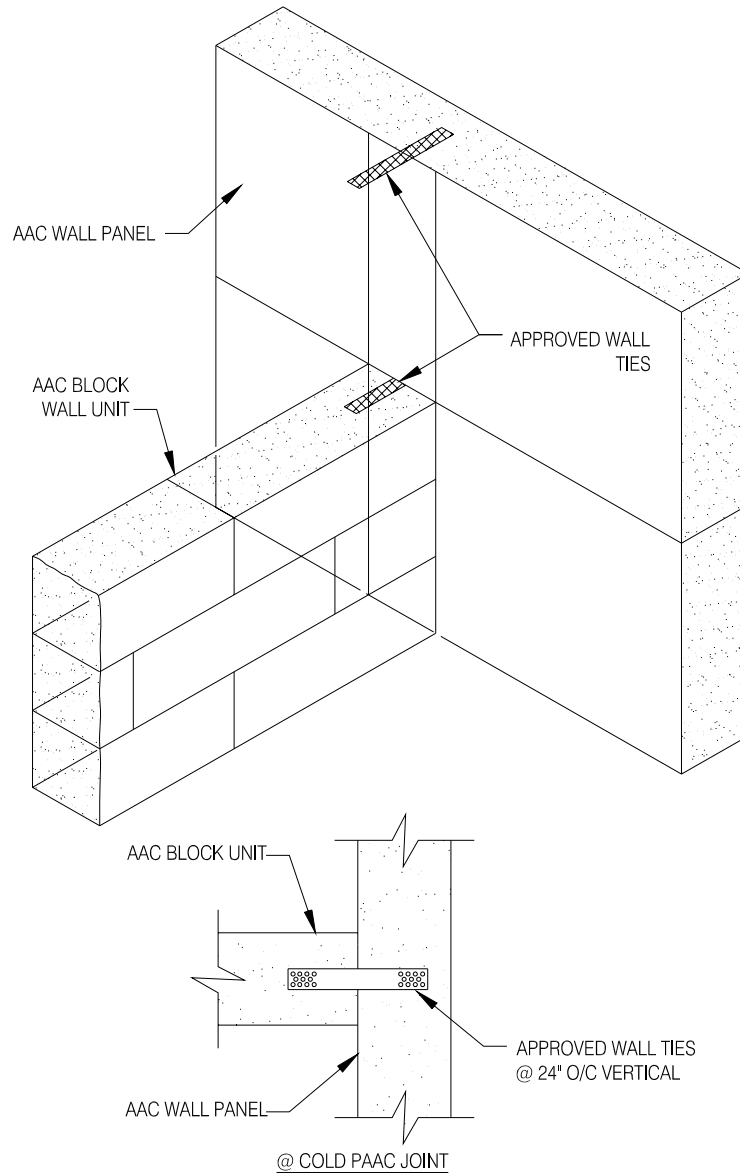


**5.2.4.1 EXTERIOR WALL PANEL @ CMU STEM WALL AND FOOTING**

1" = 1'-0"

**B.5.2.5**

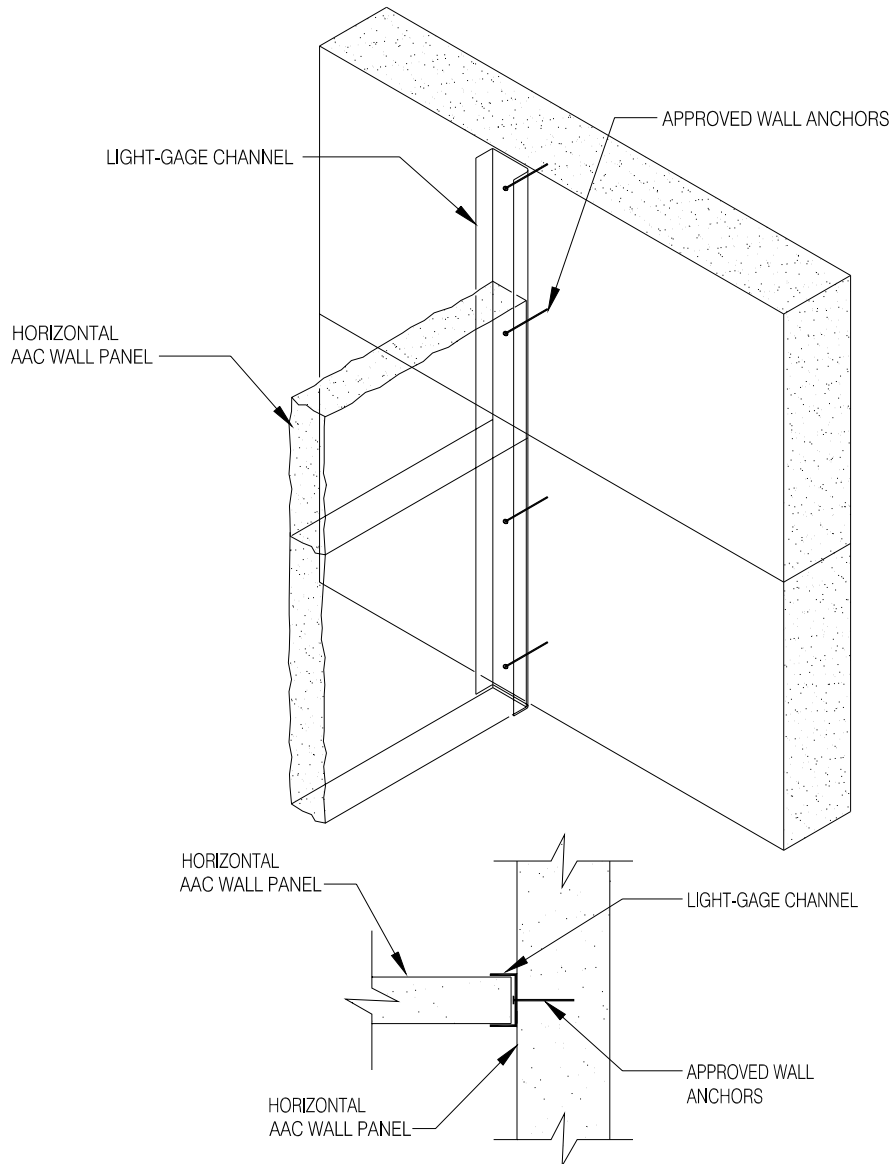
**B.5.2.5.1 Intersection of AAC Panel / Blocks**



**5.2.5.1 INTERSECTION OF AAC PANELS/BLOCKS**

1" = 1'-0"

***B.5.2.5.2 Intersection of Interior Partition Panels***

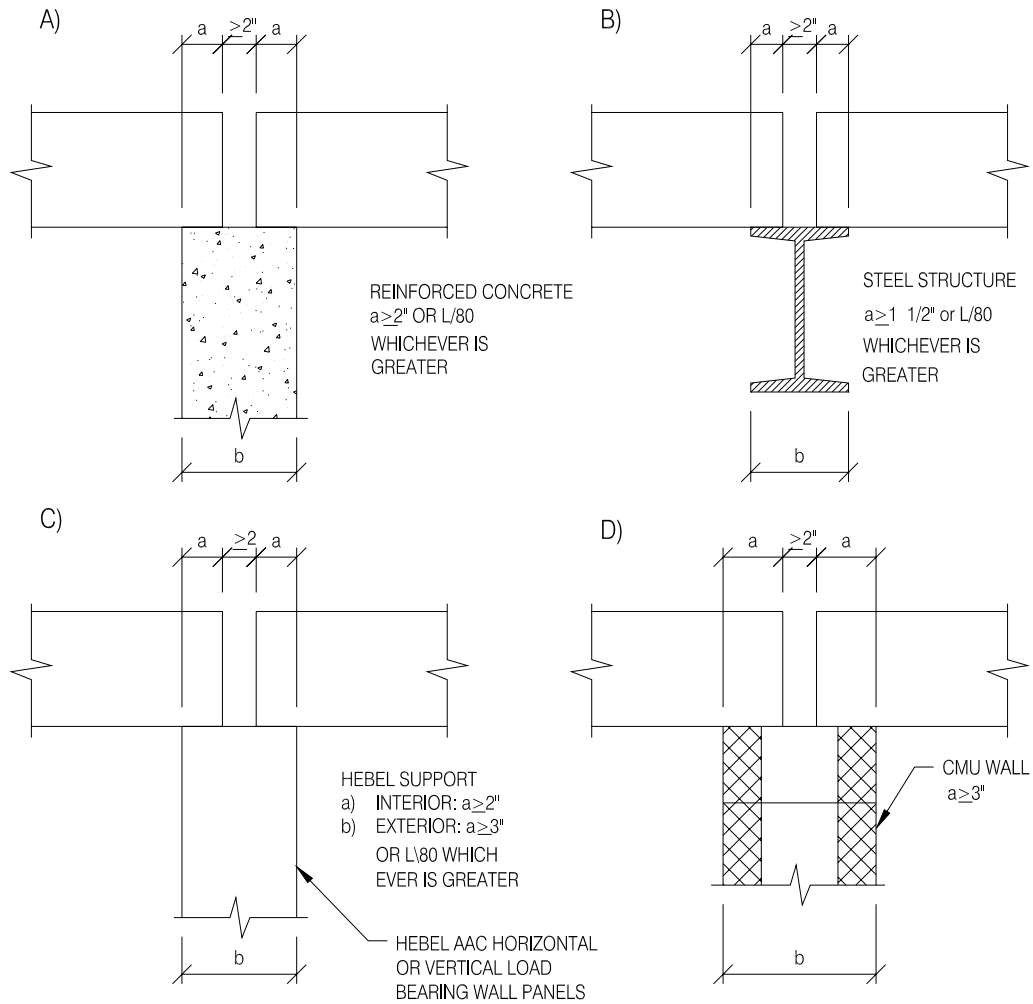


**5.2.5.2 INTERSECTION OF INTERIOR PARTITION PANELS**

1"=1'-0"

## B.5.3 Floor and Roof

### B.5.3.1 Minimum Bearing Details

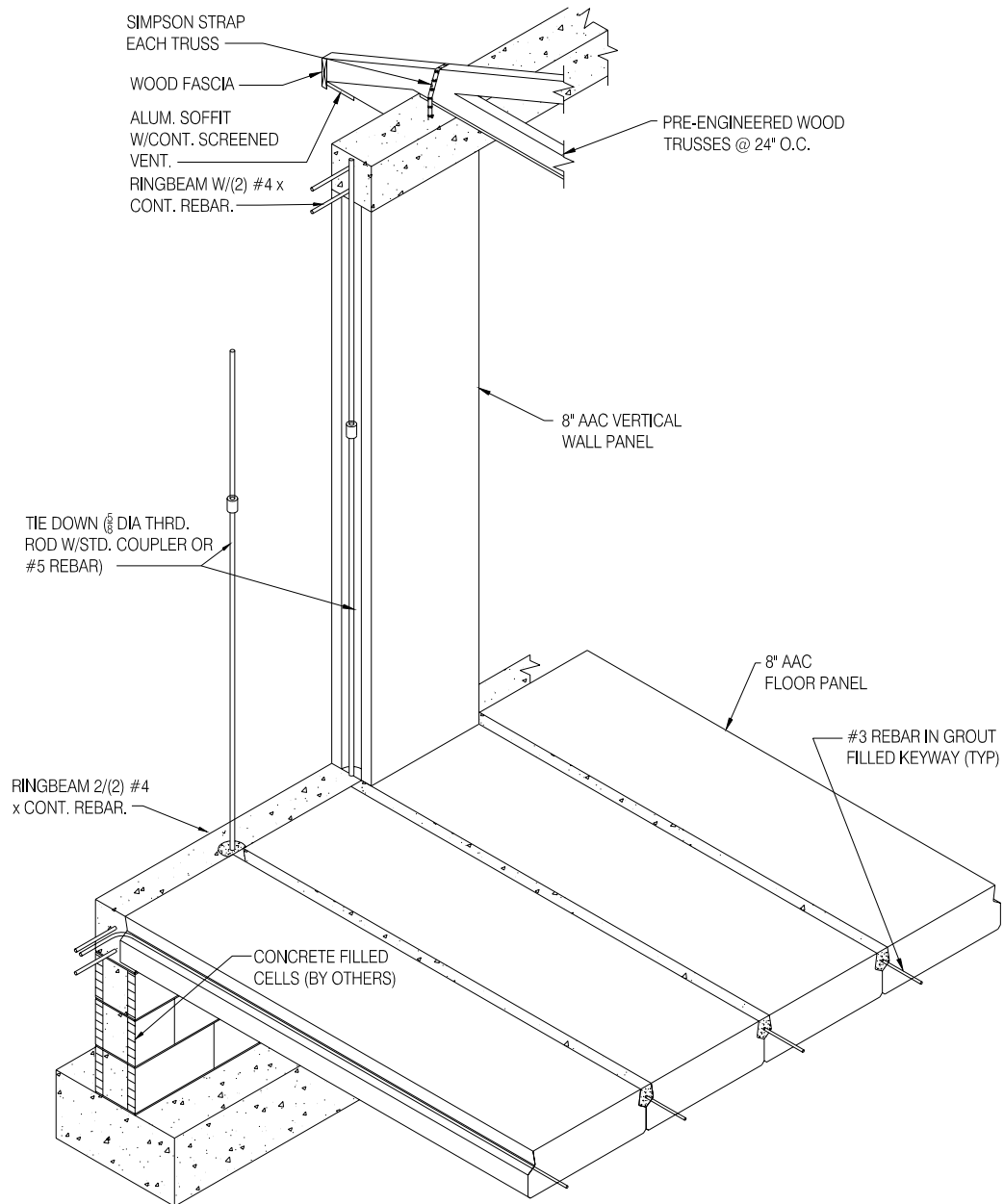


NOTE:  $L = \text{CLEAR SPAN} + a + L = (\text{TOTAL PANEL LENGTH})$   
 $b = a + a + 2"$  (MINIMUM BEARING WIDTH)

### 5.3.1 MINIMUM BEARING DETAILS

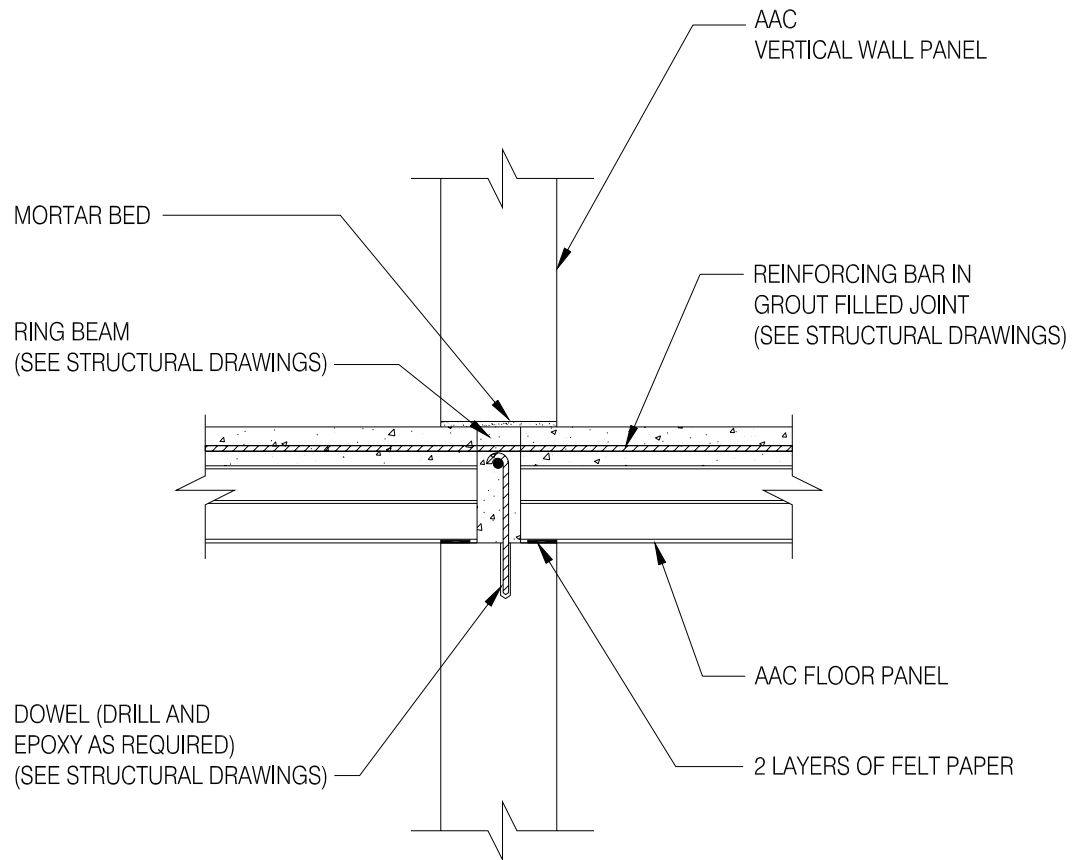
N.T.S.

**B.5.3.2 Exterior Floor Panel Support Wall Detail**



**5.3.2 EXTERIOR FLOOR PANEL SUPPORT DETAIL**  
 N.T.S.

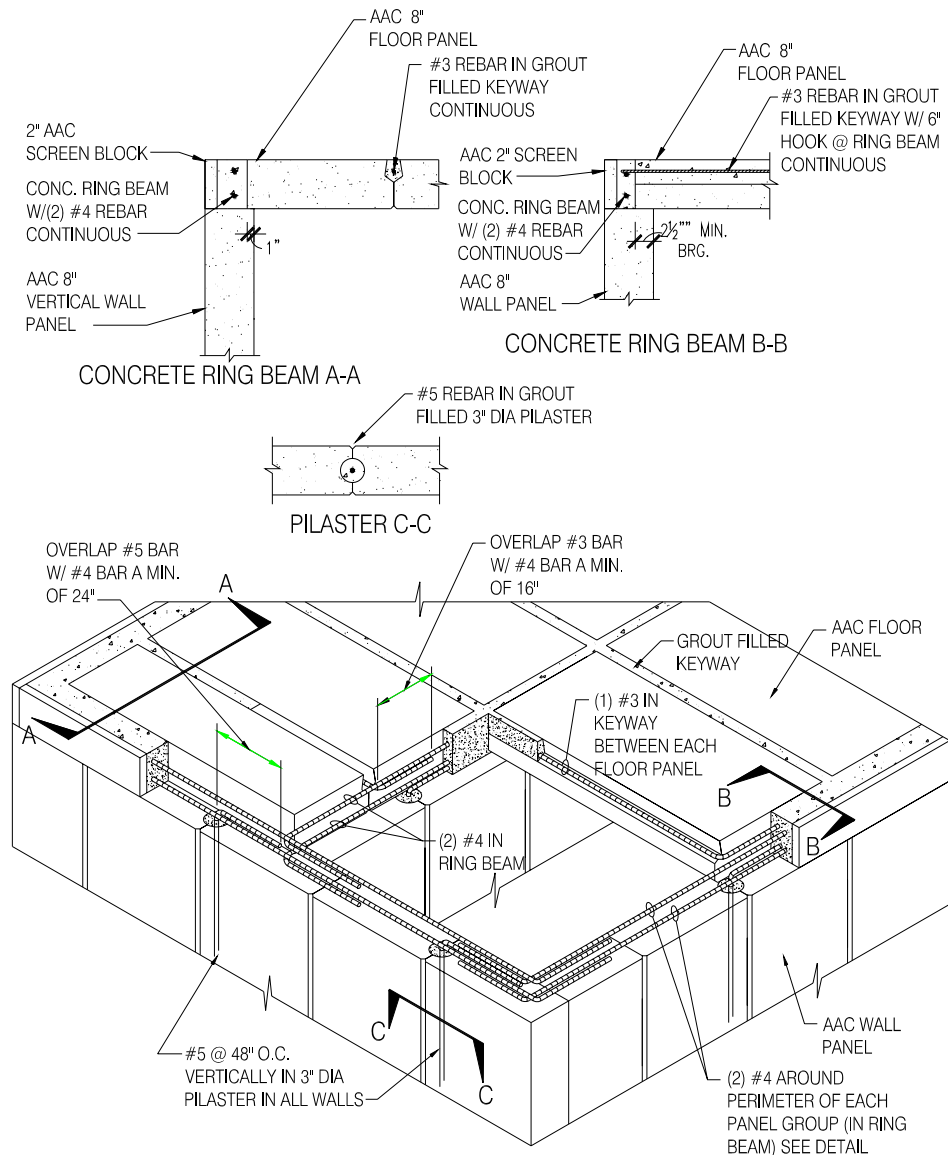
***B.5.3.3 Interior Floor Panel Support Detail***



**5.3.3 INTERIOR FLOOR PANEL SUPPORT DETAIL**

1" = 1'-0"

**B.5.3.4 Grout Key and Bond Beam Reinforcement**



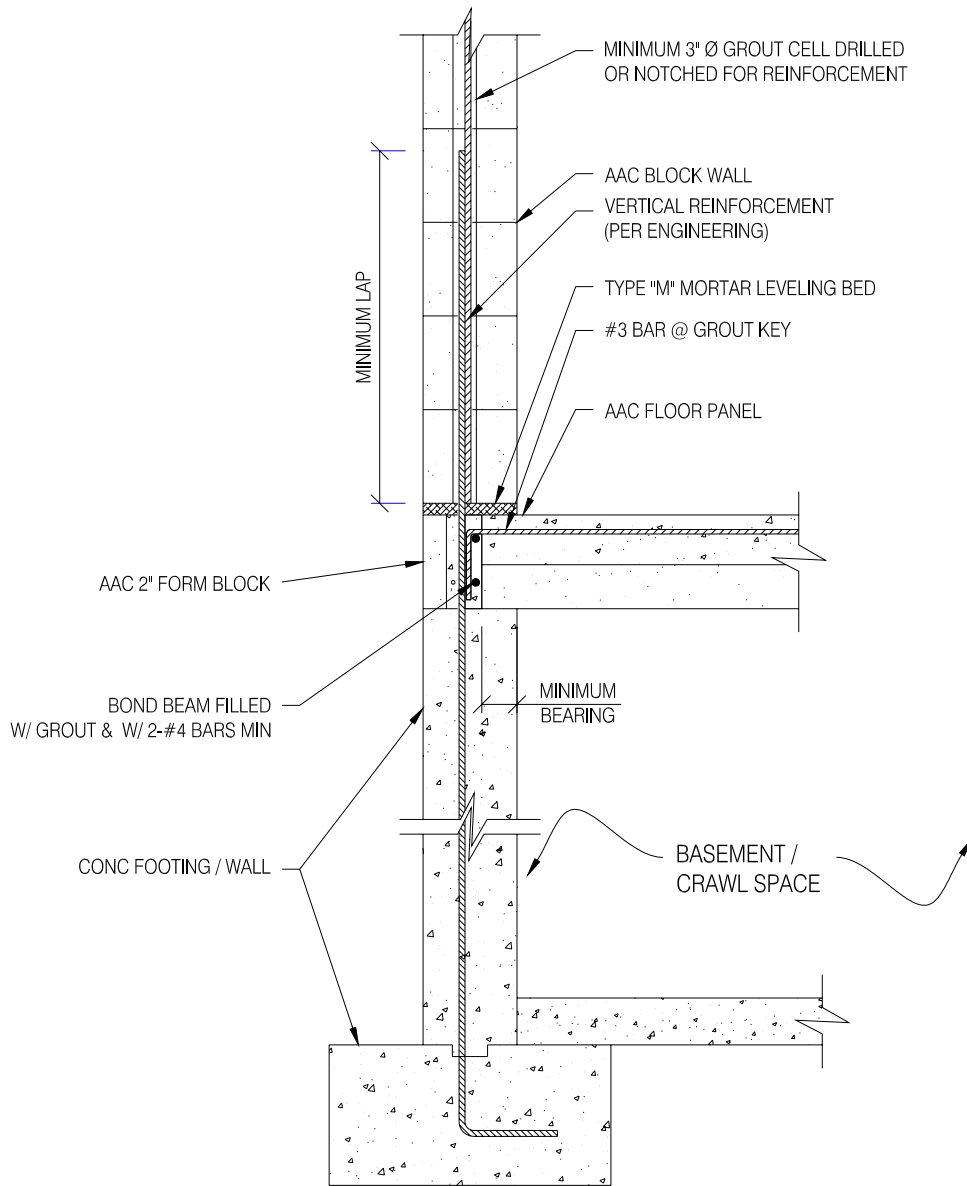
**5.3.4 GROUT KEY AND BOND BEAM REINFORCEMENT**

N.T.S.



**B.5.3.5**

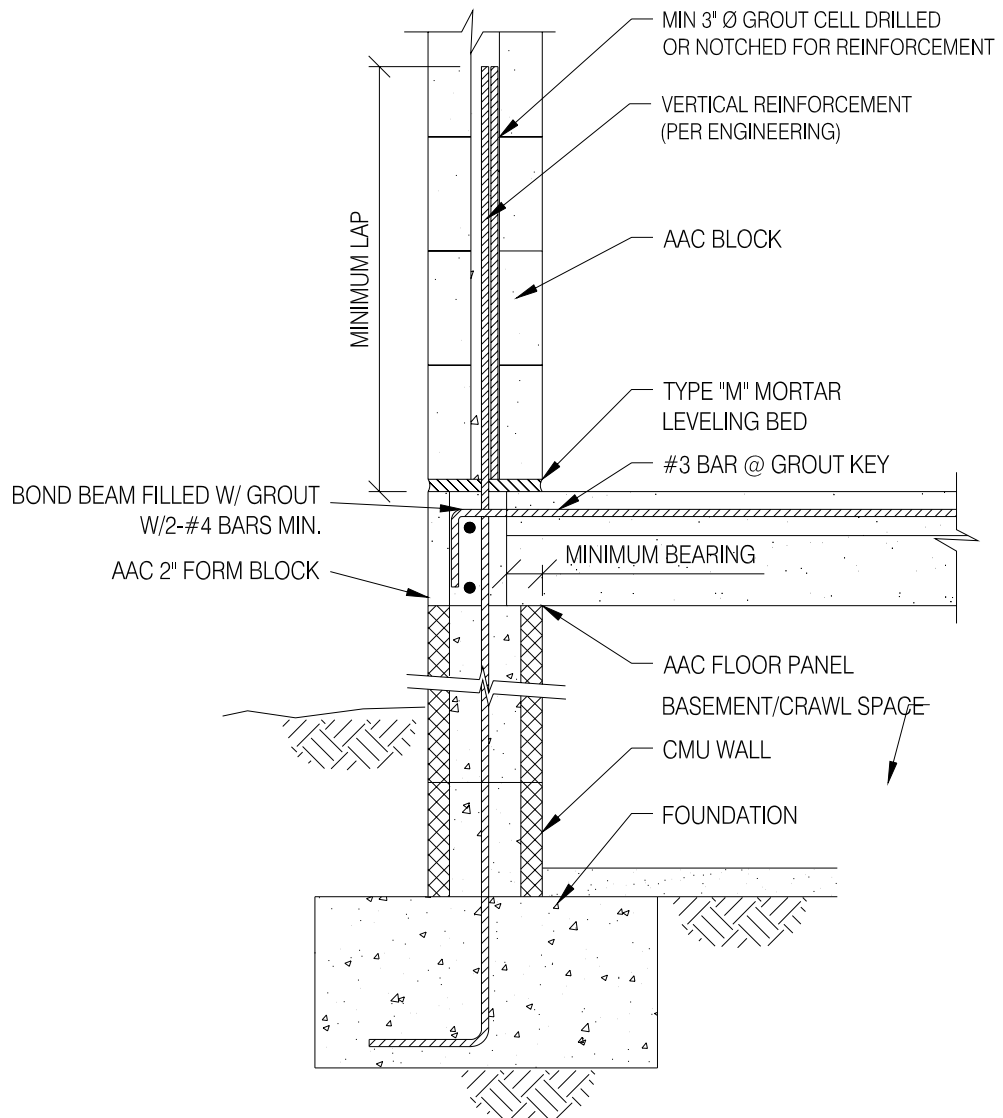
**B.5.3.5.1 Floor Panel at Concrete Basement Wall**



**5.3.5.1 FLOOR PANEL @ CONCRETE BASEMENT WALL**

1" = 1'-0"

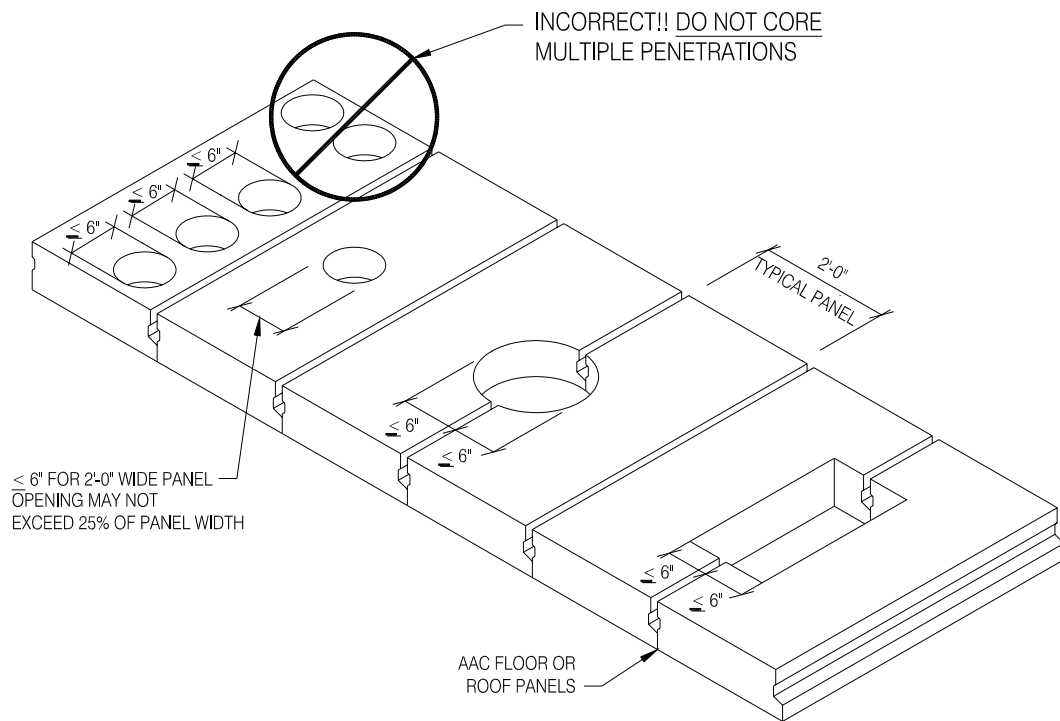
**B.5.3.5.2 Floor Panel at CMU Basement Wall**



**5.3.5.2 FLOOR PANEL @ CMU BASEMENT WALL**

1" = 1'-0"

**B.5.3.6 Allowable Sizes and Location of On-Site Coring**



5.3.6 ALLOWABLE SIZE AND LOCATION OF ON-SITE CORING

## **B.6 REFERENCES**

Argudo, J.F., “Evaluation and Synthesis of Experimental Data for Autoclaved Aerated Concrete,” *MS Thesis*, The University of Texas at Austin, August 2003.

*Autoclaved Aerated Concrete: Properties, Testing and Design*, RILEM Recommended Practice, RILEM Technical Committees 78-MCA and 51-ALC, E & FN Spon, London, 1993.

Fouad, Fouad, “*Physical and Mechanical Properties of AAC Produced in the United States*,” Report to the Autoclaved Aerated Concrete Products Association, 2002.

Tanner 2003: Tanner, J.E., “Development of Proposed Code Equations for AAC Shear Walls” *PhD Dissertation*, The University of Texas at Austin, May 2003.

# **APPENDIX C**

## **Proposed Code Design Provisions and Commentary**

### **C.1 PROPOSED CODE DESIGN PROVISIONS**

The design provisions proposed here are intended to be used in conjunction with the provisions of ACI 318-02. The provisions of that document are intended as the default, and are augmented, modified or replaced by the provisions of this Appendix. Deleted material is denoted by a strikethrough; added material is denoted by an underline.

## Chapter 2 — Definitions

*Add the following definitions, here and in the chapters where they are used.*

Autoclaved Aerated Concrete — low-density cementitious product of calcium silicate hydrates, defined in ASTM C 1386.

## **Chapter 3 — Materials**

*Add the following section, renumber subsequent sections accordingly:*

### 3.8 AAC Panels and Related Materials

3.8.1 Reinforced panels shall conform to ASTM C 1452.

3.8.2 Thin-bed mortar for AAC panels shall conform to the performance requirements of the AAC manufacturer.

3.8.2 Bedding mortar for AAC panels shall conform to ASTM C270, Types M, S, or N.

3.8.3 Grout for AAC masonry shall conform to ASTM C476.

*Renumber Section 3.9 - Referenced Standards*

*Add the following standards:*

ASTM C 270 Specification for Mortar for Unit Masonry

ASTM C 476 Specification for Grout for Masonry

ASTM C1006 Splitting Tensile Strength of Masonry Units

ASTM C 1386 Specification for Precast Autoclaved Aerated Concrete  
(PAAC) Wall Construction Units

ASTM C 1452 Specification for Reinforced Autoclaved Aerated Concrete  
Elements

ASTM C ZZZZ Method of Test for Determining the Modulus of Elasticity  
of Autoclaved Aerated Concrete (under development by ASTM C-27.60)



## Chapter 4 -- Durability Requirements

*Remove Section 4.1 on water - cementitious materials ratios.*

*Remove Section 4.2 on freezing and thawing exposures and replace by the following:*

### 4.2 Freezing and Thawing Exposures

4.2.1 - AAC shall not be used in below-grade applications where it could be subjected to cycles of freezing and thawing while critically saturated

4.2.2 - AAC masonry exposed to weather shall be protected with an exterior wythe of masonry, a cladding system, or a coating complying with the requirements of (a) and (b)

a) Vapor permeability: the PERM rating of the coating, determined in accordance with E 96, shall not be less than 5.

b) Liquid permeability: the coating shall show no leakage when tested using the following procedure:

As shown in Figure 1, prepare an AAC masonry assemblage with plan dimensions of 12 in. by 12 in. (0.3 m) and a thickness of 1 in. (25 mm). Make the assemblage using two pieces of AAC material

with a vertically oriented joint between them. Join the two pieces at the joint using thin-bed or thick-bed mortar as appropriate to the AAC masonry being tested. Cover the top surface with the coating to be tested. Affix to the top surface of the specimen, over the joint, a clear glass or plastic measurement tube with an inside diameter between 2 and 4 in. (50 and 100 mm), and a height of at least 24 in. (0.6 m). Prepare a reference tube, closed at the bottom, of the same material and dimensions as the measurement tube. Fill the measurement tube and the reference tube with water to a height of 21.6 in. (0.55 m), within a tolerance of  $\pm 1$  in. (25 mm). Note the original height of water, and the height after 5 h, in the measurement tube and in the reference tube. Record the difference between the initial height and the final height of water in the measurement tube, and in the reference tube. If those differences differ by less than 1 mm, the coating shall be considered to have shown no leakage.

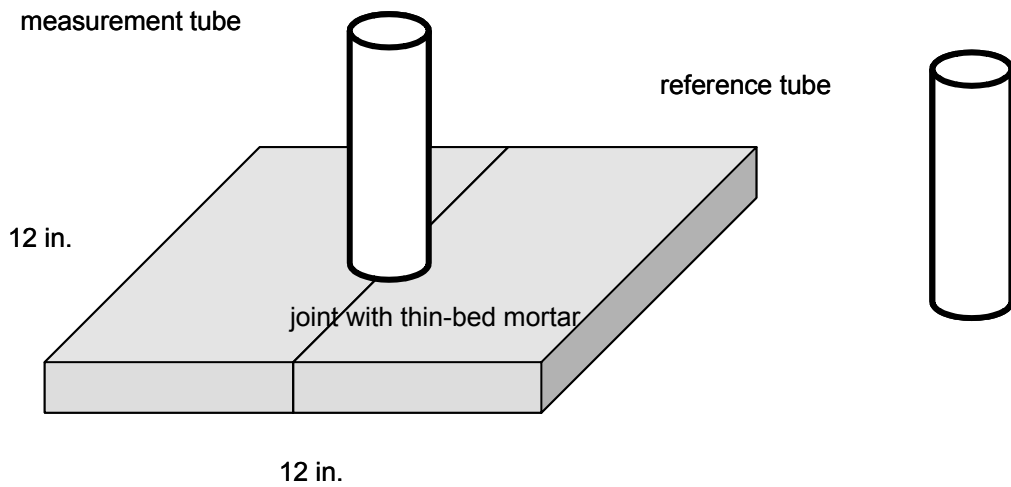


***Figure C.1*** *Assemblage for testing liquid permeability of exterior surface treatment for AAC panels*

***Delete Section 4.3.1 and replace by the following:***

**4.3.1** AAC shall be protected against injurious concentrations of sulfates as required by 4.2.

***Delete Section 4.4 on corrosion protection of reinforcement and replace by the following:***

**4.4.1** Factory-installed reinforcement for AAC panels shall be protected from corrosion in accordance with ASTM C 1452.

## **Chapter 5 -- Concrete Quality, Mixing and Placing**

*Remove 5.1 (General) and replace by the following:*

5.1.1 AAC shall comply with the provisions of ASTM C1386 for the strength class specified in the design.

*Remove 5.2 through 5.6 completely.*

*Remove 5.7 and replace by the following:*

5.7 - Preparation of equipment and place of deposit

5.7.1 - Preparation before laying of leveling mortar and placement of AAC panels shall include the following:

(a) All equipment for mixing and transporting leveling mortar shall be clean.

(b) All debris and ice shall be removed from the area where the leveling bed mortar is to be placed.

(c) Reinforcement shall be clean of ice or other deleterious coatings.

**5.7.2 - Preparation before placing grout**

(a) All cavities and keys receiving grout shall be clean and free of debris.

(b) Keys and cavities shall be wet prior to placing grout, or grout shall contain shrinkage retarding admixture.

**5.7.3- Preparation before placing thin-bed mortar**

(a) Inspect each panel for imperfections that prohibit the panel joint from sitting farther than 1/16 in. from an adjacent panel.

(b) Clean and wet each panel prior to applying the thin-bed mortar.

**5.7.4- Construction process for vertical panels**

(a) Apply thin-bed mortar to the panels on both sides of the vertical joint.

(b) Apply pressure perpendicular to the vertical joint using horizontally oriented clamps.

***Delete 5.8 through 5.11***

*Delete 5.12 and replace by the following:*

5.12 - Cold Weather Requirements

5.12.1 - All AAC materials and all reinforcement shall be free from frost.

5.12.2 - Thin-bed mortar and bedding mortar shall not be used in ambient temperatures less than 32 F without provision for proper curing and protection from freezing.

## **Chapter 6 -- Formwork, Embedded Pipes and Construction Joints**

*Delete 6.1 - Formwork*

*Remove 6.3 and replace by the following:*

### **6.3 - Conduits and Pipes Passing through AAC**

Conduits, pipes and sleeves passing through AAC elements, and the their routed openings, shall not impair significantly the strength of the construction.

*Remove 6.4 - Construction Joints.*

## **Chapter 7 -- Details of Reinforcement**

*Add 7.1 - Scope; renumber other sections as appropriate*

### **7.1 - Scope**

Factory-installed reinforcement in AAC panels shall meet the requirements of ASTM C1452. The remaining provisions of this chapter shall apply to field-installed reinforcement only.



## Chapter 8 — Analysis and Design — General Considerations

*Modify Section 8.5 — Modulus of Elasticity as follows:*

*Remove 8.5.1 (concrete) and replace by the following:*

8.5.1 — The modulus of elasticity  $E_{AAC}$  for AAC shall be taken as  $E = 6500 f_{AAC}^{0.6}$  (in psi).

*Add a new Section 8.5.2 and renumber remaining sections appropriately:*

8.5.2 - The modulus of elasticity  $E_{grout}$  for grout shall be taken as  $500 f_g'$ .

*Add a new Section 8.13 – Material properties of AAC:*

8.13.1 The splitting tensile strength  $f_{tAAC}$  shall be determined by Equation 8-1.

$$\underline{f_{tAAC} = 2.4\sqrt{f'_{AAC}} \text{ (8-1)}}$$

$f_{AAC}'$  and  $f_{tAAC}$  in psi

8.13.2 The modulus of rupture,  $f_{rAAC}$ , for AAC masonry elements shall be taken as two times the masonry splitting tensile strength,  $f_{tAAC}$ . If a section of AAC contains a horizontal leveling bed, the value of  $f_{rAAC}$  shall not exceed 50 psi (345 kPa) at that section. If a section of AAC contains a bed joint between thin-bed mortar and AAC the value of  $f_{rAAC}$  shall not exceed 80 psi (552 kPa) at that section.

8.13.3 The direct shear strength  $f_v$  shall be determined by Equation 8-2.

$$f_{vt} = 0.15 f'_{AAC} \quad (8-2),$$

$f_{AAC}$  and  $f_v$  in psi

8.13.4 The shear strength of a joint between AAC and grout shall be 36 psi (0.25 MPa). The shear strength of a joint between AAC and thin-bed mortar shall be 18 psi (0.13 MPa).

## Chapter 9 — Strength and Serviceability

*Add the following Section 9.3.2.8:*

9.3.2.8 – Adhesion.....0.67

### 9.5 - Deflections

*9.5.1 - replace “reinforced concrete” by “AAC”*

*9.5.2 -Add the following at the end of the existing 9.5.2.1:*

Footnote (2a) of Table 9.5(a) shall apply, using  $\rho_{1386}$ . Footnote (2b) shall not apply.

*Replace 9.5.2.3 by the following:*

9.5.2.3 - Immediate deflections shall be calculated using an effective flexural stiffness ( $EI_e$ ) corresponding to the unfactored moment ( $M_a$ ). The effective flexural stiffness ( $EI_e$ ) shall be obtained by linear interpolation between

the cracking point ( $M_{cr}$ ,  $\phi_{cr}$ ) and the yielding points ( $M_y$ ,  $\phi_y$ ) on a bilinear moment-curvature diagram. For these calculations, the modulus of rupture of the AAC shall be taken as twice the splitting tensile strength by ASTM C1006, at the moisture content specified by ASTM C1386.

*Replace 9.5.2.5 by the following:*

9.5.2.5 — Unless values are obtained by a more comprehensive analysis, the total long-term deflection (including the additional long-term deflection resulting from creep and shrinkage) of AAC flexural members shall be determined using Section 9.5.2.3, with an effective modulus equal to  $\frac{E_{AAC}}{1.5}$ .

## Chapter 10 – Flexure and Axial Loads

*Remove and replace “concrete” throughout by “AAC.”*

*10.2.7.3 - Remove and replace by the following:*

10.2.7.3 - The factor  $\beta_1$  shall be taken as 0.67.

*Section 10.5 - Minimum reinforcement of flexural members -- replace Equation 10-3 by the following.*

$$\underline{A_{S,\min} = \frac{4\sqrt{f'_{AAC}}}{f_y} bd}$$

*Delete Sections 10.6 through 10.16. Retain Section 10.17.*

## Chapter 11 — Shear and Torsion

*Throughout Chapter 11, replace  $V_c$  by  $V_{AAC}$ . Make additional changes as noted below.*

*Change Equation 11-3 to the following:*

$$\underline{V_{AAC} = 0.8 \sqrt{f'_{AAC}} b_w d}$$

*Change Equation 11-4 to the following:*

$$\underline{V_{AAC} = 0.8 \sqrt{f'_{AAC}} \left( 1 + \frac{N_u}{2000 A_g} \right) b_w d}$$

*Delete Section 11.3.2.*

*Delete Section 11.4.*

***Add the following to Section 11.5.6.2:***

The maximum shear strength provided by wire reinforcement bar embedded in AAC ( $V_{sb}$ ) shall be limited by  $V_{sb} \leq d_{long} \cdot s \cdot f'_{AAC}$ , the bearing capacity of the AAC on the longitudinally oriented cross-wires. Shear strength provided by the wire shall be included for resisting gravity loads only.

***Delete Section 11.6 - Torsion.***

***Modify Section 11.7.4.1 as follows:***

The shear strength  $V_n$  for AAC shall be computed as:

$$V_n = (N) \cdot \mu \text{ Eq.}$$

(11-xx)

At an interface where uncracked thin-bed mortar is present, the nominal sliding shear capacity shall be calculated as the greater of Eq. (11-xx) and the capacity calculated by the shear strength of AAC at a thin-bed mortar joint, defined in Section 8.14.1, multiplied by the area of a thin-bed mortar joint. In an AAC shear wall, it shall also be permitted to include the force in the tensile steel at a given cross-section ( $A_s f_s$ ) in the axial load.

**Add the following to Section 11.7.4.3:**

<u>AAC placed against leveling mortar.....</u>	<u>1.0</u>
<u>AAC placed against AAC .....</u>	<u>0.75</u>

**Delete Section 11.8 - Deep beams**

**Delete Section 11.9 - Special provisions for brackets and corbels.**

**In Section 11.10, replace Equation (11-29) by the following:**

$$V_{AAC} = 0.9 \ell_w h \sqrt{f'_{AAC}} \sqrt{1 + \frac{N_u}{2.4 \sqrt{f'_{AAC}} \ell_w h}}$$

**In Section 11.10, replace Equation 11-30 by the following:**

$$V_{AAC} = \frac{0.17 h f'_{AAC} \ell_w^2 h_{wall}}{h_{wall}^2 + \left(\frac{3}{4} \ell_w\right)^2}$$



*Remove Section 11.10.7 and replace by the following:*

**11.10.7 — Special provisions for shear walls with AAC panels oriented vertically** – Nominal shear strength and flexural strength shall be determined assuming that vertical cracks exist at each vertical joint. The shear capacity shall be determined using Equation (11-4) if the panel height divided by the panel width exceeds 3. It shall be permitted to design assuming vertical cracks at every third joint, using Equation (11-29), if the construction requirements of Section 5.7.4 are met.

*Delete Section 11.10.8.*

*Remove Section 11.10.9 and replace by the following:*

**11.10.9 — Design of shear reinforcement for walls**

**11.10.9.1** — Where factored shear force  $V_u$  exceeds shear strength  $\phi V_{AAC}$ , horizontal shear reinforcement shall be provided to satisfy Eq. (11-1) and (11-2), where shear strength  $V_s$  is computed by

$$V_s = \frac{A_v f_y d}{s_2} \quad (11-31)$$

where  $A_v$  is the area of deformed horizontal reinforcement embedded in grout within a distance  $s_2$  and distance  $d$  is in accordance with 11.10.4.

*Delete Sections 11.10.9.2 through, 11.10.9.5*

*Delete Sections 11.11, 11.12.*

## Chapter 12 — Bond and Development Length

*Add New 12.1 - Scope. Renumber following sections accordingly.*

### 12.1 - Scope

12.1.1 - Unless stated otherwise, the requirements of this Chapter refer to reinforcement embedded in grout. Those requirements shall apply to field-installed reinforcement.

12.1.2 - When so stated, the requirements of this Chapter shall refer to factory-installed reinforcement embedded in AAC.

**12.1.3** – The maximum ratio of vertical reinforcement to area of a grouted cell shall be 3%. It shall be permitted to use ratios of vertical reinforcement up to 4.5% if the reinforcement remains elastic throughout its entire length and the available splitting tensile strength of the grout is greater than the acting splitting tensile strength as defined by Equation (12-xx)

$$f_t = \frac{Vd_{bar}}{jd \cdot d_{bar} \cdot (d_{core} - d_{bar})} \quad \text{Equation (12-xx)}$$

The splitting tensile strength of the grout shall be taken as  $4\sqrt{f'_g}$ . If  $f'_g$  is not specified it shall be permitted to be taken as 2000 psi.

12.1.4 – Splices of longitudinal reinforcement shall not be permitted in potential plastic hinge zones.

*Add new Section 12.20:*

**12.20 - Design of Factory-Installed Reinforcement Embedded in AAC**

Factory-installed reinforcement embedded in AAC shall be designed to satisfy either 12.20.1 or 12.20.2.

12.20.1 - The spacing of cross-wires shall be less than or equal to the value required to satisfy Eq. (12-4).

12.20.2 - The number of cross-wires within a distance of 1/6 of the clear span of the panel, measured in each direction from each support, shall equal or exceed the value required to satisfy Eq. (12-5). In that equation,  $a$  is the shear span or 1/6 of the clear span of the panel. In other sections, the spacing shall not exceed  $2s_{min}$ .

$$s_{min} = \frac{V_u / \phi}{0.85 d \cdot d_{cross} \cdot l_{cross} \cdot f'_{AAC}} \quad \text{Equation (12-4)}$$

$$n_{cross,min} = \frac{V_u / \phi}{0.85 d \cdot d_{cross} \cdot l_{cross} \cdot f'_{AAC}} \cdot a \quad \text{Equation (12-5)}$$

*Delete Chapter 13*

## **Chapter 14 — Walls**

*Delete 14.1.2*

### **14.3 — Minimum reinforcement**

*Delete 14.3.1 through 14.3.6.*

*Rewrite 14.3.7 as follows:*

14.3.7 — In addition to the minimum reinforcement required by 14.2.1, not less than one No. 4 bar shall be provided around all window and door openings. Such bars shall be extended to develop the bar beyond the corners of the openings but not less than 24 in.

*Delete 14.5 (Empirical Design of walls)*

*Delete Sections 14.7 and 14.8.*

*Delete Chapter 15.*

## **Chapter 16 — Precast concrete**

*Throughout, replace “concrete” by “AAC.”*

*Modify 16.2.4 as shown below:*

**16.2.4** — In addition to the requirements for drawings and specifications in 1.2, include the following in either the contract documents or the shop drawings:

(a) Details of reinforcement, inserts and lifting devices required to resist temporary loads from handling, storage, transportation, and erection or reference to AAC manufacturers’ published construction practices;

(b) Specified compressive strength of AAC.

## **16.4 — Member design**

*Delete 16.4.2.*

## 16.5 — Structural integrity

*Remove Section 16.5.1.2 and replace with the following:*

16.5.1.2 — Where precast AAC elements form floor or roof diaphragms, the minimum provisions of Section 16.5.1.2.1 through 16.5.1.2.4 shall apply in addition to the requirements of Section 7.13.3.

16.5.1.2.1 — Nominal shear strength for AAC floor and roof diaphragms subject to lateral load parallel to the direction of panels shall be calculated based on Section 16.5.1.2.2 or Section 16.5.1.2.3. Nominal shear strength for AAC floor and roof diaphragms subject to lateral load perpendicular to the direction of panels shall be calculated based on Section 16.5.1.2.2 or 16.5.1.2.4.

16.5.1.2.2 — Nominal shear strength shall be based on adhesion at diaphragm joints, and shall be computed as the product of the contact area of grout and AAC and the shear strength of a grout and AAC joint plus the product of the contact area of thin-bed mortar and AAC and the shear strength of thin-bed mortar. The shear strengths of joints between thin-bed mortar and AAC and grout and AAC are defined in Section 8.14.4.

16.5.1.2.3 — Nominal shear strength of AAC floor and roof diaphragms shall be based on a truss mechanism subject to the minimum provisions of Section 16.5.1.2.3.1 through Section 16.5.1.2.3.4.

16.5.1.2.3.1 — Compression struts shall not be permitted to cross panel joints and shall intersect with tension ties in grouted keys and tension ties (chords) in ring beams.

16.5.1.2.3.2 — Tension ties shall consist of the reinforcement in grouted keys or in a ring beam. The reinforcement in the grouted keys shall be hooked around the longitudinal reinforcement in the ring beam with standard 90-degree hooks oriented in a vertical plane.

16.5.1.2.3.3 — Compression struts shall be defined within the panel. Their dimension perpendicular to the plane of the panel shall be taken equal to the thickness of the panel. Their dimension in the plane of the panel, measured perpendicular to the axis of the strut, shall be taken as 6 in. The nominal strength of compression struts shall be calculated as the product of 85 percent of the specified compressive strength of the AAC, multiplied by the cross-sectional area of the strut.

16.5.1.2.3.4 — The strength of the tension ties shall not exceed the product of the cross-sectional area of the reinforcement and the specified yield strength of the reinforcement.

16.5.1.2.4 — Nominal shear strength shall be based on dowel action of reinforcement in the grouted keys perpendicular to the lateral load. The nominal shear strength shall be computed as the product of 60 percent of the cross-sectional area of the reinforcement and the specified yield strength of the reinforcement.

**16.5.1.3** — Vertical tension tie requirements of 7.13.3 shall apply to all vertical structural members, except cladding, and shall be achieved by providing connections at horizontal joints in accordance with the following:

(a) Precast columns shall not be made of AAC;

(b) Precast wall panels that comprise shear walls shall be connected at wall intersections, at locations of longitudinal reinforcement;

(c) When design forces result in no tension at the base, the ties required by 16.5.1.3(b) shall be permitted to be anchored into an appropriately reinforced concrete slab on grade.

**16.5.1.4** — Except for sliding shear resistance in a shear wall, connection details that rely solely on friction caused by gravity loads shall not be used.

**16.5.2** — For precast autoclaved aerated concrete bearing wall structures three or more stories in height, the minimum provisions of 16.5.2.1 through 16.5.2.5 shall apply.

**16.5.2.1** — Longitudinal and transverse ties shall be provided in floor and roof systems to provide a nominal strength of 1500 lb per ft of width or length, and shall be designed to transfer shear to lateral force-resisting elements. Ties shall be provided over interior wall supports and between members and exterior walls. Ties shall be positioned in or within 2 ft of the plane of the floor or roof system. Longitudinal ties shall only be required parallel to the direction of span of the panels.



**16.5.2.2** — Longitudinal ties parallel to floor or roof slab spans shall be spaced not more than 10 ft on centers. Provision shall be made to transfer forces around openings.

**16.5.2.3** — Transverse ties perpendicular to floor or roof slab spans shall be spaced not greater than the bearing wall spacing.

**16.5.2.4** — Ties around the perimeter of each floor and roof shall resist the design loads acting at that level.

**16.5.2.5** Continuous vertical reinforcement in AAC shear walls shall be sufficient to resist the design moments.

***Rewrite 16.6.2.2 as follows:***

**16.6.2.2** — Unless shown by test or analysis that performance will not be impaired, the following minimum requirements shall be met:

(a) Each member and its supporting system shall have design dimensions selected so that, after consideration of tolerances, the distance from the edge of the support to the end of the precast member in the direction of the span is at least 1/180 of the clear span  $l$ , but not less than:

For solid or hollow-core slabs	2 in.
For beams or stemmed members	3 in.
<u>For autoclaved aerated concrete panels</u>	<u>2 in.</u>

(b) Bearing pads at unarmored edges shall be set back a minimum of 1/2 in. from the face of the support, or at least the chamfer dimension at chamfered edges.

**16.6.2.3** — The requirements of 12.11.1 shall not apply to the positive bending moment reinforcement for statically determinate precast members. At least one-third of such reinforcement, however, shall extend to the center of the bearing length.

### **16.8 — Marking and identification**

**16.8.1** — Each precast member shall be marked to indicate its class, production identification code, location and orientation in the structure and date of manufacture. Pallets should also identify the class of AAC, production identification code and unit dimensions.

**16.8.2** — Identification marks shall correspond to placing drawings.

**Delete Chapter 17, 18, 19, and 20.**

## Chapter 21 - Special Provisions for Seismic Design

### *Rewrite 21.2.1.3 as follows:*

**21.2.1.3** – In regions of moderate seismic risk or for structures assigned to intermediate seismic performance or design categories, intermediate or special moment frames, ordinary, intermediate, ~~or special structural walls~~, or intermediate or special AAC structural systems shall be used to resist forces induced by earthquake motions. Where the design seismic loads are computed using provisions for special concrete systems or intermediate or special AAC structural walls, the requirements of Chapter 21 for special systems, as applicable, shall be satisfied.

**21.2.1.4** – In regions of high seismic risk for structures assigned to high seismic performance or design categories, special moment frames, ~~or special structural walls~~, or special AAC structural systems, complying with 21.2 through 21.10, and 21.15 shall be used to resist forces induced by earthquake motions. Frame members not proportioned to resist earthquake forces shall comply with 21.11.

### *Add Section 21.14 – Intermediate AAC structural systems*

**21.14.1** - The provisions of this section apply to design of intermediate AAC structural walls and their associated horizontal diaphragms to resist forces induced by earthquake motions. The design provisions of Chapters 1-18 shall apply except as modified in this section.

21.14.2 – The design shear force  $V_e$  shall be determined from consideration of the maximum forces that can occur in an AAC element. Forces in the longitudinal reinforcement shall be determined assuming that the stress in the flexural tensile reinforcement is  $1.25f_y$ .

21.14.3 – The horizontal diaphragm shall be designed to resist the design shear force,  $V_e$  of Section 21.14.2. Design according to Section 16.5.1.2.2 shall not be permitted.

**Add Section 21.15 – Special AAC structural wall systems**

21.15.1 - The design provisions of this section apply to special AAC structural walls and horizontal diaphragms to resist forces induced by earthquake motions.

21.15.2 – The design provisions of Chapters 1-18 and Section 21.14 shall apply except as modified in this Section.

21.15.3 – Lateral load between horizontal diaphragms and AAC structural walls shall be transferred through connectors embedded in grout in accordance with Section 16.

## APPENDIX E - NOTATION

*Add the following:*

$\underline{d_{cross}}$  = diameter of cross-wires, in. (mm)

$\underline{d_{long}}$  = diameter of longitudinal reinforcement, in. (mm)

$\underline{E_{AAC}}$  = modulus of elasticity of AAC, psi (MPa)

$\underline{f_{AAC}'}$  = specified compressive strength of AAC, psi (MPa)

$\underline{f_g'}$  = specified compressive strength of grout, psi (MPa)

$\underline{f_{AAC}}$  = splitting tensile strength of AAC by ASTM C1386, psi  
MPa)

$\underline{h_{wall}}$  = height of AAC shear walls between stories, in. (mm)

$\underline{l_{cross}}$  = length of reinforcement bearing on AAC, in. (mm)

$\underline{V_{AAC}}$  = nominal shear strength provided by AAC, kips (kN)

$\underline{V_{S_b}}$  = maximum usable shear strength provided by each wire of  
shear reinforcement, kips (kN)

$\underline{\rho_{1386}}$  = air-dried density of AAC by ASTM C1386, lb/ft<sup>3</sup> (kg/m<sup>3</sup>)

$\underline{w_{strut}}$  = horizontal projection of the width of the compression strut,  
in. (m)

## C.2 COMMENTARY ON PROPOSED DESIGN PROVISIONS

*The Commentary provisions proposed here are intended to supplement the Commentary of ACI 318-02. Where no new Commentary provisions are indicated, the current Commentary of ACI 318-02 applies. Where Code provisions of ACI 318-02 are deleted, the corresponding Commentary is also deleted. Added Commentary provisions are denoted by an underline.*

### Chapter 3 — Materials

*Add the following section, renumber subsequent sections accordingly:*

Renumbered Section 3.9 - Referenced Standards

*Add the following:*

ASTM C ZZZZ Method of Test for Determining the Modulus of Elasticity of Autoclaved Aerated Concrete is currently under development by ASTM C-27.60. If it has not been developed by the time this document is completed, this reference will be changed to a footnote.

## Chapter 4 -- Durability Requirements

*Remove Section 4.2 on freezing and thawing exposures and replace by the following:*

### **R4.2 Freezing and Thawing Exposures**

Because AAC can deteriorate when subjected to cycles of freezing and thawing while critically saturated, no below-grade applications of AAC are permitted where the AAC could become critically saturated, and coatings are also required to prevent the infiltration of liquid water into AAC in above-grade applications.

*Add the following to Section 4.4 on corrosion protection of reinforcement:*

### **R4.4 - Corrosion protection of reinforcement**

Provisions for coating on AAC welded wire fabric are included in ASTM C1452.

## Chapter 5 -- Concrete Quality, Mixing and Placing

### *Add the following:*

R5 - Code 5.1.1 links the designer's specified value with the producer-verified strength class. Corresponding material specifications and tolerances are prescribed in ASTM C1386. The mixture design for the AAC is factory-adjusted to produce the required strength class. The design engineer and the contractor are not involved in AAC production or curing. Construction techniques are based on industry practices and construction techniques, and have been verified by laboratory testing at UT Austin (Tanner 2003, Varela 2003) and elsewhere. The Committee may consider imposing more specific hot- and cold-weather construction requirements.

## Chapter 6 -- Formwork, Embedded Pipes and Construction Joints



*Delete Chapter 6 and replace by the following:*

R6 - Formwork is not required because AAC is a precast product. Conduits and pipes are not cast-in; openings for them may be cut or routed, and the effect of those openings on structural performance must be checked.

## Chapter 7 -- Details of Reinforcement

*Add the following:*

R7 - Conventional reinforced concrete is constructed with cast-in-place reinforcement or post-installed reinforcement such as post-tensioning tendons. AAC is constructed with factory-placed welded-wire reinforcement, and possibly also with cast-in-place, deformed reinforcement installed in grouted cores in the field. Detailing requirements for deformed reinforcement in grout are prescribed in the existing Chapter 7. Detailing requirements for the factory-installed reinforcement are prescribed by the provisions of ASTM C1452.

## Chapter 8 — Analysis and Design — General Considerations

*Add the following:*

R8.5.1 — The expression for modulus of elasticity of AAC is based on combined test data from UT Austin (Argudo 2003, Tanner 2003) and UAB.

*Add a new Section 8.5.2 and renumber remaining sections appropriately:*

R8.5.2 - The expression for modulus of elasticity of grout is based on the 2002 MSJC Code.

*Add a new Section 8.13:*

R8.13.1 – The equation for splitting tensile strength is based on ASTM C1006 tests performed at The University of Texas at Austin (Tanner 2003).

R8.13.2 --The modulus of rupture is based on ASTM C78 tests carried out at the University of Alabama at Birmingham<sup>2</sup> for different AAC compressive strengths (Argudo 2003). Modulus of rupture tests show that a thin-bed mortar joint can fail prior to the material if the modulus of rupture exceeds the tensile-bond strength of the thin-bed mortar. This critical value is 80 psi (552 kPa). The data are consistent with the formation of cracks in thin-bed mortar joints in AAC shear wall specimens at The University of Texas at Austin (Tanner 2003). Shear wall tests performed at The University of Texas at Austin show if a

---

<sup>2</sup> Internal report by Fouad H. Fouad, *Physical and Mechanical Properties of AAC Produced in the United States*, The University of Alabama at Birmingham, August 10, 2002.

leveling joint is present, flexural cracking capacity may be controlled by the tensile bond strength across the interface between the AAC and the leveling mortar which is usually less than the modulus of rupture of the AAC material itself.

**R8.13.3** – The equation for direct shear strength is based on shear tests performed at the University of Alabama at Birmingham<sup>1</sup> (Argudo 2003).

**R8.13.4** – The equation for shear strength of joints is based on direct shear tests performed at The University of Texas at Austin (Tanner 2003). Data on shear strength of joints from The University of Alabama at Birmingham<sup>1</sup> indicate the value for thin-bed mortar is conservative (Argudo 2003).

## Chapter 9 — Strength and Serviceability

### *Add the following:*

R9.3.2.8 — The value of the strength reduction factor reflects the brittle nature of an adhesion failure in an AAC joint.

R9.5.2.1 — The minimum-thickness requirements of Table 9.5(a) of ACI 318-02 can be applied to reinforced AAC elements if the following constraints are applied:

- 1) Footnote (a) to Table 9.5(a) of ACI 318-02 should be applied. It specifies that for structural lightweight concrete having unit weight in the range 90-120 pcf, the minimum thickness shall be multiplied by  $(1.65 - 0.005w_c)$ , where  $w_c$  is the unit weight in pcf. The footnote is applicable, because AAC is comparable to lightweight concrete in terms of its flexural stiffness. For the reinforced AAC panels tested at UAB, the corresponding factor from Footnote (a) to Table 9.5(a) is 1.47, making the ratios of calculated to observed deflections all comfortably above unity.
  
- 2) Footnote (b) to Table 9.5(a) of ACI 318-02 requires that for  $f_y$  other than 60,000 psi, calculated deflection values be multiplied by  $(0.4 + f_y/100,000)$ . This requirement is believed not to apply to AAC, because the bond between smooth wire and AAC differs considerably from the bond between deformed reinforcement and conventional concrete. Also, the specified yield strength of AAC reinforcement ( $f_y = 80,000$  psi) would

correspond to a factor of 1.2, which would result in an over-estimate of deflections if the RILEM effective inertia were used.

**R9.5.2.2** - The deflection-calculation provisions of Section 9.5.2.2 and 9.5.2.3 of ACI 318-02 can be applied to reinforced AAC elements, with the following modifications:

Short-term deflections should be calculated using an effective flexural stiffness ( $EI_e$ ) corresponding to the unfactored moment ( $M_a$ ). The effective flexural stiffness ( $EI_e$ ) should be obtained by linear interpolation between the cracking point ( $M_{cr}, \phi_{cr}$ ) and the yielding points ( $M_y, \phi_y$ ) on a bilinear moment-curvature diagram. This procedure is recommended by RILEM<sup>3</sup>. The short-term deflections so obtained should then be multiplied by the factor from Footnote (a) of Table 9.5(a). When this approach is used, calculated deflections are 0.9 to 1.2 times the experimentally observed values.

**R9.5.2.5** - For calculation of additional long-term deflections resulting from creep and shrinkage of AAC flexural members, Section 9.5.2.5 of ACI 318-02 is not applicable because the reinforcement ratio for compressive reinforcement ( $\rho'$ ) is generally much smaller for AAC than for reinforced concrete. To calculate total deflections, including long-term deflections, a simplified approach based on RILEM specifications can be adopted. Total deflections can be calculated using an effective modulus of elasticity ( $E_{AAC'}$ ) equal to the modulus of elasticity ( $E_{AAC}$ ) divided by 1.5.

---

<sup>3</sup> RILEM Recommended Practice, RILEM Technical Committees 78-MCA and 51-ALC, Section 5.4.1, 1983.

## Chapter 10 – Flexure and Axial Loads

*Add the following:*

**R10.2** - Evaluation of AAC panel tests at UAB, confirmed by shear wall tests at UT Austin, shows that the behavior of reinforced AAC elements under combinations of flexure and axial loads can be described by conventional beam theory, using plane sections and an equivalent rectangular compressive stress block.

**R10.2.7.3** – The factor  $\beta_1$  is determined based on stress-strain relationships for AAC tested at the University of Alabama at Birmingham and at The University of Texas at Austin (Argudo 2003).

**R10.5.1** - Eq. (10-3) is intended to produce an AAC section whose nominal moment capacity is approximately twice its flexural cracking capacity.

## Chapter 11 — Shear and Torsion

*Add the following:*

**R11.3** - For reinforced concrete beams without shear reinforcement, the mean diagonal tensile strength ( $f_t$ ) can be taken equal to  $6\sqrt{f'_c}$  (US customary units). Equation (11-5) of ACI 318-02 uses a nominal unit strength in shear that decreases from  $3.5\sqrt{f'_c}$  for low ratios of shear span to depth, to  $1.9\sqrt{f'_c}$  for high ratios. For simplicity, the current Equation (11-3) can be used, with a corresponding unit strength of  $2\sqrt{f'_c}$ . That unit strength is one-third of the mean diagonal tensile strength.

On that basis, the current Equations (11-3) and (11-4) of ACI 318-02 can be rewritten in terms of the splitting tensile strength ( $f_t$ ) for use with AAC elements. The corresponding shear capacity ( $V_{AAC}$ ) is given by the new Eq. (11-3) for members subjected to shear and flexure only, and by the new Eq. (11-4) for members subjected to axial compression as well.

**R11.5.6.2** —Under monotonic loading conditions the shear reinforcement is effective. The resistance in the reinforcement comes from bearing of perpendicular reinforcement on surrounding AAC or from dowel action of the reinforcement. Tests at The University of Texas at Austin (Tanner 2003) show that shear reinforcement is not effective in resting shear under reversed cyclic loads due to crushing of the surrounding grout or AAC. Under reversed cyclic loading only deformed bars in grout contribute to the shear strength.



**R11.5.6.9** — In traditional reinforced concrete a maximum shear strength of the stirrups is determined based on a truss mechanism. In shear reinforcement in AAC the maximum shear strength of the shear reinforcement is limited by the bearing capacity of the perpendicular reinforcement. This is explained pictorially in Figure C.2. If a cut is taken at the center of a stirrup, the available capacity from the top and bottom reinforcement can be determined,  $V_s^1$  and  $V_s^2$ , using the following equation  $V_s = n_{bars} d_{bars} f'_{AAC} \cdot s$ . The number of bars may be different for  $As^-$  and  $As^+$  which would result in different values for  $V_s^1$  and  $V_s^2$ ; the minimum of these values is the limiting shear strength of the reinforcement.

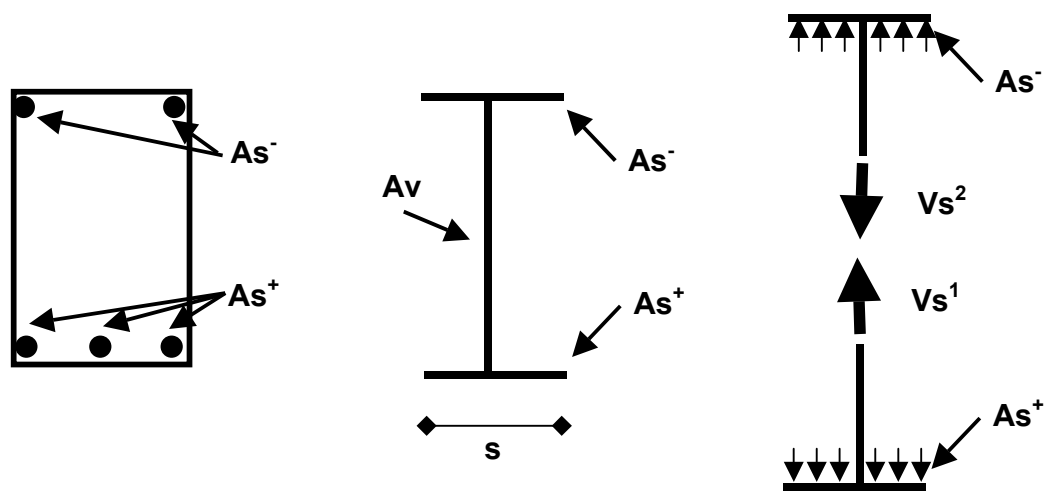


**Figure C.2** *Shear strength in shear reinforcement limited by bearing of the longitudinal reinforcement*

### **11.7 — Shear-friction**

**R11.7.4.1** — Sliding shear resistance is the product of the coefficient of friction across an interface, and the force acting perpendicular to that interface.

This mechanism is referred to in ACI 318 as “shear friction.” This resistance can come from reinforcement crossing the interface and applied axial load.

In the traditional shear friction mechanism, sliding over a rough joint causes one section of the crack to lift upwards; this results in yielding of the vertical reinforcement, which provides additional clamping force. Under reversed cyclic loading of AAC, the roughness of the bed joints can decrease, and resistance to sliding shear is provided by dowel action of reinforcement crossing the bed joints. Sliding was observed in shear wall tests at UT Austin (Tanner 2003). Vertical reinforcement contributed significantly to the capacity for several cycles until the onset of local crushing and spalling of the grout in the cells surrounding that reinforcement. Therefore, for reversed cyclic loading, the shear friction resistance mechanism is limited to resistance provided due to axial load. The nominal sliding shear capacity should be based on the frictional capacity consistent with the total force on the compressive stress block required to equilibrate the tensile force in the tensile reinforcement at a given cross-section.

At an unbonded interface the calculated sliding shear resistance should be based on friction only. At an interface where uncracked thin-bed mortar is present, the nominal sliding shear capacity should be based on the greater of the capacity based on initial adhesion, and the frictional capacity after that adhesion is overcome. At an interface where leveling-bed mortar is present, the interface is probably cracked due to in-plane flexure, and initial adhesion should not be counted on.

**R11.7.4.3** — The coefficient of friction  $\mu$  in Eq. (11-25) and Eq. (11-26) should be 1.0 between AAC and leveling bed mortar and 0.75 between AAC and

AAC. Direct shear tests performed at The University of Texas at Austin (Tanner 2003) determined a coefficient of friction,  $\mu$  between AAC and AAC. The average coefficient of friction was 0.85, with a 10% lower fractile it was 0.76. Based on this data the ACI 318-02 value of  $\mu=1.0\lambda$ , with  $\lambda=0.75$  for lightweight concrete is nearly a 10 % lower fractile. Since all AAC is lightweight concrete,  $\lambda$  is included in the design coefficient of friction for AAC.

**R11.8.1** — Provisions on the use of AAC in deep beams have not been developed to date.

**R11.10** —

**R11.10.1** — Design for shear in out-of-plane loading cases is based on beam design for one-way slabs. Beam design is based on out-of-plane loading of individual floor panels.

R 11.5.6 - Shear strength provided by shear reinforcement ( $V_s$ ) can be calculated using Section 11.5 of ACI 318-02, with the following qualifications:

- a) Vertical or inclined wires designed to provide shear strength need to be welded to the longitudinal reinforcement; and
- b) The maximum usable shear strength provided by each shear reinforcement bar ( $V_{sb}$ ) is limited by the bearing capacity of the AAC on the longitudinal reinforcement.

The nominal shear capacity ( $V_n$ ) is equal to the sum of the nominal shear capacity of AAC ( $V_{AAC}$ ) and the shear strength provided by the shear

reinforcement ( $V_s$ ). The design shear capacity ( $\phi V_n$ ) is obtained by multiplying the nominal shear capacity  $V_n$  by the appropriate capacity-reduction factor.

**R11.10.6** — Shear strength of AAC shear walls may be limited by web-shear cracking, crushing of the diagonal strut and sliding shear. A suite of 14 shear wall specimens was tested at The University of Texas at Austin (Tanner 2003, Varela 2003), and the results of those tests were combined with results from 12 shear wall specimens tested at Hebel Germany<sup>4</sup>. The equation for web-shear cracking addresses the cases of mortared head joints and unmortared head joints. Each equation is verified by 11 or 9 tests, respectively, performed on the shear-dominated shear wall specimens. The aspect ratios of the specimens ranged from 0.6 to 3. Crushing of the diagonal strut was based on the observed response of Shear Wall Specimen 1 performed at The University of Texas at Austin (Tanner 2003). The equation was confirmed as an upper bound based on the results of the remaining 8 tests performed on walls with aspect ratios less than 2. Flexure-shear cracking was observed in the 6 flexure-dominated specimens. In each wall, after the formation of a flexure-shear crack at least one load cycle was performed without an associated decrease in strength or stiffness. In addition, the flexural reinforcement provided additional strength in the wall. If design requirements for flexure-shear cracking are eliminated, the design provisions of Section 11.10.7 are no longer required. They are replaced by special provisions for shear walls constructed with panels oriented vertically.

**R11.10.7** — **Special provisions for shear walls with AAC panels oriented vertically** – Tests conducted at The University of Texas at Austin

---

<sup>4</sup> Personal communication, Violandi Vratsanou, Hebel AG, Germany, November 2000.

(Tanner 2003) showed that vertical cracks formed at the head joints in shear wall specimens with vertically oriented panels (Tanner 2003, Varela 2003). If these cracks formed in a specimen, they were limited to every third joint when following the construction techniques presented in Section 5.7.4. If vertical cracks are present, the strength and stiffness of an AAC shear wall will decrease and the behavior will be different, which must be considered in design. As the aspect ratio of an individual panel exceeds 3 the cracks will be governed by beam shear, rather than the equation for walls and Equation (11-3) should be used instead of Equation (11-29).

**R11.10.8** — Based on the shear wall specimens tested at The University of Texas at Austin and Hebel Germany the behavior of a shear wall can be predicted. Since the behavior can be predicted additional shear reinforcement is not required. Additional shear reinforcement, in the form of welded wire fabric in panels is not effective under reversed cyclic loads. Deformed bars embedded in grout or reinforced concrete are the only shear reinforcement effective under reversed cyclic loads.

**R11.10.9 — Design of shear reinforcement for walls**

**R11.10.9.2 through R11.10.9.5** Tests performed at The University of Texas at Austin show that the shear behavior of walls can be predicted satisfactorily (Tanner 2003, Varela 2003). In addition, flexural behavior can be achieved with vertical reinforcement concentrated at the ends. If shear behavior can be avoided and flexural behavior is ensured, the prescriptive reinforcements can be relaxed.

## Chapter 12 — Bond and Development Length

*Add the following:*

R12.1 - Bond and development requirements for deformed reinforcement in grout are identical to those used for concrete or masonry construction. Given the small sizes of deformed bars used in AAC construction, bond between the grout and the AAC itself does not govern the bond capacity.

Bond and development requirements for welded-wire fabric embedded in AAC are quite different from those for conventional concrete, however. Because the welded-wire fabric has a corrosion-resistant coating, bond strength between the coated wire and the AAC itself is negligible. Bond strength comes from bearing of the cross wires against the AAC. For typical cross-wire spacings, local crushing of the AAC under the cross wires can be assumed to redistribute the bearing stresses under the cross wires, leading to a uniform bearing strength of  $f_{AAC}'$  under every cross-wire. Multiplying this stress by the number of cross wires and by the bearing area of each cross-wire gives the maximum force that can be developed in the welded wire fabric (Figure C.3).

This maximum force in the welded-wire mesh can limit the flexural capacity of a reinforced AAC panel.

R12.1.3 – Splitting of AAC around vertical reinforcement in a grouted cell was observed in shear wall specimens tested at The University of Texas at Austin (Tanner 2003). This splitting occurred in cells with ratios of reinforcement to area of grouted cells of 4.5%. Splitting was not observed in shear walls with a ratio of reinforcement to area of grouted cells of 3%.

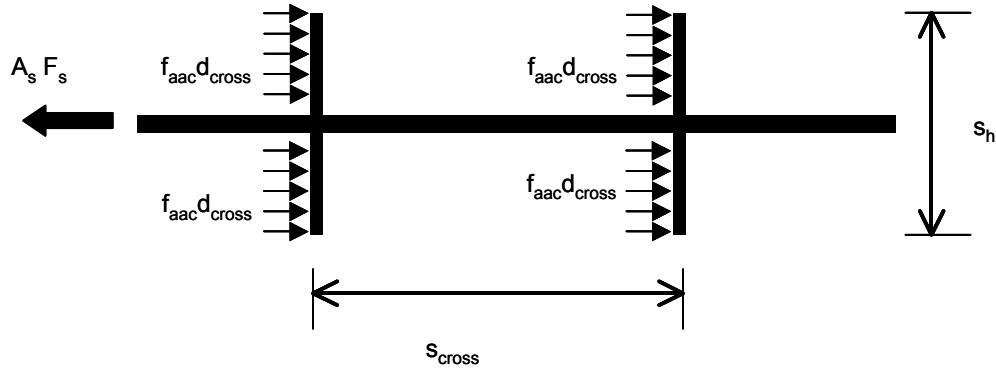


**Figure C.3 Bond mechanism of welded-wire mesh in AAC**

A reinforcement-to-core area ratio as high as 4.5% (equivalent to a No. 5 bar in a 3-in. grouted core) is acceptable provided that the bar remains elastic and an analysis to determine the acting splitting tensile stress due to radial stresses of the reinforcement is performed. This value is compared to the splitting tensile strength of the grout.

**R12.1.4** – Splices shall not be permitted at locations of potential plastic hinges due to the possibility of increasing the design strength at that location. In addition, the probability of vertical cracks forming due to splitting is increased at the location of a splice.

**R12.20.2** – The minimum number of cross-wires is intended to prevent an anchorage failure in AAC panels (Argudo 2003). Eq. (12-5) prescribes the required number of cross-wires in a distance  $a$ , the length of the panel divided by 6. Beyond this distance the twice the maximum spacing prescribed by Eq. (12-4).

*Delete Chapter 13*

*Add the following:*

R13.1 - The deletion of Chapter 13 essentially means that AAC slabs are designed as one-way slabs.

**Chapter 14 — Walls**

*Add the following:*

R14.3 - Tests performed at the University of Texas at Austin (Tanner 2003, Varela 2003) show that walls with reinforcement concentrated at the ends performed satisfactorily and the maximum horizontal and vertical spacing requirements can be relaxed.

R14.3.7 — Using a No. 5 bars around window openings may cause cracks parallel to the direction of the reinforcement or other local damage if the reinforcement yields. No. 4 bars will resist cracks formed around the openings and reduce the damage if the reinforcement yields.



*Delete Chapter 15.*

## **Chapter 16 — Precast concrete**

*Add the following:*

**R16.2.3** - Tolerances for AAC elements are specified in ASTM C 1452.

**R16.5.1.2** — In general, floor diaphragms composed of AAC elements are not topped. General structural integrity provisions for this type of construction were verified in the seismic testing of a Two-story AAC Assemblage Specimen at the University of Texas at Austin (Tanner 2003, Varela 2003). The assemblage was designed using the vertical tension ties, transverse tension ties and longitudinal tension ties of Section 7.13.3. The continuous steel (chord) perpendicular to the orientation of lateral load provides reinforcement for in-plane flexural resistance of the diaphragm. Sections 16.5.1.2 through 16.5.1.4 present design options to transfer shear from the diaphragm to the AAC shear walls.

**R16.5.1.2.2** — Lateral load was successfully transferred through adhesion in the Two-story Assemblage Specimen (Tanner 2003, Varela 2003). Since adhesion failure is brittle, a strength reduction factor of 0.67 is used. The shear strength of a joint was determined based on direct shear tests performed on joints between thin-bed mortar and AAC and grout and AAC (Tanner 2003). The values presented in Section 8.13.4 represent lower 7% fractiles of these tests.

**R16.5.1.2.3** — A secondary resistance mechanism exists in which the entire floor diaphragm system acts like a truss: the bond beam comprises the tension and compression chords; the reinforcement between floor panels and in

the ring beam parallel to the panels connect to the chords; and the panels themselves act as compression diagonals (Figure C.4). The shear strength of AAC diaphragms with panels oriented parallel to the direction of loading can be checked using a truss mechanism.

**R16.5.1.2.3.1** — Compression struts are not allowed to cross panel joints, since the effect of joint cracks on the strength of AAC compression struts is unknown.

**R16.5.1.2.3.2** — The reinforcement in the grouted keys is anchored into the ring beam using a vertically oriented hook that extends beyond the ring beam reinforcement. This mechanical connection enhances the in-plane integrity of the horizontal diaphragm (Figure C.5). The truss model assumes uniform tension in the reinforcement. This assumption is valid even with damage at joints.

**R16.5.1.2.3.3** — The area of the compression strut is 6 in. in the plane of the panel, multiplied by the panel thickness.

**R16.5.1.2.3.4** — The strength of tie elements (reinforcement in grouted keys or ring beams) is calculated as the cross-sectional area of the longitudinal reinforcement in those elements, multiplied by the specified yield strength of the reinforcement.

**R16.5.1.2.4** — The nominal shear strength of an AAC diaphragm with panels oriented perpendicular to the direction of loading can be generated through dowel action in the reinforcement. The available resistance of an AAC

diaphragm can also be determined by the transfer of load through shear in the reinforcement, which is computed by  $0.6f_yA_s$ .

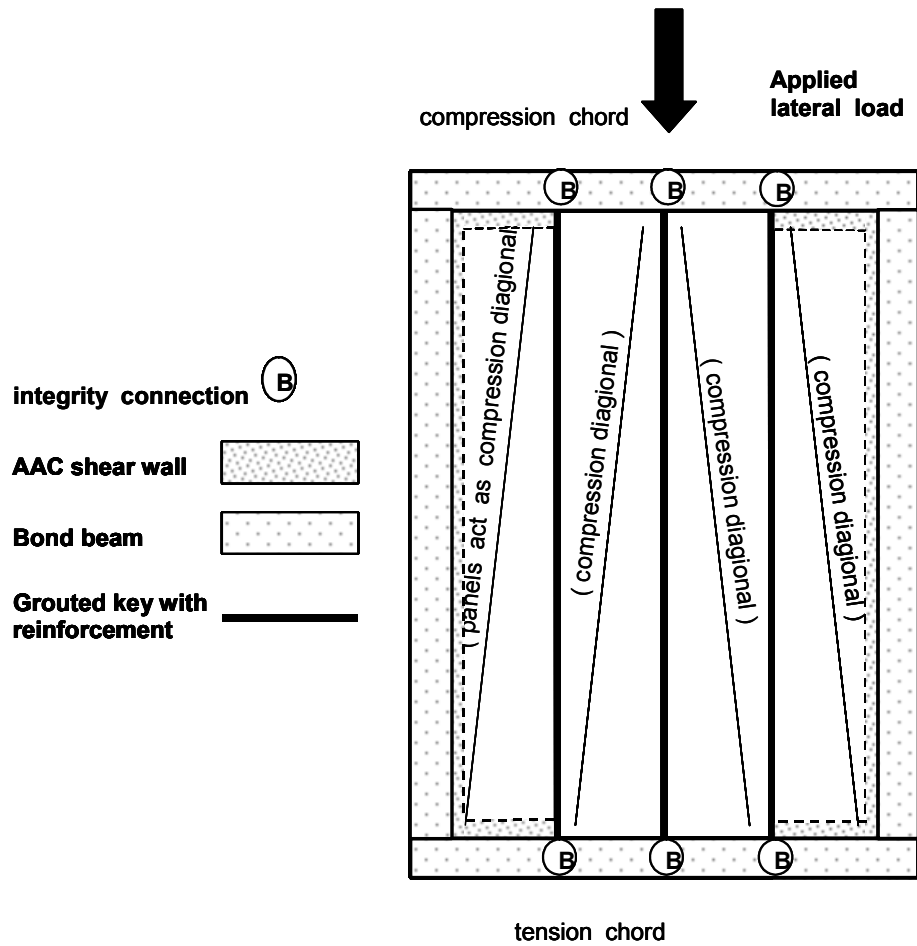


*Figure C.4 Truss mechanism in an AAC floor or roof diaphragm*

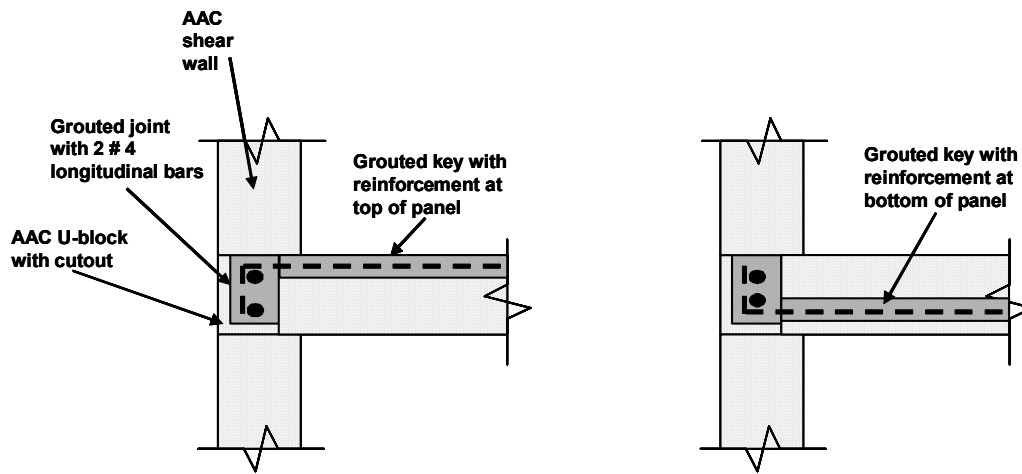


*Figure C.5 Detail of grouted key reinforcement with 90° hook oriented vertically and hooked around the ring beam reinforcement*

R16.5.1.4 — Connections between shear walls in stories depends on sliding shear resistance. Tests performed on shear walls at The University of Texas at Austin (Tanner 2003) indicate that sliding shear resistance can be accurately predicted based on frictional resistance.

R16.5.2.1 — These longitudinal ties are intended to support the diaphragm in the event a supporting bearing wall is removed from the structure. The ties are shown in Figure C.6; the effect of losing an interior wall is shown in Figure C.7. Since the mechanism will only form in the direction parallel to the direction the slab is spanning, they are not required perpendicular to the direction a slab is spanning.

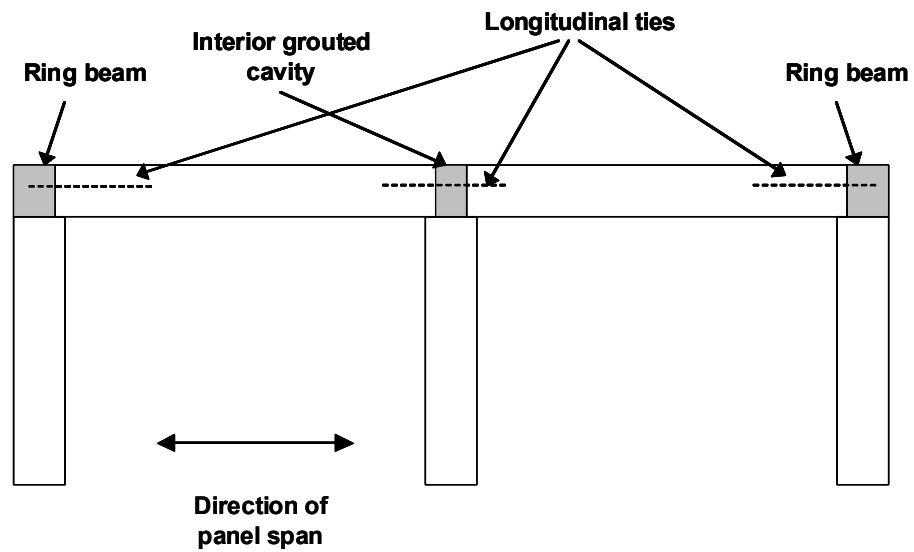


**Figure C.6** Elevation of two exterior shear walls and one interior shear wall with two interior panels connected by longitudinal ties

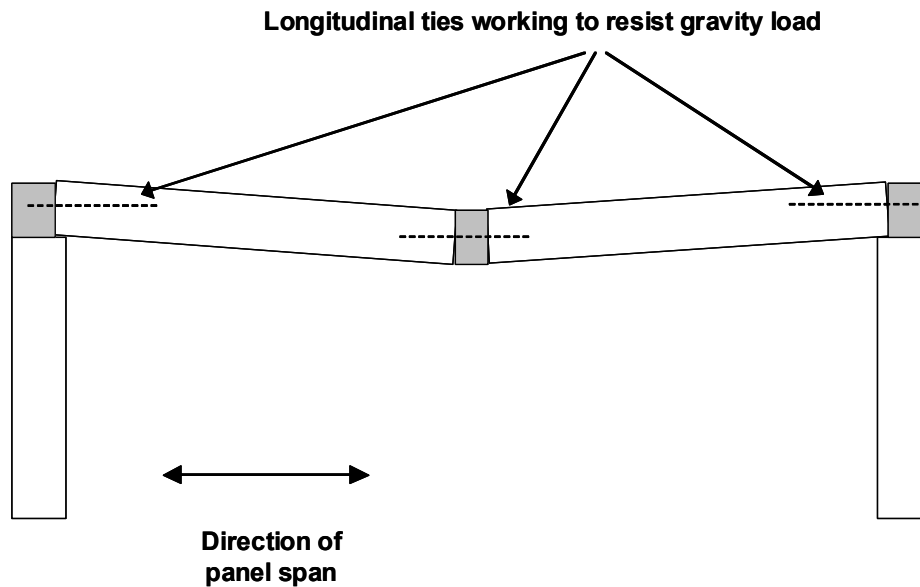


**Figure C.7** Elevation of shear walls with interior bearing wall missing and longitudinal ties serving as reinforcement

**R16.6.2** - Bearing must be checked wherever AAC floor or roof panels rest on AAC walls. An example of the critical section to be used in this calculation is shown in Figure C.8. The Two-story Assemblage Specimen tested at The University of Texas at Austin (Tanner 2003, Varela 2003) performed satisfactorily with an average bearing length of 2 in. The minimum bearing length was 1.75 for any given panel.

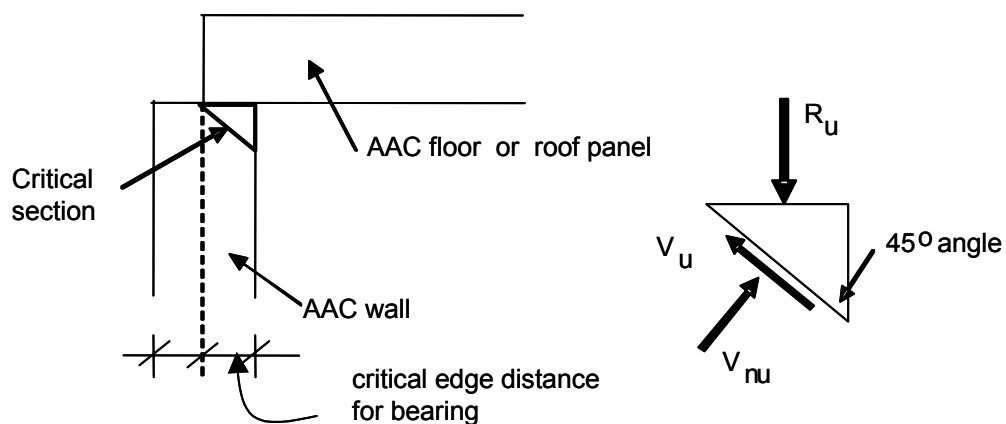


**Figure C.8** *Critical section at bearing of AAC floor or roof panel on AAC wall*

## Chapter 21 — Special Provisions for Seismic Design

### *Add the following:*

R21.14.2 – In order to ensure the failure of an AAC member is not governed by shear the design shear force is based on the design flexural capacity multiplied by an overstrength factor of 1.25.

R21.14.3 – Design through adhesion is a brittle failure mechanism and therefore not permitted in regions of moderate seismic risk.

R21.15.3 – Additional connectors are provided to ensure a ductile failure at the diaphragm AAC joint.

## APPENDIX D

### Complementary sections to Chapters 3 and 4

#### D.1 TO CHAPTER 3 (EVALUATION AND SYNTHESIS OF AVAILABLE DATA ON MECHANICAL PROPERTIES OF AAC)

The material presented in this Appendix is repeated from Tanner (2003).

##### D.1.1 Discussion of Results for Stress-Strain Relationship

Tests performed at UT Austin measured the strains up to failure of the core. Strains were measured with a set of rings attached to the cylinder (Figure D.1). The lower ring remains fixed and the upper ring pivots around a vertical pin. The vertical displacement is measured and converted into a strain. The center ring is optional and measures transverse strain. It was used in all tests except Contec Shipment 1 and Babb Shipment 2. Once the specimen begins to lose strength the reported strains may be smaller than the actual value.

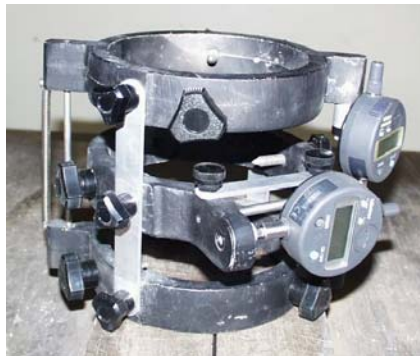


*Figure D.1 Test setup for measuring compressive stress versus strain*



The stress-strain curves for each specimen are presented in Figure D.2 through Figure D.7. All but two specimens (Contec Shipment 2 and Babb Shipment 2) reached a strain of 0.003. Although Contec Shipment 2 does not reach strains greater than 0.003, data from that shipment are at variance with data from other shipments. Data from Babb Shipment 2 indicate strains above 0.003 for initial tests; one reason for low strains in the remaining specimens may be slip between the specimen and the extensometer rings. Contec Shipment 1 results indicate that strains up to 0.004 can be obtained while still carrying half of the maximum load. These results, combined with the results from the other shipments, support using a maximum useful strain of 0.003.

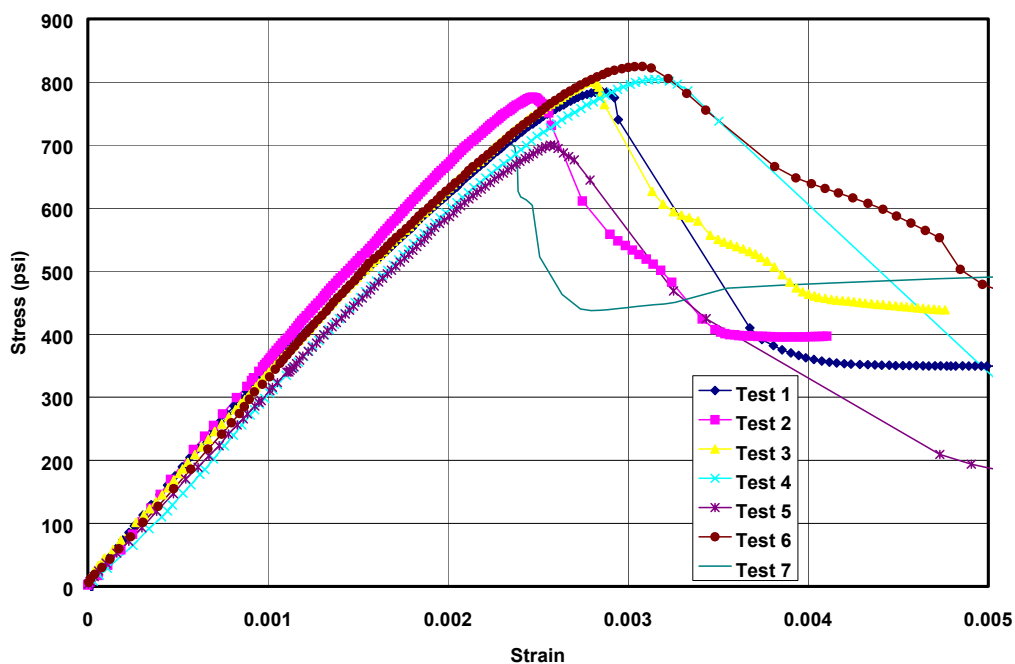


*Figure D.2 Compressive stress versus strain for Contec Shipment 1*

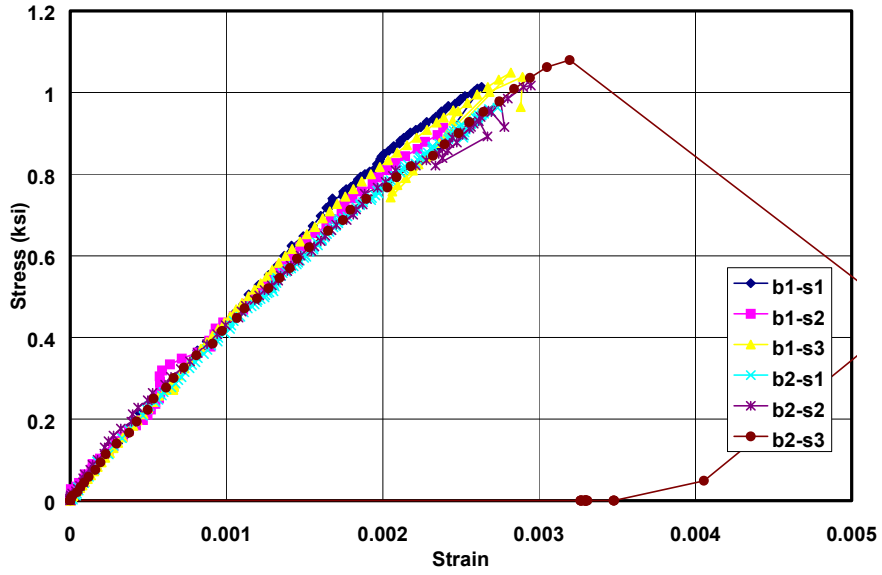


Figure D.3 Compressive stress versus strain for Contec Shipment 2

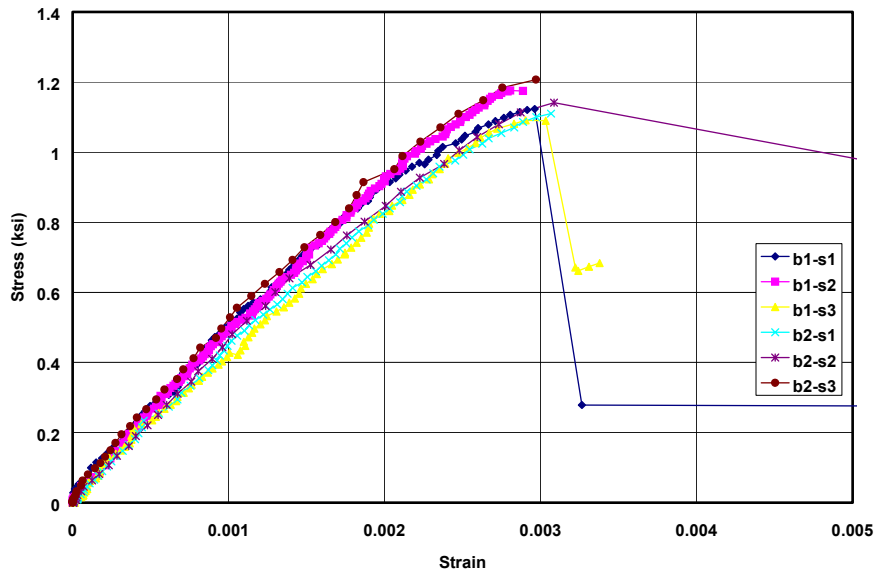


Figure D.4 Compressive stress versus strain for Babb Shipment 1

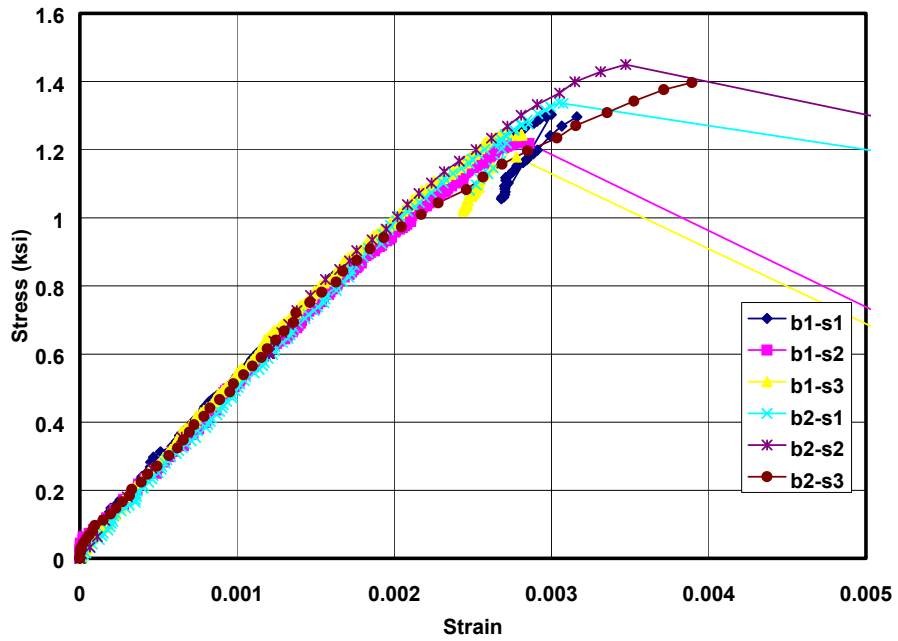


Figure D.5 Compressive stress versus strain for Hebel Shipment 2

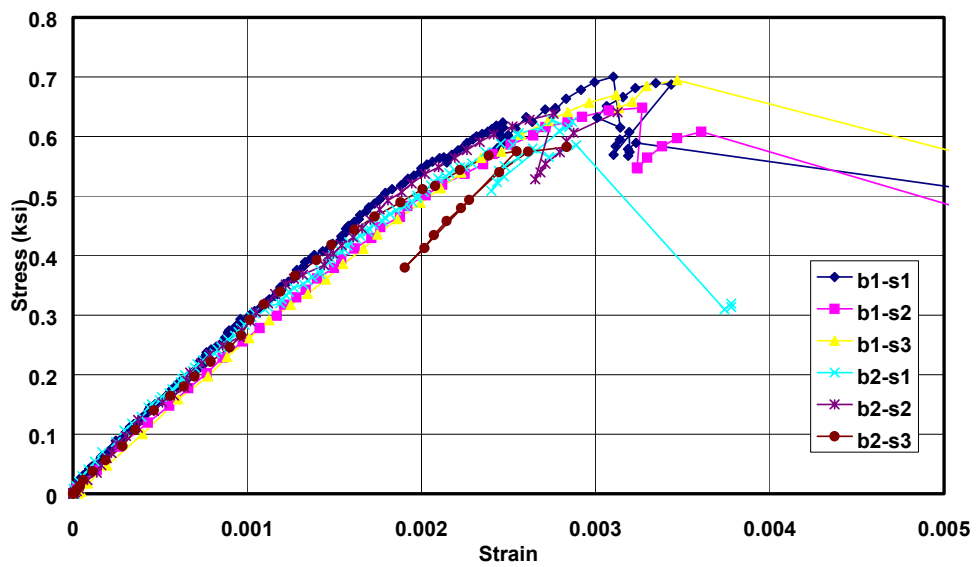
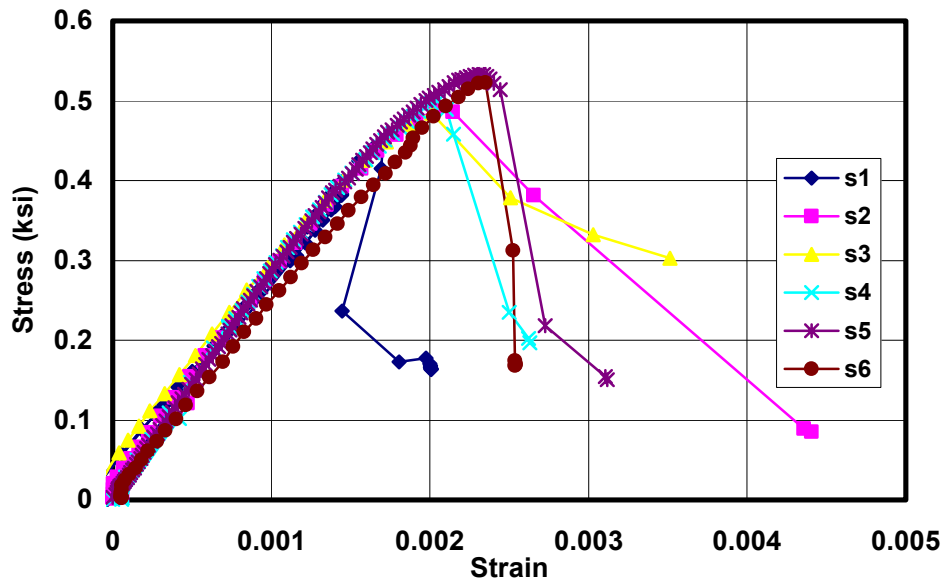


Figure D.6 Compressive stress versus strain for Ytong Shipment 2



*Figure D.7 Compressive stress versus strain for Babb Shipment 2*

### D.1.2 Discussion regarding Tensile Bond Strength between AAC and Type S Bedding Mortar for UT Austin Results

Flexural cracking was observed in 11 shear-wall specimens tested at UT Austin. Flexural cracking is governed by the modulus of rupture of the AAC, or by the tensile bond strength across a leveling bed joint if such a joint is present in the element under consideration. In all cases, these flexural cracks formed between the AAC and the masonry leveling bed, indicating tensile bond failure between the two materials. The flexural cracks occurred in both ends of the wall because the walls were subject to reversed cyclic load. General agreement exists between the lateral load and the first and second occurrence of flexural cracking ( $V_{cr}$ ). The lateral loads at which flexural cracking was observed and back-calculated tensile bond strength for each shear wall are listed in Table D.1.

**Table D.1**      *Calculated modulus of rupture of AAC shear walls tested at UT Austin*

<b>Specimen</b>	<b>Axial Load kips (kN)</b>	<b>First tested <math>V_{cr}</math> kips (kN)</b>	<b>Second tested <math>V_{cr}</math> kips (kN)</b>	<b>First calculated <math>f_{bond}</math> psi (MPa)</b>	<b>Second calculated <math>f_{bond}</math> psi (MPa)</b>
3	120 (534)	65.9 (293)	78.9 (351)	67.1 (0.47)	92.6 (0.64)
4	120 (534)	90.0 (400)	71.5 (318)	117.9 (0.82)	80.9 (0.56)
5	60 (267)	53.9 (240)	54.5 (243)	74.8 (0.52)	75.9 (0.53)
7	80 (356)	29.4 (131)	30.8 (137)	91.1 (0.63)	98.8 (0.69)
9	60 (267)	12.4 (55)	11.4 (51)	77.5 (0.54)	64.7 (0.45)
11	25 (111)	6.8 (30)	4.9 (22)	269.5 (1.87)	175.7 (1.22)
13	25 (111)	7.0 (31)	5.9 (26)	111.7 (0.78)	88.0 (0.61)
14b	5 (22)	2.9 (13)	2.9 (13)	76.5 (0.53)	76.5 (0.53)
15a	5 (22)	8.5 (38)	10.6 (47)	40.3 (0.28)	55.8 (0.39)
15b	25 (111)	7.8 (35)	8.3 (37)	35.1 (0.24)	38.8 (0.27)
16	25 (111)	13.1 (58)	2.4 (11)	74.2 (0.52)	NA
Assemblage	30 (134)	40.8 (0)	36.5 (162)	62.7 (0.44)	54.6 (0.38)
				Mean	683
				COV (%)	33

Shear Wall Specimens 4 (first occurrence) and 11 (both occurrences) show the highest modulus of rupture. In both specimens, at least one flexural crack was not observed until it had propagated more than one-quarter the plan length of the wall. Those specimens were not included in the mean calculation and coefficient of variation. The mean modulus of rupture is 68 psi, and the corresponding 20% fractile is 49.4 psi. The proposed design value for modulus of rupture should not exceed 50 psi if a leveling bed joint is present in the AAC element. In the above table, data are not presented for three shear-wall specimens. Shear Wall Specimen 1 and Shear Wall Specimen 14b had a shrinkage cracks along the bedding mortar joint prior to testing, and multiple flexural cracks had formed in Shear Wall Specimen 2.

### **D.1.3 Shear Bond between AAC and Grout**

#### ***D.1.3.1 Information regarding Shear Bond between AAC and Grout***

The following source of information is available:

- a) Direct shear tests from UT Austin on AAC elements connected by grout invariably show a combined shear bond failure and material failure.

#### ***D.1.3.2 Design and Description of Direct Shear Tests***

In an AAC structure, floor slabs are commonly composed of panels, joined by grouted keys and panels adjacent to a bond beam. Reasonably reliable predictive equations for shear bond between AAC and grout are necessary to check the capacity of those joints. To that end, direct shear tests were designed and performed at UT Austin. The tests are described here, and the results are discussed in the following section.

The direct shear specimen developed to determine the shear capacity between grout and AAC is shown in Figure D.8 and Figure D.9. The specimen height was 27 in., and the joint length was 22 in. The grout-only specimens were constructed by placing AAC along the entire length of the joint, to reproduce the loss of water associated with placing grout adjacent to AAC. Where the grout did not touch the AAC, an AAC block was placed next to the grout, and a paper towel was used as a permeable bond breaker. The AAC units created the formwork for the grout, and were pre-wetted before the grout was placed.

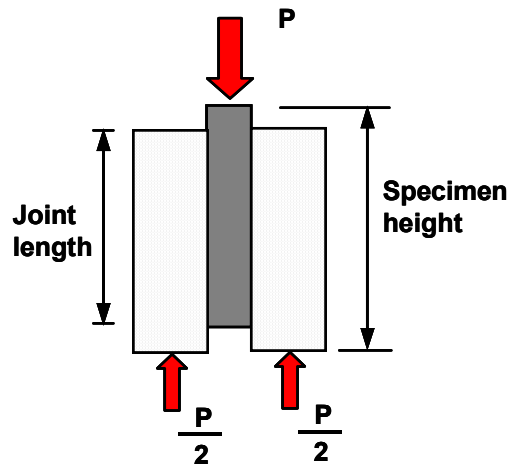


*Figure D.8 Elevation of direct-shear specimens (grout only)*

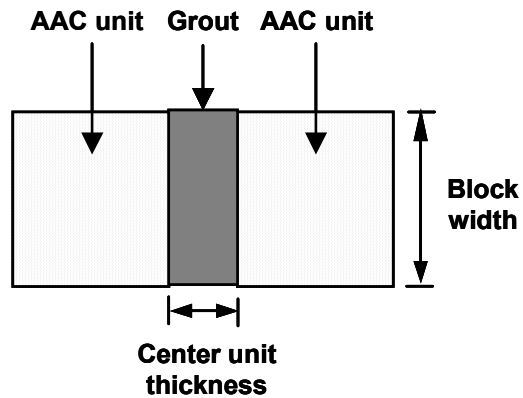


*Figure D.9 Plan view of direct-shear specimens (grout only)*

### *D.1.3.3 Discussion regarding Shear Bond between AAC and Grout*

Three specimens were tested, and the results are presented in Table D.2. The average shear stress for each joint is the total load divided by the observed failure area (Equation (D.1)). The mean shear strength is 58 psi (0.4 MPa), with a COV of 22%. In each case, a peak load was reached, and the load dropped at the

same time as a crack formed in one joint. The load then increased to another peak. The second increase in load is evidently due to a redistribution of the load at the cracked joint.

**Table D.2: Summary of results from direct-shear tests on joints between grout and AAC**

Specimen	Test date	Construction date	Test age, days	Maximum load, kips (kN)	Maximum stress, psi (MPa)
DS-GR-1	4/11/02	3/26/02	16	16.9 (75)	49.6 (0.34)
DS-GR-2	4/11/02	3/26/02	16	24.8 (110)	72.7 (0.5)
DS-GR-3	4/11/02	3/26/02	16	17.5 (78)	51.3 (0.35)

$$\tau_{ave} = \frac{P}{A}$$

Equation (D.1)

Each failure can be classified as a shear bond failure, a material failure or a combination of the two. A shear bond failure is characterized by a smooth surface along the grout side of the failure. A material failure has AAC along the grout side of the joint failure. In the case of the direct shear specimens at UT Austin, the failure is combined. This can be observed by the presence of smooth surfaces and AAC material along the grout failure surface (Figure D.10). For all failure surfaces, at least 30% of the surface area was covered by AAC, indicating that failure was governed by the strength of the AAC material itself, rather than by shear bond or the strength of the grout. Pre-wetting of the AAC units may have increased the shear-bond capacity of the interface, and forced the failure to occur in the AAC material.





*Figure D.10 Failure surface of Direct Shear Specimen DS-GR-1*

#### **D.1.4 Coefficient of Friction of AAC**

##### ***D.1.4.1 Information regarding Coefficient of Friction of AAC***

The following sources of information are available:

- a) UT Austin has information on the coefficient of friction between AAC and Type S leveling bed.
- b) UT Austin has information about the coefficient of friction of un-mortared AAC joints based on direct shear tests.

#### ***D.1.4.2 Discussion of Results for Coefficient of Friction between AAC and ASTM C270 Leveling Mortar***

The coefficient of friction between AAC and ASTM C270 Type S leveling mortar was determined based on sliding observed at four different times during the testing of Shear Wall Specimen 1 at UT Austin. Since no vertical reinforcement was present in the wall, the sliding shear resistance came from axial load alone. The coefficient of friction was calculated by dividing the lateral load by the corresponding applied axial load at each time sliding occurred. The average of those four values is 1.0, with a COV of 4%.

$$V_{sliding} = \mu N \quad \text{Equation (D.2)}$$

#### ***D.1.4.3 Discussion of Results for Coefficient of Friction between AAC and AAC***

Since the coefficient of friction between AAC and AAC may differ from that between AAC and leveling mortar, additional direct-shear tests were performed using un-mortared AAC units clamped together with threaded rods (Figure D.11), running through the centerline of a 3 in. (76 mm) core in each AAC modular block. Three specimens were constructed, and each was subjected to three levels of applied clamping force: 5 kips (22 kN); 10 kips (44 kN); and 15 kips (67 kN). No damage was observed from these tests. Each test is labeled with the specimen number and the value of clamping force in kips. The test results are presented in Table D.3. The coefficient of friction is determined by Equation (D.3), where  $N$  is the clamping force. The average coefficient of friction

is 0.8, with a COV of 8%. A 10% lower fractile is 0.76, and the proposed design value for coefficient of friction between AAC and AAC is 0.75.

$$\mu = \frac{P}{2N}$$

Equation (D.3)

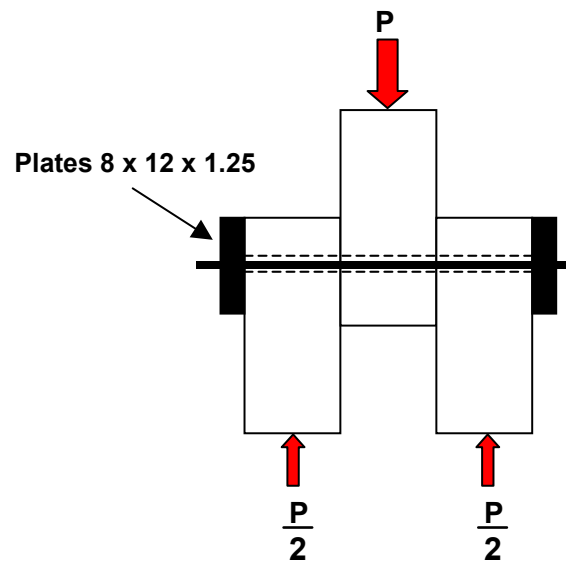


*Figure D.11 Direct shear specimen to determine coefficient of friction for AAC*

**Table D.3 Results for coefficient of friction between AAC and AAC**

<b>Specimen</b>	<b>Maximum Vertical Load kips (kN)</b>	<b>Measured Clamping Force kips (kN)</b>	<b>Coefficient of Friction</b>
1 – 5	7.7 (34)	4.8 (21)	0.80
2 – 5	9.3 (41)	5.3 (24)	0.87
3 – 5	8.8 (39)	4.8 (21)	0.93
1 – 10	13.7 (61)	9.2 (41)	0.75
2 – 10	20.3 (90)	10.6 (47)	0.96
3 – 10	17.1 (76)	10.3 (46)	0.83
1 – 15	24.4 (109)	14.1 (63)	0.86
2 – 15	27.9 (124)	16.1 (72)	0.87
3 – 15	21.5 (96)	14.0 (62)	0.77

## **D.2 TO CHAPTER 4 (DESIGN PROVISIONS FOR REINFORCED AAC FLOOR PANELS)**

### **D.2.1 Discussion regarding Anchorage Behavior of Tensile Reinforcement for Shear Walls Tested at UT Austin**

Three shear-dominated wall specimens, tested at UT Austin, were made of horizontal panels with welded-wire reinforcement. The response of those walls gives additional information on the average bond strength associated with bearing of the cross-wires on the AAC. The difference between their maximum shear capacity ( $V_n$ ) and the base shear at web-shear cracking ( $V_{AAC}$ ) provides an estimate of the contribution of the welded-wire reinforcement. The estimate depends on the following assumptions:

- a) All cross-wires in a critical length of panel bear on the AAC with a maximum stress equal to the compressive strength of the AAC; and

- b) All cross-wires that cross the web-shear crack participate equally.

The transfer of shear across the web-shear crack is unknown. The average bond strength can be estimated for two limiting conditions: 1) all of  $V_{AAC}$  is resisted by shear across the crack; and 2) none of  $V_{AAC}$  is resisted by shear across the crack. Based on that evaluation, the bond strength does not exceed 86 psi. (Table D.4).

**Table D.4** *Calculated range of bond strengths for welded-wire fabric based on shear walls tested at UT Austin*

Specimen	Maximum Capacity $V_n$ (kips)	Observed $V_{AAC}$ (kips)	$u$ with $V_{AAC}$ (psi)	$u$ without $V_{AAC}$ (psi)
1	167.6	164.2	3	86
4	126.4	82.4	15	23
9	42.4	42.2	0.2	29

Using the information from UAB previously presented in Chapter 4 (Table 4.1), calculated bond strengths range from 72 to 128 psi, slightly higher than the range of 23 to 86 psi calculated for the UT Austin specimens neglecting  $V_{AAC}$ .

## REFERENCES

- Comité Euro-international du Béton (CEB): "Autoclaved aerated concrete: CEB manual of design and technology," Lancaster, New York, Construction Press, 1978.
- Fouad, F., Dembowski, J., and Newman, D.: "Physical and Mechanical Properties of AAC Produced in the United States," Report to the Autoclaved Aerated Concrete Products Association, Department of Civil Engineering, The University of Alabama at Birmingham, February, 2002.
- Klingner, R. E., Tanner J., Varela J., "Development of Seismic Design Provisions for Autoclaved Aerated Concrete: an Overall Strategy for the US," The Masonry Society, *Proceedings* of the 9<sup>th</sup> North-American Masonry Conference, Clemson University, Clemson, South Carolina, USA, June, 2003.
- RILEM: "Lightweight Concrete," *Proceedings* of the 1st RILEM International Symposium on Autoclaved Aerated Concrete, H. Granholm, ed., Akadmiförlaget-Gamperts, Göteborg, Sweden, 1960.
- RILEM: "Autoclaved aerated concrete, moisture and properties," *Proceedings* of the 2nd RILEM International Symposium on Autoclaved Aerated Concrete, Swiss Federal Institute of Technology in Lausanne, March, 1982, Folker H Wittmann, ed., Elsevier Scientific Publishing Co., New York, N.Y., distributed in the US by Elsevier Science Publishing Co., 1983.
- RILEM: "Standards and Regulations concerning Building and Buildings Constructed with Autoclaved Aerated Concrete," second revised edition, F. H. Wittmann and Y. Houst, eds., Laboratory for Building Materials, Swiss Federal Institute of Technology, Lausanne, Switzerland, 1984.
- RILEM: "Advances in autoclaved aerated concrete," *Proceedings* of the 3rd International Symposium on Autoclaved Aerated Concrete, Zurich, Switzerland, 14-16 October 1992, Folker H. Wittmann, ed., A.A. Balkema, Rotterdam, 1992.
- RILEM: "Autoclaved Aerated Concrete: Properties, Testing, and Design," Technical Committees 78-MCA and 51-ALC, S. Aroni, et al., eds.,

RILEM Recommended Practice, E & FN Spon, London and New York, 1993.

Tanner, J. E.: "Development of Proposed Code Equations for AAC Shear Walls," PhD Dissertation, Department of Civil Engineering, The University of Texas at Austin, August 2003.

Varela, J.: "Development of R and Cd Factors for the Seismic Design of AAC Structures," PhD Dissertation, Department of Civil Engineering, The University of Texas at Austin, May 2003.

## VITA

Jaime Fernando Argudo was born in Guayaquil, Ecuador on October 3, 1963, the son of Carlos Vicente Argudo and Alba Esperanza Rodríguez. He received his Bachelor of Science in Civil Engineering from Universidad Católica de Santiago de Guayaquil, in 1986. He is a professor to the School of Engineering of Universidad Católica de Santiago de Guayaquil since 1987 and, from 1998 to 2001; he served as Director for its Research and Development Institute (IIFIUC). From September 1989 to July 1990, he attended the Earthquake Engineering Course in the International Institute of Seismology and Earthquake Engineering (IISEE), in Tsukuba, Japan. He also attended courses in Peru (1992), Italy (1993), Mexico (1998), and Sweden (2001), in the area of Disaster Mitigation and Management. From 1992 to 2001, he worked as consultant to various organizations, such as the United Nations, the Organization of The American States, the World Health Organization, and the Municipal Government of Guayaquil, in the fields of Structural Vulnerability Assessment and Seismic Risk Mitigation. From 1996 to 2001, he worked as a researcher and project manager to Universidad Católica and the National Foundation for Science and Technology in the fields of Earthquake Engineering and Low-cost Housing. In July 2001, he became a member to the International Existing Building Code Committee (IEBC) of the International Code Council (ICC). In January 2002, he entered the Graduate Program in Structural Engineering at The University of Texas at Austin.

Permanent Address: Urdesa Norte, Ave. 4ta #418 y Calle Quinta (Planta Baja)  
Guayaquil, Ecuador

The author typed this thesis.